



U.S. Department
of Transportation
**Federal Railroad
Administration**

STUB SILL TANK CAR RESEARCH PROJECT: FULL-SCALE DAMAGE TOLERANCE TEST

Office of Research and
Development
Washington, D.C. 20590

DOT/FRA/ORD-

December 1998
Final Draft Report

This document is available to the
U.S. public through the National
Technical Information Service
Springfield, Virginia 22161

Disclaimer: This document is disseminated under the sponsorship of the Department of Transportation in the interest of information exchange. The United States Government assumes no liability for the contents or use thereof. The United States Government does not endorse products or manufacturers. Trade or manufacturers' names appear herein solely because they are considered essential to the object of this report.

METRIC CONVERSION FACTORS

Approximate Conversions to Metric Measures

Symbol	When You Know	Multiply by	To Find	Symbol
--------	---------------	-------------	---------	--------

LENGTH

in	inches	*2.50	centimeters	cm
ft	feet	30.00	centimeters	cm
yd	yards	0.90	meters	m
mi	miles	1.60	kilometers	km

AREA

in ²	square inches	6.50	square centimeters	cm ²
ft ²	square feet	0.09	square meters	m ²
yd ²	square yards	0.80	square meters	m ²
mi ²	square miles	2.60	square kilometers	km ²
	acres	0.40	hectares	ha

MASS (weight)

oz	ounces	28.00	grams	g
lb	pounds	0.45	kilograms	kg
	short tons	0.90	tonnes	t
	(2000 lb)			

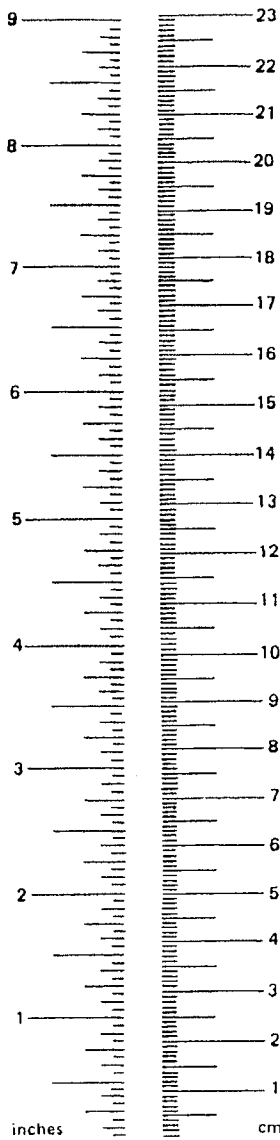
VOLUME

tsp	teaspoons	5.00	milliliters	ml
Tbsp	tablespoons	15.00	milliliters	ml
fl oz	fluid ounces	30.00	milliliters	ml
c	cups	0.24	liters	l
pt	pints	0.47	liters	l
qt	quarts	0.95	liters	l
gal	gallons	3.80	liters	l
ft ³	cubic feet	0.03	cubic meters	m ³
yd ³	cubic yards	0.76	cubic meters	m ³

TEMPERATURE (exact)

°F	Fahrenheit temperature	5/9 (after subtracting 32)	Celsius temperature	°C
----	------------------------	----------------------------	---------------------	----

* 1 in = 2.54 cm (exactly)



Approximate Conversions from Metric Measures

Symbol	When You Know	Multiply by	To Find	Symbol
--------	---------------	-------------	---------	--------

LENGTH

mm	millimeters	0.04	inches	in
cm	centimeters	0.40	inches	in
m	meters	3.30	feet	ft
m	meters	1.10	yards	yd
km	kilometers	0.60	miles	mi

AREA

cm ²	square centim.	0.16	square inches	in ²
m ²	square meters	1.20	square yards	yd ²
km ²	square kilom.	0.40	square miles	mi ²
ha	hectares	2.50	acres	
	(10,000 m ²)			

MASS (weight)

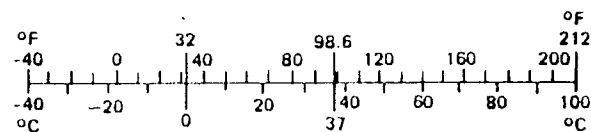
g	grams	0.035	ounces	oz
kg	kilograms	2.2	pounds	lb
t	tonnes (1000 kg)	1.1	short tons	

VOLUME

ml	milliliters	0.03	fluid ounces	fl oz
l	liters	2.10	pints	pt
l	liters	1.06	quarts	qt
l	liters	0.26	gallons	gal
m ³	cubic meters	36.00	cubic feet	ft ³
m ³	cubic meters	1.30	cubic yards	yd ³

TEMPERATURE (exact)

°C	Celsius temperature	9/5 (then add 32)	Fahrenheit temperature	°F
----	---------------------	-------------------	------------------------	----



FINAL DRAFT

FINAL DRAFT

List of Acronyms**Organizations:**

AAR	Association of American Railroads
ARI	American Railcar Industries
CMA	Chemical Manufacturers Association
FRA	Federal Railroad Administration
GE	General Electric Capital Railcar Services
RPI	Railway Progress Institute
SSWG	Stub-Sill Working Group
SwRI	Southwest Research Institute
TC	Transport Canada
TTC	Transportation Technology Center
TTCI	Transportation Technology Center, Inc.

Terminology:

DTA	Damage Tolerance Analysis
FEA	Finite Element Analysis
FEEST	Freight Equipment Environmental Sampling Test
LCF	Longitudinal Coupler Force
LLBUF	Loaded Longitudinal (coupler force), Buff only
LLDFT	Loaded Longitudinal (coupler force), Draft only
LVPU	Loaded Vertical (coupler force), Positive is Up
OTR	Over-the-Road
REPOS	Road Environment Percentage Occurrence Spectrum
ULBUF	Unloaded Longitudinal (coupler force), Buff only
ULDFT	Unloaded Longitudinal (coupler force), Draft only
UVPU	Unloaded Vertical (coupler force), Positive is Up
VCF	Vertical Coupler Force

FINAL DRAFT

1. Report No. DOT/FRA/ORD-	2. Government Accession No.	3. Recipient's Catalog No.	
4. Title and Subtitle Stub Sill Tank Car Research Project: Full-Scale Damage Tolerance Test		5. Report Date November 1998	
		6. Performing Organization Code	
7. Authors Keith B. Smith		8. Performing Organization Report No.	
9. Performing Organization Name and Address Transportation Technology Center, Inc. P.O. Box 11130, 55500 DOT Road Pueblo, CO 81001		10. Work Unit No. (TRAIS)	
		11. Contract or Grant No.	
12. Sponsoring Agency Name and Address U.S. Department of Transportation Federal Railroad Administration Office of Research and Development 400 Seventh Street, SW Washington, DC 20590		13. Type of Report or Period Covered	
		14. Sponsoring Agency Code	
15. Supplemental Notes			
16. Abstract The Federal Railroad Administration, with supplemental support from the Association of American Railroads (AAR), Railway Progress Institute, and Chemical Manufacturers Association, contracted with the Transportation Technology Center, Inc., a subsidiary of the AAR (then organized as AAR, Transportation Technology Center), to conduct a full-scale damage tolerance analysis (DTA) validation test on a tank car using the Simuloader. This is one of five companion reports that detail North American tank car industry efforts since 1992 to assess the operating environment and apply DTA principles to tank car design. These efforts included: an over-the-road operating environment survey, material spectrum variable testing, a full-scale fatigue crack growth test, fractographic analysis of the full-scale test vehicle, and DTA analytical model validation and application guidance. This document covers only the details of the 300,000-spectrum-mile full-scale DTA validation test.			
17. Key Words Beach Mark, Clipping, Coherence, Compliance, Marker Band, Precrack, Preflaw, Rainflow, Spectrum, Transient, Truncation		18. Distribution Statement This document is available through National Technical Information Service Springfield, VA 22161	
19. Security Classification <i>(of the report)</i>	20. Security Classification <i>(of this page)</i>	21. No of Pages 82	22. Price

EXECUTIVE SUMMARY

In 1992, the National Transportation Safety Board recommended that tank car structures be designed using a damage-tolerant philosophy similar to that utilized by the aircraft industry. Toward that end, the Southwest Research Institute was engaged to assist in the development and implementation of a damage tolerance analysis (DTA) methodology for railroad tank cars. To help validate the resulting methodology, the Federal Railroad Administration (FRA), with supplemental support from the Association of American Railroads (AAR), Railway Progress Institute (RPI), and Chemical Manufacturers Association (CMA), contracted with the Transportation Technology Center, Inc. (TTCI), a subsidiary of the AAR (then organized as AAR, Transportation Technology Center), to conduct a full-scale fatigue crack growth test on a tank car. This report is one of several that detail North American tank car industry efforts since 1992 to assess the operating environment and apply DTA principles to tank car design. These efforts include an over-the-road (OTR) environmental survey, coupon spectrum variable testing, a full-scale fatigue crack growth test, a fractographic analysis of the full-scale test pieces, and DTA analytical model validation and application guidance. This document covers only the details of the 300,000-spectrum-mile full-scale DTA validation test.

Prior to the full-scale test, a 15,000-mile OTR test was performed to enhance data for 100-ton tank cars published in the AAR *Manual of Standards and Recommended Practices*. This revised tank car data was used to create the 10,000-spectrum-mile load schedule used in the full-scale test program, as well as for industry DTA models. Subsequent to this OTR test, a coupon test program was conducted to investigate effects of spectrum variables on fatigue crack growth rates. These preliminary coupon studies indicated that for accelerated tests of common tank car steels, the omission of relatively small cycles (truncation) and peak load attenuation (clipping) might have minimal effects on crack growth behavior.

While the full-scale test was assembled, a finite element analysis (FEA) of the test car was used to find locations of high stress (critical regions), estimate stress-to-load ratios for truncation, and provide input into the crack growth model to estimate test duration. In general, the FEA predicted stress concentrations at the same critical regions identified by the SS-II

database, a compilation of stub-sill inspections performed by the tank car industry. However, the predicted stress magnitudes were understated by a nominal weighted-average factor ranging from one to three. It is important to note that this factor was an engineering estimate based on several measurements and many parameters, and warrants further study.

The orphan tank car used for the full-scale validation test had neither head pads nor head braces (details that are common to current tank car designs) and no previous record of parent metal crack repairs. Initial visual inspections of the car did not reveal any cracks in the more critical stub-sill regions highlighted by both the SS-II database and the stress analysis of the car. For this reason, flaws were mechanically created in four critical regions and cyclic loading was used to initiate cracks from these 'preflaws.' Though this 'precracking' effort was only marginally successful at the preflaws, several unexpected cracks were initiated nearby within the critical regions of interest.

The Simuloader, a computer-controlled servohydraulic test bed for full-scale multiaxial fatigue and vibration testing of rail cars, was used to perform the 300,000-spectrum-mile full-scale DTA validation test. Longitudinal and vertical coupler forces were applied to the test car in series (without any corresponding bolster motions) and crack growth in critical regions was monitored. In addition, car body strains and deflections under static loads were periodically measured. These 'car body compliance' surveys showed variability in both linearity and repeatability, a likely result of stress redistribution throughout the structure due to crack propagation. Also, it was noted that upward vertical and draft longitudinal coupler loads were dominant in terms of critical region strain sensitivity, though the opposite loading directions are typically dominant for crack growth, as they usually cause critical region tension.

Because this was a DTA validation, not an OTR simulation, many simplifications were utilized to simplify the modeling, accelerate the test, and reduce costs without compromising any program objectives. To accelerate the test, the input DTA load schedule was truncated to a small percentage of the OTR cycle count, though actuator transient response added many small cycles back into the test spectra. As a setup cost reduction, vertical loads were applied to the stub sills of the car just inboard of the strikers, rather than out at the coupler pulling face (as they are

experienced in the field), which resulted in the understatement of the applied bending stresses. This changed at 200,000 DTA spectrum miles when the vertical coupler input spectrum was amplified to accelerate crack growth, which effectively corrected for the missing moment arm and doubled the applied shear (compared to OTR) in the critical regions. None of these simplifications compromised the validation effort, because the inputs into the car were identical to those into the analytical computer models (FEA and crack growth). The vertical loads were applied in the FEA at the same structural points as they were on the test car, and all loads were recorded during testing as input into crack growth models of the critical regions. It should be noted, however, that due to these simplifications, 300,000 DTA spectrum miles (the duration of the test) is not correlated with 300,000 revenue service miles of fatigue damage.

By the end of the test, 30 crack indications (unconfirmed at that point) had been documented and monitored for surface growth, five of which were from preflaws. Ten of these cracks and two preflaws were broken open for a cursory fractographic analysis (through the thickness); three cracks and one preflaw were examined more thoroughly. The application of constant-amplitude 'marker bands' proved to be effective for creating a record of crack growth rates and aspect ratios. The full-scale test and corresponding DTA results, though not directly transferable to other stub-sill tank car designs, illustrated the general applicability of the damage tolerance approach to tank car design and life extension. Sufficient stress and crack growth results have been obtained for the DTA analytical model validation.

Table of Contents

1.0 INTRODUCTION	1
2.0 BACKGROUND	1
2.1 Stub-Sill Tank Car Research	2
2.1.1 Tank Car Damage Tolerance	2
2.1.2 Task Order Evolution.....	2
2.2 Over-the-Road Test	4
2.2.1. Motivation and Results	4
2.2.2 Data Information and Publishing	5
2.3 Coupon Test Programs.....	6
2.3.1 Truncation and Clipping Effects	6
2.3.2 Marker Banding Feasibility.....	8
2.3.3 Preflaw and Dye Penetrant Verification	9
2.4 Damage Tolerance Analysis	10
2.4.1 General Approach	10
2.4.2 Industry Progress	12
2.5 The Simuloader.....	13
2.5.1 General Description.....	13
2.5.2 Evolution and Function.....	14
2.5.3 Input Drive Files	14
2.6 Test Car Description	15
3.0 OBJECTIVE	16
4.0 KEY PERSONNEL	17
5.0 INITIAL CONDITIONS	17
5.1 Physical Setup	17
5.1.1 Jacket Removal.....	17
5.1.2 Initial Inspection.....	18
5.1.3 Test Car Mounting on the Simuloader.....	20
5.1.4 Water Lading	24
5.2 System Characterization	24
5.3 Preliminary Analysis.....	26

Table of Contents (continued)

5.3.1	DTA Predictions	26
5.3.2	Critical Region Selection	26
5.4	Test Car Flaw Induction	27
5.5	Transducer Setup	29
5.5.1	Data Collection Channel Count	29
5.5.2	Car Body Response Strains	31
5.6	Simulation Inputs	37
5.6.1	DTA Validation; Not OTR Simulation.....	37
5.6.2	Drive File Development	38
6.0	TEST OPERATIONS	40
6.1	Crack Initiation	41
6.2	Spectrum Loading	42
6.2.1	Spectrum Crack Growth	42
6.2.2	Car Body Compliance	44
6.2.3	System Control and Response.....	45
6.3	Mid-Test Procedure Adjustments.....	45
6.3.1	Inspection Technique	45
6.3.2	Input Load Spectrum	45
6.4	Post-Test Analysis	48
6.4.1	Final Critical Region Inspection.....	48
6.4.2	Sill Sectioning and Fractography.....	48
6.4.3	Damage Tolerance Validation	48
7.0	RESULTS AND DISCUSSION	49
7.1	Spectrum Crack Growth.....	49
7.1.1	Initial Precracking Success	49
7.1.2	Spectrum Cracking Success	50
7.1.3	Marker Banding Success Indications	56
7.2	Car Body Compliance	57
7.2.1	Compliance Test Results	57
7.2.2	Sill Deflections and Bending Strains.....	58

Table of Contents (continued)

7.2.3	Tank Head Gradients and Summations	60
7.2.4	Sill Web Gradients and Summations.....	66
7.2.5	Sill Top Flange Gradients	68
7.3	System Control and Response	68
7.4	Post-Test Analysis	69
8.0	SIGNIFICANT OBSERVATIONS.....	71
8.1	OTR and Coupon Testing	71
8.2	Orphan Tank Car NATX 22746.....	71
8.3	Pre-Test Damage Tolerance Analysis	72
8.4	Preflawing and Precracking.....	72
8.5	Validation Load Schedule.....	73
8.6	Marker Band Application	73
8.7	Spectrum Crack Growth	73
8.8	Car Body Compliance.....	74
8.9	VCF Placement and Amplification	75
8.10	DTA Validation	75
	Acknowledgements	77
	Bibliography	79
	Glossary.....	81
	Appendix A: SwRI 10,000-Mile Tank Car Load Schedule.....	A-1
	Appendix B: Full-Scale Damage Tolerance Test Crack Indication Log.....	B-1
	Appendix C: Piecewise Car Body Compliance Test Data	C-1
	Appendix D: Car Body Compliance Sensitivities	D-1
	Appendix E: Rainflow Cycle Counted Drive and Response Data.....	E-1

List of Figures

Figure 1.	Coupon Test Setup at SwRI	7
Figure 2.	Marker Bands on Coupon Fracture Surface	9
Figure 3.	Schematic of Tank Car on Simuloader	14
Figure 4.	Test Car NATX 22746 Upon Arrival at the Transportation Technology Center	18
Figure 5.	SS-II Critical Regions (SS-II Codes Indicated)	20
Figure 6.	Test Car NATX 22746 on Simuloader	21
Figure 7.	B-End of Test Car, LCF Connection	21
Figure 8.	Schematic of VCF Attachment to Stub Sill.....	22
Figure 9.	B-End of Test Car, VCF Connection.....	23
Figure 10.	VCF System Transfer Function	25
Figure 11.	Basic Critical Region Structural and Weld Details	27
Figure 12.	B-End Right Corner Flaw and Tank Head Rosette	28
Figure 13.	B-End Left Strain Gages and Preflaw	32
Figure 14.	B-End Right Strain Gages and Preflaw.....	33
Figure 15.	A-End Left Strain Gage.....	34
Figure 16.	A-End Right Strain Gages and Preflaw.....	35
Figure 17.	Sill Bending Strain Gages (at Both Ends of Car)	36
Figure 18.	Segment of VCF Input Sinusoid	39
Figure 19.	B-End Left Seal Weld Cracks	51
Figure 20.	B-End Left Flange Weld Cracks and Preflaw.....	51
Figure 21.	B-End Right Seal Weld Cracks and Preflaw	52
Figure 22.	A-End Left Seal Weld Cracks and Preflaw	53
Figure 23.	A-End Left Sill Top Flange Crack	53

List of Figures (continued)

Figure 24.	A-End Right Seal Weld Cracks.....	54
Figure 25.	A-End Right Sill Top Flange Cracks	54
Figure 26.	A-End Right Flange Weld Crack and Preflaw	55
Figure 27.	VCF Load Stud Fracture Surface at 6.6x Magnification.....	56
Figure 28.	Schematic of Potential LCF Load Path.....	59
Figure 29.	Principal Stress Magnitudes and Directions at B-End Left Tank Head	63
Figure 30.	Principal Stress Magnitudes and Directions at B-End Right Tank Head..	64
Figure 31.	Principal Stress Magnitudes and Directions at A-End Left Tank Head	65
Figure 32.	Principal Stress Magnitudes and Directions at A-End Left Sill Web	67

List of Tables

Table 1.	Orphan Tank (Test Car) Characteristic.....	16
Table 2.	Orphan Tank (Test Car) Material.....	16
Table 3.	Basic Simuloader Actuator Characteristic.....	24
Table 4.	Induced Flaw (Preflaw) Location	27
Table 5.	Data Collection Channel List	30
Table 6.	Validation Test Strain Gage Summary.....	31
Table 7.	10,000-Mile Validation Load Schedule Breakdown	40
Table 8.	Sequence of Significant Full-Scale Test Events	41
Table 9.	Precracking Loads Applied in Full-Scale Test	42
Table 10.	Marker Bands Applied in Full-Scale Test.....	44
Table 11.	Empirical/Analytical Comparison Matrix Example.....	46

1.0 INTRODUCTION

The Federal Railroad Administration (FRA), with supplemental support from the Association of American Railroads (AAR), Railway Progress Institute (RPI), and Chemical Manufacturers Association (CMA), contracted with the Transportation Technology Center, Inc. (TTCI), a subsidiary of the AAR (then organized as AAR, Transportation Technology Center), to conduct a full-scale damage tolerance analysis (DTA) validation test on a tank car using the Simuloader, a full-scale fatigue and vibration test bed. This test is the final subtask of Task Order 108 – Stub-Sill Tank Car Research; this document covers only this final subtask.

2.0 BACKGROUND

This report contains descriptions of the Simuloader, a full-scale multiaxial servohydraulic fatigue and vibration test machine for railcars, and DTA, a fracture mechanics based methodology used to establish inspection intervals for fatigue cracked structures. This report concentrates on the use of the Simuloader to validate the DTA methodologies in the North American railroad tank car industry's stub-sill tank car research. After some evolution, Task Order 108 has been subdivided into three distinct, consecutive phases:

1. Over-the-Road (OTR) Operating Environment Survey
2. Spectrum Variable Investigation with Coupon Testing
3. Full-Scale Damage Tolerance Test

Cogburn (1995) and McKeighan et al. (1997) provided detailed discussions of the first two phases in previously published reports; details from the third phase are the primary focus of this document and a companion report by Benac et al. (1998). Cardinal et al. (1998) discussed the actual DTA program performed in parallel with this task order, and Williams (1997) reported on the finite element analyses (FEA) of the orphan tank car that was tested.

Before the third phase of Task Order 108 is discussed, some background information on the various components of this multidimensional tank car research program has been assembled here. Section 2.1 provides a historical perspective with a few of the events that have shaped decisions of both the tank car industry and the FRA as both the DTA program and Task Order 108 have evolved. Following that, Sections 2.2 and 2.3 give a brief summary of some of the

goals and relevant findings of the first two phases of Task Order 108. Finally, Sections 2.4 and 2.5 include general descriptions of DTA and the Simuloader.

2.1 STUB-SILL TANK CAR RESEARCH

2.1.1 Tank Car Damage Tolerance

Throughout the first half of the 20th century, the prevailing design for railroad tank cars employed a continuous center sill, above which a tank was mounted. In the late 1950's the stub-sill design was introduced in which short draft sills were welded onto each end of the tank (thus, coupler loads were transmitted through the tank itself). Because a large portion of the sill weight was eliminated, the stub-sill design proved to be more efficient than that of the through sill. With this improved efficiency, stub-sill tank cars rapidly became preferred by the industry and soon came to dominate the North American tank car fleet. During the early 1990's, at least 12 sill separations occurred in this fleet of stub-sill tank cars. A resulting inspection of 1,100 cars showed fatigue cracking at the attachment of the sill to the tank in a significant number of these designs. At that time, the North American railroad tank car industry agreed to inspect and repair stub sills and their attachment welds on all tank cars built before 1984.

At the same time, the tank car industry also agreed to undertake a DTA program to establish safe inspection intervals for the newly repaired cars. Toward this end, a technical committee was formed including several individual car builders and owners, the FRA, AAR, RPI, CMA, and Transport Canada (TC). This committee employed the Southwest Research Institute (SwRI) to act as an independent third-party program manager providing guidance during the industry's adoption of DTA principles. This committee, hereafter referred to as the Stub-Sill Working Group (SSWG), reports to the AAR/RPI Tank Car Committee. In addition to Cardinal et al. (1998), Stone et al. (1997) has documented the efforts of the SSWG. FRA support for industry-led projects to refine and use DTA techniques to ensure tank car reliability was discussed by Hattery et al. (1997).

2.1.2 Task Order Evolution

From 1990 to 1993 under contract DTFR53-82-C-00282, Task Order 43, the FRA funded the AAR Transportation Test Center (which has since privatized as TTCI) to study fatigue crack

growth in stub-sill tank cars. Cackovic et al. (1993) used the Simuloader to replicate 300,000 miles of fatigue significant service on a stub-sill tank car. The fatigue loads simulated were obtained by combining tank car bolster vibration waveforms recorded during an over-the-road (OTR) test with coupler loads measured during the Freight Equipment Environmental Sampling Test (FEEST). This combination was based on the assumption that coupler forces experienced in revenue service were typically incoherent (linearly unrelated at frequencies of interest) with truck bolster motions. Though no formal report was issued for the FEEST program, some details can be found in papers by Richmond et al. (1981) and Sharma et al. (1984). The data obtained from the FEEST program was published as Road Environment Percentage Occurrence Spectrums (REPOS) in Chapter VII of Specification M-1001, part of the AAR *Manual of Standards and Recommended Practices* (AAR-MSRP).

In 1992, while the tank car industry embarked on a program of stub-sill tank car inspections and DTA training, the FRA, under contract DTFR53-93-C-00001, awarded Task Order 108: Stub-Sill Tank Car Research. This contract was divided into three phases, the first of which was to determine the OTR environmental loading spectrums for a representative stub-sill tank car. The data obtained in this phase was used to augment the existing FEEST data for 100-ton tank cars, as well as to provide input for the latter two phases of the task order and the tandem DTA program in progress. In 1995, the resources for the second phase (the squeeze test) were reallocated to investigate the effects of two spectrum variables (truncation and clipping) on fatigue crack growth in a coupon test program at SwRI.

The Simuloader test (the third phase of Task Order 108) was originally planned to be an accelerated full-scale multiaxial fatigue test of the tank car used in the OTR test. However, much had developed since the inception of the program. Because Task Order 108 was permitted to evolve with the efforts of the SSWG, the scope of this final phase was both changed and expanded to validate the DTA methodologies under industry evaluation. In order to accommodate the modified scope of this phase, additional funding for the task order was secured in early 1997 from the FRA, AAR, RPI, and CMA. An orphan tank car was located, instrumented, and mounted on the Simuloader. The longitudinal and vertical coupler forces (LCF and VCF, respectively) from the modified REPOS tables were input into the car body sequentially for a period corresponding to approximately 300,000 miles of 'fatigue significant

revenue service;’ no other actuators were used to apply loads to the car. Critical region stresses and crack growth rates were monitored throughout the test and have been compared to analytical predictions by Cardinal et al. (1998) for the actual DTA validation.

2.2 OVER-THE-ROAD TEST

2.2.1 Motivation and Results

A complete recount of the motivations behind the operating environment survey (the first phase of Task Order 108) that began in 1994 is beyond the scope of this report; however, a brief summary of these is appropriate. Prior to 1988, the environmental load data used for tank car design was contained in fatigue analysis guidelines from a previous AAR study by Przybylinski et al. (1977). This road test data, collected in 1970, was processed with range-mean cycle counting methods and reported a maximum VCF of 12.5 kilopounds (kips). In 1988, this spectra was replaced with the FEEST data from 1986, which was processed with relatively more conservative rainflow cycle counting techniques and reported VCF events as high as 50 kips. Following this change, the relatively high load levels and the overall repeatability of the FEEST program were questioned. As a result of this questioning, the OTR test of 1994 was conceived.

A side benefit of the 1994 OTR test was the vertical coupler load investigation that was launched during the instrumentation of the test car. The VCF measurement was originally designed to repeat the configuration used in the 1986 FEEST program. However, the setup was enhanced to determine whether more accurate VCF loads under both static and dynamic conditions could be obtained. The resulting five measurements of vertical coupler loading used the following strains, calibrated to force:

- Coupler shank shear strain
- Vertical sill bending strain
- Striker/carrier strain
- Yoke support plate shear strain
- Vertical sill shear strain

For reasons discussed by Cogburn (1995), vertical sill shear became the measurement of choice for the tank car design guidelines. It is important to note that this measurement, the data

from which has subsequently been published in the AAR-MSRP, is not a direct measurement of VCF. Rather, it represents the vertical force acting at the striker/carrier resulting from a load applied at the coupler pulling face.

The five primary load cases measured in the 1994 OTR testing duplicated those of the earlier FEEST program. These were:

- Vertical center plate force
- Vertical bolster force
- Vertical side bearing force
- Longitudinal coupler force
- Vertical coupler force

The side bearing load cells failed early in the test and were neither repaired nor replaced, as it was determined to be cost-prohibitive given the relative importance of the measurement. Effectively, this meant that the center plate measurement was abandoned as well, because it was calculated from the difference between the bolster load and the total side bearing load. The effect of this decision was realized when the data was integrated and published.

2.2.2 Data Integration and Publishing

The rainflow cycle counted data acquired during the 1994 OTR test was reviewed and integrated into the AAR-MSRP with the 1986 FEEST data for 100-ton tank cars in general service. The most recently published version of these REPOS tables includes data from both test programs.

As discussed in Section 2.2.1, the 1994 test failed to produce both the vertical side bearing and the corresponding vertical center plate spectrums; therefore, the REPOS tables now contain only 1986 data for both of these load cases. Because one of the primary goals of the 1994 test was to replace the questionable 1986 VCF spectrum, the AAR-MSRP now contains only 1994 data for VCF. The remaining two load cases, vertical bolster force and LCF, are represented with a combination of both the 1986 and 1994 data. The motivation behind this decision is described below for the case of LCF.

Stress-life fatigue calculations were performed in 1996 to qualify the relative differences between the 1986 and 1994 LCF spectra. Through these, it was demonstrated that absolute differences are extremely difficult to quantify due to the logarithmic nature of fatigue and the dependency of the calculations on variables such as stress concentrations, material properties, and processing effects. Relative differences are much easier to characterize. The calculations showed that, in general, the loaded car data from 1986 is more conservative (more severe) than that of 1994. In contrast, similar calculations showed a reverse trend for the empty car data (the spectrum from 1986 was less conservative than that of 1994). To complicate matters further, the spectrum from 1986 was clipped at 300 kips draft and 500 kips buff (due to data acquisition limitations concerning the total number of bins allowable); thus reducing its potential severity. Ultimately, the decision was made to combine the spectra from 1994 with that of 1986 for the AAR-MSRP REPOS tables.

2.3 COUPON TEST PROGRAMS

2.3.1 Truncation and Clipping Effects

The spectrum variable investigation (the third phase of Task Order 108) was launched shortly after the completion of the OTR test in late 1995. To a large extent, a paper written by Orringer (1994) originally prompted the investigation into simulation acceleration techniques. An underlying assumption in accelerated simulation work is that a large percentage of revenue service data consists of load levels that do not produce fatigue-significant structural stresses. Whether this concept of a stress 'threshold' applies in the case of fatigue crack growth is the subject of many debates. The determination of a threshold stress level for a typical tank car steel was the primary purpose of the coupon testing program run by McKeighan et al. (1997).

Toward this end, seven test specimens were machined from normalized ASTM A572 Grade 50 steel from the remnants of stub-sill production at Union Tank Car Company and tested with the loaded VCF spectrum from the 1994 OTR test. The two main parameters varied for this study were the number of low-amplitude cycles omitted (truncated) from each spectrum pass and the stress-to-force scale factor for the spectrum. This scale factor results from the fact that the fatigue spectrums for this program were recorded in terms of a force applied at a relatively remote point on the structure from where the critical stress responses (thus, fatigue) actually

occur. In addition to this study of truncation, a brief study into the effects of clipping was performed in parallel with the same coupons. Clipping differs from truncation in that load cycles are not removed from the input spectrum; rather, their individual magnitudes are limited to (not allowed to exceed) a preset value. Figure 1 is a photograph of the coupon test setup at SwRI.

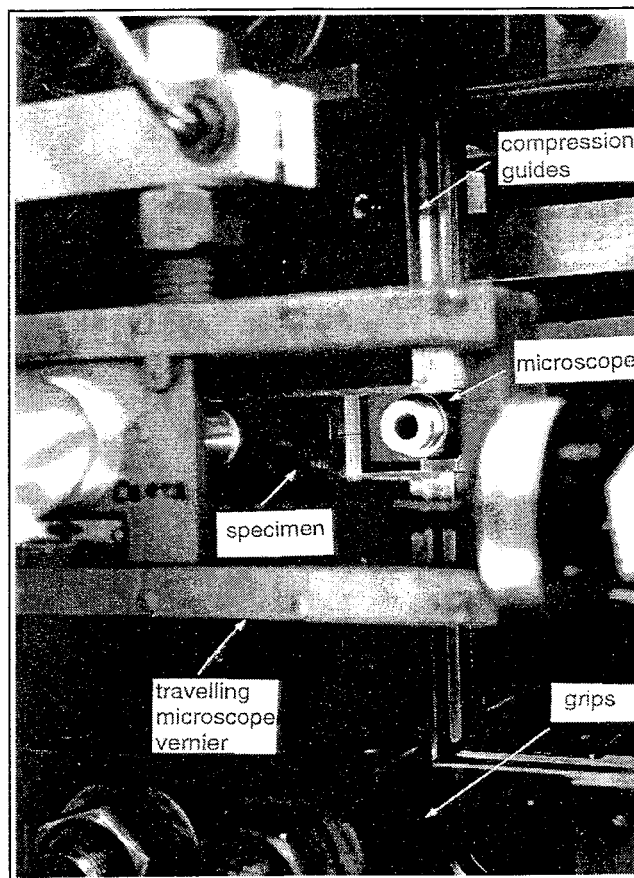


Figure 1. Coupon Test Setup at SwRI

This preliminary study indicated that load cycles producing critical region stress ranges of less than 5.1 kilopounds per square inch (ksi) do not appear to contribute to crack growth and can be removed from the spectrum as a means of accelerating the test. In addition, tensile and compressive peak load clipping did not affect coupon life significantly outside the bounds of normal specimen variability. It is important to note that these conclusions were based on limited testing and a more rigorous coupon test program was recommended for achieving more definitive conclusions. For the purposes of validating the analytical damage tolerance methodology, however, truncation was deemed an acceptable test acceleration method and

clipping was deemed tolerable, provided that identical load spectra are input into both the analysis and the test article.

2.3.2 Marker Banding Feasibility

For the DTA model validation, accurate crack length measurements during the full-scale test were crucial. Toward this end, a technique was utilized to supplement the visual inspection methods. The technique is referred to as ‘marker banding’ and has been used for many years during full-scale and laboratory aircraft testing to ensure accurate post-test measurements of both crack length and aspect ratio. Fracture surface marking in the form of thin bands can be achieved with the application of a block of constant-amplitude cycles interspersed periodically throughout variable-amplitude spectrum loading.

Prior to the setup of the full-scale test, a laboratory coupon was manufactured from representative tank car steel and potential fracture surface marking techniques were tested. A coupon of ASTM A572 Grade 50 steel (left over from the previous coupon studies) was loaded with the same spectrum used for the truncation studies, with periodic marker bands applied. To achieve marking, constant-amplitude periodic marking cycles were applied at a maximum of 90 percent of the peak spectrum load and a load ratio (minimum/maximum load) of 0.8. For this feasibility study, the number of marking cycles varied from 38,000 (the initial band) to 1,000 (the final band), so as to apply marks on the fracture surface approximately 0.004 inch wide. Figure 2 is a photograph of the coupon fracture surface at the conclusion of testing.

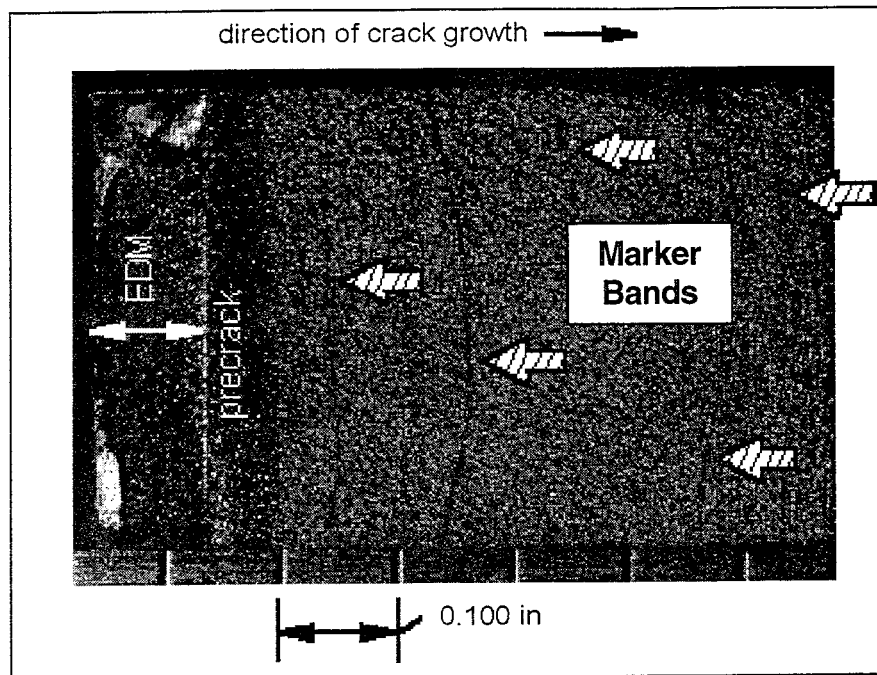


Figure 2. Marker Bands on Coupon Fracture Surface

The preliminary study into marker banding feasibility was successful. The technique was optimized (i.e., the necessary cycle count, load magnitude, and load ratio were estimated), based on the results of the coupon test, for use in the full-scale test. In addition to band-application optimization, the potential benefits and drawbacks of two different load sequence scenarios (in this case, minimum-ordered versus mean ordered) were evaluated. For this specific case, it was found that the order of the loads within a single spectrum pass had little effect on whether the marker bands were discernible on the fracture surface. Both studies were carried out to increase the likelihood of accurate crack length and depth measurements in the event that a crack tip was not clearly visible at the surface (due to geometry, rust, and weld surface complexity).

2.3.3 Preflaw and Dye Penetrant Verification

A crack induction methodology was planned to provide the necessary cracks to propagate for the DTA validation because the initial visual inspections of the orphan test car did not reveal any cracks in the regions of interest. This methodology consisted of the insertion of a notch (with a rotary grinder) near a stress concentration and the application of constant-amplitude cyclic loading to the specimen to initiate cracking from a corner of the new flaw. These processes are referred to as 'preflawing' and 'precracking,' respectively. Before the full-scale test began, this methodology was benchmarked against more reliable but less portable approaches (e.g.,

electrical discharge machining) with another coupon test. Also, the use of dye penetrant was investigated and was determined to have little effect on the readability of the fracture surface.

2.4 DAMAGE TOLERANCE ANALYSIS

2.4.1 General Approach

DTA principles have been used for many years in the aircraft industry to establish structural lifetimes and determine safe inspection intervals, and are now being adapted for the analysis of stub-sill cracks in railroad tank cars. These principles are well documented in a number of handbooks and textbooks (Gallagher et al., 1984; Broek, 1989; Barsom et al., 1987; DOT/VNTSC/FAA, 1993). A more complete description of the parallel DTA efforts that have guided the development of Task Order 108 is contained in the companion report by Cardinal et al. (1998). However, the philosophy, assumptions, and procedures for performance of a DTA have been synopsized from this report in the following paragraphs.

A number of specific technology areas comprise the damage tolerance approach to structural integrity. As a result, performance of a DTA is a multidisciplinary effort requiring inputs from a diverse but related number of fields, including: load spectra and stress analysis, fracture mechanics and fatigue crack growth analysis, laboratory and full-scale testing, nondestructive evaluation, and field experience.

Damage tolerance can be defined as the capability of a structure to resist failure and continue to operate safely with damage (e.g., fatigue cracks) in the primary structure. The goal of a DTA is to demonstrate that structural integrity will be maintained for a designated or desired amount of time using some measure of life (hours, cycles, or miles). This goal is accomplished by computing fatigue crack growth curves and critical crack lengths for different critical locations in the structure. These calculations are subsequently used, along with nondestructive inspection sensitivity levels, to determine inspection intervals.

Damage tolerance analyses are based upon the supposition of pre-existing flaws, idealized as planar fatigue cracks, in the structure. Most fatigue cracks in welded joints can be represented in this fashion. For new, unused structural elements, an initial flaw size

representative of manufacturing quality is specified. Initial flaw sizes for in-service structural elements are based on the resolution of the inspection technique. Flaws are presumed to exist at the 'worst' locations (usually regions containing stress concentrations) in the structure; these areas are typically referred to as fatigue critical locations. The two primary sources of information used to identify these critical areas are field data and the results of global and fine-mesh FEA.

Performing a crack growth calculation for a fatigue critical location requires the availability of three types of data: the load (stress) history, material and crack growth properties, and the assumed crack geometry along with its local stress field. To determine internal loads and stresses caused by remotely applied operational loads, global (coarse grid) and local (fine grid) finite element analyses are usually required. From these analyses, the stress gradient normal to the plane of anticipated crack growth is determined and used as input to a solution for the stress intensity factor (crack driving force) for a specific geometry and loading. The fatigue crack growth prediction methodology uses the stress intensity range, which is the variation of the stress intensity factor during a stress cycle. The stress intensity factor, K , is generally expressed as a function of the nominal far-field stress, σ , a geometry and loading mode dependent factor, β , and the crack length, a , as follows:

$$K = \beta\sigma(\pi a)^{1/2}$$

Geometry factor solutions (tabulated values or empirical expressions) for many structural geometries and loading conditions are available in fracture mechanics literature. They have also been incorporated into crack growth analysis software such as NASGRO (Forman et al., 1994), originally developed by the National Aeronautics and Space Administration for the ongoing Space Shuttle Program.

For computation of crack growth, a number of equations are available relating stress intensity range, ΔK , to crack growth rate, da/dN . The appropriate growth law used in an analysis is chosen based on the amount and rates of growth anticipated, the extent of available empirical

data and how well the chosen model represents the empirical crack growth data. For structural steels, the Paris equation is often deemed to be suitable (Hudak et al., 1985):

$$da/dN = C\Delta K^m$$

The Paris coefficient, C, and the exponent, m, can be based on both material properties and the degree of conservatism required by the application. Several crack growth expressions have been incorporated into software to predict crack growth under specified stress histories (or variable-amplitude stress spectra).

Crack growth analysis predicts growth, but does not specify when a crack will become critical. The computation of critical crack length, a_{cr} , is accomplished with a substitution of the material's fracture toughness (resistance to unstable fracture), K_c , into the stress intensity factor equation and solving for the critical crack length. Thus, with the crack growth curve and the critical crack size defined for a particular fatigue critical location, safety limits can be obtained. The initial safety limit is defined as the time required for a crack to propagate from a manufacturing flaw size to a critical crack size. The field safety limit is defined as the time required for a crack to grow from a detectable flaw size to a critical crack size.

Damage tolerance results (crack growth curves) must be transformed into specified inspection intervals that can be incorporated into a maintenance program. The basic concept here is to provide a safety factor of two (or more) on life for the structural integrity of the component. This is accomplished by considering two categories of inspections: the initial inspection and subsequent in-service inspections. Assuming a safety factor of two, the initial inspection interval would be half of the initial safety limit. Likewise, recurring inspection intervals (in service) would be half of the field safety limit, specified by non-destructive evaluation techniques and reliabilities along with the corresponding detectable flaw sizes.

2.4.2 Industry Progress

For the specific application of DTA to tank car stub sills, the SSWG has assembled the *Stub-Sill Inspection Database* (AAR/RPI, 1996), hereafter referred to as the SS-II database. This database, based on the tank car fleet currently in service, has documented the locations of frequently occurring cracks. Statistical analyses of this database were performed by SwRI to

prioritize the severity of various fatigue critical locations in different car designs. In addition to providing input for this database, each of the RPI members of the SSWG have proceeded with a preliminary DTA on at least one car design with guidance from SwRI. The full-scale test results have been used by Cardinal et al. (1998) to adjust some of the input parameters (both to the FEA and NASGRO portions of the process) that will be recommended for future DTA efforts.

2.5 THE SIMULoader

2.5.1 General Description

The Simuloader is a computer-controlled servohydraulic test bed built for the full-scale multiaxial fatigue and vibration testing of railcars. Through the input of both longitudinal and vertical forces into the center sill of a test vehicle (through solid load transfer blocks), as well as both vertical and lateral displacements into a truck bolster interface underneath the vehicle, this machine can excite a test car with profiles and waveforms that represent an actual railroad environment. Simulations are typically done in an accelerated fashion with the utilization of only those events that produce significant stresses on the structure, combined with an overall compression of events in time.

Originally donated to the FRA in 1983 by Union Tank Car Company, the Simuloader was later installed at TTC in Pueblo, Colorado, and is now operated by TTCl. Manufactured by MTS Systems Corporation, this test system includes 13 hydraulic actuators of various capacities and their associated analog controllers. An IBM computer is used, in conjunction with a panel of Measurements Group signal conditioning amplifiers and a VXI-based chassis of digital/analog and analog/digital converters, to send drive signals to the controllers and collect actuator and test vehicle response data from up to 64 transducers. A schematic drawing of a tank car mounted on the Simuloader is pictured in Figure 3.

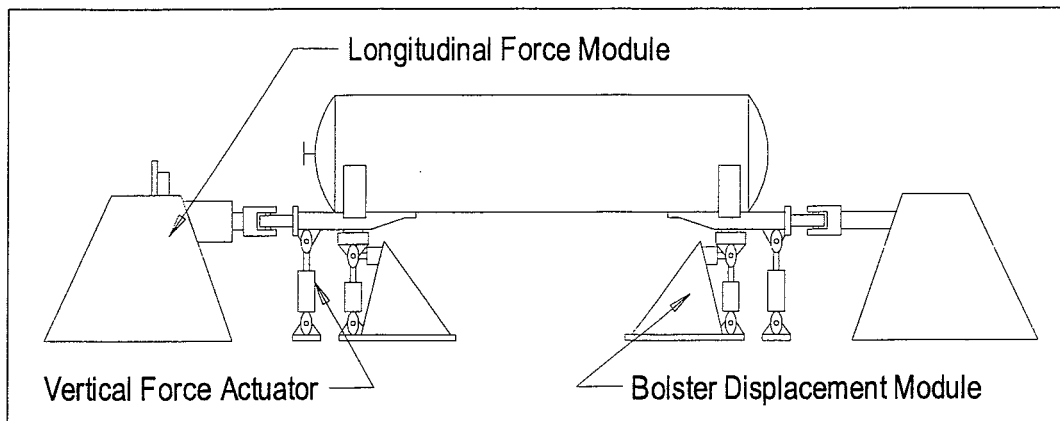


Figure 3. Schematic of Tank Car on Simuloader

2.5.2 Evolution and Function

Historically, freight car bodies and components were over-designed to minimize in-service fatigue failures. High safety factors were used to keep stress levels in critical locations at a minimum. Increased fuel costs combined with competition from the trucking industry in recent decades, however, has made these heavy designs uneconomical. The resulting design optimization effort created the need for accelerated fatigue testing of prototypes.

Controlled laboratory environments have been available for the fatigue testing of relatively small components, such as truck bolsters and brake beams. The Simuloader was built to meet the need for a facility where a multiaxial fatigue test of an entire car body could be performed. This machine has been used by various car builders to verify analyses, reveal design deficiencies, test design modifications, and provide safety from fatigue failures not accounted for in standard specification testing. In a typical test, the effects of 30 years of fatigue damage can be simulated within a few months.

2.5.3 Input Drive Files

Drive files are computer data files that contain waveforms (time histories) used to animate the Simuloader and simulate the environment to which a particular freight car will be subjected over the course of its life. To date, simulation inputs have been created from various combinations of two sources of data: actual time history data and rainflow cycle counted data.

To obtain time history data, a manned instrumentation car is sent with an instrumented test car over an applicable route. Due to the expense involved, a test of this nature is usually only about 2,000 miles long. Data from vertical and lateral accelerometers on the truck bolsters, strain gage bridges on the couplers, and a variety of car body response transducers is recorded continuously over the route. After the uneventful miles are edited out (the process of truncation), the remaining bolster accelerometer time history data is double integrated into displacement signals to drive the Simuloader bolster modules and the remaining coupler strain data is scaled into force signals to drive the solid load blocks. The primary advantage to this type of testing is that the sequence and phase relationships between the various inputs to the car body are preserved. This methodology was demonstrated by Sharma (1990).

Rainflow cycle counted data (Society of Automotive Engineers, 1988), though typically only used for analytical fatigue studies, can be used to create sinusoidal time histories to drive the center sills of a car on the Simuloader. In this case, an unmanned data collection system is attached to an instrumented test car and sent over several applicable routes. Because rainflow data takes comparatively less computer memory storage space (thus, the cost of acquiring it greatly reduced), these tests are often on the order of 15,000 miles long. Force calibrated strain gage bridges are used to collect truck bolster and coupler loads. Additional car body response transducers are used in known critical regions. Though sequence and phase information is lost in this latter scenario, a better statistical sample of the car body inputs can be obtained. It is believed that train handling is more representative of normal conditions when the crew is unaware of a test car in the train, as is usually the case with unmanned tests. The AAR has tested several car body designs extensively in this manner (Sharma et al., 1984) and compiled a database of the results in the AAR-MSRP. The data used for the Full-Scale Damage Tolerance Test was rainflow cycle counted.

2.6 TEST CAR DESCRIPTION

The tank car that was used for the full-scale damage tolerance analysis validation test was an orphan (the designer/builder is no longer in business) of stub-sill design with about 300,000 miles of accumulated usage. The tank car had been in storage for approximately 8 years before being pulled for this program. Donated to the program by GE Capital Railcar Services (GE), it

had neither head braces nor pads and had no previous record of parent metal crack repairs. A listing of test car and material characteristics of interest is contained in Tables 1 and 2.

Table 1. Orphan Tank (Test Car) Characteristics

CATEGORY	DATA
Date of Manufacture	October 1967
Classification	DOT 111, Exterior Coiled and Insulated
Car Number	NATX 22746
Length Over Strikers	51 feet X 11 3/8 inches
Length Over End Sills	51 feet X 7 7/8 inches
Length Over Tank Heads	49 feet X 3 5/8 inches
Length Over Tank Seams	44 feet X 2 5/8 inches
Length Over Truck Centers	39 feet X 11 3/8 inches
HeightXRail to Jacket Top	12 feet X 1 7/8 inches
HeightXExtreme (to Platform Handrail)	14 feet X 11 7/8 inches
Outer Tank Diameter	104 inches
Total Capacity	20,670 gallons
Light Weight	75,000 pounds
Gross Rail Load (Full)	263,000 pounds
Truck Characteristics	100-ton, D3 springs and Roller Side Bearings

Table 2. Orphan Tank (Test Car) Materials

CATEGORY	DATA
Sill Web Material	AAR M116-Grade A Steel (Analogous to ASTM A7)
Sill Web Thickness	5/8 inch Specified, 19/32 inch Measured
Sill Top Flange Material	ASTM A285 (Reportedly)
Sill Top Flange Thickness	5/8 inch Specified and Measured
Tank Head Material	ASTM A515-Grade 70 (Reportedly)
Tank Head Thickness	1/2 inch Specified and Measured

3.0 OBJECTIVE

The objective of the Full-Scale Damage Tolerance Test was to experimentally validate the analytical damage tolerance methodologies under the consideration of the SSWG. In this test, a stub-sill tank car was subjected to both the longitudinal and vertical coupler forces normally experienced in revenue service, thereby propagating cracks throughout the structure. The stress distribution and crack growth results obtained have been compared to a finite element stress analysis of the car and the associated fatigue crack growth predictions obtained from the combination of computer models.

4.0 KEY PERSONNEL

The principal contacts for this program were as follows:

- Jose Pena, FRA - Task Order Monitor
- Dan Stone, TTCI - Damage Tolerance Program Manager
- Joe Cardinal, SwRI - Damage Tolerance Project Engineer
- Keith Smith, TTCI - Simuloader Test Project Engineer
- Pete McKeighan, SwRI - Coupon Test Experimentalist
- Mike Williams, ARI - Orphan Test Vehicle Analyst

5.0 INITIAL CONDITIONS

This section of the report includes detailed descriptions of the various stages of setup for the full-scale test. Section 5.1 contains information regarding the initial inspection of the test car, as well as some minor modifications that were made to prepare it for the test. In Section 5.2, the characterization of the test system (the machine, with the test car mounted on it) is discussed. Following that, the preliminary DTA analysis of the test car, which helped guide subsequent decisions concerning strain measurement locations (documented in Section 5.4) and overall test expectations, is discussed in Section 5.3. The preflawing of the tank car is described in Section 5.5 and the spectral inputs to the car are explained in Section 5.6.

5.1 PHYSICAL SETUP

5.1.1 Jacket Removal

Shortly after the test car arrived on site in August of 1996, large portions of the non-structural insulation jacket were removed by TTCI in the areas surrounding the stub sills. This was done to expose the stub-sill welds and facilitate their visual inspection. A photograph of the test car, upon its arrival on site, is shown in Figure 4.

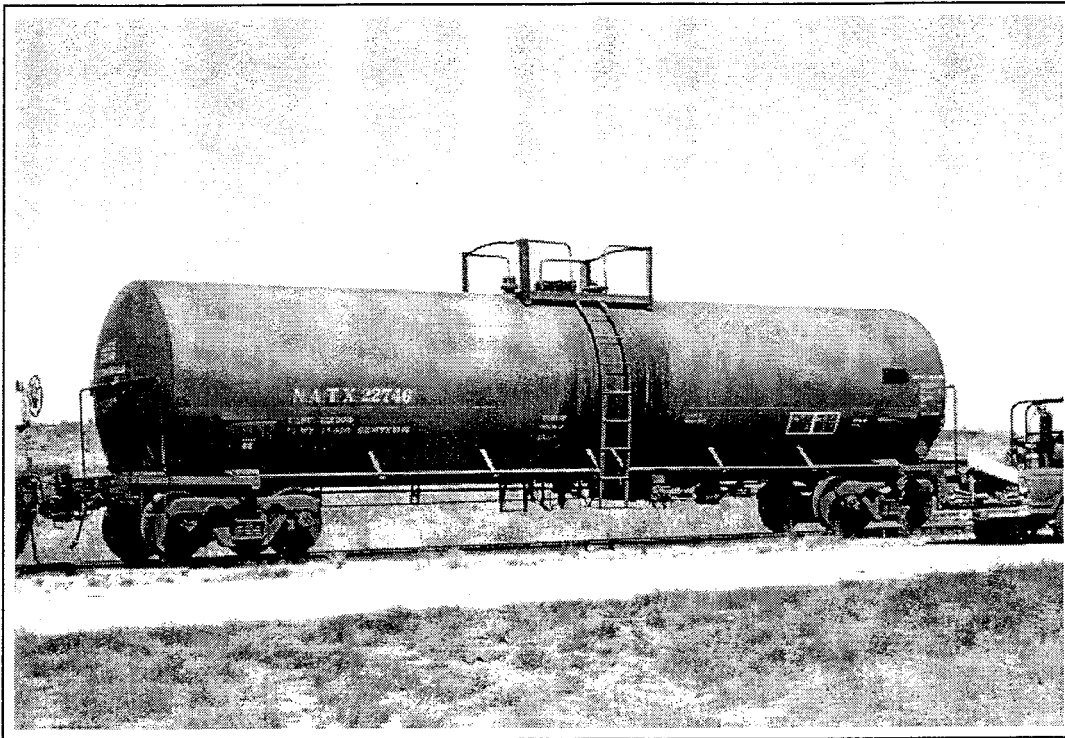


Figure 4. Test Car NATX 22746 Upon Arrival at TTC

After portions of the jacket were removed from the car, the stub sill and bolster web welds were lightly sand blasted for the removal of rust and scale buildup. This was done, despite the risk of effectively shot peening the surface, because the corrosion near the welds of interest was as much as 1/8-inch thick in some areas, rendering visual inspection ineffective.

5.1.2 Initial Inspection

Personnel from TTCI, American Railcar Industries (ARI), and GE performed initial visual and fluorescent dye penetrant inspections. In general, these inspections revealed the following attributes:

- Poor fit-ups (gaps) between many welded parts
- Much undercutting and porosity in all welds
- Many lug and center-filler weld cracks in both draft pockets
- Several bolster web weld cracks at both ends
- Evidence of torch cutting without grinding on bolster webs

On a macroscopic scale, it was observed that the B-end welds appeared to possess a higher quality of workmanship than those of the A-end. In addition, it was apparent that the center plate, draft gear, and yoke at the B-end had been replaced at some point while the A-end retained all of the original components. Also, the original trucks were still with the car. The car was in better condition than was expected, given its age. Some contributing factors for this may have been:

- 51-pound/foot stub sills (relatively heavy)
- 3/16-inch thick exterior coils with oversize welds
- Considerable amount of time spent in storage
- Light weight is approximately 5-7 kips heavier than cars today

This initial inspection did not, however, reveal any cracks in the critical regions highlighted by the SS-II database. For this reason, and because cracks in the draft pocket would not be accessible once the car was on the Simuloader, the car was deemed free of critical region cracks and preparations for precracking the test car began (refer to Section 5.3). As a precaution, many of the weld cracks inside the draft pockets were repaired to avoid premature test abortion due to draft lug failure. A schematic of three of the SS-II critical regions of interest is contained in Figure 5.

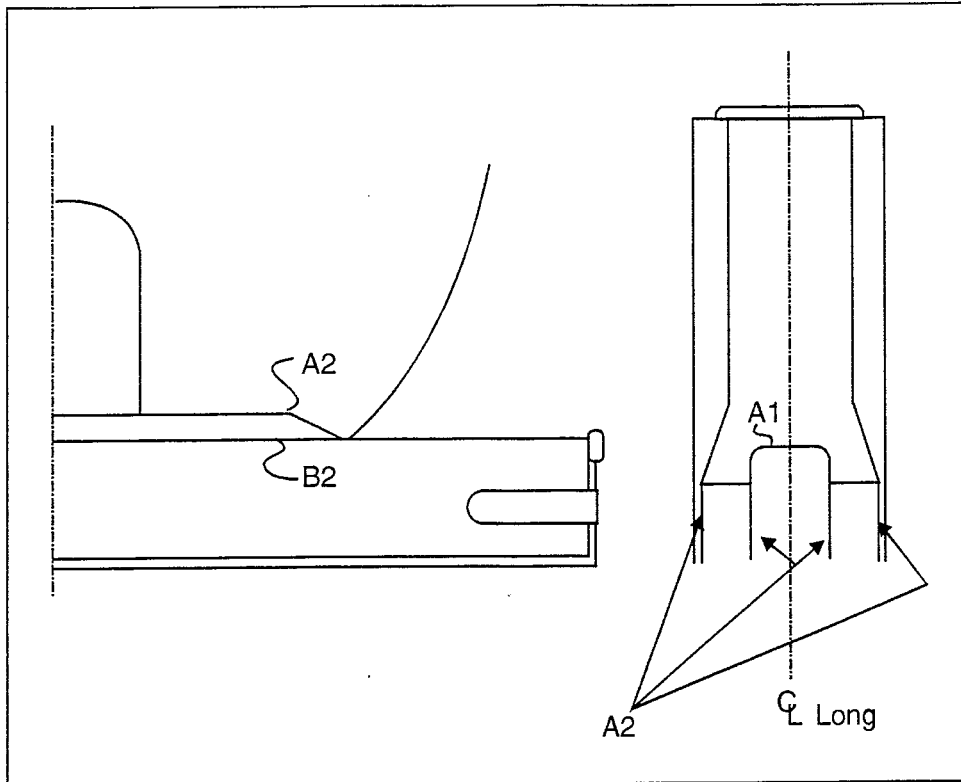


Figure 5. SS-II Critical Regions (SS-II Codes Indicated)

5.1.3 Test Car Mounting on the Simuloader

An instrumented load block system (solid draft gear) was installed into the sills of the test car to be used as a measurement and control transducer for the longitudinal coupler loads. The B-end of the car interfaced with the LCF actuator at the east end of the machine, and the A-end interfaced with the reaction mass at the west end, through spherical bearing arrangements which allowed the car lateral and vertical degrees of freedom. Figures 6 and 7 are pictures of the test vehicle mounted on the machine and the solid block LCF arrangement at the B-end of the car.

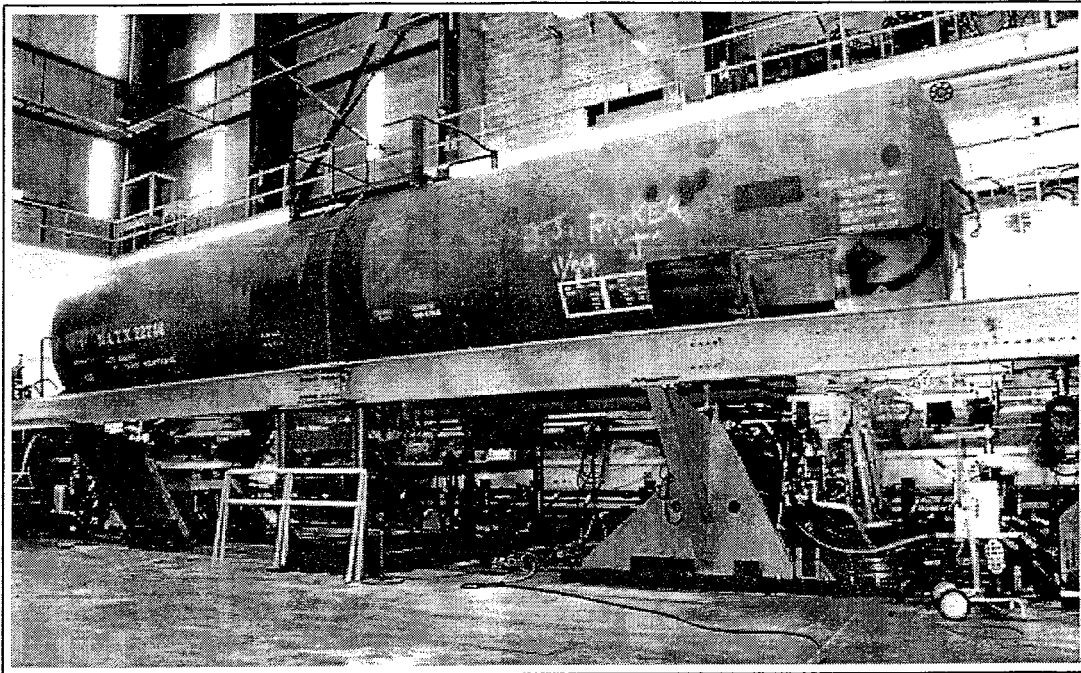


Figure 6. Test Car NATX 22746 on Simuloader

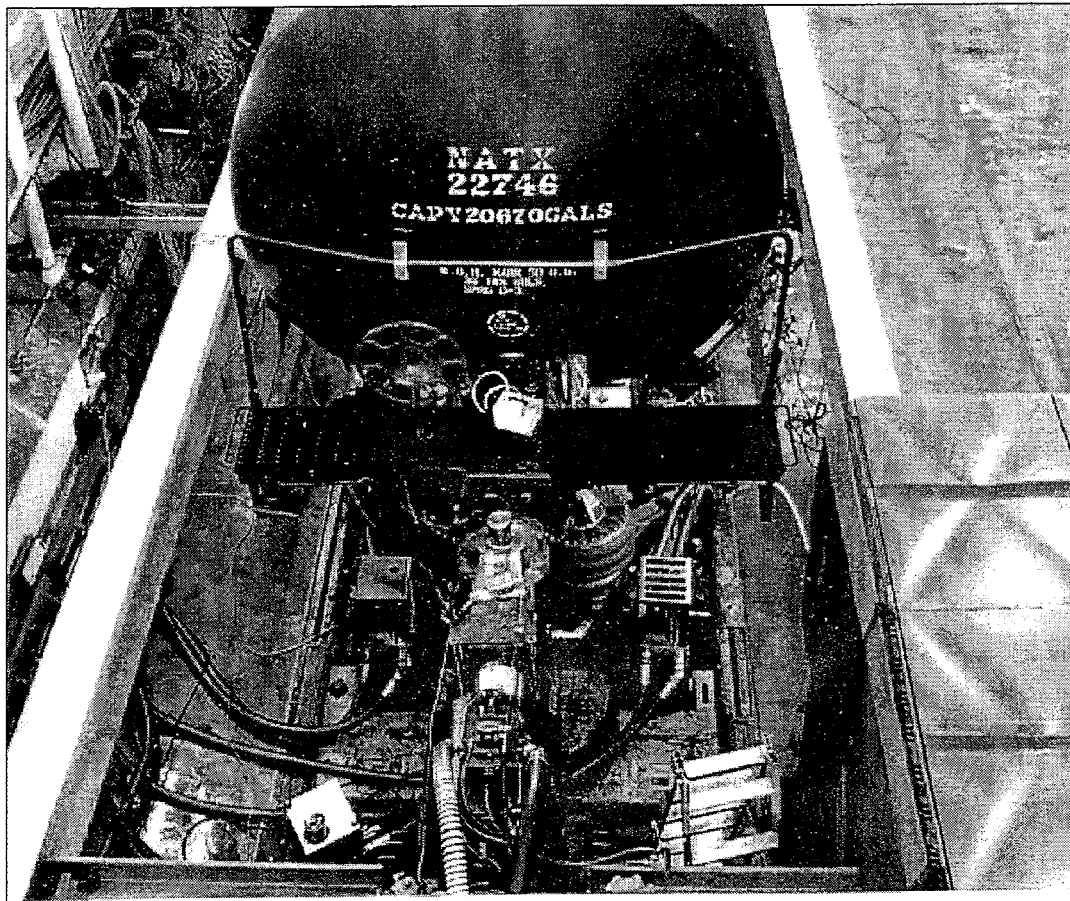


Figure 7. B-end of Test Car, LCF Connection

Each VCF actuator (in series with a standard load cell) was attached to a 2-inch thick ASTM A36 steel plate welded beneath the center sill at each end of the car, slightly inboard of the respective coupler carriers. As demonstrated in the schematic of Figure 8, this put the centerline of the applied vertical coupler load 10 inches inboard of the outer face of the striker plate (about 8 inches outboard of the front draft lug face). This effectively placed it halfway between the tank head seal weld and the coupler pulling face for the fully extended draft position. Figure 9 is a photograph of the B-end VCF actuator. This was done to reduce cost (to apply VCF at the coupler pulling face would have required much additional fixturing).

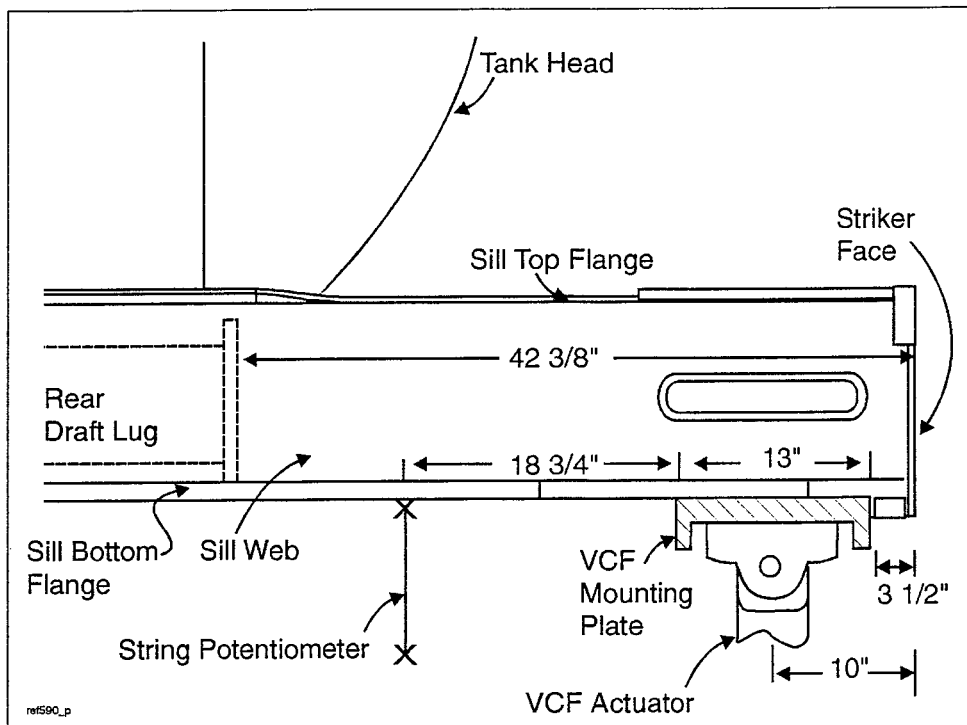


Figure 8. Schematic of VCF Attachment to Stub Sill

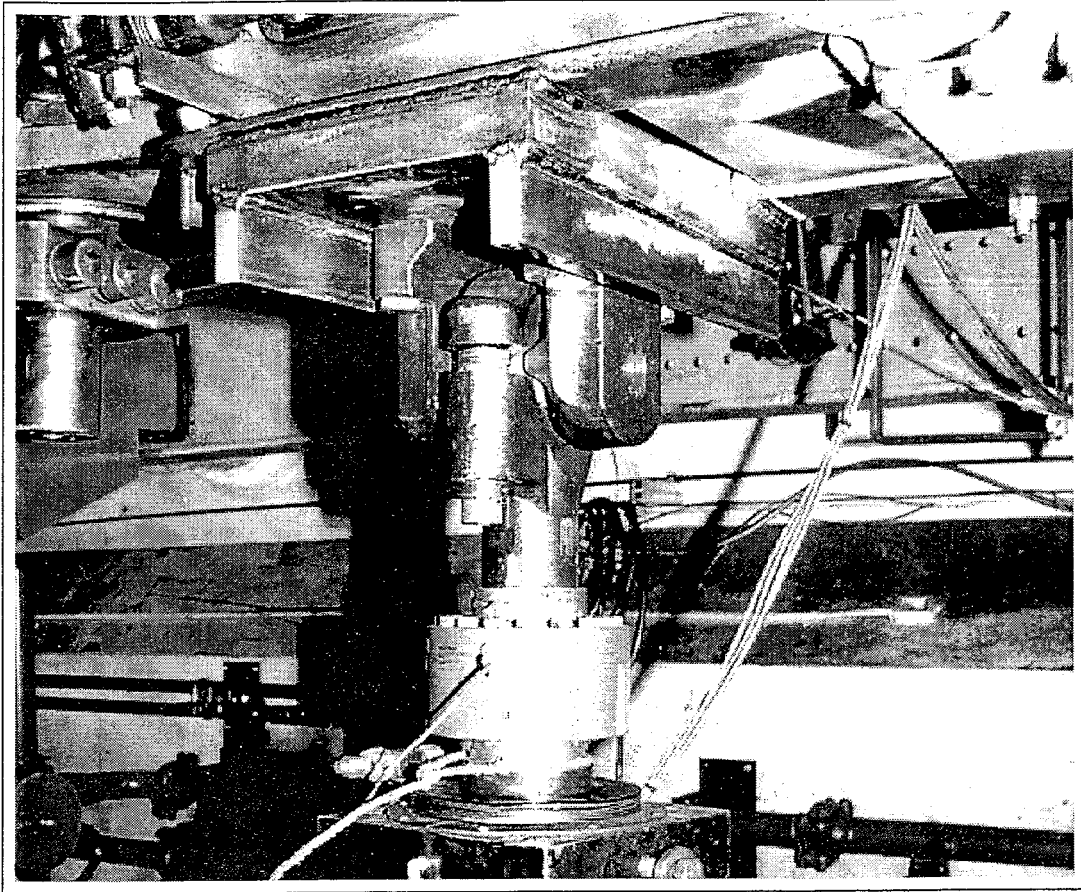


Figure 9. B-end of Test Car, VCF Connection

This placement reduced the applied VCF moment to the seal weld by as much as a factor of two from the extreme possibility (full coupler extension during an OTR VCF event); the applied VCF shear in the simulation was the same as during the OTR test. Though this placement proportionally reduced stress magnitudes throughout the vehicle, it did not affect their stress concentration locations resulting from applied VCF. It should be noted that this VCF actuator placement was reflected in the preliminary FEA of the test car. The primary motivation for this placement of the VCF actuator had to do with space constraints, as the actuators were too long to fit underneath the LCF spherical bearing arrangement with moment arm extension fixtures. This loss of moment arm from the OTR situation was determined to be acceptable for the validation test for reasons discussed in Section 5.6.1.

Another irregularity in this Simuloader VCF setup involved actuator capacities. The VCF actuators used with this machine have a maximum force capacity of 55 kips under normal conditions. In anticipation of the possible need to amplify loads during the test (in the absence of

crack growth), a spare 110-kip actuator was used at the B-end of the car. Because there was only one of these available, the A-end of the car was fixtured with the standard 55-kip jack. The decision to use the larger actuator at the B-end was based on the initial observations of B- versus A-end weld quality. Because the B-end appeared to possess better workmanship, load amplification to drive crack growth was anticipated to be more likely at that end. In Table 3, a few of the basic characteristics are listed.

Table 3. Basic Simuloader Actuator Characteristics

ACTUATOR	STROKE CAPACITY	LOAD CAPACITY	FLOW CAPACITY
LCF (at B-end of Car)	12 inches, Static and Dynamic	500 kips Tension, 750 kips Compression	400 gallons/minute, 3-Stage Servo valve
B-end VCF	6 inches, Static and Dynamic	110 kips, Double Ended	180 gallons/minute, 3-Stage Servo valve
A-end VCF	10.4 inches Static, 10 inches Dynamic	55 kips, Double Ended	90 gallons/minute, 3-Stage Servo valve

It is important to note that the Simuloader bolster modules (vertical, lateral and yaw bolster actuators) were not used for dynamic load application during the test; rather, they were only used to raise and align the test car for the application of both LCF and VCF. This, along with VCF jack capacities, is also discussed further in Section 5.6.1.

5.1.4 Water Lading

After the mounting procedures were complete, the car was filled to capacity with water. The underlying assumption was that lading had little or no effect on crack growth in the areas of interest (the stub sills) and that loading the tank with water served merely to increase the reaction mass. In other words, the use of a loaded tank for both the loaded and unloaded applied force regimes was determined to be acceptable for test simplification.

5.2 SYSTEM CHARACTERIZATION

The Simuloader actuators were controlled with proportional derivative feedback loops based on force and displacement signals. The outer loop of this test system, however, was open. That is, there is no automated feedback mechanism for the real-time adjustment of drive signals based on the machine's response to system cross talk. For multiaxial test beds, remote parameter control systems are typically used to meet this need. To date, it has been TTCI's experience that these

do not converge at the lower frequencies at which railcars are typically tested. Due to this outer loop, some transient responses were expected and observed during testing. As with a few other simplifications, this did not adversely affect the goals of this program for the reasons discussed in Section 5.6.1.

After all of the actuators were calibrated and tuned and the test car was mounted on the machine, constant-force frequency sweeps of the system were performed to determine optimum actuator response (and any system resonant frequencies). Through calculated response/command transfer functions, it was determined that longitudinal and vertical coupler force response deteriorates at frequencies above 2 and 5 hertz, respectively. One explanation for the relatively poor response of the longitudinal actuator (in addition to the sheer volume of hydraulic oil it requires) may be the inertial nature of the mass being pushed against (the mechanical “slop” in the system). There were small longitudinal gaps between contact points throughout the Simuloader/test car system, creating a series of tiny impacts and nonlinearities every time the actuator changed direction and crossed through the null position. These nonlinearities, when combined with any excited system resonances, could increase longitudinal force control difficulty at higher frequencies. The empirical system transfer function for the west vertical coupler actuator (acting independently) is plotted in Figure 10.

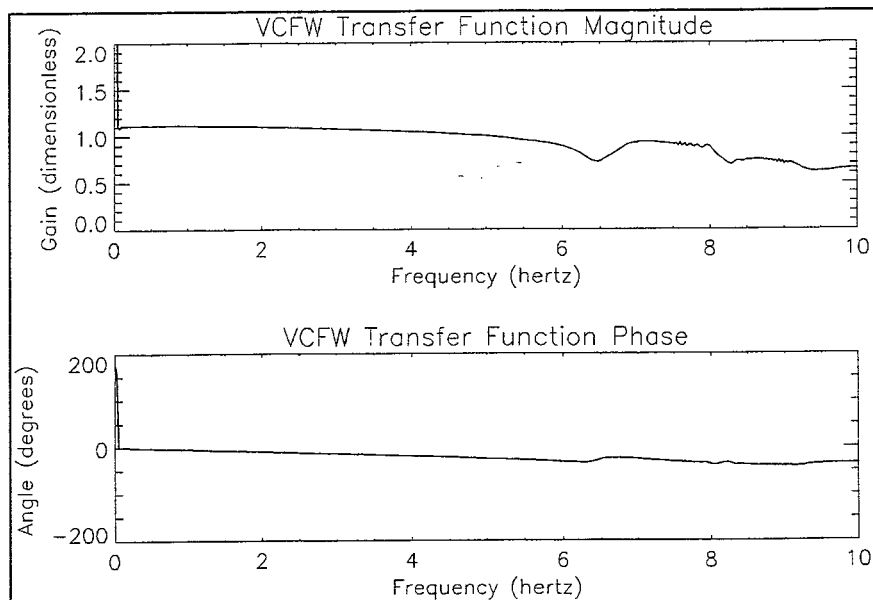


Figure 10. VCF System Transfer Function

5.3 PRELIMINARY ANALYSIS

5.3.1 DTA Predictions

Before the orphan test car was mounted on the Simuloader and instrumented, a preliminary DTA was performed with the loads that would be applied in the test (same LCF and VCF loads, and application points). The FEA of the test car was completed by ARI and SwRI made some preliminary crack growth predictions. The details concerning these predictions include proprietary information and will not be discussed here. They are, however, discussed to a limited extent by Cardinal et al. (1998) and further by Williams (1997). Through these analyses, fatigue critical locations were identified. Stress-to-input force ratios were defined for these locations and some estimates of crack life to fracture were calculated (based on these stress-to-force ratios and the tank car load spectrum). This information was critical to the test setup. With the aid of these analytical models and the inspection database mentioned earlier, the preflaw locations and strain gage layout for the full-scale test were determined. A rough estimate of test duration was also established at 300,000 equivalent simulated railroad spectrum miles.

5.3.2 Critical Region Selection

Because there were no cracks of consequence evident from the initial inspections of the orphan car, it was necessary to preflaw the car for the fatigue crack growth test. The critical regions chosen as the primary focus for this preflawing and subsequent instrumentation were selected based upon the following four criteria:

- Location identified in SS-II database
- Location identified as a FEA hot spot
- Location accessible while car is on Simuloader
- Preflaws spaced to minimize interaction effects

In general, the FEA of the orphan tank car predicted hot spots (areas with high stress concentrations) at the same locations identified by the SS-II database. Critical locations in the areas of the sill top flange and tank head seal weld were chosen for testing so crack growth could be monitored while the car was mounted on the machine. To minimize any interaction of cracks (through load redistributions and resulting local stress changes), it was decided to position only

one preflaw at each corner of the test car. This preliminary DTA analysis, along with the resulting selection of preflaw locations, guided the strain gage location decisions. Figure 11 is an isometric view of the sill, with structural and weld labels for reference in subsequent portions of this report.

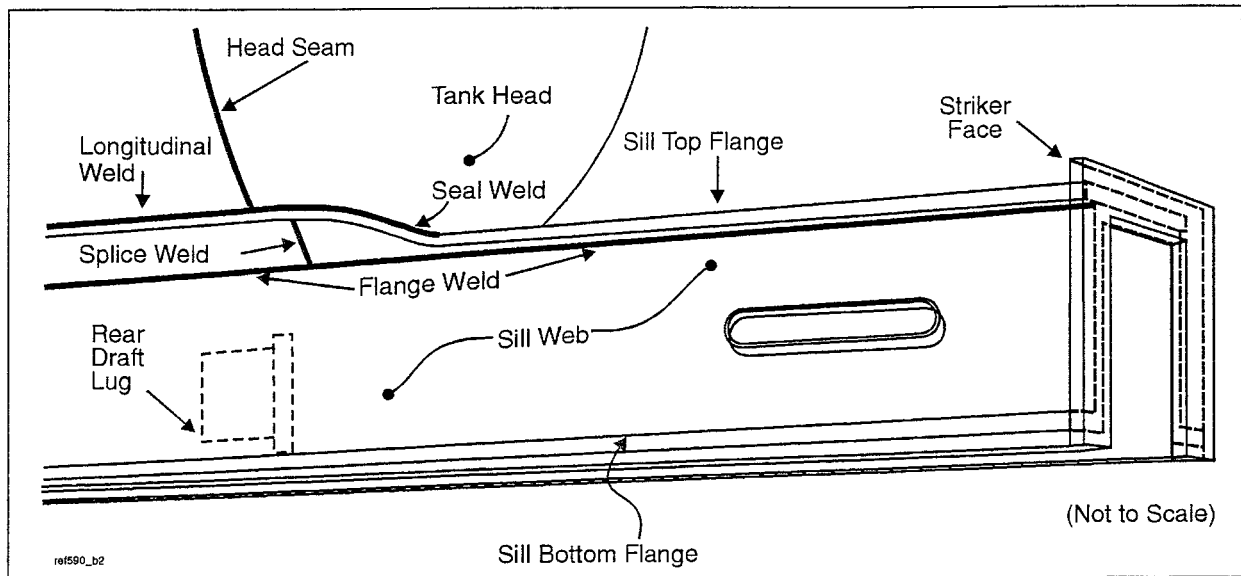


Figure 11. Basic Critical Region Structural and Weld Details

5.4 TEST CAR FLAW INDUCTION

Both variation (in weld geometries and the resulting local stress spectrums) and repeatability (in crack growth characteristics between two similar regions) were desirable for this full-scale DTA validation. In an attempt to simultaneously accomplish both with only four flaws (at the time, only four to eight resulting cracks were expected), three of the preflaws were characteristically different, while the fourth was a repeat case. Both the B-end left and the A-end right corners of the test car were preflawed in the same relative location. Table 4 lists the four preflaws and their respective characteristics. Preflaw locations are included in the instrumentation schematics of the next section.

Table 4. Induced Flaw (Preflaw) Locations

TEST CAR CORNER	WELD AREA	FLAW TYPE	FLAW ACRONYM
B-end Left	Flange Weld Bottom Toe (in Sill Web)	Surface	SW@FW-B
B-end Right	Sill Top Flange, Near Seal Weld Corner	Corner	STF@SW
A-end Left	Seal Weld Top Toe (in Tank Head)	Surface	TH@SW
A-end Right	Flange Weld Bottom Toe (in Sill Web)	Surface	SW@FW-A

The region underneath and surrounding each flaw was polished to a mirror finish before the tank car was preflawed to aid in the subsequent crack growth measurements. The three surface flaws (0.625 inch long) and one corner flaw (0.125 inch long) were created with a rotary grinder and a jeweler's saw, respectively. The nominal depth and width measurements for all four flaws were 0.125 inch and 0.010 inch, respectively. These dimensions were based on target aspect ratios for the flaws, as well as the limitations of the preflawing technique used. The goal here was to insert a stress riser in each of the four critical regions that were to be tested, which would in turn be cycled in the hope of initiating at least one crack. At a microscopic level, the saw and the grinder leave rectangular notches, the width of the blade, in the metal. Any resulting cracks are expected to grow from one corner of these notches. Figure 12 is a photograph of the B-end right corner of the car, complete with the corner flaw and the tank head strain rosette.

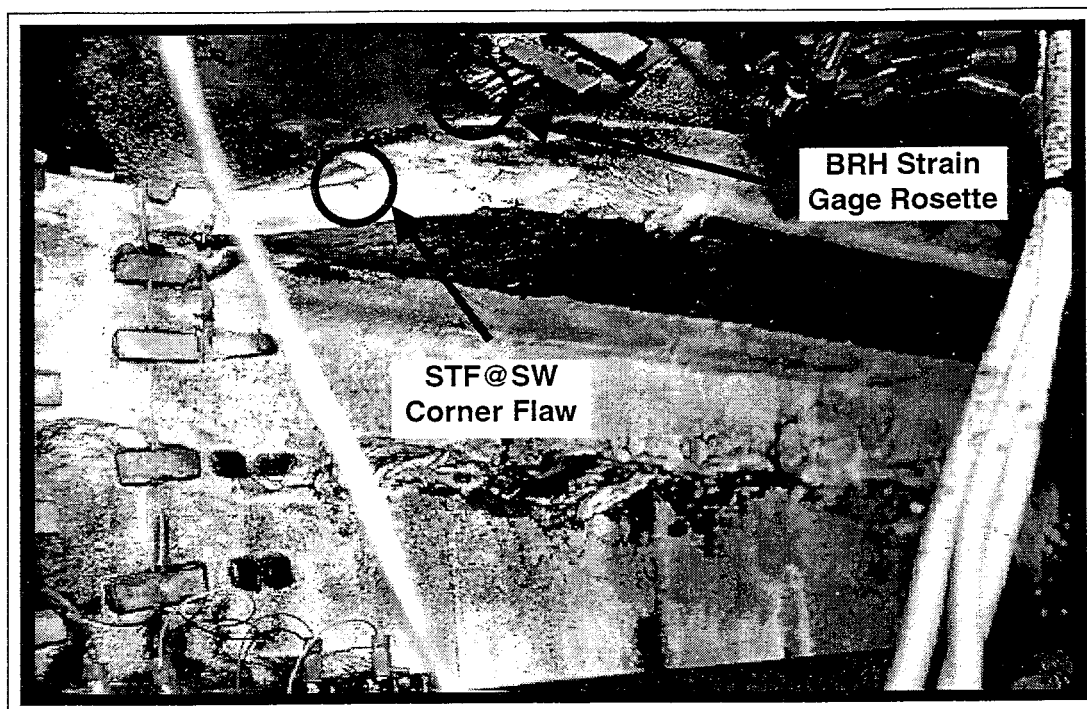


Figure 12. B-end Right Corner Flaw and Tank Head Rosette

5.5 TRANSDUCER SETUP

5.5.1 Data Collection Channel Count

An array of 36 strain gages was applied to the car as a monitor of absolute stress field and gradient values, as well as any changes in car body compliance due to crack propagation. Two string potentiometers were mounted vertically, inboard of the vertical coupler force actuators, to be used in conjunction with the actuator displacement measurements to monitor the relative vertical deflections of each stub sill. In addition to these strain and displacement measurements, the applied forces at each actuator were recorded (the feedback signals from the control transducers). All channels are listed in Table 5.

The string potentiometers were 25.25 inches inboard of the VCF actuators at both ends of the car, which put them about 35.25 inches inboard of the striker face. This arrangement was depicted in Figure 8, Section 5.1.3 of this report.

All signals were set up to be externally low-pass filtered at 15 hertz and sampled at a rate of 200 points per second with a 16-bit digitizer. Because the measurements of interest were acquired in a quasi-static manner, the filter cut-off frequencies and rates at which they were sampled is of little consequence. They are recorded here for documentation purposes.

Table 5. Data Collection Channel List

CHANNEL	NAME	UNITS	DESCRIPTION
0	LCF	kilopounds	Longitudinal Coupler Force (B-end)
1	VCFE	kilopounds	East Vertical Coupler Force (B-end)
2	VCFW	kilopounds	West Vertical Coupler Force (A-end)
3	VCDE	inches	East Vertical Actuator Displacement (B-end)
4	VCDW	inches	West Vertical Actuator Displacement (A-end)
5	BLH1	microstrain	B-end Left Head Strain #1 (Vertical Rosette Leg)
6	BLH2	microstrain	B-end Left Head Strain #2 (Diagonal Rosette Leg)
7	BLH3	microstrain	B-end Left Head Strain #3 (Longitudinal Rosette Leg)
8	BLH4	microstrain	B-end Left Head Strain #4 (Vertical Uniaxial Leg)
9	BLW1	microstrain	B-end Left Web Strain #1 (Top Inboard Leg)
10	BLW2	microstrain	B-end Left Web Strain #2 (Top Outboard Leg)
11	BLW3	microstrain	B-end Left Web Strain #3 (Bottom Inboard Leg)
12	BLW4	microstrain	B-end Left Web Strain #4 (Bottom Outboard Leg)
13	BRH1	microstrain	B-end Right Head Strain #1 (Longitudinal Rosette Leg)
14	BRH2	microstrain	B-end Right Head Strain #2 (Diagonal Rosette Leg)
15	BRH3	microstrain	B-end Right Head Strain #3 (Vertical Rosette Leg)
16	BRH4	microstrain	B-end Right Head Strain #4 (Vertical Uniaxial Leg)
17	BRF1	microstrain	B-end Right Flange Strain #1 (Inner Leg)
18	BRF2	microstrain	B-end Right Flange Strain #2 (Inboard Edge Leg)
19	BRF3	microstrain	B-end Right Flange Strain #3 (Middle Edge Leg)
20	BRF4	microstrain	B-end Right Flange Strain #4 (Outboard Edge Leg)
21	ALH1	microstrain	A-end Left Head Strain #1 (Longitudinal Rosette Leg)
22	ALH2	microstrain	A-end Left Head Strain #2 (Diagonal Rosette Leg)
23	ALH3	microstrain	A-end Left Head Strain #3 (Vertical Rosette Leg)
24	ALH4	microstrain	A-end Left Head Strain #4 (Vertical Uniaxial Leg)
25	ALW1	microstrain	A-end Left Web Strain #1 (Longitudinal Rosette Leg)
26	ALW2	microstrain	A-end Left Web Strain #2 (Diagonal Rosette Leg)
27	ALW3	microstrain	A-end Left Web Strain #3 (Vertical Rosette Leg)
28	ALW4	microstrain	A-end Left Web Strain #4 (Vertical Uniaxial Leg)
29	ARF1	microstrain	A-end Right Flange Strain #1 (Inner Leg)
30	ARF2	microstrain	A-end Right Flange Strain #2 (Inboard Edge Leg)
31	ARF3	microstrain	A-end Right Flange Strain #3 (Middle Edge Leg)
32	ARF4	microstrain	A-end Right Flange Strain #4 (Outboard Edge Leg)
33	BLBT	microstrain	B-end Left Top Flange Bending Strain
34	BLBB	microstrain	B-end Left Bottom Flange Bending Strain
35	BRBT	microstrain	B-end Right Top Flange Bending Strain
36	BRBB	microstrain	B-end Right Bottom Flange Bending Strain
37	ALBT	microstrain	A-end Left Top Flange Bending Strain
38	ALBB	microstrain	A-end Left Bottom Flange Bending Strain
39	ARBT	microstrain	A-end Right Top Flange Bending Strain
40	ARBB	microstrain	A-end Right Bottom Flange Bending Strain
41	SPE	inches	East Vertical Sill Displacement (B-end)
42	SPW	inches	West Vertical Sill Displacement (A-end)
43	LCF_D	kilopounds	Longitudinal Coupler Force Drive Signal
44	VCFE_D	kilopounds	East Vertical Coupler Force Drive Signal
45	VCFW_D	kilopounds	West Vertical Coupler Force Drive Signal

5.5.2 Car Body Response Strains

The strain gages were located along the stub sills and in the vicinity of the induced flaws. There were 24 uniaxial gages and four rectangular rosettes (all with 0.125-inch grids); each gage was individually wired in a quarter-bridge configuration. Eight of the gages were mounted along the sill of the car to measure remote sill bending and macro car body sensitivity to crack growth. The rest of the gages were used near the induced flaws for both FEA correlation and to measure local sensitivity to crack growth measurement. The monitoring of stress fields inside the tank was considered before the test began in order to get a sense of the bending gradient through the thickness of the shell. This was abandoned primarily due to the complexity (and resulting cost) of strain gage installation inside the tank and the necessary protection of their leads from the water. Table 6 is a summary of the strain gage layout.

Table 6. Validation Test Strain Gage Summary

TEST CAR CORNER	APPLIED STRAIN GAGES	MOUNTING SURFACE
B-end Left	1 Rosette, 1 Uniaxial	Tank Head
B-end Left	4 Uniaxial	Sill Web
B-end Right	1 Rosette, 1 Uniaxial	Tank Head
B-end Right	4 Uniaxial	Sill Top Flange
A-end Left	1 Rosette, 1 Uniaxial	Tank Head
A-end Left	1 Rosette, 1 Uniaxial	Sill Web
A-end Right	4 Uniaxial	Sill Top Flange
All Four (Bending)	2 Uniaxial	Sill Top and Bottom Flange

Figures 13 through 17 contain the strain gage layout information for the orphan test car. As can be seen in Table 5, the first two letters of each channel designation indicate the corner of the vehicle on which each particular gage is located. The third letter indicates whether the gage is mounted on the tank head (H), sill web (W) or sill top flange (F). Finally, the number (the last digit) is used to differentiate other nearby gages. This last number is the only portion of the channel acronym that is indicated next to each gage in the schematic of each test car corner. The channel designation system differs slightly for the bending gages in the last two letters; the third letter stands for bending (B) and the last letter indicates whether the gage is on the top (T) or bottom (B) flange. In addition to the strain gage locations in the figures, the preflaw locations are called out.

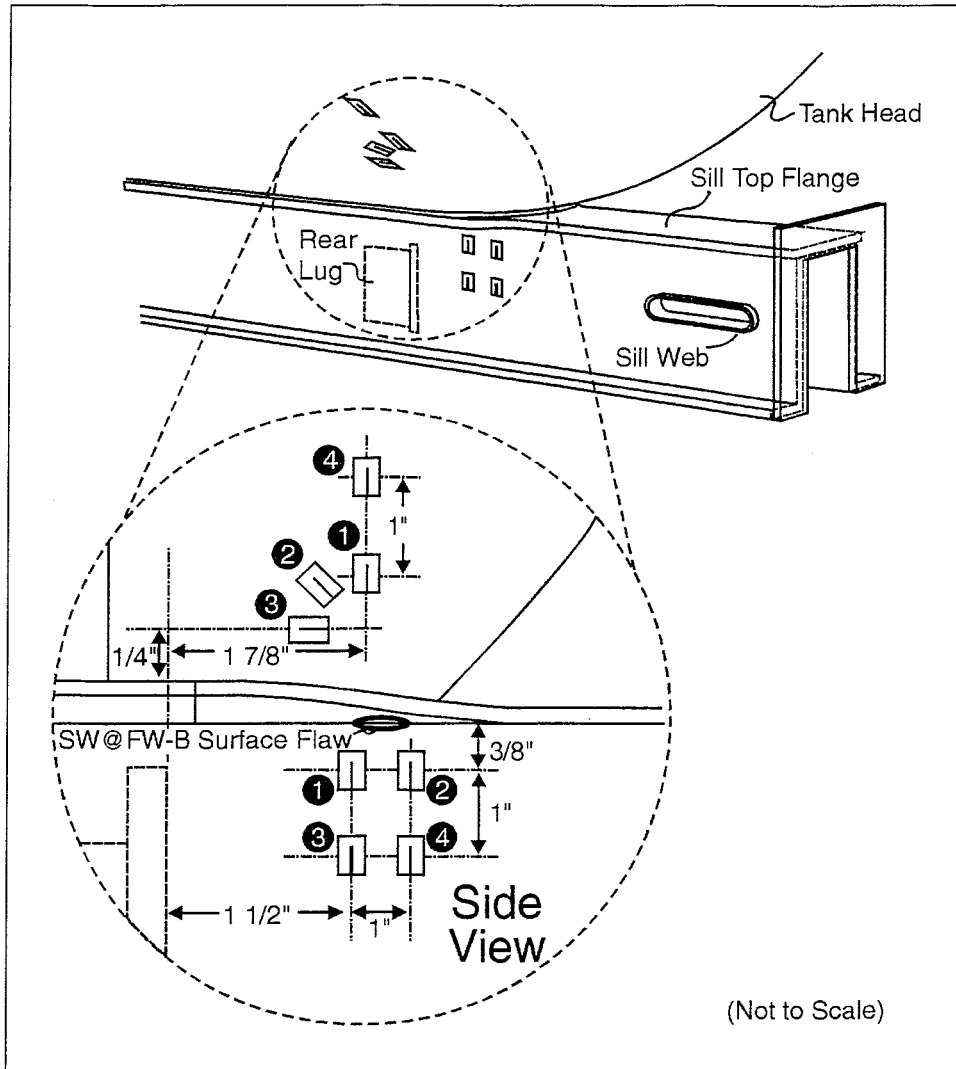


Figure 13. B-end Left Strain Gages and Preflaw

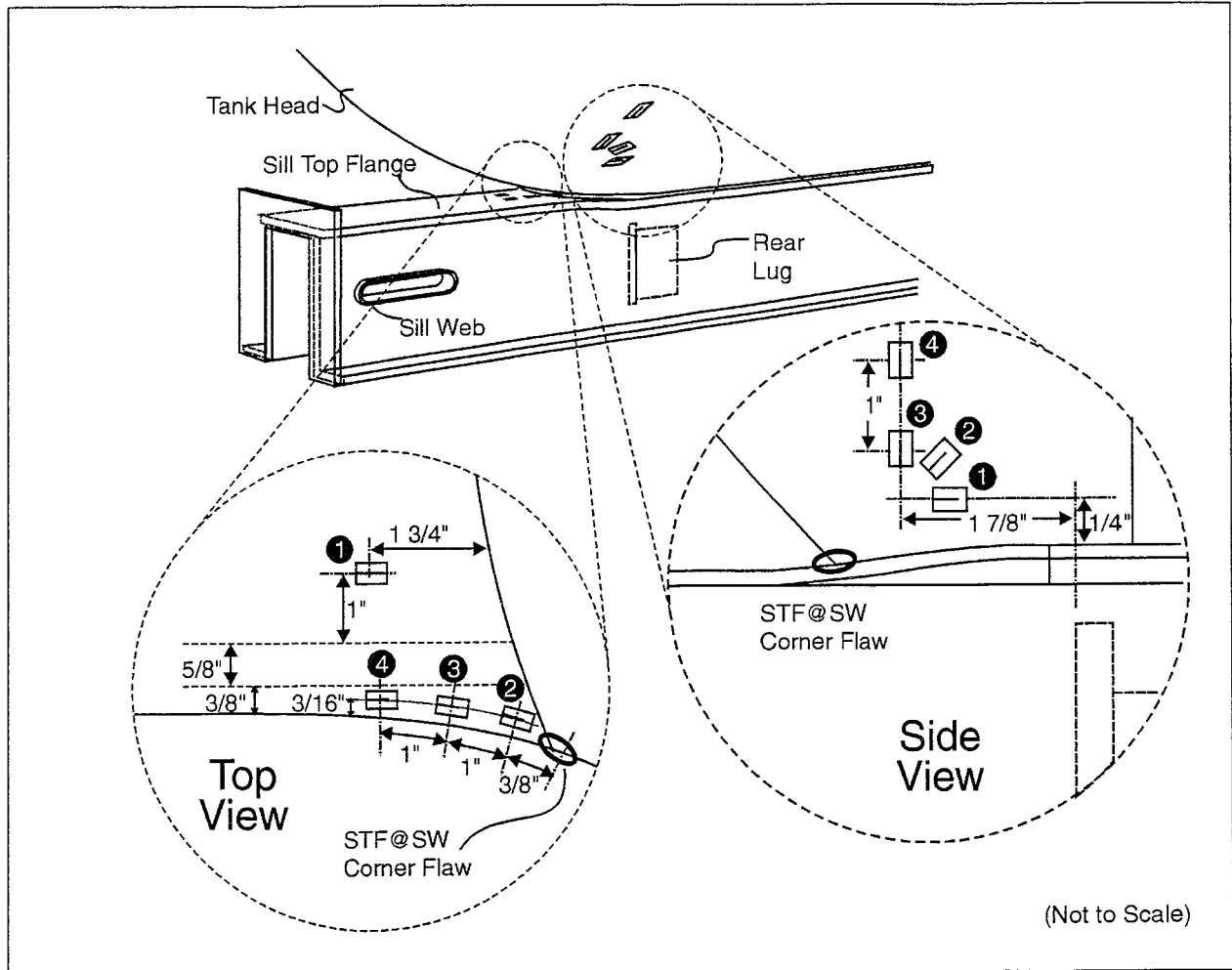


Figure 14. B-end Right Strain Gages and Preflaw

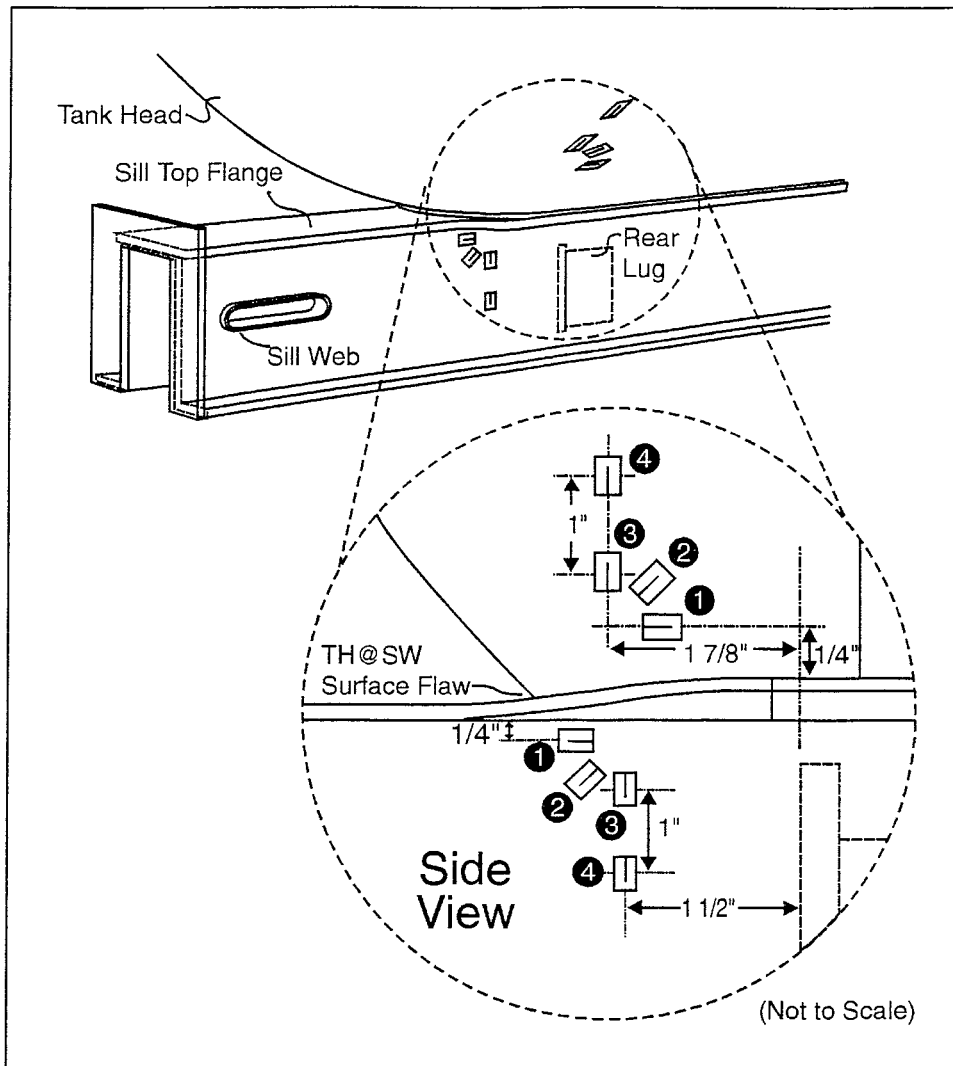


Figure 15. A-end Left Strain Gages

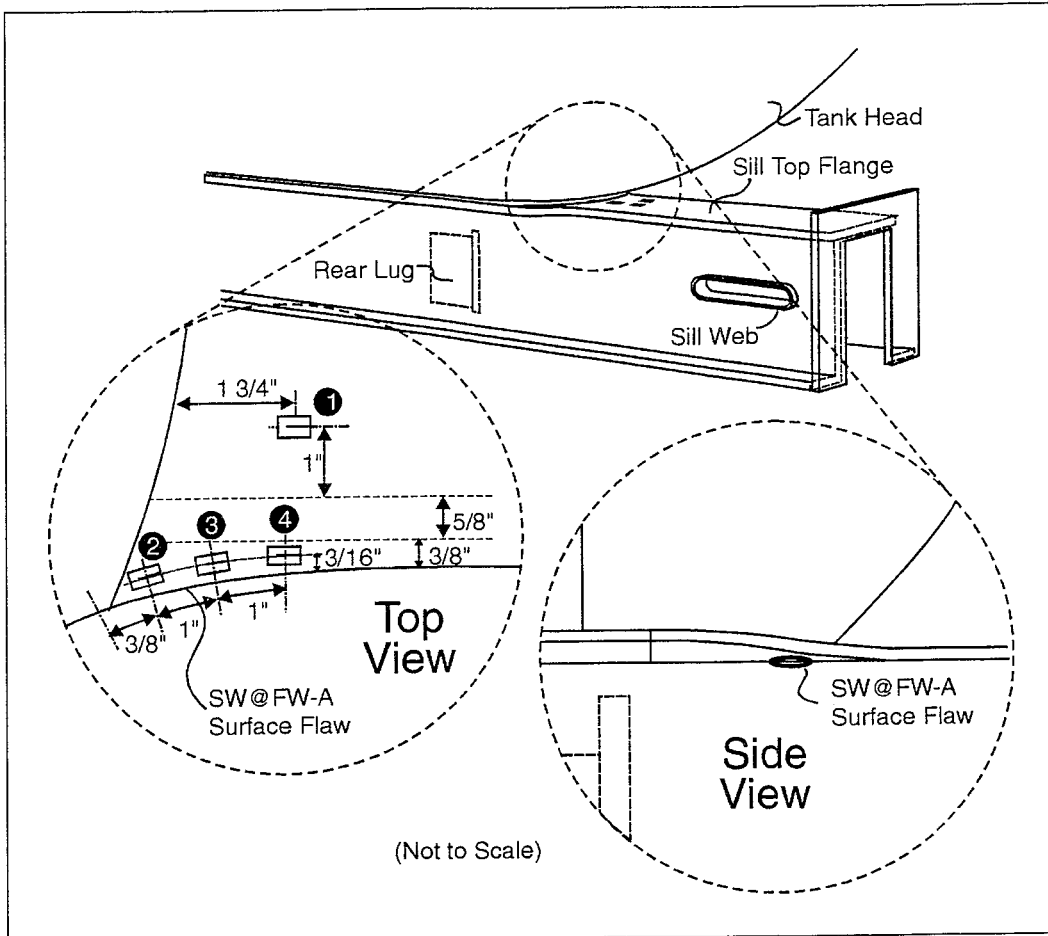


Figure 16. A-end Right Strain Gages and Preflaw

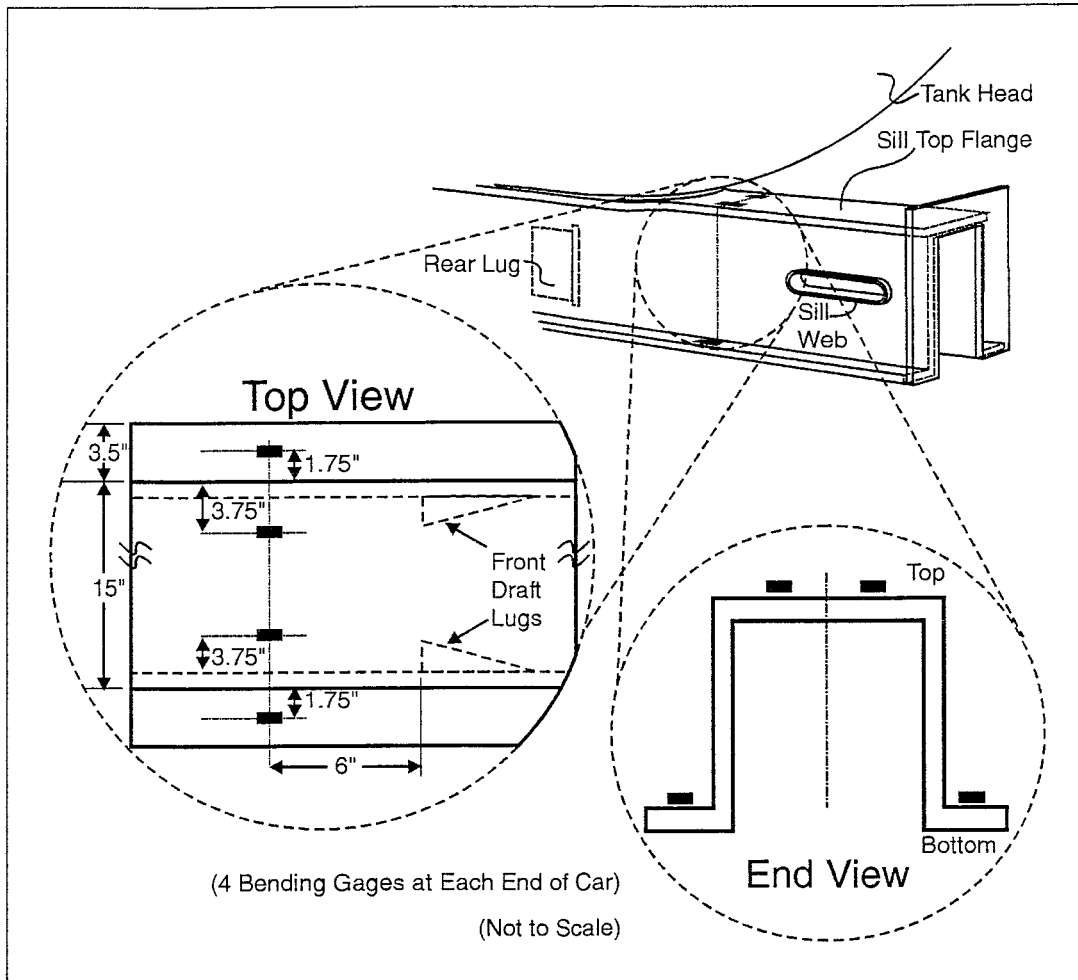


Figure 17. Sill Bending Strain Gages (at Both Ends of Car)

5.6 SIMULATION INPUTS

5.6.1 DTA Validation; Not OTR Simulation

For the purposes of this validation test, the precise loading of the vehicle with values from the OTR target spectra was not important, as the response of the actuators was collected as input for the DTA model. This represents a departure from typical simulations where OTR spectral reproduction is of utmost importance.

In the case of transient response (see Section 5.2), if the B-end VCF actuator overshoot the target load of 35 kips by 5 percent on average (to 36.75 kips), the overshoot was reflected in the input for the DTA model of this car. The same was true for clipping (see Section 6.3.2). Because the collected machine inputs to the car were used in the crack growth analyses performed for the validation, transient responses and clipping were initially determined to be acceptable for this test and warranted no further attempts at correction.

As mentioned in Section 5.1.3, the VCF actuator was mounted underneath the sill, effectively cutting the applied moment to the seal weld in half. This was a cost saving measure and was accounted for in the preliminary DTA of the test car. In other words, the VCF was applied in the FEA at the same position as it was in the test.

It is important to note that LCF and VCF spectra were applied to the test car in series without corresponding bolster motions. Thus, the relative phasing between various OTR car body inputs, and corresponding summation effects on the stress spectra of critical regions, was lost. This series application reduced the number of variables necessary for the DTA model validation, and was reflected in the crack growth analyses performed.

And finally, as will be discussed in the next section, the inputs to the test car were truncated to reduce test time. This was also reflected in the crack growth analyses performed.

In short, many test simplifications were used to reduce the cost of the program without compromising its objectives. Because of these, 300,000 DTA spectrum miles (the duration of the test) is in no way correlated with 300,000 revenue service miles of fatigue damage. Again, this was a DTA validation, not an OTR simulation.

5.6.2 Drive File Development

SwRI developed a scaled 'load schedule' from the most recent release of the tabulated rainflow cycle-counted data published in the AAR-MSRP (the first phase of Task Order 108) that represents a 10,000-mile block of longitudinal and vertical coupler loading for 100-ton tank cars. This is the load schedule currently in use by the tank car industry for the DTA program; the portion of it used to develop inputs for the full-scale validation test is listed in Appendix A. Cardinal et al. (1998) further describes the methodology behind the distillation of this load schedule from the AAR-MSRP data.

For Simuloader input development, six components of this DTA load schedule were extracted to create what is hereafter referred to as the validation load schedule:

- Loaded tank VCF events, positive = upward (LVPU)
- Unloaded tank VCF events, positive = upward (UVPU)
- Loaded tank LCF buff events, negative = buff (LLBUF)
- Unloaded tank LCF buff events, negative = buff (ULBUF)
- Loaded tank LCF draft events, positive = draft (LLDFT)
- Unloaded tank LCF draft events, positive = draft (ULDFT)

Because these components were extracted from rainflow cycle-counted data, the number and magnitude of the events were known but their frequency content and relative sequencing were not. For the creation of drive files for this test, two basic assumptions were utilized. First, metal fatigue (in a single degree of freedom system) is generally independent of the frequency of the applied stresses. Second, if the ratio of accumulated mileage per spectrum pass to total simulated mileage (in this case, 10,000/300,000 miles) is small, then the load sequence is effectively random as far as fatigue crack growth mechanisms are concerned (both large and small magnitude cycles are evenly distributed throughout the test).

The FEA of the test car was used to determine the most sensitive critical region weld for each loading regime (LCF buff, LCF draft, VCF downward, VCF upward), and the corresponding stress/force ratios. Again, these issues are discussed further by Williams (1997) and Cardinal et al. (1998). These stress/force ratios were used to truncate the input spectra at the

aforementioned threshold level of 5.1 ksi. This truncation level resulted in a 97.3-percent reduction in the total number of cycles needed for fatigue crack propagation. Next, the remaining cycle counts for each component of the validation load schedule were rounded off to the nearest whole number because partial cycles cannot be applied in the laboratory as they can in the numerical model.

Sinusoidal drive signals for each actuator were created in an 'ordered random' fashion from the remaining cycles of each of the six loading regimes. In other words, the positive peaks of the loads were ordered (descending from the highest LCF draft and VCF upward loads) while the alternating components were applied randomly (within this positive peak superstructure) at constant frequencies of 2 and 5 hertz X the frequencies determined in the initial system characterization. The loads within a spectrum pass were applied in this fashion because a complete random structuring would introduce unnecessary additional fatigue causing cycles that were not in the original tabulated data. The segment of the vertical coupler drive signal in Figure 18 demonstrates this resultant 'stair stepping' of values, with ranges sharing peak values occurring together in series.

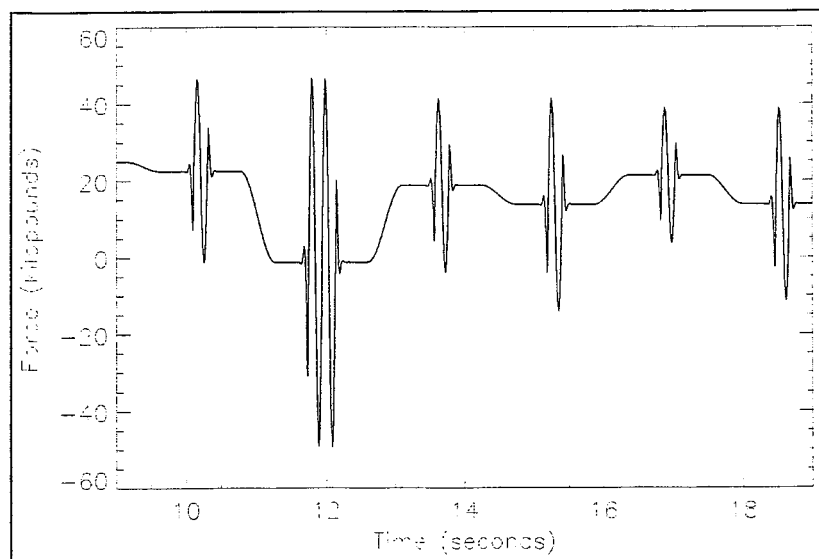


Figure 18. Segment of VCF Input Sinusoid

In summary, there were six individual drive files created: two for the VCF actuators and four for the LCF actuator. These six files, combined in a sequence, simulated 10,000 miles of fatigue damage and constituted a test cycle (with 30 test cycles completing the 300,000-mile

test). With the aid of truncation, the test was accelerated to a rate of approximately 7,936 spectrum miles per hour of actual run time. It should be noted, however, that this estimate does not include inspection time, pauses between drive files, or any of the other various sources of machine down time. The six drive files are listed in Table 7, along with some characteristics.

Table 7. 10,000-Mile Validation Load Schedule Breakdown

DRIVE FILE (LOAD CASE)	ORIGINAL DTA CYCLE COUNT	TRUNCATED CYCLE COUNT	SINUSOID DURATION	COMMAND MAXIMUM - UP/DRAFT	COMMAND MINIMUM - DOWN/BUFF
LVPU	394,996.0	9,161	35.8 minutes	61.25 kips	- 51.25 kips
UVPU	159,738.0	6,189	22.6 minutes	33.75 kips	- 41.25 kips
LLBUF	7,558.6	197	6.3 minutes		- 830 kips
ULBUF	7,963.4	194	4.5 minutes		- 650 kips
LLDFT	22,801.4	227	4.8 minutes	410 kips	
ULDFT	15,747.2	109	1.8 minutes	300 kips	

6.0 TEST OPERATIONS

The third phase of Task Order 108 (Full-Scale Damage Tolerance Test) was further subdivided into three major portions. First, the car was precracked with the application of constant-amplitude cyclic loading. When four surface cracks were apparent in the critical regions of interest, the spectrum loading of the car was initiated. After the accumulation of 200,000 spectrum miles, the test was paused and the VCF loads were amplified to increase crack growth. At 300,000 spectrum miles, the car underwent a final visual inspection, was removed from the machine, and then was sectioned for a fractographic analysis.

This section of the report includes descriptions of the procedures that were used during the program. Section 6.1 contains information regarding the crack initiation procedures that were used to precrack the test vehicle. Section 6.2 presents the fatigue crack growth and car body compliance measurements as the test progressed. In Section 6.3, the adjustments to testing procedures that were made two-thirds of the way through the full-scale test are discussed. Finally, Section 6.4 covers the post-test inspections, fractography and analysis that occurred after the spectrum loading was complete. An overview of the sequence of significant testing events is contained in Table 8.

Table 8. Sequence of Significant Full-Scale Test Events

ACCUMULATED FATIGUE DAMAGE	TASKS COMPLETED, EVENTS OF INTEREST
300,000 Miles of Revenue Service Estimated, Several Years in Storage	Initial Car Inspection, Instrumentation, System Characterization and Preflating
156,500 LCF and VCF Constant Amplitude Cycles	Test Car Precracking Completed
70,000 DTA Test Spectrum Miles	Inspection Technique Change – No VCF Preload, Dye Penetrant to Aid Measurement
200,000 DTA Test Spectrum Miles	VCF Loads Doubled to Increase Crack Growth Rates
300,000 DTA Test Spectrum Miles	End of Test, Fiber Optic Scope Inspection with VCF Preload, Sill Sectioning and Fractography

6.1 CRACK INITIATION

As discussed, the car was polished and preflawed at each of the four corners. These induced flaws were subsequently precracked with the application of constant-amplitude cyclic load blocks with maximum levels not exceeding approximately 80 percent of the peak spectrum load. Precracking was performed under tensile-only as well as fully-reversed loading (perpendicular to the crack surfaces), using both the longitudinal and vertical coupler actuators of the Simuloader. Approximately 156,500 load cycles were necessary to create fatigue cracks with a surface length of at least 0.15 inches from any of the flaws. The precracking process was terminated when what was eventually designated as seven cracks had initiated on the structure (the goal was four). Discussed further in Section 7.1, these initial cracks were lettered A, B, C, D, E, F and G. The breakdown of the precracking cycles that were applied is listed in Table 9.

Table 9. Precracking Loads Applied in Full-Scale Test

LOAD CASE	DIRECTION	ENDPOINTS	CYCLE COUNT
VCF	Downward	4 to 40 kips	5,000
LCF	Buff	75 to 445 kips	5,000
VCF	Downward	4 to 40 kips	3,500
LCF	Buff	75 to 505 kips	5,000
VCF	Downward	4 to 40 kips	10,000
LCF	Buff	55 to 550 kips	10,000
VCF	Fully Reversed	40 kips	5,000
VCF	Fully Reversed	40 kips	15,000
VCF	Fully Reversed	40 kips	30,000
VCF	Fully Reversed	37 kips	15,000
VCF	Upward and Downward	42 kips and 48 kips	15,000
VCF	Upward and Downward	42 kips and 48 kips	10,000
VCF	Upward and Downward	41 kips and 48 kips	22,500
LCF	Fully Reversed	425 kips	5,000
LCF	Buff and Draft	630 kips and 400 kips	500

The logic behind this precracking load schedule was based on SwRI experience. SwRI engineers were present to give real-time guidance based on laboratory results during this part of the program. At 1.30 inches after precracking, crack E (in the tank head at the A-end left) was the primary motivator to start spectrum loading the test vehicle.

6.2 SPECTRUM LOADING

6.2.1 Spectrum Crack Growth

The variable-amplitude spectrum loading portion of the test was broken into 10,000-mile increments, corresponding to the length of the input validation load schedule. Within the schedule, the loaded and unloaded VCF and LCF cycles were applied sequentially to the stub sill. One pass through the validation load schedule began with the VCF cycles applied to each end of the car (applied simultaneously to both ends, in parallel), followed in series by LCF cycles applied at the B-end and reacted at the A-end. The Simuloader bolster modules (vertical, lateral, and yaw actuators) were not used for dynamic load application during the test; they were only used to position the test car for the application of the LCF and VCF loads.

The test was paused for crack inspections between validation load schedule passes (at 10,000-mile intervals). At that time, existing crack lengths were measured with the aid of clear plastic flexible scales and magnifying glasses. For the precracking, the first seven test inspections (the first 70,000 spectrum miles of the test), and the post-test fiber optic scope inspection, these inspections were done with the Simuloder energized and a static vertical load of 50 kips applied to the stub sills in a downward direction. This loading was done to open up the crack tips and make them more easily visible against the polished metal background.

The entire car was visually inspected for new cracks at 20,000-mile intervals (every other validation load schedule pass). Also at these intervals, constant-amplitude marker bands were applied to the car with the VCF actuators. As with the coupons before the full-scale test (see Section 2.3.2), these marker bands were applied at a maximum of 90 percent of the peak downward spectrum load, with a load ratio of 0.8 (at 5 hertz). This translated to cyclic loading with a 41.5-kip mean and a 4.5-kip amplitude (fully reversed around that mean preload) at both ends of the car. For the first band, the number of such cycles applied was 40,000. The marker band cycle count was then decreased by 2,500 cycles every 20,000 spectrum miles to account for increased crack growth rates as the test progressed, thereby keeping all marker bands approximately the same width. Because it was not known whether this marker banding effort was successful during the test, the cycle count reduction was frozen to 17,500 cycles at 200,000 spectrum miles. Table 10 contains the details pertaining to the loads that were applied to the car.

Table 10. Marker Bands Applied in Full-Scale Test

VCF MARKER BAND	CYCLE COUNT (LENGTH)	SPECTRUM MILES ACCUMULATED
1	40,000	20,000
2	37,500	40,000
3	35,000	60,000
4	32,500	80,000
5	30,000	100,000
6	27,500	120,000
7	25,000	140,000
8	22,500	160,000
9	20,000	180,000
10	17,500	200,000
11	17,500	220,000
12	17,500	240,000
13	17,500	260,000
14	17,500	280,000
15	17,500	300,000

6.2.2 Car Body Compliance

Before the precracking process and subsequently at 50,000-mile test intervals, quasi-static sensitivity tests were performed to quantify changes in the compliance (linear stiffness) of the vehicle as the test progressed. Longitudinal loading was applied to the car in static increments of 100 kips, spanning the range of 0 to 500 kips, for a duration of a few seconds at each step. This was done in both buff and draft. Vertical loading was also applied in 10-kip increments from 0 to 50 kips in the same fashion (both upward and downward). As these incremental loads were applied, a strain survey was continuously recorded on all channels. In addition to FEA critical region stress-to-force ratio verification, these periodic tests provided information concerning load path and stiffness changes in the presence of propagating cracks.

Strain circuit integrity was also checked on all bridges at 50,000-mile intervals. This was done with two processes. First, a strain indicator was used at the gage (removing all data acquisition cabling and conditioning from the signal) to check for any offsets due to material yielding or gage peeling. Second, all signals were balanced and a resistance calibration was performed to ensure that the gain of any individual signal conditioner had not changed.

6.2.3 System Control and Response

Finally, system response was monitored throughout the full-scale test. The feedback from the actuators was recorded periodically for both the validation load schedule (every 50,000 spectrum miles) and the marker band drive files (every other band). Due to reasons already discussed, actuator transient response was expected, which would add many low-amplitude cycles to the full-scale test. The extent of this was quantified with rainflow cycle counting and the resulting files were used for the actual DTA parameter adjustments and validation. In other words, the exact loads that were input into the test car were put into the model. This was done to eliminate any validation error associated with Simuloader/vehicle system response errors during the application of the loads.

6.3 MID-TEST PROCEDURE ADJUSTMENTS

6.3.1 Inspection Technique

The crack inspection at 70,000 spectrum miles was the last to be done with a vertical load on the sills of the car. Safety considerations concerning the cutting power of the pilot pressure hoses (in the event of a break) ended this practice, as the crack inspections put the inspector within a few feet of several of these hoses. From that point on (all inspections after and including the one performed at 80,000 spectrum miles), dye penetrant was routinely used to assist in locating the crack tips. With the sills vertically loaded (as with the past inspections), red dye was sprayed onto all known cracks. After that, the machine was shut down, developer was applied, and crack lengths were measured with the aid of clear plastic flexible scales and magnifying glasses. The car was only loaded for the application of the dye to open the crack tips for better penetration. For the final inspection with a fiber optic scope (at 300,000 spectrum miles), however, the car was repositioned so that the entire Simuloader would not need to be energized, the pressurized pilot hoses were shielded (from the scope operator), and the sills were again loaded.

6.3.2 Input Load Spectrum

After the accumulation of 200,000 spectrum miles, the test was stopped for further data analysis. At that point, the critical region cracks had not grown appreciably; reasons for this were under investigation. The end result of this analysis was the amplification of the VCF portion of the validation load schedule for the remainder of the test. The motivations for this are discussed in

the following paragraphs. Due to the length of the hiatus, car body compliance and existing crack lengths were measured twice before testing resumed, once before and once after the pause in testing.

At 200,000 spectrum miles, an in-depth comparison was made between the test vehicle FEA and the stresses recorded during the compliance tests. A comparison matrix was formed between the measured strains (scaled to stress with $E = 29,000$ ksi), the calculated von Mises stress summations (for the rosettes) and the FEA stresses at longitudinal loads of 500 kips (buff and draft) and vertical loads of 50 kips (upward and downward). After outliers were discarded, nominal weighted averages were calculated from a matrix that contained 40 empirical measurements (36 strains and 4 displacements) from six different compliance strain surveys (taken at different points throughout the test). When combined with the analytical FEA results, this yielded a 40 by 7 array of values to compress for each of the four load cases. As stated previously, the details of this comparison are proprietary and are discussed by Williams (1997) and Cardinal et al. (1998). Through the nominal weighted averages, the initial FEA of the test car was determined to be conservative by a factor ranging from one to three, depending on the critical region and load case of interest. In other words, the FEA predicted stresses that were anywhere from accurate to three times higher than what was observed in the laboratory. It is important to note, however, that these nominal weighted-average factors are based on a linear FEA of the uncracked structure and that they do not distinguish changes in car body compliance as cracks progressed throughout the test. This issue warrants further study. An example of the comparison matrix that was constructed for the seal weld critical regions is shown in Table 11.

Table 11. Empirical/Analytical Comparison Matrix Example

	First Strain Survey (Before Precracking)	Average of Next Five Strain Surveys	FEA Prediction	FEA/Test #1 Ratio	FEA/Tests #2-6 Ratio	Nominal FEA/Test Ratio
BLHvM						
BLH1						
BLH4						
BRHvM						
BRH3						
BRH4						
ALHvM						
ALH3						
ALH4						

[Refer to Williams (1997) and Cardinal et al. (1998)]

To ensure sufficient crack growth for DTA model validation during the pending last segment of the full-scale test, it was decided that the VCF portion of the validation load schedule would be amplified by a factor of two and clipped at 55 kips. In other words, the VCF loads were increased to 200 percent of their original OTR values, and any cycle of the amplified input that exceeded 55 kips was attenuated to that same value. This amplification of the VCF portion of the validation load schedule was in effect for the remainder of the full-scale test (100,000 spectrum miles).

The logic behind the amplification amounted to a moment arm correction. As discussed previously, the vertical coupler actuator was approximately halfway between the seal weld and the fully extended coupler pulling face. Though the shear stresses in the critical regions were relatively unaffected by this placement, the applied moment was as little as half its extreme potential. This was initially determined to be acceptable for DTA model validation and was accounted for in the preliminary analysis of the car. However, when it was discovered that the initial stress predictions were conservative by such a large degree, this loss of applied moment became more important.

The logic driving the decision to clip the amplified VCF load spectrum was to protect the car from unintentional catastrophic sill damage, as well as to allow identical load application to both ends of the car. Clipping was justified because the most recent car design guidelines specify that a tank car must withstand vertical loads of 50 kips (in both directions) and the A-end actuator had a peak capacity of 55 kips (compared to 110 kips at the B-end). Supporting this was the brief coupon investigation mentioned earlier that suggested the impact of clipping on crack growth behavior may be small in specific variable-amplitude situations. At the 55-kip clipping level, only 115 cycles (99 LVPU and 116 UVPU) were clipped. This represented less than 1 percent of the total VCF cycle count.

After this FEA/test comparison, SwRI computed NASGRO fatigue crack growth predictions with the amplified and clipped load schedule and the revised stress/load ratios for the critical regions, based on strain data from the test. A low R-ratio (load ratio) model was used to add a conservative degree to the predictions (a prediction of slower growth would indicate a need for more amplification). With a twofold increase in VCF, incremental crack growth was

predicted to increase by a factor as large as 9. However, because the crack aspect ratios were still assumed at this stage of the test and the stress gradients through the thickness of the material were unknown, the confidence level in these predictions was limited.

6.4 POST-TEST ANALYSIS

6.4.1 Final Critical Region Inspection

At 300,000 spectrum miles, sufficient crack growth had been achieved for the validation of the DTA model. The test was stopped and personnel from both General American Transportation Corporation and SwRI joined with TTCI in the final car inspection. In addition to the dye penetrant inspection typical of the entire test, a fiber optic scope was used to inspect and document crack measurements and geometries. The fiber optic scope was used in conjunction with a partial machine shutdown and some protective tarps so cracks could be inspected safely with a vertical load on the sills of the car. The scope proved to be quite helpful in determining the existence of cracks (especially in hard-to-reach locations), but difficult to use for actual surface length measurements.

6.4.2 Sill Sectioning and Fractography

At the conclusion of the full-scale test, the instrumentation was removed from the test car and the car was then removed from the Simuloader for sill sectioning. The car was rolled on its side and each sill was flame-cut out of the tank car with a frame of tank head material about 12 inches wide. The regions containing both the seal weld and the flange weld (the inboard portions where flaws had been inserted) were then removed from these sections and sent to SwRI for post-test fractographic analysis. There, the pieces were further sectioned and the fracture surfaces were exposed for more accurate crack length and depth measurements. The details of this fractographic analysis and the crack growth rate behavior are contained in the companion report by Benac, et al. (1998).

6.4.3 Damage Tolerance Validation

The actual DTA model validation was done by SwRI as part of the overall industry program and is documented by Cardinal et al. (1998). In that report, a correlation analysis has been performed between the empirical data (both Simuloader and fractographic) and analytical data (FEA and

NASGRO). Recommendations for the SSWG, including model parameter adjustments, are included in that document.

7.0 RESULTS AND DISCUSSION

This section includes discussions of the various results of the full-scale test that are not addressed in any of the companion reports referenced. Section 7.1 contains details concerning the surface crack growth measurements that were made throughout the program. Section 7.2 details the compliance test results and contains a few notes on the strain measurements. In Section 7.3, the response of the Simuloader/vehicle system is described and quantified with the aid of rainflow cycle counting. Finally, Section 7.4 provides brief introductions and references to the companion reports.

In this report, anything suspected to be a crack has been referred to as a crack. During the final inspection (with the fiber optic scope) and the fractographic analysis, a few of these ‘cracks’ were shown to be surface aberrations, not true cracks. This is addressed to some degree here, and to a larger degree in the companion reports. In addition, the presentation and discussion of all data is hereafter in accordance with the following sign conventions:

- LCF draft - positive
- LCF buff - negative
- VCF upward - positive
- VCF downward - negative
- Stress/strain tension - positive
- Stress/strain compression - negative
- Displacement extension - positive
- Displacement retraction - negative

7.1 SPECTRUM CRACK GROWTH

7.1.1 Initial Precracking Success

After what was eventually designated as seven cracks initiated in the critical regions of the car, the precracking process was terminated. These cracks (lettered A, B, C, D, E, F, and G) are

sketched in Figures 20, 22, and 26 of Section 7.1.2. Cracks A and B extended from either side of the SW@FW surface flaw at the B-end left corner of the car and remained unconfirmed (possible scratches, rather than cracks) throughout the test. Like A and B, cracks C and D extended from either side of the TH@SW surface flaw at the A-end left corner of the car. Cracks E and F were also at the A-end left corner in the top toe of the seal weld. These cracks (E and F) were actually the same crack, divided into a lateral and longitudinal portion along the seal weld, respectively. All four of the A-end left cracks were difficult to distinguish due to the poor weld quality in that area. Finally, at the A-end right corner of the car, crack G extended from the outboard side of the SW@FW surface flaw. Interestingly, crack G apparently disappeared or was no longer visible on the surface at the 80,000-mile inspection. This also occurred with cracks A and B at the same time. The 80,000-mile inspection was the first inspection with dye penetrant and no vertical preload, due to safety concerns.

7.1.2 Spectrum Cracking Success

Appendix B contains a complete log of all surface crack measurements that were made during this full-scale validation test. Where a crack was growing at both tips (and both were observable), a reference mark was scribed into the metal and the crack was given two letter designations, one for each tip. This is reflected in the crack figures and in the appendix table. Figures 19 through 26 are schematic diagrams of all these cracks at 300,000 spectrum miles (the end of the test).

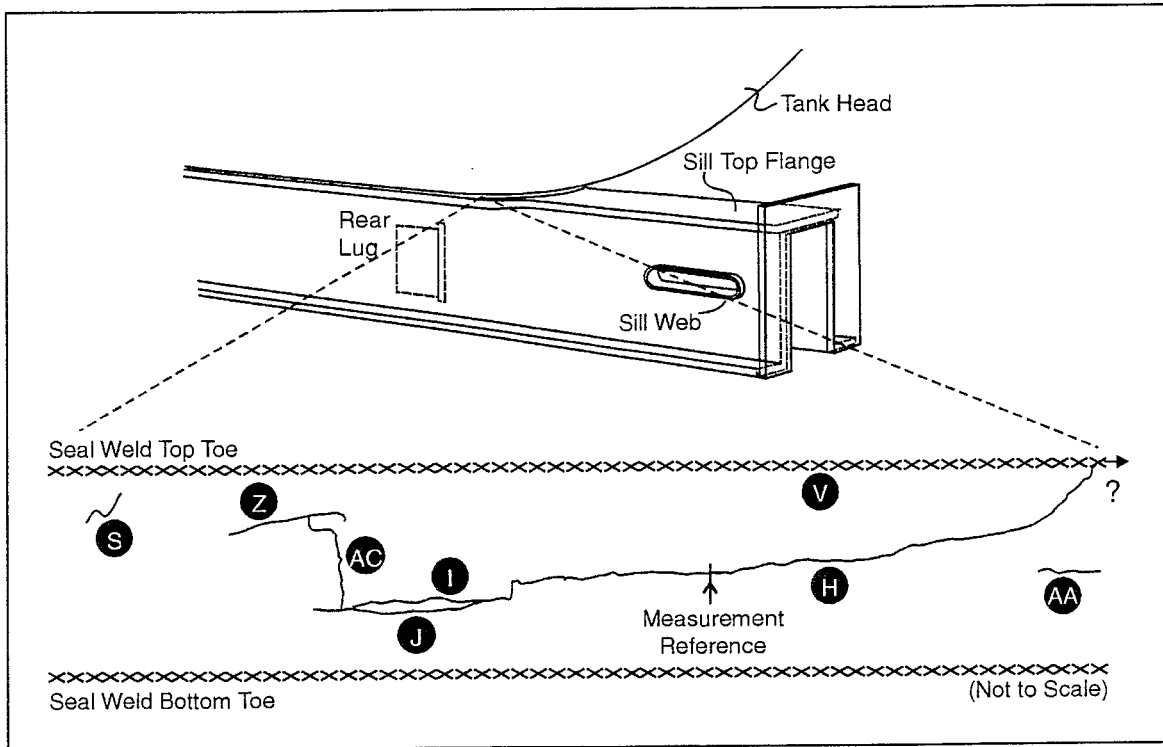


Figure 19. B-end Left Seal Weld Cracks

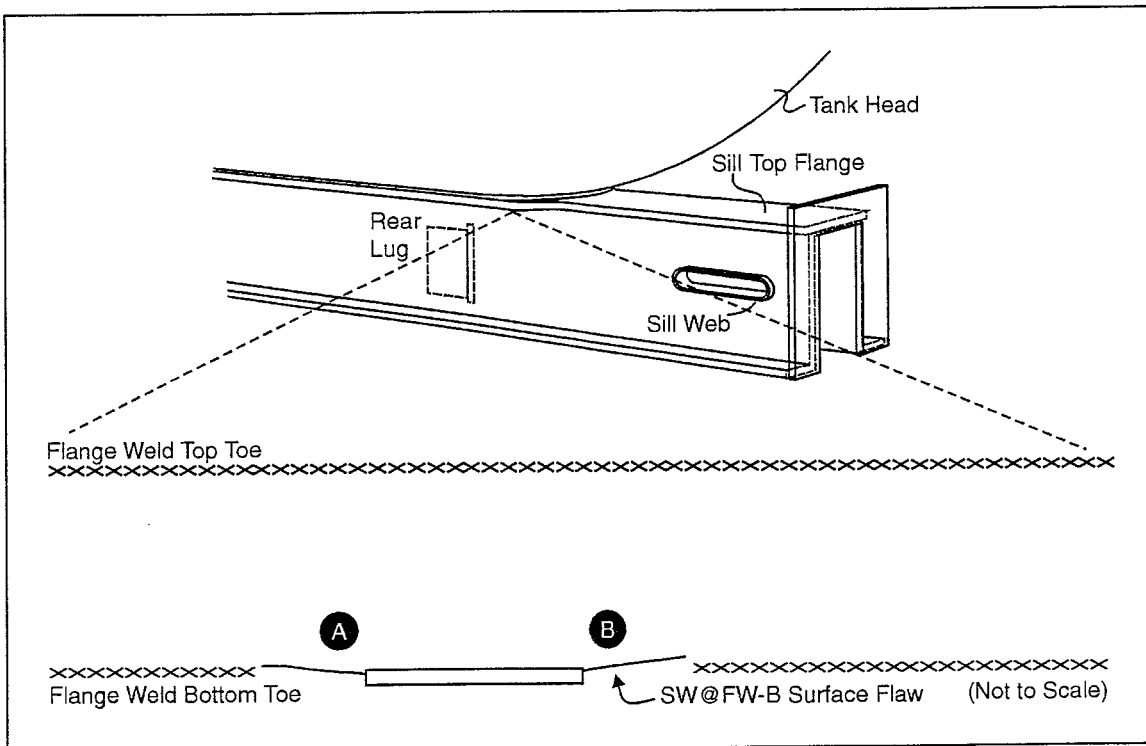


Figure 20. B-end Left Flange Weld Cracks and Preflaw

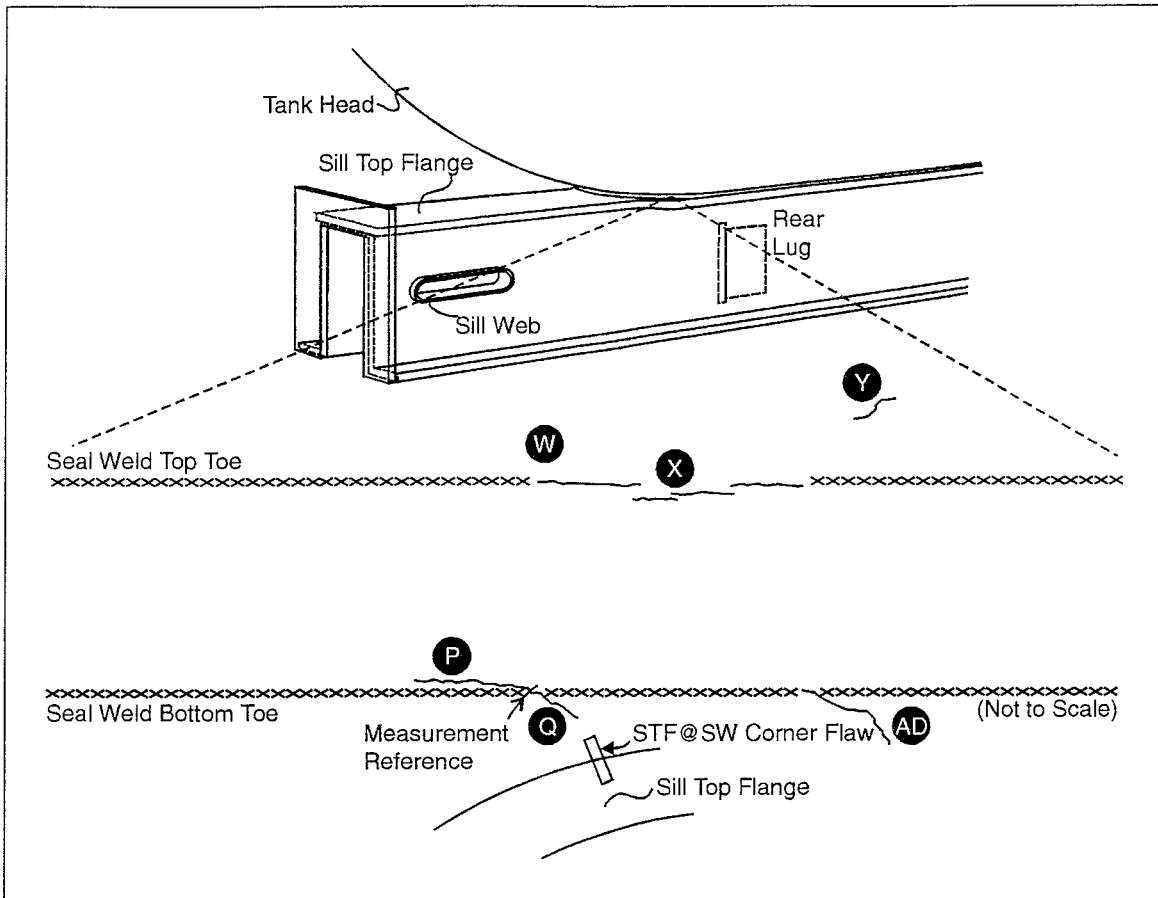


Figure 21. B-end Right Seal Weld Cracks and Preflaw

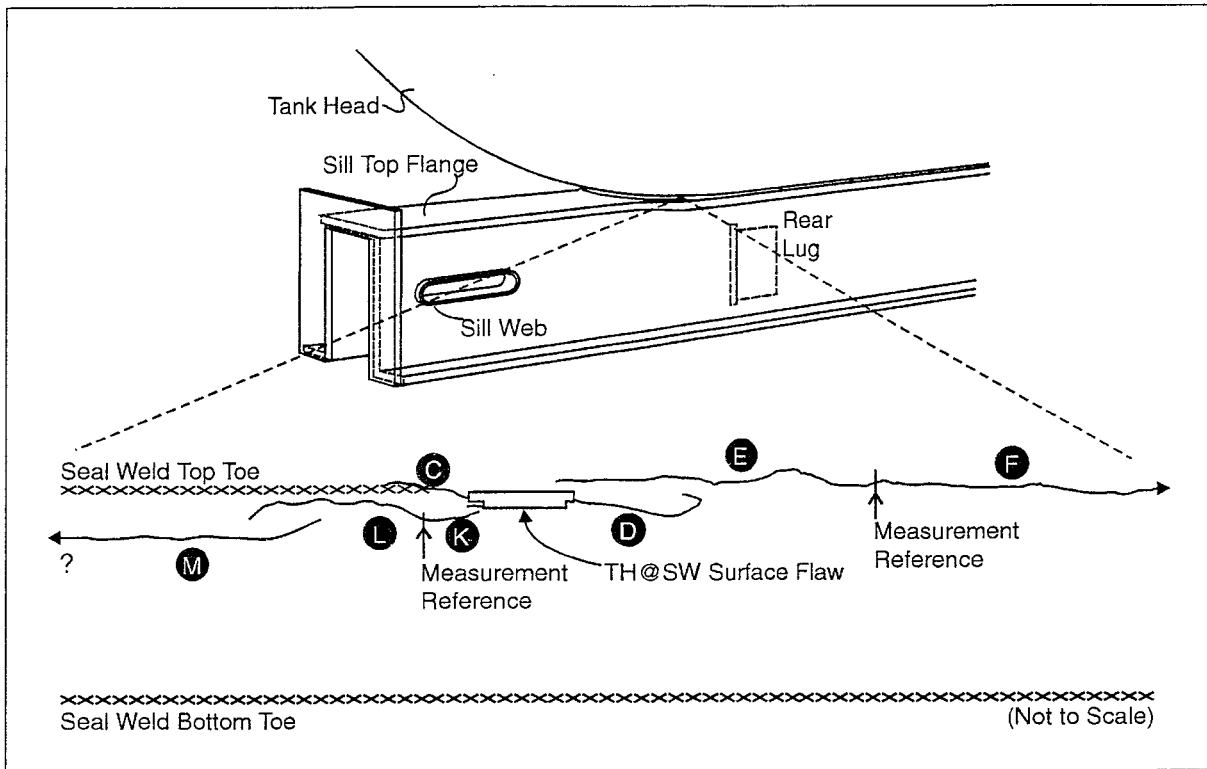


Figure 22. A-end Left Seal Weld Cracks and Preflaw

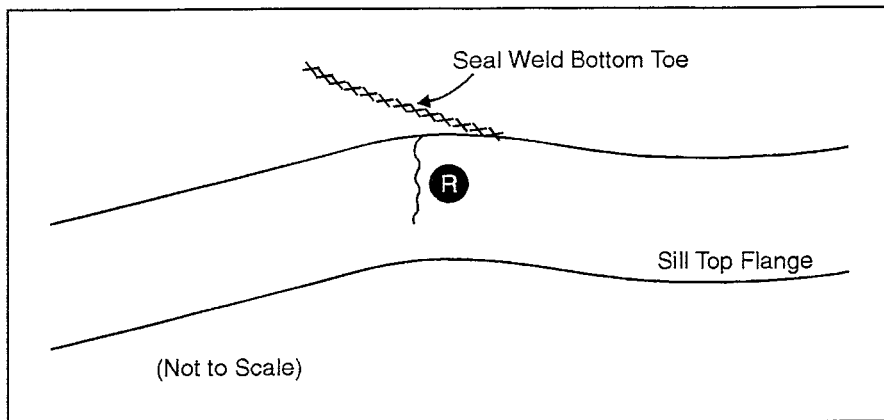


Figure 23. A-end Left Sill Top Flange Crack

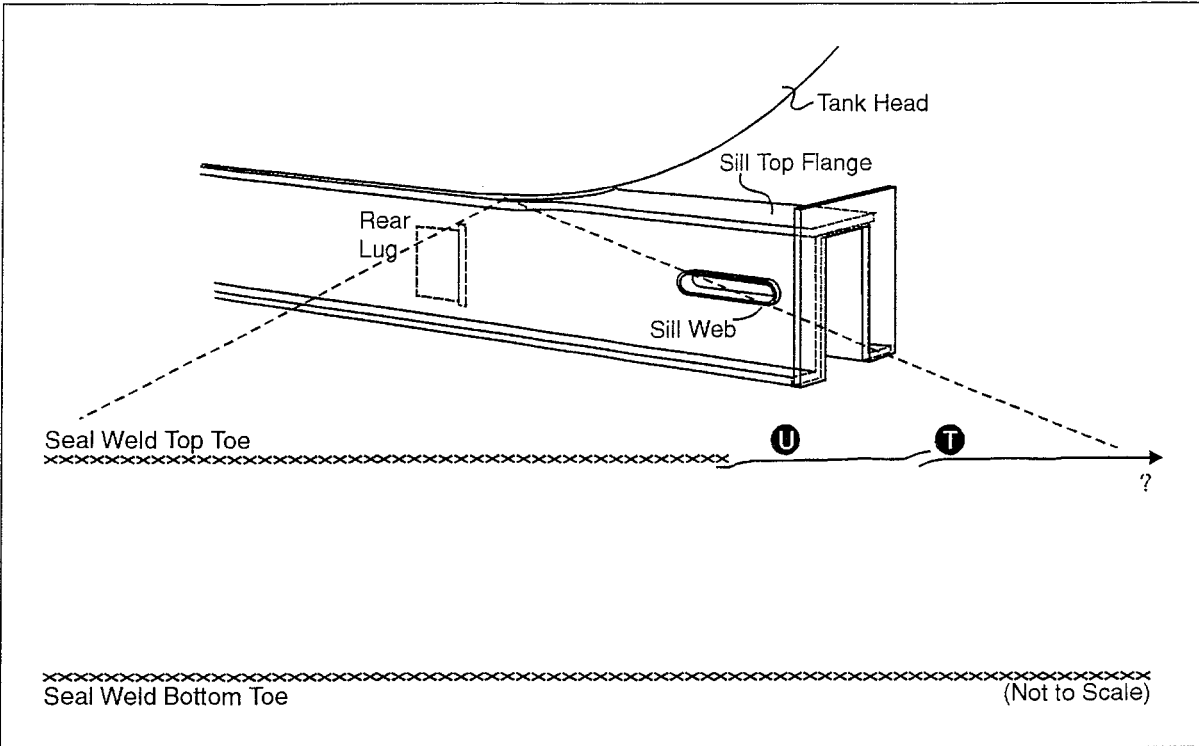


Figure 24. A-end Right Seal Weld Cracks

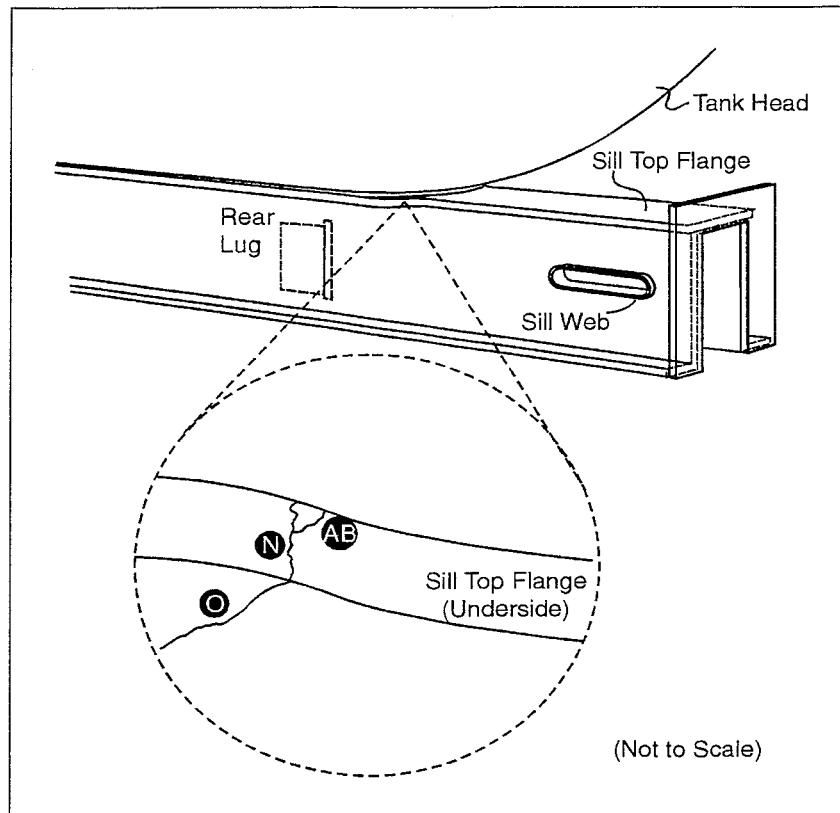


Figure 25. A-end Right Sill Top Flange Cracks

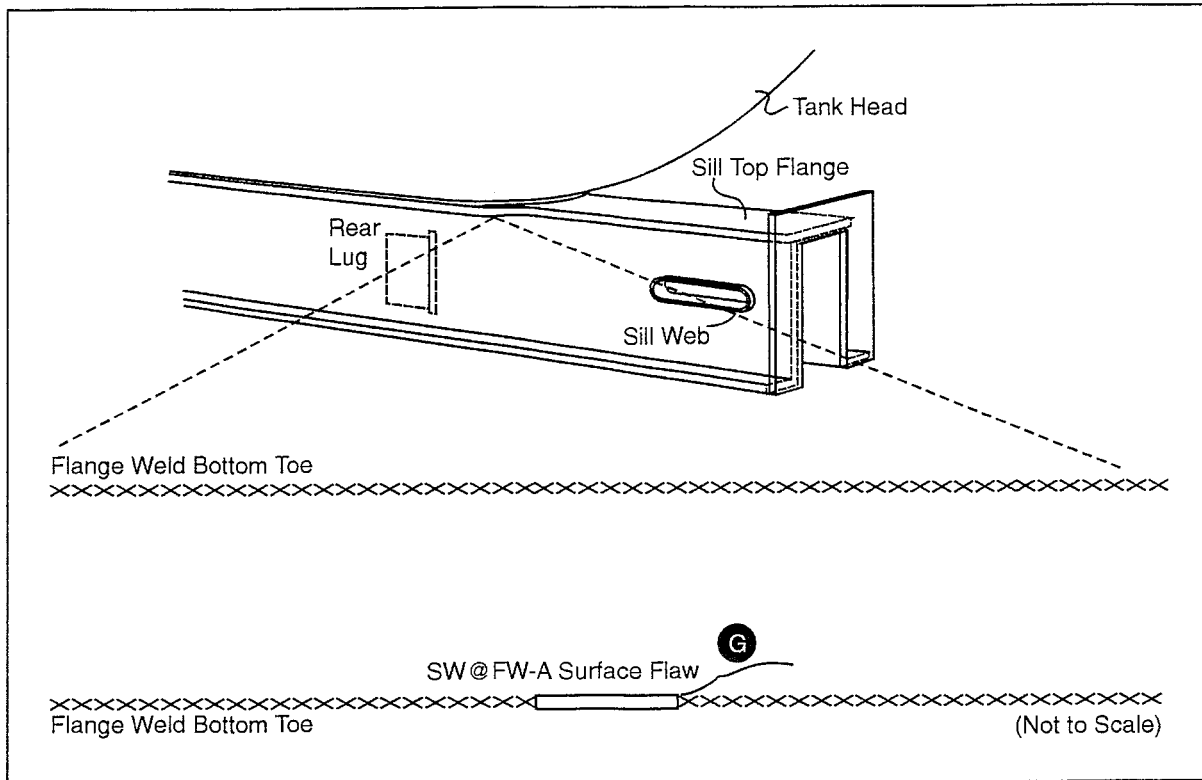


Figure 26. A-end Right Flange Weld Crack and Preflaw

Several of the 30 cracks listed in the spectrum crack growth log occurred in weld toes. Their existence (or lack thereof) was only proven in the post-test fractographic efforts at SwRI. Their approximate measurement uncertainty ranged from ± 0.01 to ± 0.05 inch, depending upon the accessibility of the critical region.

There were three discontinuities in the surface crack length measurements, reflected in the crack growth log by heavier dividing lines. The first of these appeared after 70,000 spectrum miles, when the inspection technique changed. At that point, the vertical preload was discontinued and dye penetrant was added to the process. This change may have influenced the measurements in two conflicting ways: the crack tips were not held open (making the cracks appear shorter) and the dye penetrant led the crack tips (making the cracks appear longer). It was not determined whether these two effects cancelled each other. The second discontinuity occurred at 200,000 miles. Because the mid-test hiatus lasted a few months, a second inspection was performed before testing resumed. A few of the cracks appeared to look different after the hiatus; a few of the previous reference marks were difficult to distinguish and were scribed into

the metal again. The last discontinuity was at 300,000 miles, when the final inspection was performed twice. The second-to-last inspection was done with routine procedures at the conclusion of the test. The final inspection, however, was done with the aid of both a fiber optic scope and a vertical preload on the sills of the car. The car was positioned and the operator was shielded to remove safety risks from pilot pressure hoses.

7.1.3 Marker Banding Success Indications

During the last leg of the test (at about 293,000 spectrum miles), a stud from the A-end VCF actuator broke and the test was paused for machine repair. Upon examination of this stud, it was apparent that it had fractured by fatigue (as opposed to a static overload fracture), and the cracks had been growing through it during several previous tests. In addition, beach marks (striations) from the marker banding in this test were evident even on a macroscopic scale. The stud was sent to SwRI for further inspection and confirmation of these conclusions, which is detailed by Benac et al. (1998). This was significant, as it was the first indication (before the post-test sectioning of the car) that the marker banding techniques used during the full-scale test were effective. Figure 27 depicts one of the load stud fracture surfaces.

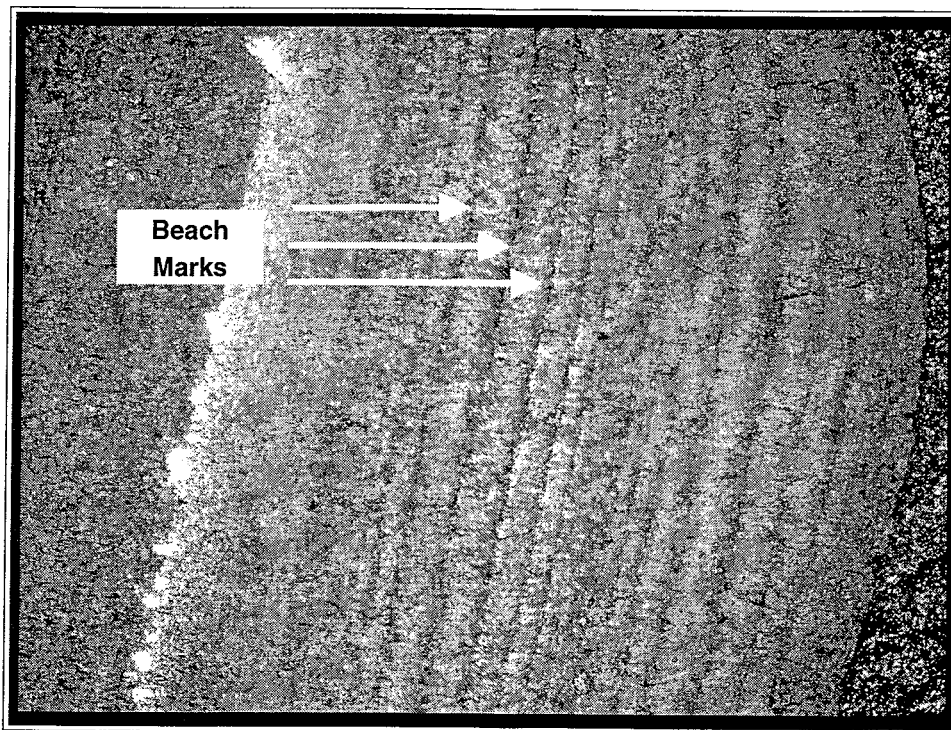


Figure 27. VCF Load Stud Fracture Surface at 6.6x Magnification

7.2 CAR BODY COMPLIANCE

7.2.1 Compliance Test Results

During this program, a total of nine measurements of critical region stiffness were taken with static strain surveys at the following intervals (in sequence):

1. Before precracking cycles were applied to the car
2. After the precracking process, prior to spectrum loading
3. After the application of 50,000 spectrum miles
4. After the application of 100,000 spectrum miles
5. After the application of 150,000 spectrum miles
6. After the application of 200,000 spectrum miles, before the hiatus
7. After the application of 200,000 spectrum miles, after the hiatus
8. After the application of 250,000 spectrum miles
9. After the application of 300,000 spectrum miles, at the end of the test

The calculated stress data from these nine surveys is plotted in Appendix C. For comparison purposes, the data was organized into the following nine major channel groups:

- Vertical sill deflections: VCDE, VCDW, SPE, SPW
- B-end sill bending stresses: BLBT, BLBB, BRBT, BRBB
- A-end sill bending stresses: ALBT, ALBB, ARBT, ARBB
- Vertical head stresses: BLH1, BLH4, BRH3, BRH4, ALH3, ALH4
- Von Mises head stresses: ALHvM, BLHvM, BRHvM
- Vertical web stresses: BLW1, BLW2, BLW3, BLW4, ALW3, ALW4
- A-end Von Mises web stress: ALWvM
- B-end longitudinal flange stresses: BRF1, BRF2, BRF3, BRF4
- A-end longitudinal flange stresses: ARF1, ARF2, ARF3, ARF4

The data from these nine groups of channels was further subdivided into the three different compliance load cases (LCF, B-end VCF = VCFE, and A-end VCF = VCFW). In all, Appendix C contains 243 plots (nine channel groups, nine strain surveys for each group, and three load cases for each survey).

The tables in Appendix D present compliance data from the nine strain surveys at force levels of 500 kips LCF buff, 500 kips LCF draft, 50 kips upward VCF, and 50 kips downward VCF, as well as calculated principal (p1 and p2) and von Mises (vM) stress data for the four rosettes. It is important to note that the principal stress direction results (BLHang, BRHang, ALHang, and ALWang) represent the acute angle from the axis of gage 1 (different for each corner) to the nearest principal axis, regardless of whether it is the maximum or minimum principal stress axis. When positive, this angle is in the direction of the gage numbering. When negative, this angle is in the opposite direction. The first four tables of Appendix D are dominated by raw strain data. The subsequent four tables are comprised mostly of calculated stress and standard deviation data for three groupings (compliance test 1, tests 2 through 6, and tests 3 through 9). The stress calculations in these tables were performed with Young's modulus equal to 29,000 ksi and 0.275 for Poisson's ratio.

7.2.2 Sill Deflections and Bending Strains

The sill deflections and bending strains were essentially linear and repeatable for both LCF and VCF at both ends of the car, with the exception of the A-end during the first buff strain survey (before precracking). This initial A-end discrepancy may have been caused by load path changes within the structure, strain gage 'break-in,' or a combination of both. The initial sensitivity change between the first and second compliance test (before and after precracking) is apparent in some of the other measurements as well. This change in sensitivity seemed the most pronounced in the case of buff, which may be a consequence of the fact that buff was the most variable load case in terms of load application geometry (the car and machine may have shifted relative to one another between strain surveys).

There was an unexpected result in the bending response of the test car to LCF buff. In the initial FEA, longitudinal tension in the top flange and compression in the bottom flange was expected. However, the reverse of this proved to be the case at both ends of the car. Under a buff load, the top flanges (at the location of the strain gages) went into longitudinal compression and the bottom into tension. This may have been due to a vertical reaction force (of the gross car body reaction to LCF) applied just inboard of the striker, as demonstrated in Figure 28.

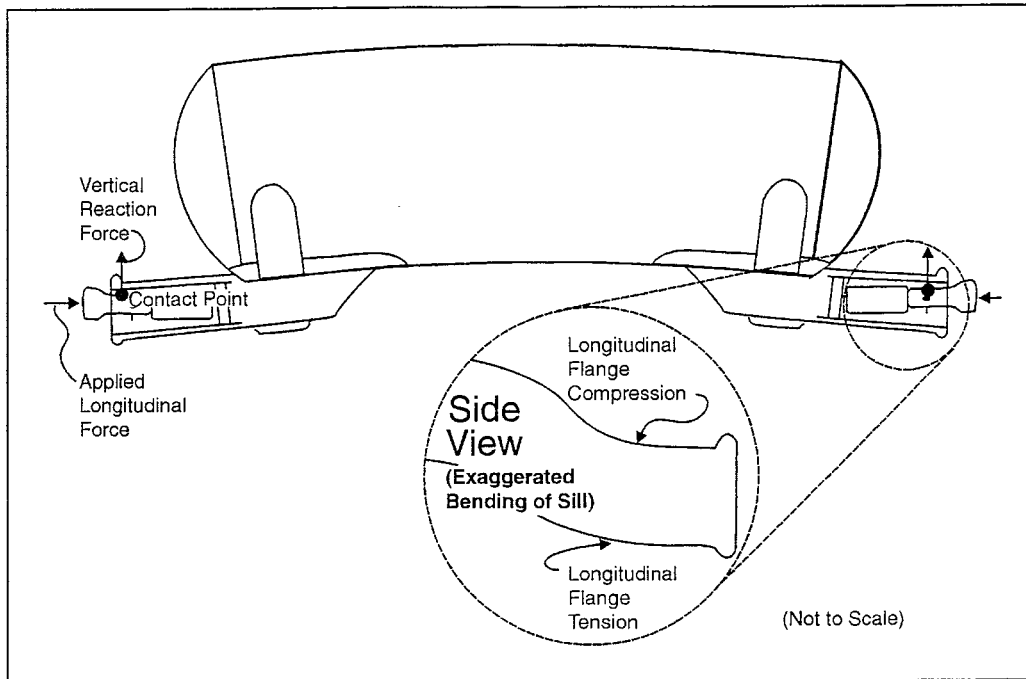


Figure 28. Schematic of Potential LCF Load Path

This polarity (compression in the top flanges and tension in the bottom) was also the case for upward VCF; the reverse was true for downward loading (tension in the top flanges and compression in the bottom). Both the top and bottom flanges were in tension when draft loads were applied to the car. And finally, the sill was forced down at all four vertical displacement measurement locations under both buff and downward loads; the sill was forced up under both draft and upward loads. This latter observation was expected in the FEA of the test car.

Other qualitative observations that were made concerning the sill bending strains and displacements include:

- Vertical displacement magnitudes at the string potentiometers were greater for LCF buff than draft, yet approximately the same for upward and downward VCF
- Vertical displacement magnitudes at the actuators were greater for upward VCF than downward, yet approximately the same for both LCF buff and draft
- Vertical displacements at the actuators were more linear and repeatable than those inboard at the string potentiometers
- Downward VCF caused the most vertical displacement at the actuators, but LCF buff caused the most at the string potentiometers

- Bending strain response magnitudes to LCF draft were greater than to buff, though upward and downward VCF were similar
- Both ends of the car had about the same compliance strain levels
- The highest uniaxial strain magnitudes (on these bending gages) were recorded during LCF draft

All data from all channels is plotted and tabled in Appendices C and D, respectively. The string potentiometers SPE and SPW were not used during the first strain survey (they were added later). Also, the completion bridge for strain gage ARBB had a loose wire during the second survey, which was fixed shortly afterward. The data from these channels during the referenced surveys may be disregarded.

7.2.3 Tank Head Gradients and Summations

Tank head strains were measured with both uniaxial gages and rosettes at three corners of the test car: the B-end left, the B-end right and the A-end left. At each corner, comparisons were made between the pair of uniaxial strains perpendicular to the seal weld (e.g., channels BLH1 and BLH4) and between the calculated von Mises stresses (from each rosette). Linearity and repeatability varied between corners, but were better under VCF than under LCF. Discrepancies may be primarily due to stress redistributions due to crack propagation.

The A-end left tank head strain response to LCF buff was dissimilar from those observed at either the B-end left or right corners of the tank car. The vertical strain perpendicular to the seal weld (channel ALH3) was compressive under LCF buff, while the same response at both of the B-end corners was tensile. In addition, the relative magnitude of the vertical strain measured 1 inch outboard of the rosette (channel ALH4) was small, though the region was in tension like its counterparts at the B-end of the car. Surprisingly, these relative differences were observed under LCF buff only, and not under any of the other three load types (LCF draft, upward VCF, and downward VCF). With this A-end exception, the strains perpendicular to the seal weld were tensile under LCF buff and downward VCF, and compressive under draft and upward loading.

Other qualitative observations that were made concerning the tank head strain measurements and stress calculations include:

- Across the 1 inch between strain measurements perpendicular to the seal weld, vertical tank head sensitivity to both LCF and VCF generally dropped by a factor of two (e.g., BRH4 \approx 0.5*BRH1)
- The B-end corners of the car were more sensitive to LCF buff than to draft, with the reverse case at the A-end left
- At the B-end, upward and downward VCF caused about the same magnitudes of strain; upward was dominant at the A-end left

An interesting exercise that was briefly visited involved the calculation of the magnitudes and directions of the principal stresses for the three tank head rosettes at the various stages of the test. The relationship between this data and the incremental seal weld crack growth data, as well as an overall examination of the load redistribution phenomenon, has not been addressed in detail here. However, some preliminary observations were noted through these calculations and include the following:

- Maximum principal stresses occurred in directions perpendicular to the seal welds for all load types at both B-end corners of the car, minimum principal stresses were parallel (longitudinal to the car)
- Principal stress angles were similar between buff and draft, as they were between upward and downward loading, at the B-end
- Maximum principal stresses were oriented slightly inboard of vertical for VCF and slightly outboard for LCF at the B-end
- Principal stress magnitudes were similar for upward and downward VCF, but not for LCF buff and draft at the B-end
- At the B-end, VCF caused higher stress magnitudes than LCF
- The principal stress magnitudes and directions at the A-end left did not follow clear patterns, such as those at the B-end corners
- Upward VCF and LCF draft caused the highest stress magnitudes at the A-end left, contrary to the B-end corners

As demonstrated by these conclusions, there were several similarities between the B-end left and B-end right tank head strains. However, the A-end left did not follow the same patterns. Benac et al. (1998) discussed the fractographic analysis that has been performed to date at each of these three corners, as well as crack growth rate behavior from the full-scale test. It is interesting to note here that of the three, the A-end left was the only strain-gaged corner of the car that had confirmed cracks growing through the tank head itself. In addition, recall that the workmanship at the A-end of the car was of a lesser quality than that of the B-end. The B-end left corner had cracks through seal weld material (a very porous, low-quality weld) and the B-end right corner was never opened up for further analysis. It is possible that this contributed to the observed stress patterns. Figures 29 through 31 are schematic diagrams of the average relative relationships between the principal stresses for each of the three tank head measurements over the course of the test (these average values include all nine compliance strain surveys). The arrows indicate both relative magnitude (distance from center) and whether the stresses were compressive (pointing toward the center) or tensile (pointing away from center); the axes indicate stress directions relative to the rosettes. Again, the tables in Appendix D contain the actual calculated values for these schematics.

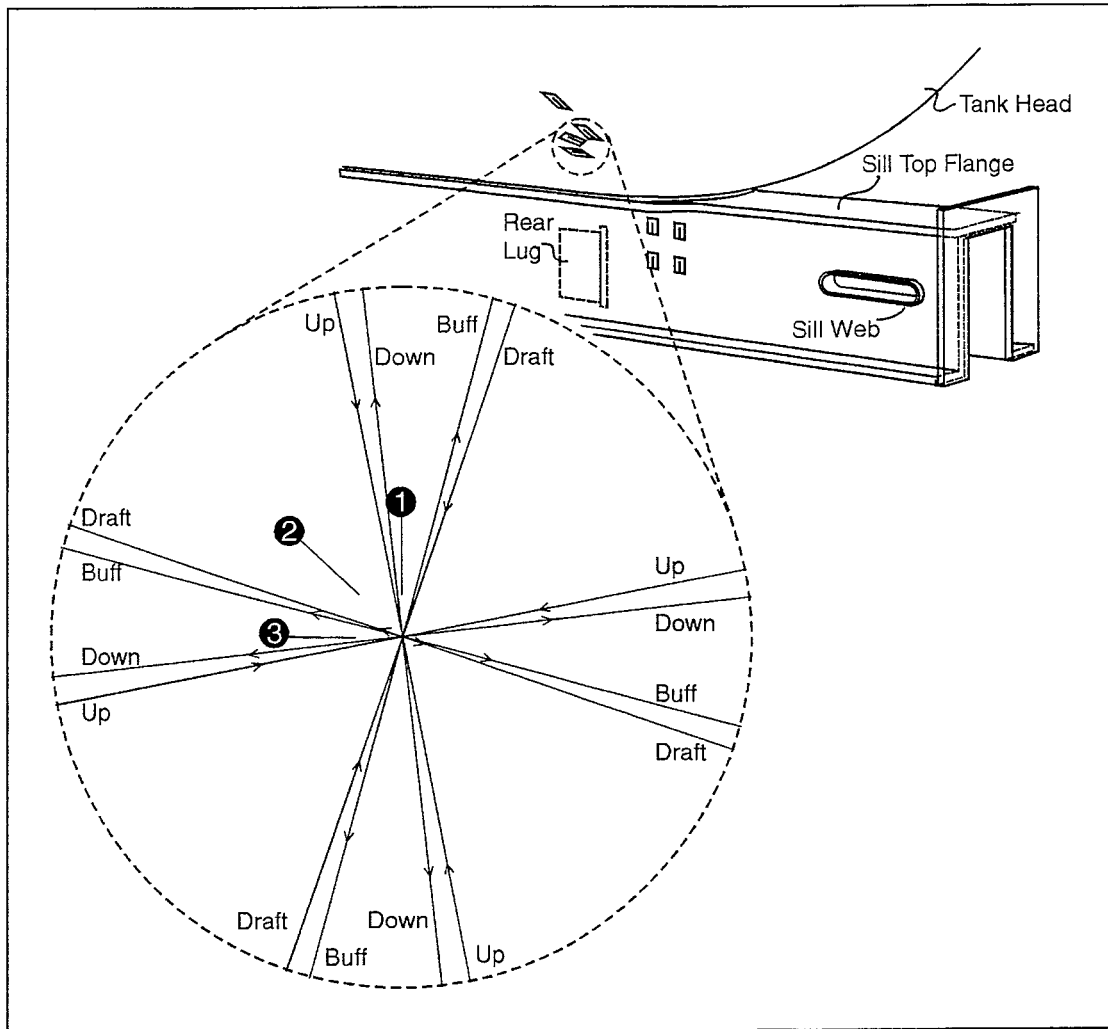


Figure 29. Principal Stress Magnitudes and Directions at B-end Left Tank Head

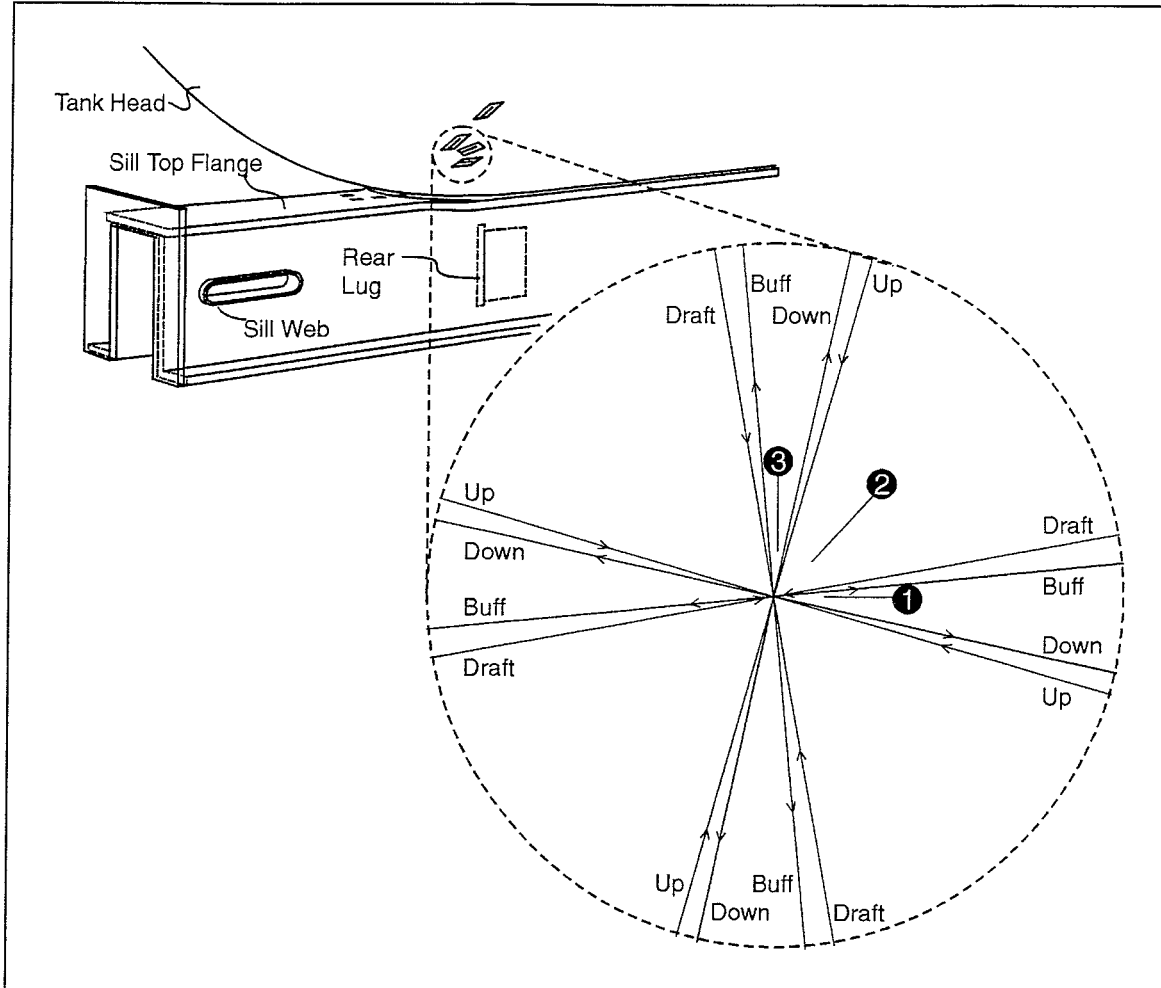


Figure 30. Principal Stress Magnitudes and Directions at B-end Right Tank Head

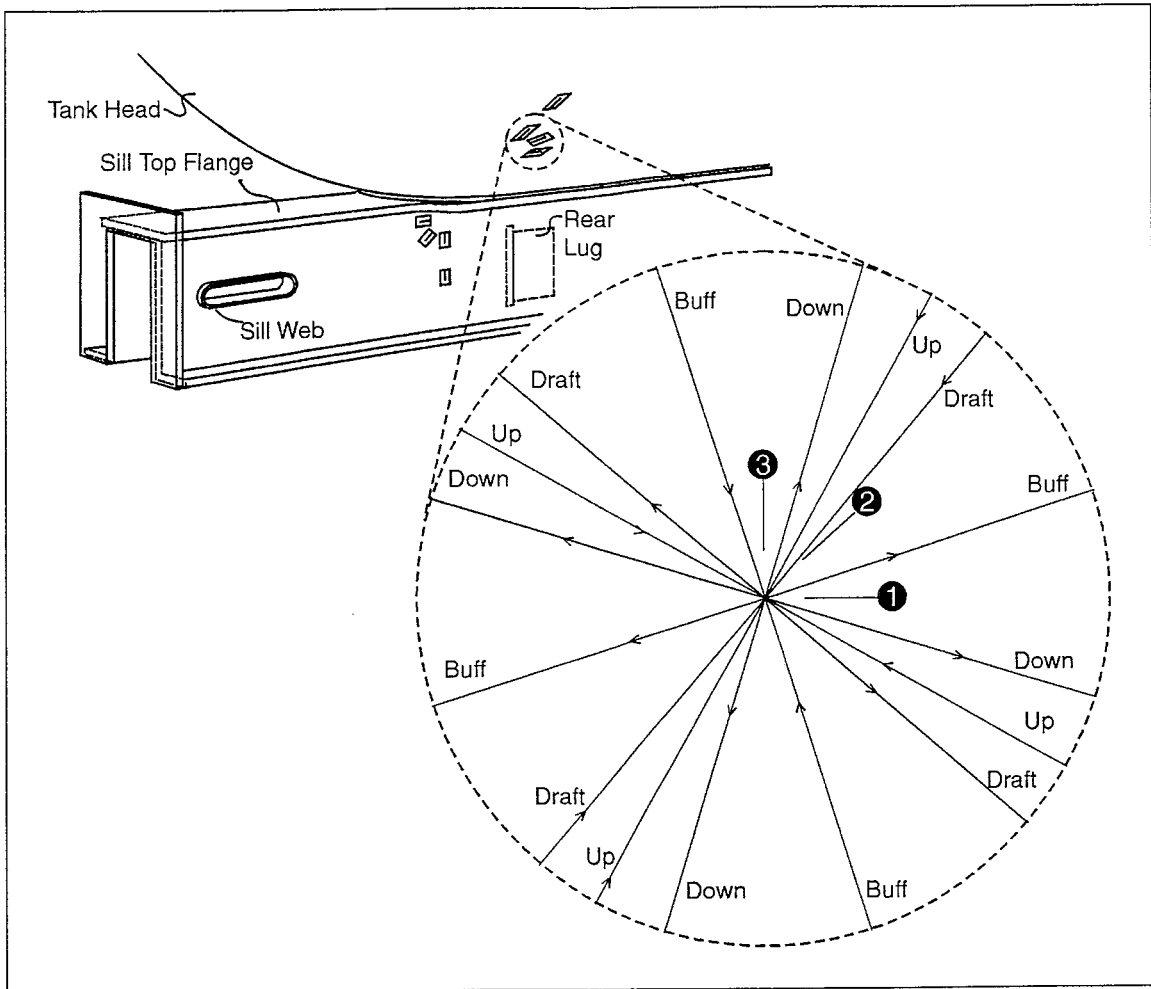


Figure 31. Principal Stress Magnitudes and Directions at A-end Left Tank Head

7.2.4 Sill Web Gradients and Summations

A quantification of vertical sill web stress gradients was achieved with the strain gages at the b- and A-end left corners of the test car. In addition, the web surface strain was measured at the A-end with a rosette. The data taken from these channels indicated that the stresses were for the most part linear for the duration of the test. However, repeatability appears to be poor, as the standard deviations between the sill web channels often had magnitudes as large as some of the individual measurements. This low repeatability was primarily due to the low sensitivity of the area to longitudinal and vertical coupler loading (the measurements taken were very small). Vertical strain sensitivities may have been low either because the gages were not located close enough to measure them or because the gages were not oriented to observe them (e.g., if the maximum principal strains were perpendicular to the gages, and the minimum principal strains were small, a vertical gradient may not have existed under the conditions tested).

Though the measured strains were relatively small, certain patterns were distinguishable. With the possible exception of channel BLW1, vertical tension on the sill web was caused by LCF buff and downward VCF, while draft and upward loads caused vertical compression. However, LCF buff and upward VCF primarily caused compression on the surface at the location of the A-end left rosette, while draft and downward loads caused mostly tension. This is a direct result of the longitudinal orientation of the principal axes. These effects are best illustrated in the schematic diagram of Figure 32. Like Figures 29 through 31, Figure 32 contains the average relative relationship between the principal stresses for all load cases at the A-end left sill web rosette location; the conventions used are the same.

Three qualitative observations that were made concerning the sill web strain measurements and stress calculations are:

- Vertical sill web strain sensitivity to force appeared to increase as the measurement location moved upward toward the flange weld and outboard toward the striker
- Maximum principal stresses occurred in directions approximately parallel to the flange weld (longitudinal to the car) for all load types at the A-end left; minimum principal stresses were perpendicular
- LCF caused the highest von Mises stresses at the A-end left, though upward VCF was vertically dominant at the B-end left

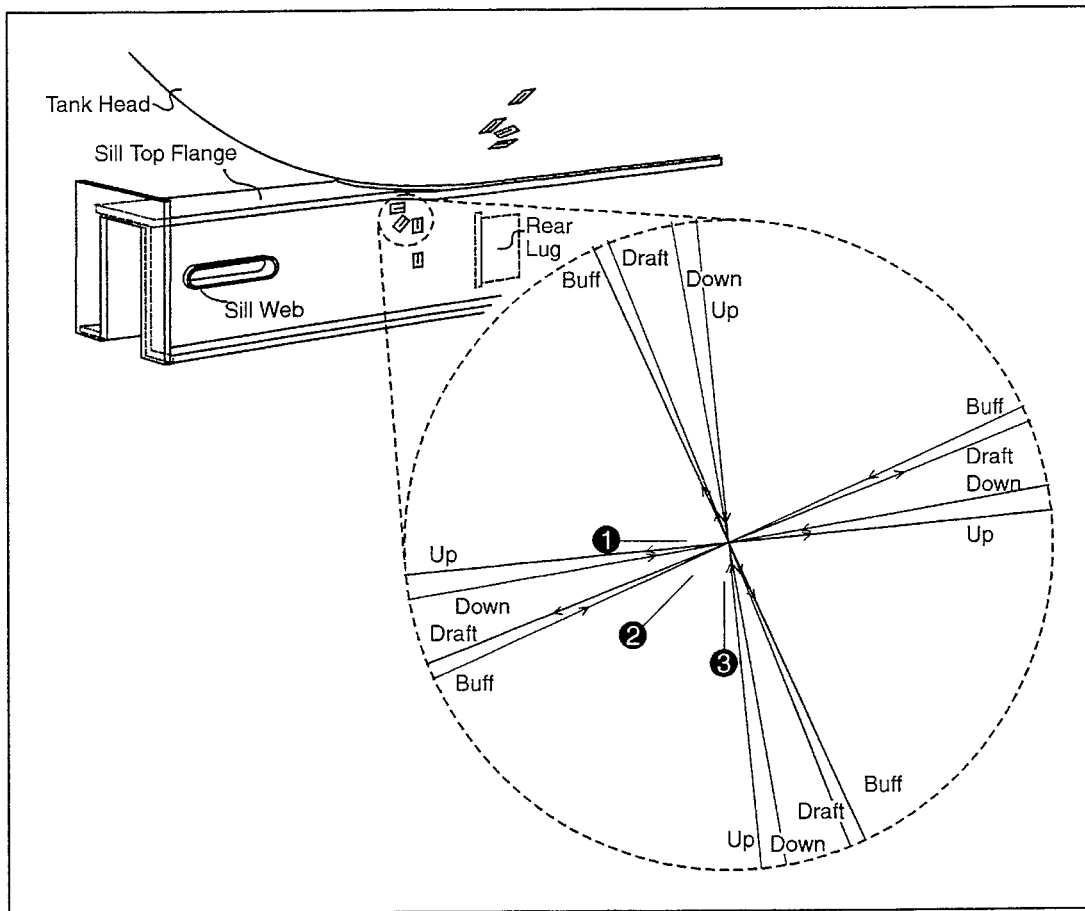


Figure 32. Principal Stress Magnitudes and Directions at A-end Left Sill Web

7.2.5 Sill Top Flange Gradients

Much like the bending strains, the sill top flange sensitivities near the seal welds at the b- and A-end right corners of the car exhibited marked differences after the first compliance strain surveys. This effect was more dramatic at the A-end of the car, where the LCF buff response went from tensile to compressive. Again, this may be due to stress redistribution within the structure, strain gage ‘break-in,’ or a combination of both. As a result, overall linearity and repeatability at the A-end right was marginal, while both were good at the location of the B-end right flange gages. With the exception of the first strain survey, LCF buff and upward VCF caused longitudinal compression in the flange, while draft and downward loads caused longitudinal tension.

Sill top flange qualitative observations include:

- In general, LCF draft caused higher sill top flange longitudinal strain magnitudes than buff though VCF sensitivity magnitudes were about the same, regardless of application direction
- Higher longitudinal strains were observed at the flange edge (versus inboard)
- The B-end right was more compliant than the A-end right flange
- Of the four load cases, draft caused the highest strain magnitudes at the a- and b- end right sill top flange measurements

Aside from the initial A-end right flange measurements, outliers of interest included channels BRF2 and BRF4. The strain gage BRF2 was damaged during an inspection after precracking; all measurements from that point on were rejected. The gage BRF4 showed a brief inconsistency during strain surveys at 0 and 50,000 spectrum miles. For both of these surveys, its sensitivity to the applied loads was about half of what it later achieved.

7.3 SYSTEM CONTROL AND RESPONSE

As discussed in Section 5.6.1, the LCF and VCF spectra were applied to the test car in series without any corresponding bolster motions and the response of the actuators was collected as input into the DTA model. This system response data was collected at 50,000 spectrum-mile intervals, and rainflow cycle counted for convenience. These cycle counted forces are listed in Appendix E. For simplicity, the histograms of Appendix E contain only two-dimensional

information (force ranges versus number of counts) and do not contain the associated mean load levels. Over the course of the entire full-scale test, the mean levels were on target and the ranges were slightly undershot at times; and as expected, actuator transient response and ramp functions between cycles added many low-amplitude cycles back into the applied spectra.

Because the actuator response spectra were used for the DTA validation, the various sources of differences between the inputs to and the response of the system were deemed acceptable and no additional time was spent further tuning the Simuloader actuators. For the DTA validation (Cardinal et al., 1998), the VCF response at the A-end of the test car (VCFW LVPU and UVPU) was used at both 150,000 and 250,000 spectrum miles. LCF response to the buff portion of the validation load schedule (LCF LLBUF and ULBUF) at 100,000 spectrum miles was also used.

7.4 POST-TEST ANALYSIS

The final critical region inspection under a VCF preload, with the aid of a fiber optic scope, revealed that of the 30 suspected cracks A, B, P, U, W, and Y did not seem to exist. The other 24 crack lengths were both verified and modified, as is reflected in the crack growth log of Appendix B.

After the test car was removed from the Simuloader, the sills were sectioned and sent to SwRI for a fractographic analysis. The results of this analysis are contained in the companion report by Benac, et al. (1998). The fractographic evaluation included two types of assessments. The first was a general examination noting the fracture surface features, origin, and size. The cracks assessed solely in this fashion were cracks C, H, I, J, N, O, T, U, Z, AB, and the preflaws SW@FW-B and SW@FW-A. The second type of assessment was a more detailed evaluation of each fracture, including the precrack zone, marker band identification, and marker band measurement to determine crack growth rate. The cracks that were assessed in this fashion were cracks K, L, R, and the preflaw TH@SW. These latter four were chosen for detailed analyses because they contained the largest quantity of distinguishable fracture surface features, as assessed in the initial examination.

In the report by Cardinal et al. (1998), the actual DTA validation is discussed, along with the industry DTA efforts as a whole. To some extent, 'validation' is a misnomer as the results of this test were used to modify the input parameters to the DTA model in addition to validating those previously assumed. The response data files (rainflow cycle counted) used for this effort were:

- VCFW LVPU at 150,000 and 250,000 spectrum miles
- VCFW UVPU at 150,000 and 250,000 spectrum miles
- LCF LLBUF at 100,000 spectrum miles
- LCF ULBUF at 100,000 spectrum miles

8.0 SIGNIFICANT OBSERVATIONS

Key observations from the full-scale test have been summarized in this final section. Other conclusions concerning recent cooperative efforts of the government and the tank car industry can be found in five additional reports. Cogburn (1995) discussed the most recent tank car OTR test procedures and the data that was acquired to be put into the AAR-MSRP. McKeighan et al. (1997) discussed the coupon tests that were performed to investigate both spectrum truncation and clipping. In a proprietary report by Williams (1997), the pre- and mid-test FEA of the orphan test car are reviewed. The details from the full-scale damage tolerance validation test were covered in this document. The post-test fractographic efforts, full-scale fatigue crack growth rates, and their implications were documented by Benac et al. (1998) in a companion report. And finally, the actual tank car DTA program and its validation, using the information from the full-scale test and the post-test fractography, is detailed by Cardinal et al. (1998).

8.1 OTR AND COUPON TESTING

- AAR REPOS data for 100-ton tank cars now includes a combination of both 1986 and 1994 FEEST data for LCF, but only 1994 data for VCF. These are the two primary load spectra employed by the tank car DTA program.
- It was assumed that if the ratio of simulated mileage per spectrum pass to the total test mileage is small (in this case, 1/30), the test load sequence is effectively randomized for fatigue crack growth mechanisms, regardless of the sequence within each pass.
- Preliminary coupon tests indicated that for common tank car steels, 4 to 5 ksi may be an acceptable truncation level in accelerated testing and that peak load clipping may have minimal effects on crack growth behavior. Additional testing is recommended.

8.2 ORPHAN TANK CAR NATX 22746

- The orphan test car had neither head pads nor head braces and no previous record of parent metal crack repairs. Though different from most cars in service, this was deemed acceptable for the analytical model validations. It arrived at TTC with approximately 300,000 mile of accumulated usage and had been in storage for about eight years.

- For the initial inspections of the stub-sill critical regions, portions of the jacket were removed and the seal weld areas were lightly sand blasted. The rust and scale was as much as 1/8-inch thick in some areas, which hindered visual inspection.
- Despite evidence of poor workmanship in several areas on the car, initial visual inspections did not reveal any cracks in the critical stub-sill regions highlighted by both the SS-II database and the FEA of the test car.

8.3 PRE-TEST DAMAGE TOLERANCE ANALYSIS

- In general, the FEA of the orphan test car predicted stub-sill stress concentrations at the same locations identified by the SS-II database.
- The FEA of the car was conservative by a factor of one to three, an engineering estimate based on 36 strain and displacement measurements from 6 car body compliance tests, and a linear FEA of the uncracked structure. However, this nominal weighted-average factor does not distinguish changes in car body compliance as cracks progressed throughout the structure. This issue warrants further study.
- The initial LEFM analysis of the car, based on the conservative FEA, predicted a necessary duration of about 300,000 spectrum miles to achieve sufficient crack growth for model validation. Crack aspect ratios (a critical parameter) were assumed.

8.4 PREFLAWING AND PRECRACKING

- A relatively small amount of confirmed crack initiation and growth was observed at the mechanically inserted flaws during precracking X an unexpected result.
- In retrospect, precracking was occurring elsewhere on the car, at stress concentrations that were sometimes more difficult to observe; crack E motivated the suspension of precracking.
- A total of 156,500 precracking cycles were applied to the car with a maximum force of 80 percent peak spectrum load, resulting in deep crack growth through the thickness in regions later sectioned for fractographic analysis. Visual surface measurements did not reveal this relative severity during the precracking phase of the test.

8.5 VALIDATION LOAD SCHEDULE

- From the 10,000-mile DTA load schedule, all cycles that caused critical region stresses less than or equal to 5.1 ksi (based on the FEA) were truncated for the validation drive files; resulting in a 97.3 percent reduction in total cycle count, or 16,100 spectrum cycles for each 10,000-spectrum-mile pass.
- Sinusoidal drive signals for each actuator were created in an 'ordered random' fashion. Ramp functions between cycles and actuator transient response caused the addition of many low-amplitude cycles back into the applied spectrum and increased test time.
- For the 300,000-spectrum-mile validation test, LCF was applied at 2 hertz and VCF at 5 hertz. These frequencies were maximized during the initial system characterization.

8.6 MARKER BAND APPLICATION

- Beach marks (striations) on the fracture surface of the VCF stud that failed at 293,000 spectrum miles indicated marker banding success. Constant-amplitude marker bands were applied to the car at 20,000-spectrum-mile intervals (375,000 total throughout the test) with a load ratio of 0.8 and a maximum of 90 percent peak spectrum load.
- The marker banding techniques utilized proved effective for creating a periodic fractographic record of crack growth through the thickness of the material, in the regions analyzed.

8.7 SPECTRUM CRACK GROWTH

- Thirty suspected cracks were monitored throughout the test; five were from preflaws.
- Ten suspected cracks and three preflaws (through the thickness) were given a cursory fractographic analysis. Three cracks and one preflaw were examined more thoroughly.
- Two of the five suspected preflaw cracks were proven to be true fatigue cracks; these were C and D from the tank head preflaw (TH@SW) at the A-end left corner.
- Visual measurements of surface crack length made during the test agreed well with the fractographic results from the cracks analyzed (cracks K, L, R, and preflaw TH@SW), including those made with dye penetrant and no preload after 70,000 spectrum miles.

- At all four corners of the car, increased crack growth rates (and some new cracks) were observed on the surface after the VCF amplification at 200,000 spectrum miles; sufficient growth for DTA model validation was achieved by 300,000 spectrum miles.
- The fiber optic scope worked well for the detection and video documentation of cracks in otherwise unobservable locations, but proved to be difficult to manage for the actual measurement of surface crack length.

8.8 CAR BODY COMPLIANCE

- A vertical reaction inside the sill near the striker may have caused the stub sills to bend irregularly under buff loading, rather than as they would under downward loads. This possibility of 's-shape' versus 'c-shape' bending needs further investigation.
- Measurement linearity and repeatability varied; this result may be a reflection of stress redistribution due to load path changes as cracks propagated through the structure.
- In the areas measured, upward VCF and LCF draft were dominant in strain sensitivity (these load directions caused higher strain magnitudes) than their downward and buff counterparts; in general, downward and buff are dominant coupler loads in driving crack growth, as they often result in critical region tension.
- Either relatively poor workmanship or cracks in the A-end left tank head parent metal (in the upper toe of the seal weld) appeared to skew the nearby principal stress directions from the case at the B-end left, where the seal weld cracks were in weld metal and the welds were of better overall quality.
- The B-end right stress magnitudes and directions were similar to the B-end left, but it was not opened for analysis
- The vertical tank head strains typically dropped by a factor of two in the 1-inch distance between strain gages.
- The vertical sill web strains (at the B- and A-end of the car) were very small; the principal stress axes for both VCF and LCF was longitudinal along the flange weld.

- Higher longitudinal strain magnitudes were observed at the edge of the sill top flange at both the B- and A-end right corners, when compared with the strains measured inboard on the flange surface.
- Strain channel BRF2 (B-end right sill top flange edge, nearest seal weld) was the only data channel lost permanently during the full-scale test.

8.9 VCF PLACEMENT AND AMPLIFICATION

- Due to actuator placement, the applied VCF moment to the seal weld was approximately half of the extreme OTR possibility (the applied shear was not affected). This moment arm reduction, as well as truncation, clipping, actuator transient response, and lack of bolster motions (i.e., the fact that this was not an OTR simulation) were all deemed acceptable simplification techniques for the DTA model validation. All of these factors were accounted for in the analyses of the car.
- To encourage crack growth in the wake of the discovery that the FEA was conservative, the VCF inputs were amplified at 200,000 spectrum miles by a factor of two (to correct for the OTR moment arm loss). Because the applied shear was doubled from the OTR situation, the inputs were clipped at 55 kips, based on both tank car design criteria and the A-end actuator capacity. This was done to prevent catastrophic sill failure, as well as to provide VCF symmetry at both ends of the car.

8.10 DTA VALIDATION

- The full-scale test and corresponding DTA results, though not directly transferable to other stub-sill tank car designs, illustrated the general applicability of the damage tolerance approach to tank car design and life extension.
- Sufficient stress and crack growth results have been obtained for the DTA analytical model validation.

Acknowledgments

The author of this report wishes to express his appreciation and thanks to Jose Pena who acted as Task Order Monitor for the Federal Railroad Administration, as well as Dan Stone who acted as DTA Program Manager for the RPI-AAR Tank Car Safety Project. Helpful discussions were also held with Joe Cardinal and Pete McKeighan from Southwest Research Institute and Mike Williams from American Railcar Industries.

In lieu of an exhaustive list of all individuals who influenced this project, the author would like to acknowledge all members of the Stub-Sill Working Group for their continuing program guidance and support. Also noted are the efforts of the lab crew, consisting of Dave Johns (TTCI), Denzel Savage (TTCI), Mike Sandoval (TTCI), Tom Roderick (TTCI), Tom Masden (SwRI) and Dan Benac (SwRI).

Additionally, the FRA is acknowledged for its permission to use information from this test program for papers and presentations at professional societies. And Joe Cardinal is personally acknowledged for his direct contribution to this report with a detailed description of damage tolerance.

FINAL DRAFT

Bibliography

Barsom, J. M., and Rolfe, S. T., 1987, *Fracture and Fatigue Control in Structures*, 2nd Edition, Prentice-Hall.

Benac, D. J., McKeighan, P. C., and Cardinal, J. W., 1998, "Fractographic Analysis of Cracks Generated During a Full-Scale Railroad Tank Car Fatigue Test," Final Report 06-8840, Southwest Research Institute, San Antonio, TX.

Broek, D., 1989, *The Practical Use of Fracture Mechanics*, Kluwer.

Cardinal, J. W., McKeighan, P. C., and Hudak, S. J., 1998, "Damage Tolerance Analysis of Tank Car Stub-Sill Cracking," Final Report 06-6965, Southwest Research Institute, San Antonio, TX.

Cackovic, D. L., 1993, "Tank Car Fatigue Crack Growth Test," Technical Report DOT\FRA\ORD\93-10, Transportation Technology Center, Inc., Pueblo, CO.

Cogburn, L. T., 1995, "Stub-Sill Tank Car Research Project: Results of a 15,000-Mile Over-The-Road Test," Technical Report FRA\ORD\95-11, Transportation Technology Center, Inc., Pueblo, CO.

Damage Tolerance Assessment Handbook, Volumes I and II, 1993, DOT-VNSTC-FAA-93-13.I.

Fatigue Design Handbook, AE-10, 1988, Society of Automotive Engineers, Warrendale, PA.

Forman, R. G., et al., 1994, "NASA/FLAGRO Fatigue Crack Growth Computer Program Version 2.0 Revision A," JSC-22267A, National Aeronautics and Space Administration.

Gallagher, J. P., et al., 1984, *USAF Damage Tolerant Design Handbook*, AFWAL-TR-82-3073.

Hattery, B. K., et al., 1997, "The Minutiae of Tank Car Structural Integrity," Proceedings, *International Symposium on Railroad Tank Cars*, Indianapolis, IN.

Hudak, S. J., Burnside, O. H., and Chan, K. S., 1985, "Analysis of Corrosion Fatigue in Welded Tubular Joints," *ASME Journal of Energy Resources Technology*, Volume 107.

McKeighan, P. C., Smith, K. B., and Cardinal, J. W., 1997, "Load Interaction Effects in Coupon Fatigue Tests Using a Railroad Tank Car Spectrum," Proceedings, *ASME 1997 International Mechanical Engineering Congress and Exposition*, Dallas, TX.

Orringer, O., 1994, "Validation of Simulated Service Load Spectra for Crack Propagation Testing in Full-Scale Structures," Working Paper, Volpe National Transportation Systems Center, Washington, D.C.

Przybylinski, P., and Halcomb, S., 1977, "Interim AAR Guidelines for Fatigue Analysis of Freight Cars," Report R-245, Association of American Railroads, Pueblo, CO.

Richmond, S., Sneed, W. H., 1981, "Freight Equipment Environmental Sampling Tests: Center Plate and Side Bearing Loads for Analysis," Proceedings, *International Conference on Wheel/Rail Load and Displacement Measurement Techniques*, Cambridge, MA.

Sharma, V., 1990, "Freight Car Fatigue: Coal Car Simuloader Demonstration Test," Report R-747, Association of American Railroads, Pueblo, CO.

Sharma, V., and Punwani, S. K., 1984, "Freight Equipment Environmental Sampling Test Description and Results," Proceedings, *ASME Rail Transportation Division Spring Conference*, Chicago, IL.

Stub-Sill Inspection Database, SS-2, 1996, Association of American Railroads – Railway Progress Institute, Washington, D. C.

Stone, D. H., and Cardinal, J. W., 1997, "Application of Damage Tolerance Principles to Stub-Sill Tank Car Cracking," Proceedings, *6th International Heavy Haul Conference*, Cape Town, South Africa.

Williams, M. R., 1997, "AMF Coiled Tank Car Damage Tolerance Analysis," Design Report 1415, ACF Industries, Inc., St. Charles, MO.

Glossary

- Beach Mark:** Beach marks are striations on the fracture surface of a fatigue crack, perpendicular to the direction of crack growth. In general, they result from variations or irregularities in the magnitudes and load ratios (minimum/maximum) of applied stresses that propagated the crack through the material.
- Clipping:** During typical laboratory simulations, loads measured in the field are applied to the structures they were collected from/for. Due to various test rig limitations, dynamic loads observed in the field are not always recreated precisely in the laboratory. If a load magnitude is reduced during a simulation, it is said to be clipped. A clipped event is reduced in magnitude, but not removed from the spectrum.
- Coherence:** For linear systems, the coherence function can be interpreted as the fractional portion of the mean square value at the response that is contributed by the input at a discrete frequencies. It can be used to measure the strength of the linear relationship between two system vibrations across a bandwidth. The concept behind coherence is similar to that of statistical correlation.
- Compliance:** As it is used here, compliance is essentially a synonym for linear stiffness, or the strain of an elastic body expressed as a function of the force producing the strain. Compliance is used to indicate structural stiffness in three-dimensional space at all measurement locations, rather than specifically along any one axis at any single location.
- Marker Band:** A marker band is an intentional beach mark applied to a test specimen at known intervals, so that crack growth information along the fracture surface may be obtained after testing is completed. In the case of this program, periodic marker bands were applied through constant amplitude cyclic loading, to create features visibly different from those created during the variable amplitude spectrum loading.
- Precrack** The term precrack refers to the cyclic loading of a test specimen to drive cracks from the stress concentrations induced by a preflaw. In the case of this program, constant amplitude loads were used along two axes of the test specimen (longitudinal and vertical) to accomplish this.
- Preflaw:** The term preflaw refers to the mechanical insertion of a flaw into a test specimen in a region of high stress. As the specimen is cyclically loaded, cracks are expected to grow into the material from the stress concentrations induced at the corners of the flaw.

- Rainflow:** For highly irregular variations of load with time, cycle counting techniques have been developed to isolate and define cycles so that Palmgren-Miner cumulative damage theory can be employed. Rainflow cycle counting has been preferred by the railroad industry to count the peaks and valleys of any load history, and produce fatigue spectra for use in stress- and strain-life calculations.
- Spectrum:** A spectrum is a description of a quantity in terms of any function of frequency. In the case of the *AAR Manual of Standards and Recommended Practices*, the term fatigue spectra refers to the histograms of freight car input load data, which are the result of rainflow counting time history data from several over-the-road operating environment tests.
- Transient:** Transient data result from short-duration nonstationary phenomena with a clearly defined beginning and end. Transient actuator response therefore refers to the portion of the actuator response that is not commanded, but is a result of its mechanical limitations. This error is observed as dynamic over- and under-shooting of target values.
- Truncation:** Spectra obtained from field measurements typically contain large numbers of ranges with small magnitudes. Since the number of events generally decreases rapidly as the range magnitude increases, test times can be reduced to a small fraction of full spectra requirements if the small ranges are excluded. This type of test compression is commonly referred to as truncation.

APPENDIX A

Relevant Portions of SwRI 10,000-Mile Tank Car Load Schedule

Section A-I: Loaded Tank VCF Events

Section A-II: Unloaded Tank VCF Events

Section A-III: Loaded Tank LCF Buff Events

Section A-IV: Unloaded Tank LCF Buff Events

Section A-V: Loaded Tank LCF Draft Events

Section A-VI: Unloaded Tank LCF Draft Events

FINAL DRAFT

Section A-I: Loaded Tank VCF Events

FINAL DRAFT

Loaded 100-Ton Tank Car Vertical Coupler Force
10,000-Mile Scaled DTA Load Schedule

Positive = Upward Loading Unloaded/Loaded Ratio = 1.06
"VCF - LVPU"

Fractional Cycle Count	Minimum Load (kips)	Maximum Load (kips)
0.2011	-41.25	61.25
0.2011	-28.75	58.75
0.2011	-18.75	51.25
0.2011	-18.75	48.75
0.2011	3.75	46.25
0.2011	-1.25	46.25
0.2011	-48.75	46.25
0.2011	38.75	41.25
0.2011	-3.75	41.25
0.2011	-13.75	41.25
0.2011	33.75	38.75
0.2011	3.75	38.75
0.2011	-11.25	38.75
0.2011	-21.25	38.75
0.2011	-26.25	38.75
0.2011	-33.75	38.75
0.2011	-36.25	38.75
0.2011	-38.75	38.75
0.2011	-48.75	38.75
0.8045	33.75	36.25
0.2011	31.25	36.25
0.2011	6.25	36.25
0.2011	3.75	36.25
0.4022	-8.75	36.25
0.2011	-13.75	36.25
0.2011	-26.25	36.25
0.2011	-31.25	36.25
2.6145	31.25	33.75
0.2011	26.25	33.75
0.2011	1.25	33.75
0.2011	-1.25	33.75
0.4022	-3.75	33.75
0.2011	-13.75	33.75
0.2011	-18.75	33.75
0.2011	-23.75	33.75
0.2011	-41.25	33.75
1.2067	28.75	31.25
1.0056	26.25	31.25
0.4022	6.25	31.25
1.0056	3.75	31.25
0.2011	-1.25	31.25
0.4022	-3.75	31.25
0.4022	-6.25	31.25
0.2011	-11.25	31.25
0.6033	-13.75	31.25
0.4022	-16.25	31.25
0.2011	-18.75	31.25
0.2011	-23.75	31.25
0.2011	-26.25	31.25
0.2011	-28.75	31.25
0.2011	-31.25	31.25
0.6033	-33.75	31.25
0.2011	-43.75	31.25
18.3015	26.25	28.75
0.6033	23.75	28.75
0.4022	21.25	28.75
0.2011	13.75	28.75
0.2011	6.25	28.75

Fractional Cycle Count	Minimum Load (kips)	Maximum Load (kips)
0.8045	3.75	28.75
0.6033	1.25	28.75
0.4022	-1.25	28.75
0.2011	-6.25	28.75
0.4022	-8.75	28.75
0.2011	-11.25	28.75
0.8045	-16.25	28.75
0.8045	-18.75	28.75
0.4022	-21.25	28.75
0.4022	-23.75	28.75
0.2011	-26.25	28.75
0.4022	-28.75	28.75
0.2011	-31.25	28.75
0.2011	-36.25	28.75
0.2011	-51.25	28.75
15.687	23.75	26.25
7.6424	21.25	26.25
0.2011	18.75	26.25
0.4022	13.75	26.25
1.0056	11.25	26.25
0.4022	8.75	26.25
0.8045	6.25	26.25
1.6089	3.75	26.25
0.6033	1.25	26.25
1.6089	-1.25	26.25
0.8045	-3.75	26.25
1.6089	-6.25	26.25
1.0056	-8.75	26.25
1.2067	-11.25	26.25
0.8045	-13.75	26.25
1.6089	-16.25	26.25
0.6033	-18.75	26.25
0.4022	-21.25	26.25
1.0056	-23.75	26.25
0.4022	-26.25	26.25
0.2011	-28.75	26.25
0.4022	-31.25	26.25
0.2011	-33.75	26.25
38.8153	21.25	23.75
36.8041	18.75	23.75
1.0056	16.25	23.75
0.6033	13.75	23.75
0.6033	11.25	23.75
0.2011	8.75	23.75
2.8156	6.25	23.75
3.0167	3.75	23.75
1.6089	1.25	23.75
0.8045	-1.25	23.75
0.4022	-3.75	23.75
1.0056	-6.25	23.75
0.8045	-8.75	23.75
1.2067	-11.25	23.75
1.0056	-13.75	23.75
1.2067	-16.25	23.75
1.2067	-18.75	23.75
1.0056	-21.25	23.75
0.6033	-23.75	23.75
0.8045	-26.25	23.75
0.4022	-28.75	23.75
0.4022	-31.25	23.75
0.2011	-38.75	23.75
65.7647	18.75	21.25
38.413	16.25	21.25

Fractional Cycle Count	Minimum Load (kips)	Maximum Load (kips)
1.2067	13.75	21.25
5.4301	11.25	21.25
7.6424	8.75	21.25
4.2234	6.25	21.25
5.229	3.75	21.25
2.4134	1.25	21.25
3.419	-1.25	21.25
2.2123	-3.75	21.25
2.0112	-6.25	21.25
4.4245	-8.75	21.25
2.6145	-11.25	21.25
1.81	-13.75	21.25
2.4134	-16.25	21.25
3.0167	-18.75	21.25
0.8045	-21.25	21.25
0.8045	-23.75	21.25
0.2011	-26.25	21.25
0.2011	-38.75	21.25
303.282	16.25	18.75
16.2903	13.75	18.75
22.9272	11.25	18.75
18.9048	8.75	18.75
8.648	6.25	18.75
9.2513	3.75	18.75
11.6647	1.25	18.75
7.6424	-1.25	18.75
7.039	-3.75	18.75
6.2346	-6.25	18.75
5.4301	-8.75	18.75
3.8212	-11.25	18.75
3.0167	-13.75	18.75
2.8156	-16.25	18.75
1.6089	-18.75	18.75
0.4022	-21.25	18.75
0.8045	-23.75	18.75
0.4022	-26.25	18.75
0.6033	-28.75	18.75
0.2011	-31.25	18.75
0.2011	-33.75	18.75
0.2011	-41.25	18.75
346.5218	13.75	16.25
163.5068	11.25	16.25
46.6588	8.75	16.25
34.5918	6.25	16.25
33.3852	3.75	16.25
25.9439	1.25	16.25
25.9439	-1.25	16.25
14.0781	-3.75	16.25
21.1171	-6.25	16.25
14.2792	-8.75	16.25
10.6591	-11.25	16.25
5.8323	-13.75	16.25
9.0502	-16.25	16.25
3.6201	-18.75	16.25
2.0112	-21.25	16.25
1.4078	-23.75	16.25
2.6145	-26.25	16.25
0.6033	-28.75	16.25
0.2011	-31.25	16.25
0.2011	-33.75	16.25
0.2011	-41.25	16.25
441.046	11.25	13.75
407.6609	8.75	13.75

Fractional Cycle Count	Minimum Load (kips)	Maximum Load (kips)
100.9599	6.25	13.75
89.4963	3.75	13.75
58.1223	1.25	13.75
49.0722	-1.25	13.75
41.4298	-3.75	13.75
33.5863	-6.25	13.75
20.916	-8.75	13.75
17.6982	-11.25	13.75
13.877	-13.75	13.75
11.4636	-16.25	13.75
6.4357	-18.75	13.75
2.8156	-21.25	13.75
2.0112	-23.75	13.75
1.0056	-26.25	13.75
0.4022	-28.75	13.75
0.2011	-38.75	13.75
814.7184	8.75	11.25
862.1816	6.25	11.25
292.0195	3.75	11.25
164.7135	1.25	11.25
147.8198	-1.25	11.25
103.1722	-3.75	11.25
85.0718	-6.25	11.25
44.4465	-8.75	11.25
30.7707	-11.25	11.25
18.1004	-13.75	11.25
10.0558	-16.25	11.25
5.4301	-18.75	11.25
3.0167	-21.25	11.25
2.0112	-23.75	11.25
0.4022	-26.25	11.25
0.2011	-28.75	11.25
0.4022	-31.25	11.25
0.2011	-36.25	11.25
0.2011	-38.75	11.25
7358.0073	6.25	8.75
1655.783	3.75	8.75
831.2098	1.25	8.75
552.4639	-1.25	8.75
291.4162	-3.75	8.75
194.2775	-6.25	8.75
94.122	-8.75	8.75
50.48	-11.25	8.75
31.374	-13.75	8.75
18.3015	-16.25	8.75
6.4357	-18.75	8.75
3.2178	-21.25	8.75
1.81	-23.75	8.75
1.81	-26.25	8.75
0.2011	-28.75	8.75
0.2011	-31.25	8.75
0.2011	-33.75	8.75
0.2011	-43.75	8.75
17374.3574	3.75	6.25
13971.8877	1.25	6.25
3534.2004	-1.25	6.25
1142.9387	-3.75	6.25
595.1004	-6.25	6.25
192.0652	-8.75	6.25
101.3621	-11.25	6.25
55.5078	-13.75	6.25
28.5584	-16.25	6.25
8.4468	-18.75	6.25

Fractional Cycle Count	Minimum Load (kips)	Maximum Load (kips)
5.0279	-21.25	6.25
4.2234	-23.75	6.25
1.4078	-26.25	6.25
1.0056	-28.75	6.25
0.2011	-31.25	6.25
0.2011	-46.25	6.25
43753.0508	1.25	3.75
33361.2188	-1.25	3.75
4204.5181	-3.75	3.75
1334.1993	-6.25	3.75
375.6835	-8.75	3.75
149.2276	-11.25	3.75
76.4238	-13.75	3.75
33.3852	-16.25	3.75
16.2903	-18.75	3.75
8.4468	-21.25	3.75
1.6089	-23.75	3.75
0.4022	-26.25	3.75
0.6033	-28.75	3.75
0.2011	-31.25	3.75
0.2011	-38.75	3.75
71885.4688	-1.25	1.25
39722.0977	-3.75	1.25
3416.3469	-6.25	1.25
743.3224	-8.75	1.25
295.8407	-11.25	1.25
122.2781	-13.75	1.25
44.0443	-16.25	1.25
12.4692	-18.75	1.25
5.0279	-21.25	1.25
0.8045	-23.75	1.25
1.2067	-26.25	1.25
0.4022	-28.75	1.25
0.8045	-31.25	1.25
0.4022	-36.25	1.25
44499.3906	-3.75	-1.25
22241.3496	-6.25	-1.25
1412.031	-8.75	-1.25
439.236	-11.25	-1.25
167.1269	-13.75	-1.25
48.2677	-16.25	-1.25
13.2736	-18.75	-1.25
7.039	-21.25	-1.25
3.419	-23.75	-1.25
1.81	-26.25	-1.25
0.4022	-28.75	-1.25
0.4022	-36.25	-1.25
62314.3906	-6.25	-3.75
2115.3315	-8.75	-3.75
561.1119	-11.25	-3.75
222.4336	-13.75	-3.75
44.8487	-16.25	-3.75
18.9048	-18.75	-3.75
6.2346	-21.25	-3.75
1.81	-23.75	-3.75
1.2067	-26.25	-3.75
0.2011	-36.25	-3.75
0.2011	-41.25	-3.75
3547.2729	-8.75	-6.25
878.0697	-11.25	-6.25
179.9983	-13.75	-6.25
46.2565	-16.25	-6.25
11.6647	-18.75	-6.25

Fractional Cycle Count	Minimum Load (kips)	Maximum Load (kips)
3.419	-21.25	-6.25
1.6089	-23.75	-6.25
0.2011	-26.25	-6.25
0.6033	-28.75	-6.25
0.2011	-31.25	-6.25
0.2011	-36.25	-6.25
1031.923	-11.25	-8.75
457.9397	-13.75	-8.75
41.4298	-16.25	-8.75
11.4636	-18.75	-8.75
6.4357	-21.25	-8.75
2.2123	-23.75	-8.75
1.0056	-26.25	-8.75
0.2011	-28.75	-8.75
0.4022	-31.25	-8.75
0.2011	-38.75	-8.75
654.2283	-13.75	-11.25
219.8191	-16.25	-11.25
11.0613	-18.75	-11.25
3.2178	-21.25	-11.25
0.8045	-23.75	-11.25
0.4022	-26.25	-11.25
0.2011	-28.75	-11.25
438.0293	-16.25	-13.75
9.6535	-18.75	-13.75
2.2123	-21.25	-13.75
1.6089	-23.75	-13.75
0.2011	-26.25	-13.75
0.2011	-28.75	-13.75
0.2011	-31.25	-13.75
96.7365	-18.75	-16.25
21.7205	-21.25	-16.25
1.0056	-23.75	-16.25
0.4022	-26.25	-16.25
0.2011	-31.25	-16.25
24.9383	-21.25	-18.75
27.7539	-23.75	-18.75
0.6033	-26.25	-18.75
0.2011	-28.75	-18.75
20.5138	-23.75	-21.25
10.6591	-26.25	-21.25
11.0613	-26.25	-23.75
0.4022	-28.75	-23.75
3.8212	-28.75	-26.25
1.4078	-31.25	-26.25
1.2067	-31.25	-28.75
0.2011	-33.75	-28.75
0.4022	-33.75	-31.25
0.2011	-36.25	-31.25
0.2011	-43.75	-31.25
0.2011	-36.25	-33.75
0.8045	-38.75	-36.25
0.2011	-43.75	-41.25
0.2011	-48.75	-46.25

Section A-II: Unloaded Tank VCF Events

FINAL DRAFT

Unloaded 100-Ton Tank Car Vertical Coupler Force
10,000-Mile Scaled DTA Load Schedule

Positive = Upward Loading Unloaded/Loaded Ratio = 1.06
"VCF - UVPU"

Fractional Cycle Count	Minimum Load (kips)	Maximum Load (kips)
1.2314	-33.75	33.75
1.2314	-11.25	31.25
1.2314	26.25	28.75
1.2314	23.75	28.75
1.2314	-13.75	28.75
1.2314	-18.75	28.75
1.2314	-41.25	28.75
1.2314	18.75	26.25
1.2314	3.75	26.25
2.4628	-6.25	26.25
1.2314	-8.75	26.25
1.2314	-11.25	26.25
1.2314	-13.75	26.25
1.2314	-26.25	26.25
1.2314	21.25	23.75
2.4628	18.75	23.75
1.2314	6.25	23.75
2.4628	3.75	23.75
2.4628	1.25	23.75
1.2314	-1.25	23.75
4.9256	-6.25	23.75
1.2314	-8.75	23.75
3.6942	-11.25	23.75
1.2314	-13.75	23.75
2.4628	-16.25	23.75
2.4628	-18.75	23.75
1.2314	-23.75	23.75
2.4628	16.25	21.25
1.2314	11.25	21.25
4.9256	3.75	21.25
1.2314	1.25	21.25
3.6942	-1.25	21.25
1.2314	-6.25	21.25
2.4628	-8.75	21.25
3.6942	-11.25	21.25
1.2314	-13.75	21.25
2.4628	-16.25	21.25
1.2314	-18.75	21.25
2.4628	-21.25	21.25
1.2314	-26.25	21.25
1.2314	-31.25	21.25
2.4628	16.25	18.75
2.4628	13.75	18.75
2.4628	6.25	18.75
17.2395	3.75	18.75
7.3884	1.25	18.75
8.6198	-1.25	18.75
7.3884	-3.75	18.75
6.157	-6.25	18.75
7.3884	-8.75	18.75
1.2314	-11.25	18.75
2.4628	-13.75	18.75
4.9256	-16.25	18.75
20.9337	13.75	16.25
61.5698	11.25	16.25
23.3965	8.75	16.25
11.0826	6.25	16.25
67.7267	3.75	16.25

Fractional Cycle Count	Minimum Load (kips)	Maximum Load (kips)
23.3965	1.25	16.25
25.8593	-1.25	16.25
12.314	-3.75	16.25
14.7767	-6.25	16.25
16.0081	-8.75	16.25
16.0081	-11.25	16.25
9.8512	-13.75	16.25
6.157	-16.25	16.25
2.4628	-18.75	16.25
2.4628	-21.25	16.25
1.2314	-23.75	16.25
130.5279	11.25	13.75
41.8674	8.75	13.75
35.7105	6.25	13.75
296.7662	3.75	13.75
70.1895	1.25	13.75
43.0988	-1.25	13.75
36.9419	-3.75	13.75
34.4791	-6.25	13.75
29.5535	-8.75	13.75
18.4709	-11.25	13.75
11.0826	-13.75	13.75
8.6198	-16.25	13.75
2.4628	-18.75	13.75
2.4628	-21.25	13.75
1.2314	-23.75	13.75
86.1977	8.75	11.25
385.4267	6.25	11.25
1422.2614	3.75	11.25
325.0883	1.25	11.25
167.4697	-1.25	11.25
130.5279	-3.75	11.25
64.0325	-6.25	11.25
32.0163	-8.75	11.25
32.0163	-11.25	11.25
13.5453	-13.75	11.25
12.314	-16.25	11.25
3.6942	-18.75	11.25
1.2314	-21.25	11.25
1.2314	-26.25	11.25
3029.2319	6.25	8.75
7569.3857	3.75	8.75
1428.4183	1.25	8.75
795.4812	-1.25	8.75
330.0139	-3.75	8.75
145.3046	-6.25	8.75
50.4872	-8.75	8.75
19.7023	-11.25	8.75
20.9337	-13.75	8.75
6.157	-16.25	8.75
2.4628	-18.75	8.75
1.2314	-28.75	8.75
12384.1406	3.75	6.25
14930.665	1.25	6.25
4094.3887	-1.25	6.25
1036.8346	-3.75	6.25
264.7499	-6.25	6.25
89.8918	-8.75	6.25
66.4953	-11.25	6.25
18.4709	-13.75	6.25
4.9256	-16.25	6.25
2.4628	-18.75	6.25
44421.3477	1.25	3.75

Fractional Cycle Count	Minimum Load (kips)	Maximum Load (kips)
21567.8848	-1.25	3.75
3644.9294	-3.75	3.75
662.4905	-6.25	3.75
190.8662	-8.75	3.75
55.4128	-11.25	3.75
18.4709	-13.75	3.75
6.157	-16.25	3.75
2.4628	-18.75	3.75
1.2314	-21.25	3.75
14385.1572	-1.25	1.25
6490.6836	-3.75	1.25
1006.0498	-6.25	1.25
369.4185	-8.75	1.25
98.5116	-11.25	1.25
24.6279	-13.75	1.25
4.9256	-16.25	1.25
5357.7998	-3.75	-1.25
3372.791	-6.25	-1.25
810.258	-8.75	-1.25
136.6849	-11.25	-1.25
19.7023	-13.75	-1.25
7.3884	-16.25	-1.25
1.2314	-33.75	-1.25
3234.875	-6.25	-3.75
1955.4554	-8.75	-3.75
189.6348	-11.25	-3.75
7.3884	-13.75	-3.75
4.9256	-16.25	-3.75
1225.2382	-8.75	-6.25
158.85	-11.25	-6.25
23.3965	-13.75	-6.25
8.6198	-16.25	-6.25
35.7105	-11.25	-8.75
17.2395	-13.75	-8.75
3.6942	-16.25	-8.75
11.0826	-13.75	-11.25
2.4628	-16.25	-11.25
1.2314	-21.25	-11.25
2.4628	-16.25	-13.75
1.2314	-18.75	-13.75
1.2314	-18.75	-16.25
1.2314	-23.75	-16.25

FINAL DRAFT

Section A-III: Loaded Tank LCF Buff Events

FINAL DRAFT

Loaded 100-Ton Tank Car Longitudinal Buff Coupler Force
10,000-Mile Scaled DTA Load Schedule

Negative = Buff Loading Unloaded/Loaded Ratio = 1.06
"LCF - LLBUF"

Fractional Cycle Count	Minimum Load (kips)	Maximum Load (kips)
0.4074	-430	0
0.8149	-370	0
178.4529	-50	0
98.801	-70	0
71.096	-90	0
17.1119	-150	0
0.8149	-330	0
44.6132	-110	0
12.6302	-170	0
4.4817	-210	0
2.6483	-250	0
0.2037	-470	0
1280.7458	-20	0
243.4374	-40	0
130.1728	-60	0
11.0005	-180	0
3.0557	-220	0
0.2037	-460	0
0.4074	-480	0
12.4265	-500	0
25.0567	-130	0
3.2594	-270	0
2.0371	-290	0
51.9469	-100	0
456.5216	-30	0
3.8706	-230	0
0.4074	-310	0
0.4074	-350	0
14.6674	-160	0
1037.512	-10	0
7.7411	-190	0
0.2037	-390	0
0.4074	-410	0
25.0567	-140	0
1.0186	-280	0
0.4074	-380	0
0.2037	-530	0
0.2037	-830	0
5.9077	-200	0
1.6297	-240	0
0.6111	-320	0
94.1156	-80	0
33.409	-120	0
1.0186	-260	0
0.2037	-490	0
0.2037	-300	0
0.4074	-340	0
0.2037	-550	0
0.2037	-400	0
658.8089	-30	-10
320.2374	-50	-10
87.5967	-70	-10
35.8535	-90	-10
11.4079	-110	-10
8.1485	-130	-10
4.0743	-150	-10
1.6297	-170	-10
1.0186	-190	-10
0.8149	-210	-10

Fractional Cycle Count	Minimum Load (kips)	Maximum Load (kips)
0.4074	-230	-10
0.4074	-270	-10
418.4272	-40	-20
130.1728	-60	-20
54.3915	-80	-20
25.4642	-100	-20
9.7782	-120	-20
5.5003	-140	-20
2.2408	-160	-20
2.0371	-180	-20
0.4074	-200	-20
0.2037	-220	-20
0.2037	-260	-20
0.4074	-280	-20
0.2037	-300	-20
0.8149	-500	-20
322.0708	-50	-30
133.0248	-70	-30
32.1867	-90	-30
9.982	-110	-30
3.6668	-130	-30
2.6483	-150	-30
0.4074	-170	-30
0.6111	-190	-30
0.2037	-210	-30
0.2037	-230	-30
0.2037	-250	-30
0.2037	-290	-30
0.2037	-450	-30
277.4576	-60	-40
81.4853	-80	-40
31.1681	-100	-40
13.2414	-120	-40
6.3151	-140	-40
1.6297	-160	-40
1.6297	-180	-40
0.4074	-200	-40
0.6111	-220	-40
0.8149	-240	-40
0.2037	-300	-40
0.4074	-500	-40
142.1919	-70	-50
68.6514	-90	-50
10.7968	-110	-50
6.7225	-130	-50
2.6483	-150	-50
1.0186	-170	-50
0.2037	-190	-50
0.4074	-210	-50
0.2037	-230	-50
0.6111	-250	-50
179.2677	-80	-60
40.3352	-100	-60
15.4822	-120	-60
4.6854	-140	-60
2.2408	-160	-60
0.4074	-180	-60
0.4074	-200	-60
0.2037	-220	-60
0.2037	-240	-60
0.2037	-260	-60
0.2037	-280	-60
0.2037	-300	-60

Fractional Cycle Count	Minimum Load (kips)	Maximum Load (kips)
0.2037	-340	-60
0.2037	-360	-60
0.2037	-380	-60
0.2037	-500	-60
76.1888	-90	-70
35.0387	-110	-70
7.5374	-130	-70
2.852	-150	-70
1.2223	-170	-70
0.6111	-190	-70
0.2037	-210	-70
0.4074	-230	-70
0.2037	-290	-70
102.2641	-100	-80
23.8345	-120	-80
4.278	-140	-80
2.4446	-160	-80
0.4074	-180	-80
0.4074	-200	-80
0.2037	-220	-80
0.6111	-240	-80
0.2037	-260	-80
0.4074	-280	-80
0.2037	-360	-80
29.7421	-110	-90
14.8711	-130	-90
2.852	-150	-90
2.4446	-170	-90
1.0186	-190	-90
0.2037	-210	-90
0.2037	-230	-90
0.4074	-250	-90
41.5575	-120	-100
8.9634	-140	-100
2.0371	-160	-100
0.8149	-180	-100
0.2037	-200	-100
0.4074	-220	-100
0.2037	-260	-100
0.2037	-280	-100
0.2037	-320	-100
0.2037	-340	-100
11.8154	-130	-110
4.8891	-150	-110
2.2408	-170	-110
0.4074	-190	-110
0.2037	-210	-110
0.4074	-230	-110
0.2037	-250	-110
0.2037	-270	-110
0.2037	-310	-110
13.2414	-140	-120
3.2594	-160	-120
1.426	-180	-120
0.4074	-200	-120
1.0186	-240	-120
0.6111	-260	-120
0.4074	-280	-120
0.6111	-300	-120
0.2037	-320	-120
7.13	-150	-130
3.8706	-170	-130
0.2037	-190	-130

Fractional Cycle Count	Minimum Load (kips)	Maximum Load (kips)
0.6111	-210	-130
0.2037	-250	-130
0.4074	-270	-130
0.2037	-290	-130
0.2037	-370	-130
6.9263	-160	-140
2.0371	-180	-140
0.8149	-200	-140
0.6111	-220	-140
0.2037	-240	-140
0.4074	-260	-140
0.6111	-280	-140
0.2037	-320	-140
0.2037	-500	-140
4.0743	-170	-150
1.0186	-190	-150
0.8149	-210	-150
0.4074	-230	-150
0.2037	-250	-150
0.2037	-290	-150
0.4074	-310	-150
4.6854	-180	-160
1.426	-200	-160
0.4074	-220	-160
0.6111	-240	-160
0.4074	-260	-160
0.4074	-280	-160
0.4074	-300	-160
0.2037	-380	-160
0.2037	-500	-160
1.2223	-190	-170
1.426	-210	-170
0.6111	-230	-170
0.2037	-250	-170
3.4631	-200	-180
1.426	-220	-180
0.4074	-260	-180
0.4074	-280	-180
0.2037	-300	-180
0.2037	-320	-180
0.2037	-420	-180
1.426	-210	-190
1.2223	-230	-190
1.2223	-250	-190
0.2037	-370	-190
0.2037	-430	-190
3.4631	-220	-200
0.8149	-240	-200
0.6111	-260	-200
0.4074	-340	-200
0.8149	-230	-210
0.6111	-250	-210
0.4074	-270	-210
0.2037	-310	-210
0.4074	-350	-210
3.2594	-240	-220
1.0186	-260	-220
0.2037	-280	-220
0.2037	-320	-220
0.2037	-340	-220
0.2037	-250	-230
0.6111	-270	-230
0.4074	-290	-230

Fractional Cycle Count	Minimum Load (kips)	Maximum Load (kips)
2.0371	-260	-240
0.6111	-280	-240
0.2037	-300	-240
0.2037	-320	-240
0.2037	-400	-240
0.2037	-420	-240
1.6297	-280	-260
0.8149	-300	-260
0.4074	-320	-260
0.2037	-340	-260
0.2037	-380	-260
0.2037	-290	-270
0.2037	-370	-270
1.6297	-300	-280
0.8149	-320	-280
0.2037	-360	-280
0.2037	-380	-280
0.6111	-310	-290
0.6111	-320	-300
0.6111	-340	-300
0.2037	-360	-300
0.2037	-330	-310
0.2037	-350	-310
0.2037	-340	-320
0.4074	-360	-320
0.2037	-380	-320
0.4074	-400	-320
0.2037	-390	-330
1.0186	-360	-340
0.2037	-380	-340
0.2037	-400	-340
0.2037	-420	-340
0.4074	-380	-360
0.2037	-400	-360
0.2037	-420	-360
0.2037	-440	-360
0.4074	-400	-380
0.4074	-420	-380
0.2037	-460	-380
0.2037	-420	-400
0.4074	-500	-400
0.2037	-440	-420
0.2037	-460	-440
0.2037	-480	-440
0.4074	-480	-460
0.6111	-500	-460
0.2037	-500	-480

FINAL DRAFT

Section A-IV: Unloaded Tank LCF Buff Events

FINAL DRAFT

Unloaded 100-Ton Tank Car Longitudinal Buff Coupler Force
10,000-Mile Scaled DTA Load Schedule

Negative = Buff Loading Unloaded/Loaded Ratio = 1.06
"LCF - ULBUF"

Fractional Cycle Count	Minimum Load (kips)	Maximum Load (kips)
1.8779	-340	0
5.0077	-270	0
1.2519	-450	0
10.0153	-160	0
4.3817	-180	0
2.5038	-310	0
35.0536	-120	0
2.5038	-220	0
9.3894	-190	0
11.8932	-210	0
10.6413	-230	0
0.626	-590	0
0.626	-650	0
3.7557	-290	0
2.5038	-350	0
1.2519	-430	0
14.397	-140	0
0.626	-400	0
173.3903	-70	0
95.1456	-90	0
50.0766	-130	0
31.2979	-150	0
18.1528	-170	0
5.6336	-250	0
3.1298	-390	0
307.3453	-20	0
169.0086	-40	0
107.6648	-60	0
71.9852	-80	0
56.3362	-100	0
0.626	-200	0
0.626	-260	0
301.7117	-50	0
59.466	-110	0
878.8449	-10	0
1.2519	-370	0
1.8779	-410	0
650.3703	-30	0
3.1298	-330	0
0.626	-320	0
0.626	-630	0
0.626	-240	0
1.2519	-280	0
1086.6628	-30	-10
592.7821	-50	-10
148.978	-70	-10
66.3515	-90	-10
30.6719	-110	-10
11.8932	-130	-10
6.2596	-150	-10
3.1298	-170	-10
6.2596	-190	-10
3.1298	-210	-10
1.8779	-230	-10
0.626	-250	-10
0.626	-290	-10
440.0484	-40	-20
134.581	-60	-20
58.84	-80	-20

Fractional Cycle Count	Minimum Load (kips)	Maximum Load (kips)
23.7864	-100	-20
8.1375	-120	-20
0.626	-140	-20
1.2519	-160	-20
0.626	-180	-20
513.2855	-50	-30
224.7189	-70	-30
63.2217	-90	-30
11.2672	-110	-30
10.0153	-130	-30
5.6336	-150	-30
1.8779	-170	-30
1.2519	-190	-30
1.2519	-210	-30
0.626	-230	-30
0.626	-250	-30
0.626	-270	-30
0.626	-430	-30
299.8338	-60	-40
67.6035	-80	-40
16.9009	-100	-40
8.1375	-120	-40
0.626	-140	-40
0.626	-180	-40
0.626	-200	-40
0.626	-220	-40
214.7036	-70	-50
105.1609	-90	-50
19.4047	-110	-50
12.5192	-130	-50
2.5038	-150	-50
3.1298	-170	-50
3.1298	-190	-50
0.626	-210	-50
0.626	-230	-50
0.626	-250	-50
0.626	-330	-50
0.626	-590	-50
102.0311	-80	-60
26.9162	-100	-60
5.6336	-120	-60
3.1298	-140	-60
0.626	-160	-60
0.626	-180	-60
0.626	-200	-60
60.092	-90	-70
43.8171	-110	-70
25.6643	-130	-70
1.2519	-150	-70
0.626	-170	-70
1.2519	-190	-70
0.626	-210	-70
0.626	-290	-70
63.2217	-100	-80
12.5192	-120	-80
1.8779	-140	-80
1.2519	-160	-80
0.626	-180	-80
0.626	-200	-80
0.626	-220	-80
0.626	-280	-80
0.626	-320	-80
43.8171	-110	-90

Fractional Cycle Count	Minimum Load (kips)	Maximum Load (kips)
32.5498	-130	-90
4.3817	-150	-90
2.5038	-170	-90
1.8779	-190	-90
1.2519	-210	-90
38.8094	-120	-100
6.8855	-140	-100
1.2519	-160	-100
1.2519	-180	-100
0.626	-280	-100
21.2826	-130	-110
10.0153	-150	-110
0.626	-190	-110
0.626	-210	-110
1.8779	-230	-110
0.626	-310	-110
4.3817	-140	-120
0.626	-160	-120
1.2519	-180	-120
1.2519	-200	-120
1.2519	-260	-120
5.6336	-150	-130
5.6336	-170	-130
1.8779	-190	-130
1.2519	-210	-130
1.2519	-230	-130
0.626	-250	-130
0.626	-350	-130
2.5038	-160	-140
1.2519	-180	-140
0.626	-200	-140
1.2519	-220	-140
0.626	-260	-140
0.626	-300	-140
0.626	-320	-140
3.1298	-170	-150
3.7557	-190	-150
1.2519	-210	-150
1.2519	-230	-150
0.626	-250	-150
1.2519	-180	-160
0.626	-200	-160
0.626	-260	-160
0.626	-280	-160
2.5038	-190	-170
5.6336	-210	-170
0.626	-230	-170
0.626	-270	-170
0.626	-290	-170
0.626	-310	-170
0.626	-370	-170
5.0077	-200	-180
1.2519	-220	-180
3.7557	-210	-190
2.5038	-230	-190
0.626	-250	-190
1.2519	-270	-190
0.626	-290	-190
1.2519	-310	-190
1.8779	-220	-200
1.2519	-240	-200
1.2519	-260	-200
0.626	-300	-200

Fractional Cycle Count	Minimum Load (kips)	Maximum Load (kips)
1.2519	-230	-210
1.2519	-250	-210
0.626	-310	-210
0.626	-350	-210
1.2519	-240	-220
0.626	-400	-220
0.626	-250	-230
1.2519	-270	-230
0.626	-290	-230
0.626	-330	-230
0.626	-410	-230
0.626	-260	-240
0.626	-280	-240
1.2519	-270	-250
0.626	-290	-250
1.2519	-330	-250
0.626	-450	-250
0.626	-280	-260
1.2519	-300	-260
1.2519	-290	-270
0.626	-310	-270
1.2519	-350	-270
0.626	-390	-270
1.8779	-300	-280
0.626	-320	-280
0.626	-340	-280
0.626	-320	-300
0.626	-330	-310
0.626	-350	-310
0.626	-340	-320
0.626	-380	-320
0.626	-390	-330
0.626	-370	-350
1.2519	-380	-360
0.626	-400	-380

Section A-V: Loaded Tank LCF Draft Events

FINAL DRAFT

Loaded 100-Ton Tank Car Longitudinal Draft Coupler Force
10,000-Mile Scaled DTA Load Schedule

Positive = Draft Loading Unloaded/Loaded Ratio = 1.06
"LCF - LLDFT"

Fractional Cycle Count	Minimum Load (kips)	Maximum Load (kips)
0.2037	0	410
0.2037	350	390
0.4074	350	370
0.2037	0	370
0.2037	330	350
0.2037	250	350
1.0186	0	350
0.8149	310	330
1.426	290	330
0.4074	270	330
0.6111	250	330
0.6111	230	330
0.2037	210	330
0.2037	150	330
0.2037	110	330
1.6297	0	330
3.6668	290	310
5.0928	270	310
1.0186	250	310
0.2037	230	310
0.8149	210	310
0.2037	190	310
0.2037	150	310
0.2037	130	310
0.2037	110	310
0.2037	0	310
12.0191	280	300
5.0928	260	300
2.4446	240	300
0.2037	220	300
0.4074	200	300
0.2037	180	300
0.6111	160	300
0.2037	100	300
0.8149	80	300
1.0186	60	300
2.6483	40	300
2.2408	20	300
14.8711	0	300
5.2965	270	290
7.13	250	290
4.278	230	290
1.0186	210	290
0.6111	170	290
0.4074	150	290
0.2037	130	290
0.4074	110	290
0.2037	30	290
2.0371	0	290
7.13	260	280
2.2408	240	280
0.8149	220	280
0.2037	200	280
0.2037	140	280
0.2037	60	280
0.4074	40	280
0.2037	20	280
1.0186	0	280

Fractional Cycle Count	Minimum Load (kips)	Maximum Load (kips)
22.6122	250	270
14.4636	230	270
5.5003	210	270
3.0557	190	270
1.0186	170	270
0.8149	150	270
0.4074	130	270
1.2223	110	270
0.4074	30	270
0.6111	10	270
3.8706	0	270
4.4817	240	260
1.8334	220	260
0.6111	200	260
0.6111	180	260
0.2037	140	260
0.2037	120	260
0.2037	80	260
0.2037	60	260
0.2037	40	260
1.2223	0	260
33.0016	230	250
36.6684	210	250
9.982	190	250
4.4817	170	250
1.426	150	250
1.6297	130	250
2.4446	110	250
0.8149	90	250
0.2037	70	250
0.6111	50	250
0.6111	30	250
1.0186	10	250
6.1114	0	250
5.704	220	240
1.0186	200	240
0.8149	180	240
0.2037	120	240
0.2037	100	240
0.4074	60	240
0.6111	40	240
0.4074	20	240
2.2408	0	240
56.2249	210	230
51.7432	190	230
18.7416	170	230
6.5188	150	230
4.0743	130	230
7.3337	110	230
2.4446	90	230
1.6297	70	230
1.6297	50	230
0.8149	30	230
0.8149	10	230
6.7225	0	230
8.1485	200	220
2.0371	180	220
1.2223	160	220
0.2037	140	220
0.4074	100	220
0.8149	60	220
0.2037	40	220
0.4074	20	220

Fractional Cycle Count	Minimum Load (kips)	Maximum Load (kips)
4.4817	0	220
147.2847	190	210
110.4126	170	210
34.0201	150	210
13.6488	130	210
13.6488	110	210
4.4817	90	210
2.6483	70	210
3.6668	50	210
4.278	30	210
1.2223	10	210
8.3522	0	210
9.5745	180	200
4.4817	160	200
1.8334	140	200
0.2037	120	200
0.8149	100	200
0.6111	80	200
0.4074	60	200
0.2037	40	200
0.4074	20	200
7.7411	0	200
283.9764	170	190
254.438	150	190
60.0954	130	190
28.9273	110	190
11.0005	90	190
5.2965	70	190
4.0743	50	190
4.278	30	190
3.0557	10	190
13.6488	0	190
15.6859	160	180
1.6297	140	180
2.2408	120	180
0.8149	100	180
1.0186	80	180
1.0186	60	180
0.6111	40	180
1.2223	20	180
11.0005	0	180
673.0689	150	170
549.2112	130	170
88.2079	110	170
16.5008	90	170
6.1114	70	170
6.3151	50	170
3.6668	30	170
4.8891	10	170
13.4451	0	170
22.6122	140	160
6.1114	120	160
2.6483	100	160
3.0557	80	160
1.2223	60	160
1.8334	40	160
1.426	20	160
19.5565	0	160
1309.0619	130	150
495.0234	110	150
51.3358	90	150
10.3894	70	150
7.5374	50	150

Fractional Cycle Count	Minimum Load (kips)	Maximum Load (kips)
8.7597	30	150
5.5003	10	150
24.0382	0	150
49.5023	120	140
16.5008	100	140
6.9263	80	140
5.0928	60	140
4.6854	40	140
0.8149	20	140
26.4827	0	140
810.3717	110	130
217.1584	90	130
36.0573	70	130
15.4822	50	130
16.0934	30	130
11.6117	10	130
28.9273	0	130
62.54	100	120
17.5193	80	120
10.1857	60	120
10.7968	40	120
4.4817	20	120
37.2795	0	120
321.2559	90	110
187.2126	70	110
44.6132	50	110
31.7793	30	110
24.2419	10	110
49.7061	0	110
119.376	80	100
41.9649	60	100
28.3162	40	100
16.0934	20	100
74.3554	0	100
382.3699	70	90
234.0666	50	90
87.5967	30	90
55.2063	10	90
90.4487	0	90
246.4931	60	80
81.0779	40	80
54.5952	20	80
124.0614	0	80
698.3293	50	70
551.6557	30	70
190.472	10	70
163.3781	0	70
583.8424	40	60
170.1006	20	60
197.8057	0	60
2044.467	30	50
1281.7643	10	50
209.4173	0	50
2134.7122	20	40
349.9795	0	40
2415.8364	10	30
482.5969	0	30
1925.7021	0	20
864.3557	0	10

Section A-VI: Unloaded Tank LCF Draft Events

Unloaded 100-Ton Tank Car Longitudinal Draft Coupler Force
10,000-Mile Scaled DTA Load Schedule

Positive = Draft Loading Unloaded/Loaded Ratio = 1.06
"LCF - ULDFT"

Fractional Cycle Count	Minimum Load (kips)	Maximum Load (kips)
1.2519	280	300
0.626	0	300
1.2519	0	270
1.2519	220	260
0.626	180	260
1.2519	0	260
0.626	0	250
2.5038	220	240
0.626	60	240
0.626	20	240
1.2519	0	240
3.7557	210	230
1.8779	190	230
0.626	170	230
0.626	90	230
0.626	10	230
4.3817	0	230
5.6336	200	220
0.626	120	220
0.626	0	220
5.0077	190	210
0.626	110	210
1.2519	10	210
4.3817	0	210
6.8855	180	200
3.7557	160	200
1.8779	140	200
1.2519	80	200
3.1298	0	200
2.5038	170	190
1.8779	150	190
0.626	130	190
2.5038	110	190
1.2519	90	190
1.8779	70	190
0.626	50	190
0.626	30	190
1.2519	10	190
10.0153	0	190
14.397	160	180
3.1298	140	180
1.2519	120	180
0.626	100	180
0.626	40	180
1.2519	20	180
11.8932	0	180
18.1528	150	170
6.8855	130	170
3.1298	110	170
2.5038	90	170
0.626	70	170
1.2519	50	170
1.8779	30	170
2.5038	10	170
10.0153	0	170
15.023	140	160
5.0077	120	160
1.8779	100	160

Fractional Cycle Count	Minimum Load (kips)	Maximum Load (kips)
1.2519	80	160
1.8779	60	160
0.626	40	160
0.626	20	160
15.023	0	160
17.5268	130	150
23.7864	110	150
10.0153	90	150
3.1298	70	150
1.8779	50	150
2.5038	30	150
5.0077	10	150
25.6643	0	150
22.5345	120	140
11.2672	100	140
7.5115	80	140
3.7557	60	140
5.0077	40	140
1.2519	20	140
23.1604	0	140
78.8707	110	130
62.5958	90	130
20.0307	70	130
18.7787	50	130
13.7711	30	130
10.0153	10	130
38.8094	0	130
51.3285	100	120
20.6566	80	120
13.1451	60	120
6.8855	40	120
9.3894	20	120
36.3056	0	120
160.2452	90	110
159.6193	70	110
61.3439	50	110
38.1834	30	110
27.5421	10	110
60.7179	0	110
142.0924	80	100
52.5805	60	100
35.6796	40	100
19.4047	20	100
58.2141	0	100
349.2845	70	90
251.0091	50	90
99.5273	30	90
77.6188	10	90
92.0158	0	90
445.682	60	80
142.0924	40	80
60.092	20	80
103.2831	0	80
959.5935	50	70
575.2553	30	70
243.4976	10	70
142.0924	0	70
1206.2209	40	60
184.0316	20	60
155.2376	0	60
2242.1812	30	50
1484.7722	10	50
194.047	0	50

Fractional Cycle Count	Minimum Load (kips)	Maximum Load (kips)
1039.7161	20	40
233.4823	0	40
1671.3076	10	30
299.8338	0	30
492.0029	0	20
1439.7032	0	10

APPENDIX B

Full-Scale Damage Tolerance Test Crack Indication Log

Section B-I: B-End Left Crack Indications

Section B-II: B-End Right Crack Indications

Section B-III: A-End Left Crack Indications

Section B-IV: A-End Right Crack Indications

FINAL DRAFT

Section B-I: B-End Left Crack Indications

B-End Left Critical Region Crack Lengths
All Measurements in Inches

SPECTRUM MILES	A (BL)	B (BL)	H (BL)	I (BL)	J (BL)	S (BL)	V (BL)	Z (BL)	AA (BL)	AC (BL)
	preflaw	preflaw								
0 (after precrack)	0.14?	0.14?								
10,000	0.14?	0.14?	>>	3.35*						
20,000	0.14?	0.14?	2.25*	1.50						
30,000	0.14?	0.14?	2.25*	1.50						
40,000	0.14?	0.14?	2.26*	1.50						
50,000	0.14?	0.14?	2.28*	1.50						
60,000	0.14?	0.14?	2.28*	1.50						
70,000	0.14?	0.14?	2.28*	1.50						
80,000										
100,000	--	--	2.25*	1.46						
120,000	--	--		1.48						
140,000	--	--		1.48		0.20?				
160,000	--	--		1.51		--				
180,000	--	--		1.52		0.20?	2.23?			
200,000	--	--		1.52		--	2.23?			
200,000	--	--	2.25*	1.59	0.39	--	2.23?			
210,000	--	--		1.59	0.39	--	2.23?	0.22		
220,000	--	--		1.61	0.39	--	2.83?~	0.24		
230,000	--	--		1.61	0.39	--	2.83?	0.31	0.20	
240,000	--	--		1.61	0.39	--	2.83?	0.31	--	
250,000	--	--		1.61	0.39	--	2.83?	0.34	--	
260,000	--	--		1.61	0.39	--	2.83?	0.34	--	0.13
270,000	--	--		1.61	0.39	--	2.83?	0.34	--	0.20
280,000	--	--		1.61	0.39	--	2.83?	0.41	--	0.20
290,000	--	--		1.61	0.39	--	2.83?	0.41	--	0.20
300,000	--	--		1.61	0.39	--	2.83?	0.43	--	0.23
300,000	x	x	2.30	1.61	0.35	0.16	2.75+	0.33	0.30	0.29

LEGEND	
?	not certain crack exists (typically in weld toe)
*	unpolished for measurement (when first found)
--	penetrant did not pick up (measurement attempted)
>>	combined measurement (with adjacent crack)
~	new reference mark (after a test hiatus)
(blank)	no measurement was made
x	no crack was discernable
()	measurement was approximated
+	crack extends beyond measurement

NOTES	
-	many cracks in weld toes, not certain of existence
-	uncertainty varies from +/- 0.01 to 0.05 inches, depending on location
-	no preload on inspection after 70,000 simulated miles
-	three month hiatus after 200,000 miles
-	second inspection at 300,000 miles with fiber scope and preload
-	cracks suspected from preflaws denoted by 'preflaw' at top
-	cracks opened up for fractographic analysis denoted by 'fracto' at top

FINAL DRAFT

Section B-II: B-End Right Crack Indications

FINAL DRAFT

B-End Right Critical Region Crack Lengths
All Measurements in Inches

SPECTRUM MILES	P (BR)	Q (BR)	W (BR)	X (BR)	Y (BR)	AD (BR)
0 (after precrack)						
10,000						
20,000						
30,000						
40,000						
50,000						
60,000						
70,000						
80,000						
100,000						
120,000	1.00?*					
140,000	1.50?*					
160,000	1.50?*					
180,000	1.50?*		1.50?	1.30?		
200,000	1.50?*		1.50?	1.30?		
200,000	1.85?*-				0.12*	
210,000		0.14	1.93?~	1.32?~	0.12*	
220,000		0.14	1.93?	1.32?	0.12*	
230,000		0.20	1.93?	1.32?	0.12*	
240,000			1.93?	1.32?	0.12*	
250,000			1.93?	1.32?	0.23?*	
260,000			1.93?	1.39?	0.23?*	0.20
270,000			1.93?	1.39?	0.23?*	0.20
280,000			1.93?	1.39?	0.23?*	0.45
290,000			1.93?	1.39?	1.05?*	0.60
300,000			1.95?	1.39?	1.10?*	0.61
300,000	x	0.18	x	1.11	x	0.38

LEGEND	
?	not certain crack exists (typically in weld toe)
*	unpolished for measurement (when first found)
-	penetrant did not pick up (measurement attempted)
>>	combined measurement (with adjacent crack)
-	new reference mark (after a test hiatus)
(blank)	no measurement was made
x	no crack was discernable
()	measurement was approximated
+	crack extends beyond measurement

NOTES	
-	many cracks in weld toes, not certain of existence
-	uncertainty varies from +/- 0.01 to 0.05 inches, depending on location
-	no preload on inspection after 70,000 simulated miles
-	three month hiatus after 200,000 miles
-	second inspection at 300,000 miles with fiber scope and preload
-	cracks suspected from preflaws denoted by 'preflaw' at top
-	cracks opened up for fractographic analysis denoted by 'fracto' at top

FINAL DRAFT

Section B-III: A-End Left Crack Indications

FINAL DRAFT

A-End Left Critical Region Crack Lengths
All Measurements in Inches

SPECTRUM MILES	C (AL)	D (AL)	E (AL)	F (AL)	K (AL)	L (AL)	M (AL)	R (AL)
	Preflaw	preflaw			fracto	fracto		fracto
0 (after precrack)	0.35*	0.16	1.30*	<<				
10,000	0.36*	0.17	1.20*	<<	>>	1.35*	2.95?*	
20,000	0.28	0.17	1.08	<<	>>	1.25	2.90?*	
30,000	0.30	0.22	1.07	<<	>>	1.28	3.00?*	
40,000	0.30	0.22	1.07	<<	>>	1.29	3.00?*	
50,000	0.30	0.22	1.07	<<	>>	1.29	3.00?*	
60,000	0.30	0.22	1.07	<<	>>	1.29	3.00?*	
70,000	0.30	0.22	1.07	<<	>>	1.32	3.08?*	
80,000	0.23	0.18	0.98	0.87?*	>>	1.85	1.00?*	
100,000	0.27	0.20	1.04	3.17?*	>>	1.21	1.00?*	
120,000	0.27	0.21	--	--	>>	1.33	1.00?*	0.11*
140,000	0.27	0.21	1.04	3.42?*	0.10	1.28	1.00?*	0.14
160,000	0.35	0.21	1.04	--	0.10	1.28	1.00?*	0.14
180,000	0.35	0.21	1.04	3.42?*	0.10	1.28	1.00?*	0.14
200,000	0.35	0.21	1.04	--	0.10	1.28	--	0.14
200,000	0.35	0.21	1.07	--	0.10	1.28		0.14
210,000	0.35	0.21	1.07	--	0.10	1.28		0.14
220,000	0.35	--	1.07	--	--	1.28		0.14
230,000	0.35	0.21	1.07	3.99?*	--	1.28		0.19
240,000	0.35	0.21	1.07	3.99?*	--	1.28		0.19
250,000	0.35	0.21	1.07	3.99?*	--	1.28		0.19
260,000	0.38	0.21	1.07	3.99?*	--	1.28		0.27
270,000	0.38	0.21	1.07	3.99?*	--	1.28		0.30
280,000	0.38	0.21	1.07	3.99?*	--	1.28		0.31
290,000	0.38	0.21	1.07	4.39?*	--	1.28		0.34
300,000	0.38	0.21	1.07	4.39?*	--	1.28		0.36
300,000	0.37	0.23	1.05	1.70	0.15	1.32	(5-3/8)	0.31

LEGEND:	
?	not certain crack exists (typically in weld toe)
*	unpolished for measurement (when first found)
--	penetrant did not pick up (measurement attempted)
>>	combined measurement (with adjacent crack)
-	new reference mark (after a test hiatus)
(blank)	no measurement was made
X	no crack was discernable
()	measurement was approximated
+	crack extends beyond measurement

NOTES:	
-	many cracks in weld toes, not certain of existence
-	uncertainty varies from +/- 0.01 to 0.05 inches, depending on location
-	no preload on inspection after 70,000 simulated miles
-	three month hiatus after 200,000 miles
-	second inspection at 300,000 miles with fiber scope and preload
-	cracks suspected from preflaws denoted by 'preflaw' at top
-	cracks opened up for fractographic analysis denoted by 'fracto' at top

FINAL DRAFT

Section B-IV: A-End Right Crack Indications

FINAL DRAFT

A-End Right Critical Region Crack Lengths
All Measurements in Inches

SPECTRUM MILES	G (AR)	N (AR)	O (AR)	T (AR)	U (AR)	AB (AR)
	preflaw					
0 (after precrack)	0.12					
10,000	0.12					
20,000	0.13	0.63	0.34*			
30,000	0.13		0.41			
40,000	0.13		0.41			
50,000	0.13		0.42			
60,000	0.13		0.42			
70,000	0.13		0.44			
80,000						
100,000	--		0.46			
120,000	--		0.52			
140,000	--		0.52			
160,000	--		0.52			
180,000	--		0.52	2.09?*	0.97?*	
200,000	--		0.52	2.09?	0.97?	
200,000	--		0.52	1.75?~	1.50?~	
210,000	--		0.56	1.75?	1.50?	
220,000	--		0.61	1.84?	1.50?	
230,000	--		0.65	1.84?	1.50?	0.34
240,000	--		0.65	1.84?	1.50?	0.34
250,000	--		0.67	1.84?	1.50?	0.34
260,000	--		0.69	1.87?	1.52?	0.34
270,000	--		0.69	1.87?	1.52?	0.34
280,000	--		0.72	1.87?	1.52?	0.34
290,000	--		0.74	1.87?	1.52?	0.34
300,000	--		0.75	1.87?	1.52?	0.34
300,000	0.12	0.63	0.78	(3-3/8)	x	0.28

LEGEND:	
?	not certain crack exists (typically in weld toe)
*	unpolished for measurement (when first found)
--	penetrant did not pick up (measurement attempted)
>>	combined measurement (with adjacent crack)
-	new reference mark (after a test hiatus)
(blank)	no measurement was made
X	no crack was discernable
()	measurement was approximated
+	crack extends beyond measurement

NOTES:	
-	many cracks in weld toes, not certain of existence
-	Uncertainty varies from +/- 0.01 to 0.05 inches, depending on location
-	no preload on inspection after 70,000 simulated miles
-	three month hiatus after 200,000 miles
-	Second inspection at 300,000 miles with fiber scope and preload
-	cracks suspected from preflaws denoted by 'preflaw' at top
-	cracks opened up for fractographic analysis denoted by 'fracto' at top

APPENDIX C

Piecewise Car Body Compliance Test Data

Section C-I: Vertical Sill Deflections

Section C-II: B-End Sill Bending Stresses

Section C-III: A-End Sill Bending Stresses

Section C-IV: Vertical Head Stresses (BL, BR, and AL)

Section C-V: Von Mises Head Stresses (AL, BL, and BR)

Section C-VI: Vertical Web Stresses (BL and AL)

Section C-VII: A-End Left Von Mises Web Stress

Section C-VIII: B-End Right Longitudinal Flange Stresses

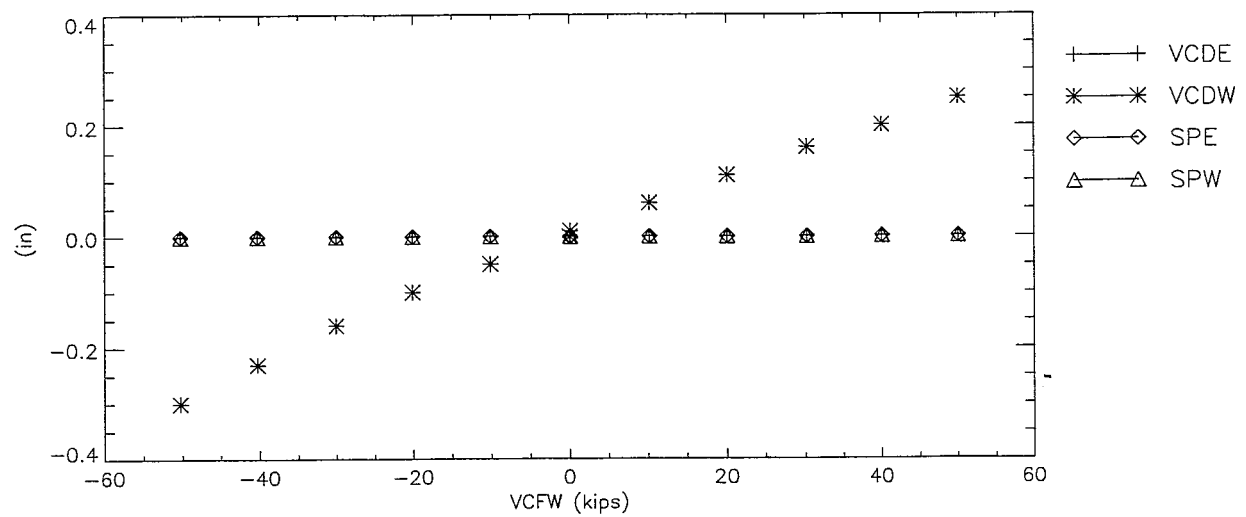
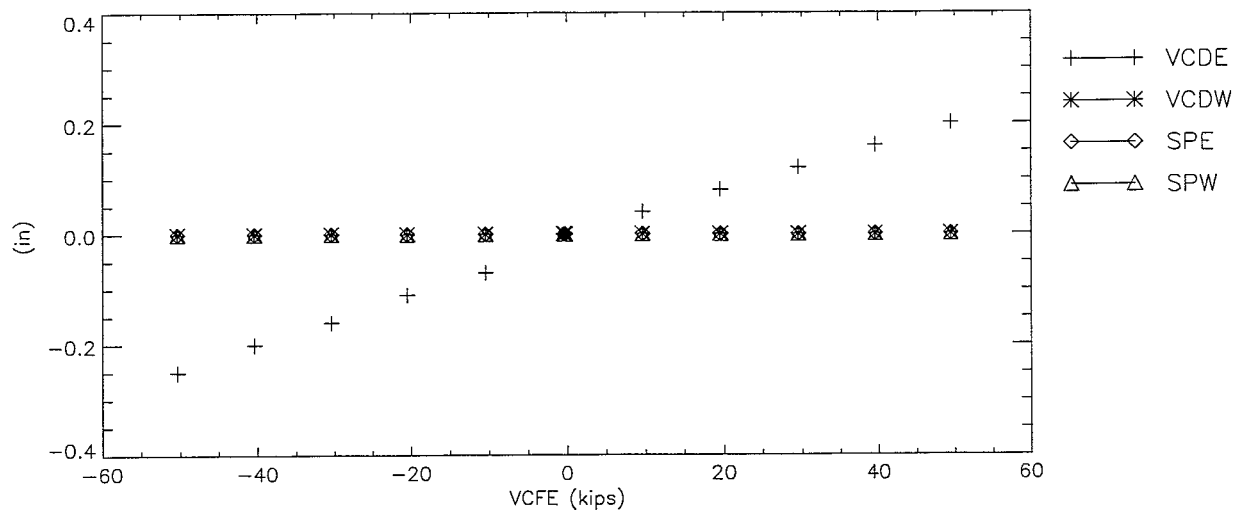
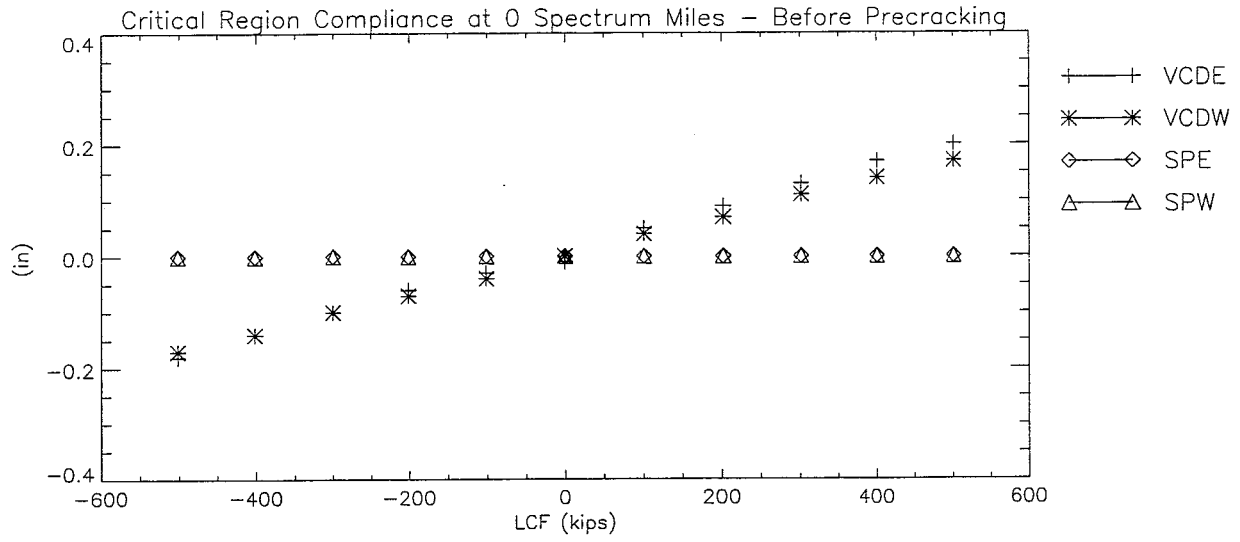
Section C-IX: A-End Right Longitudinal Flange Stresses

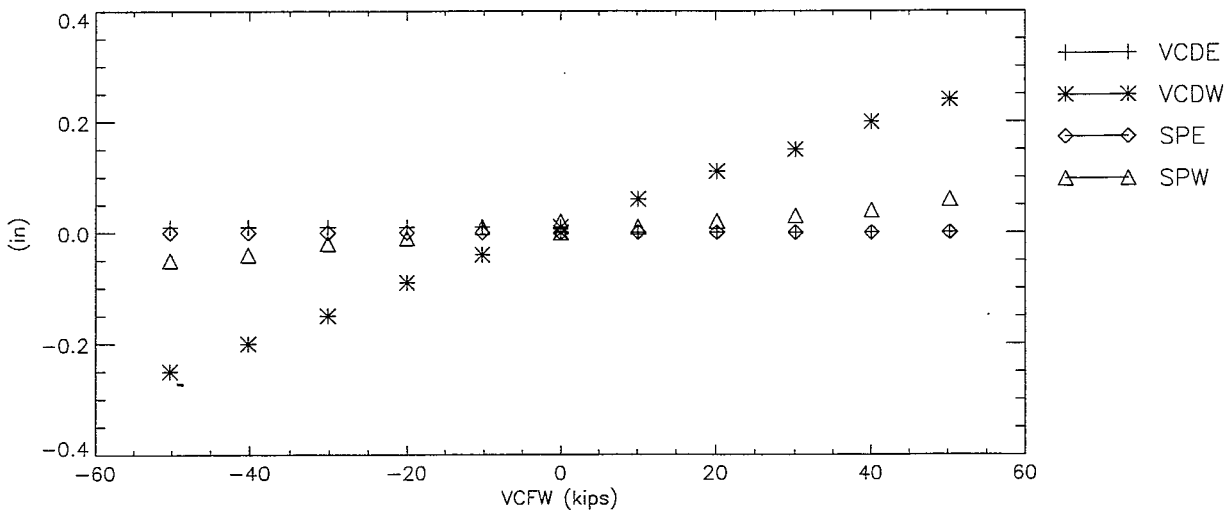
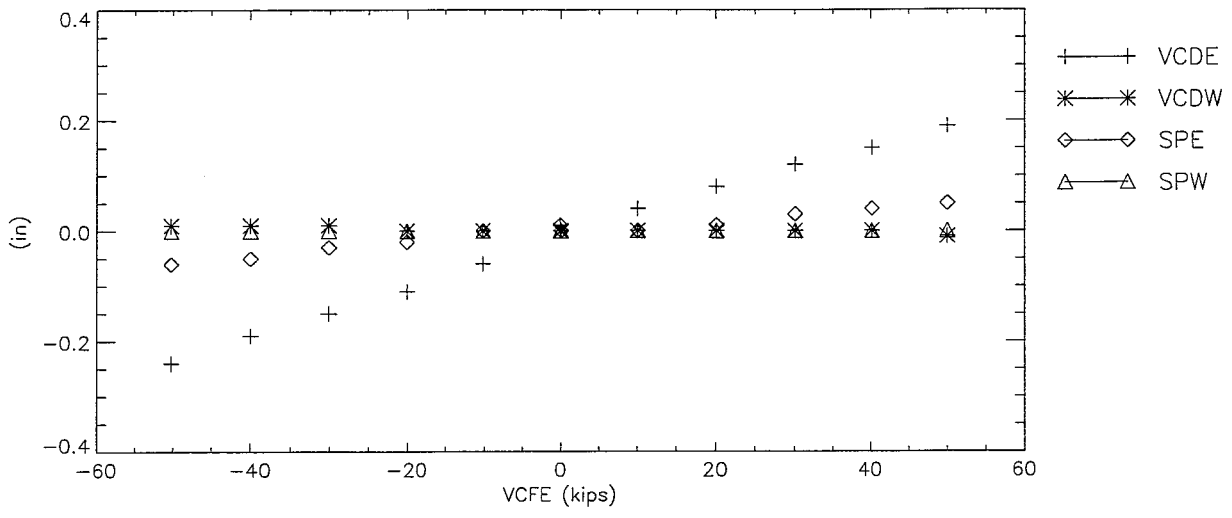
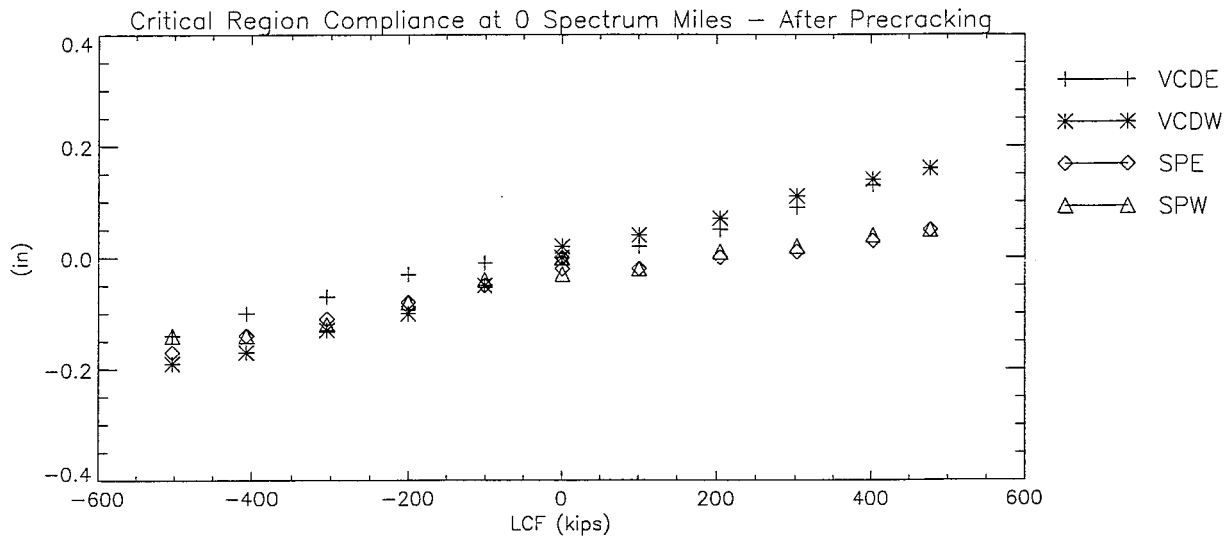
FINAL DRAFT

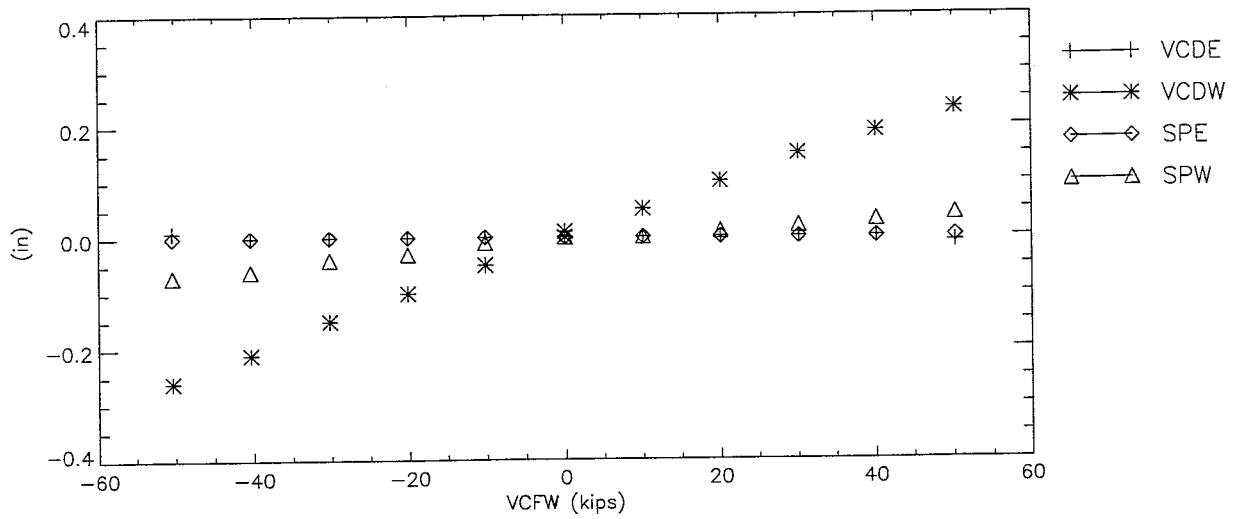
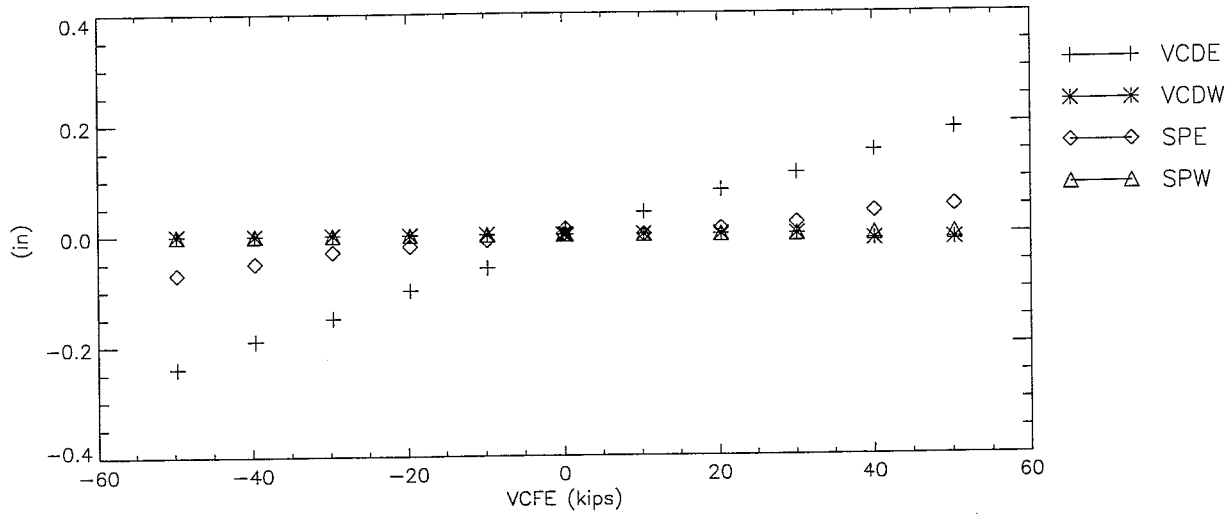
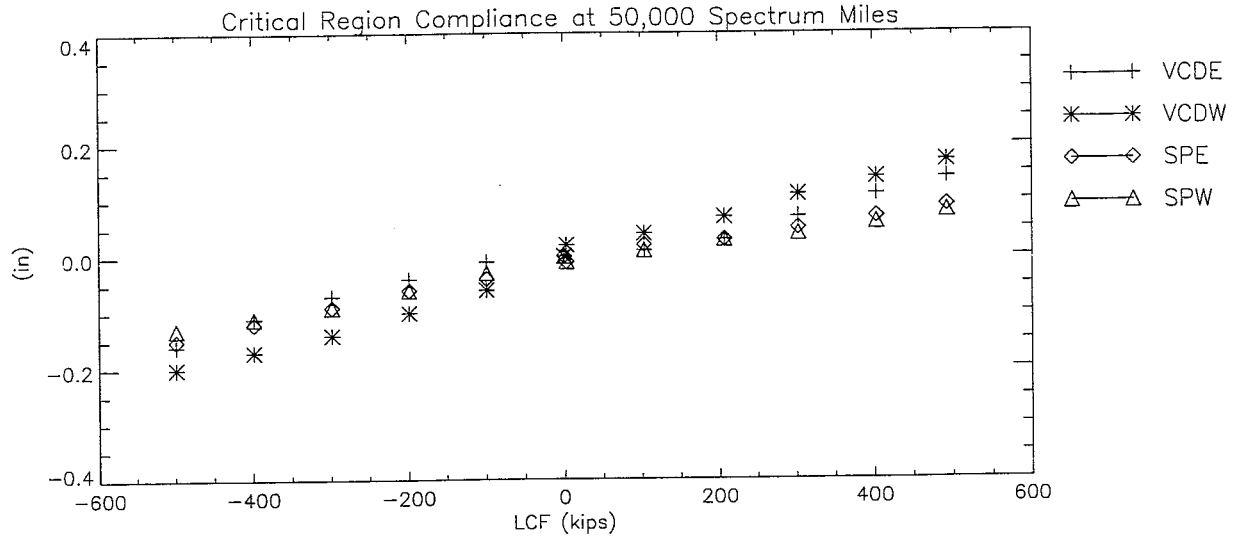
FINAL DRAFT

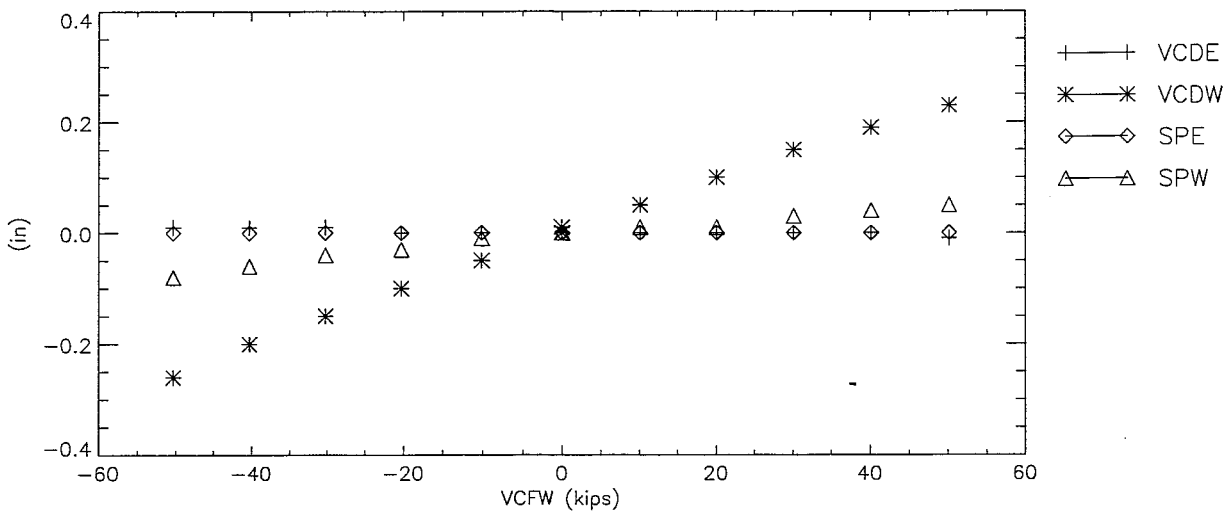
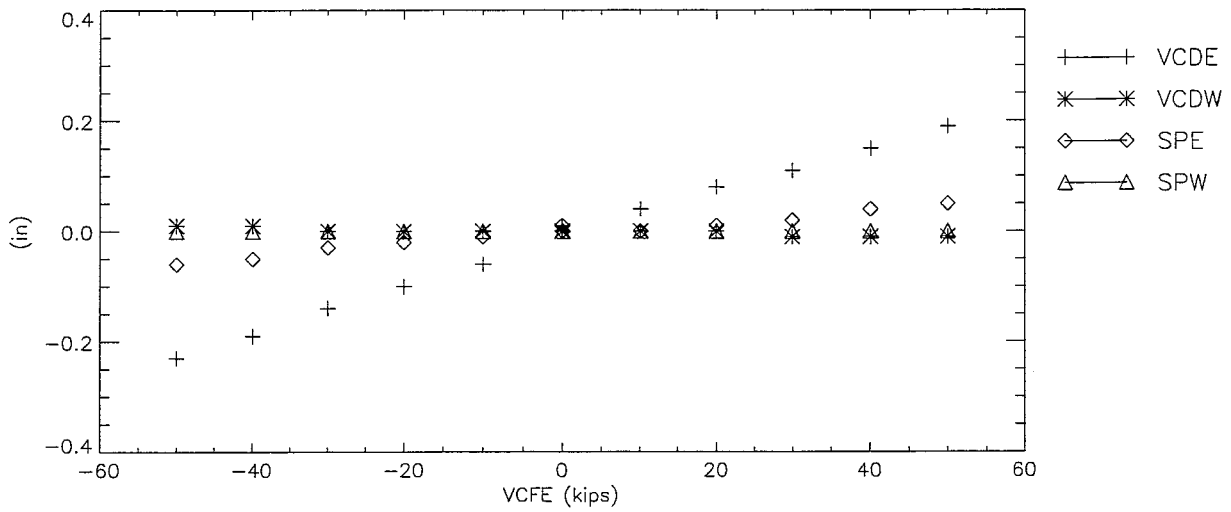
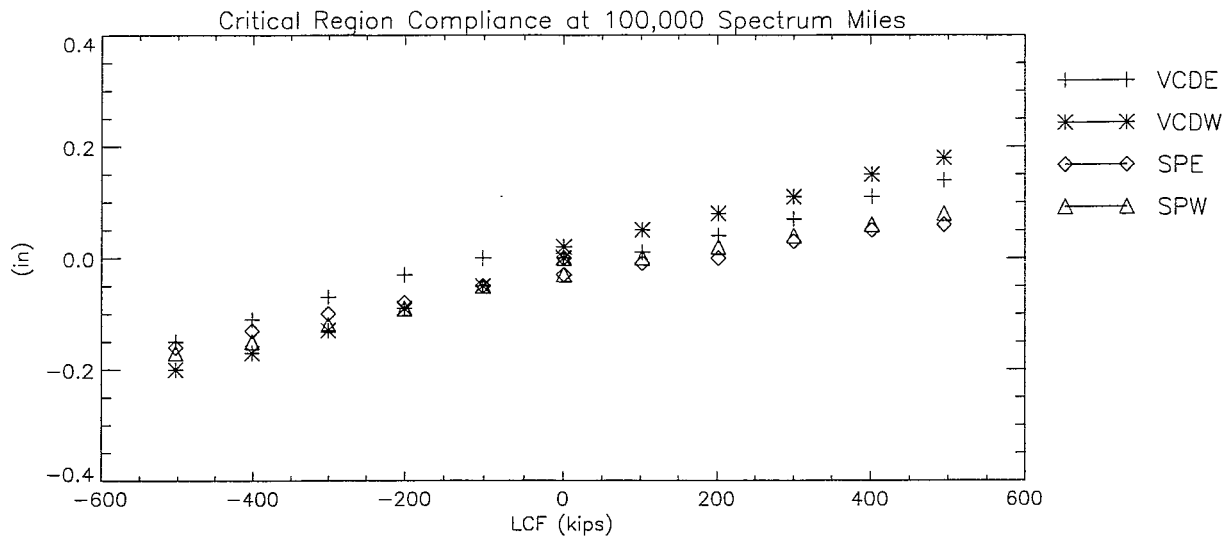
Section C-1: Vertical Sill Deflections

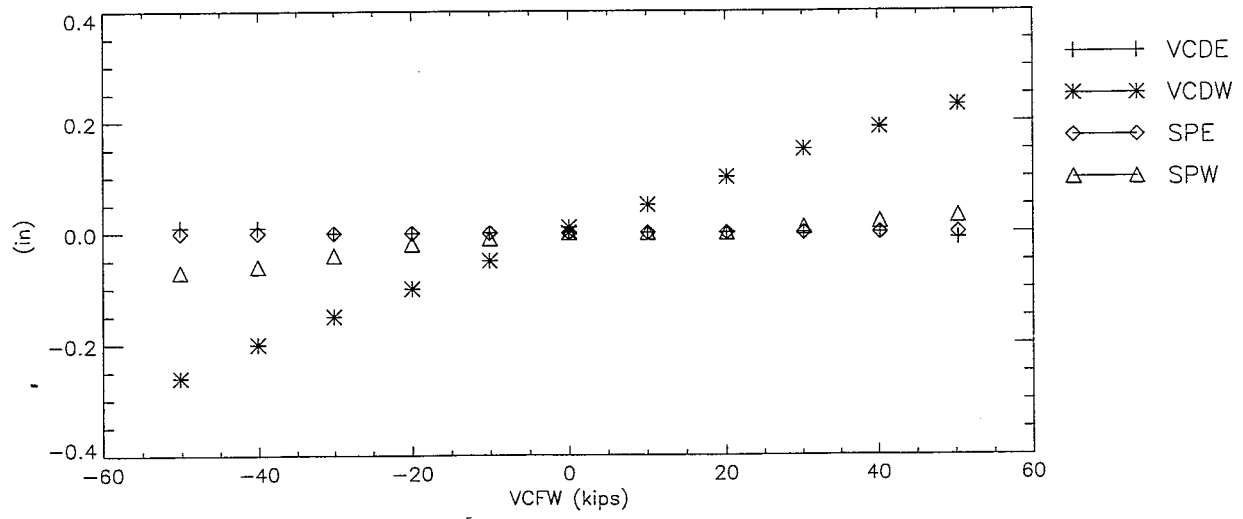
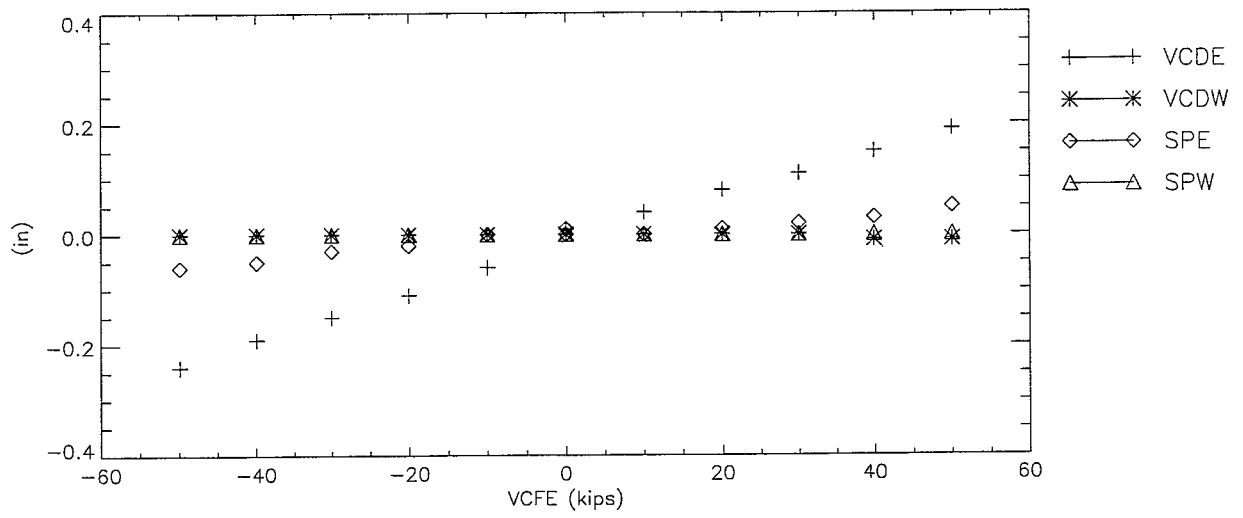
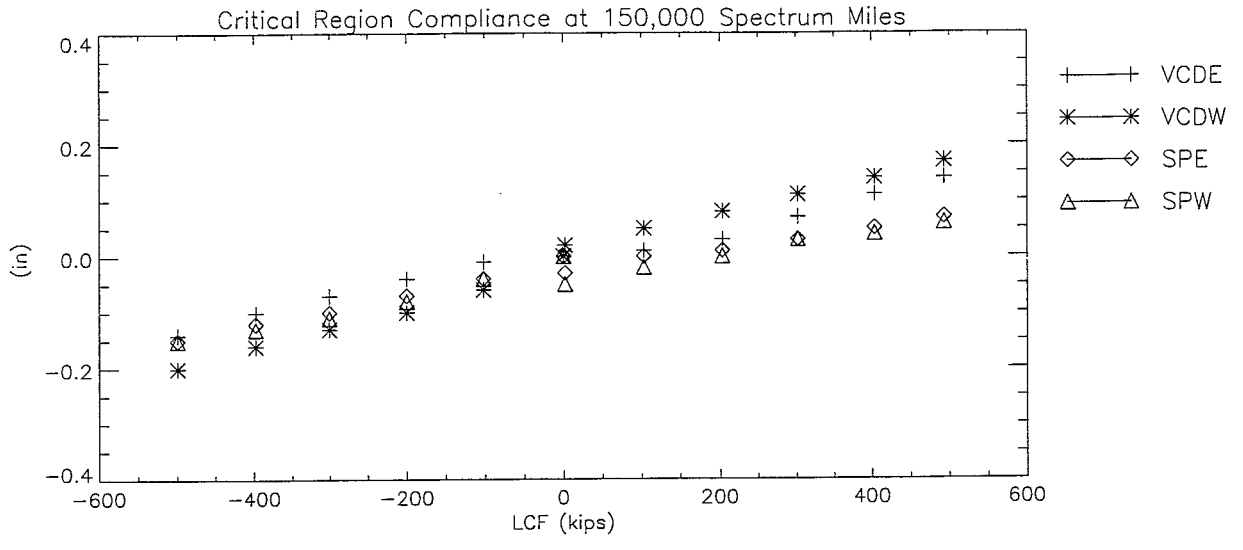
FINAL DRAFT

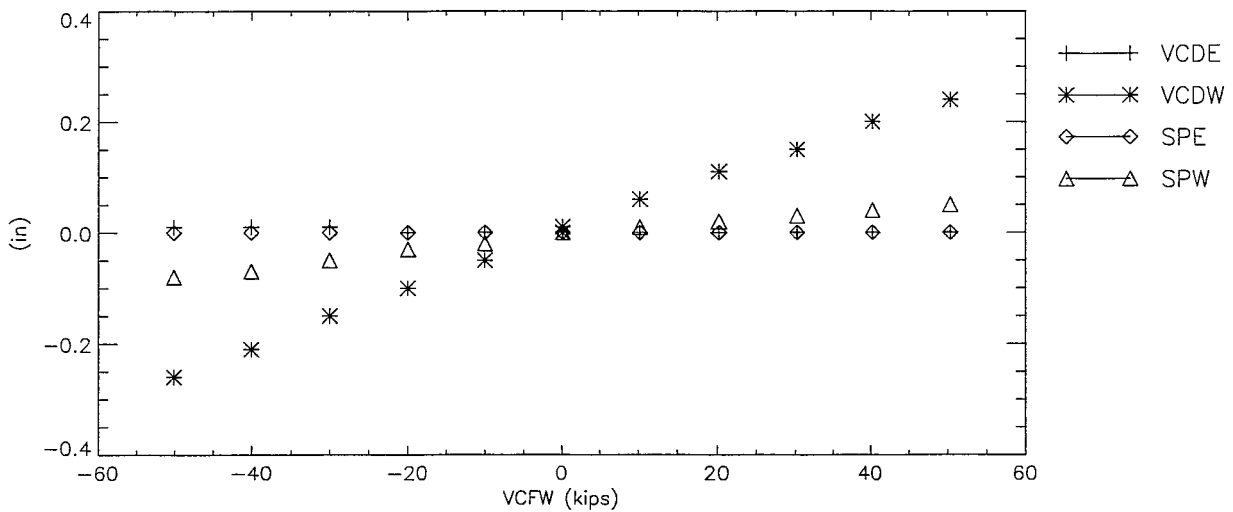
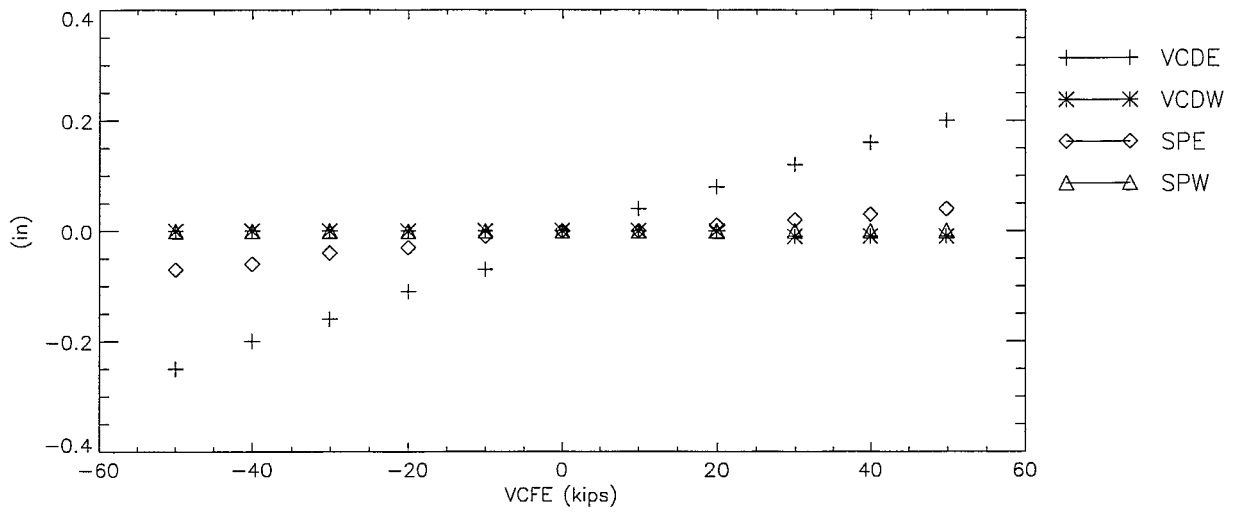
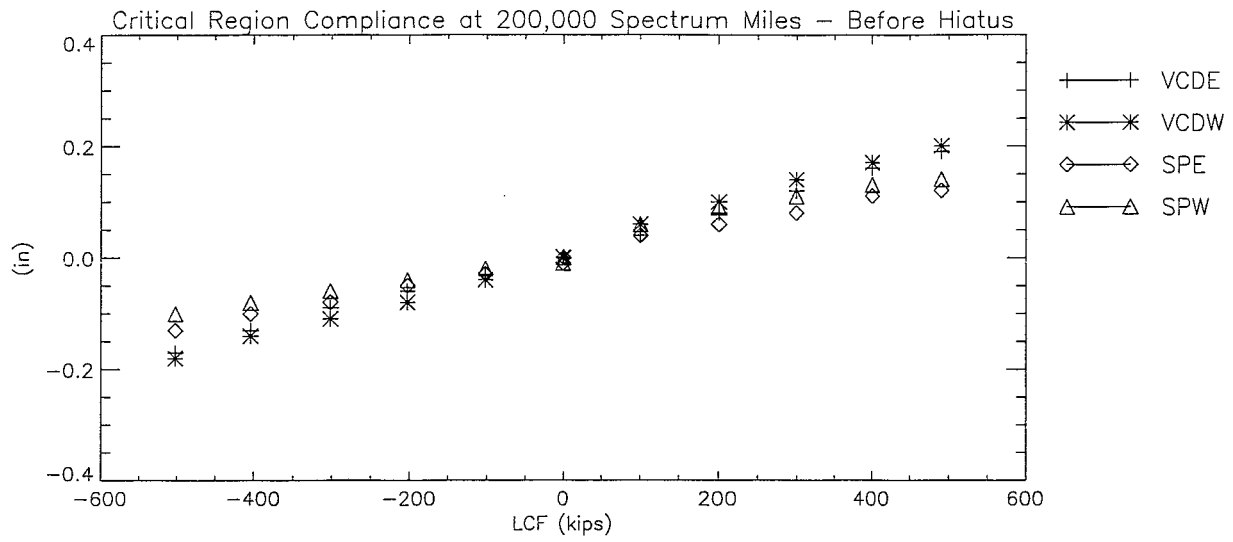


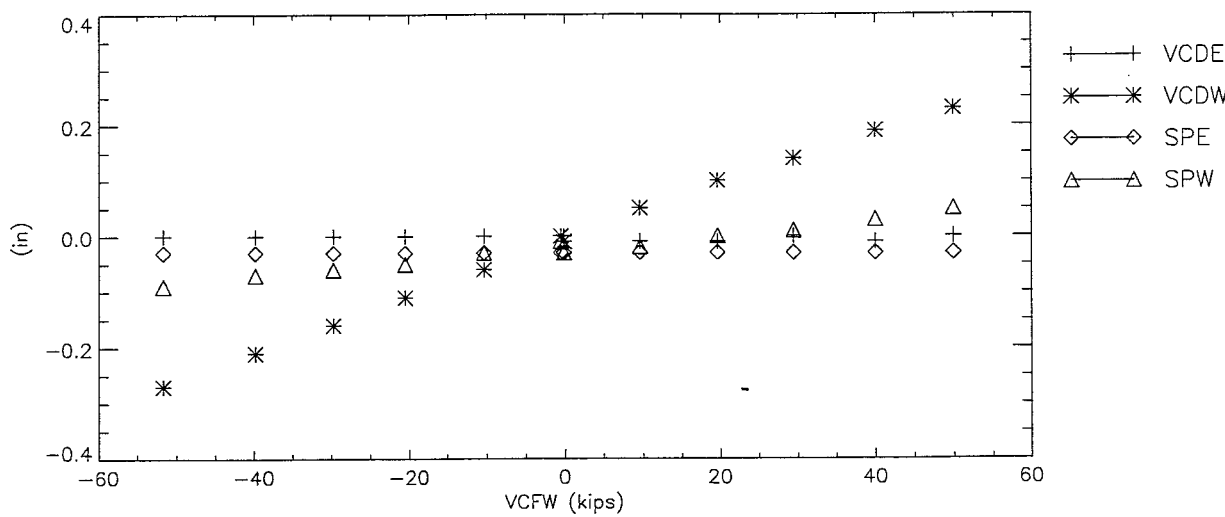
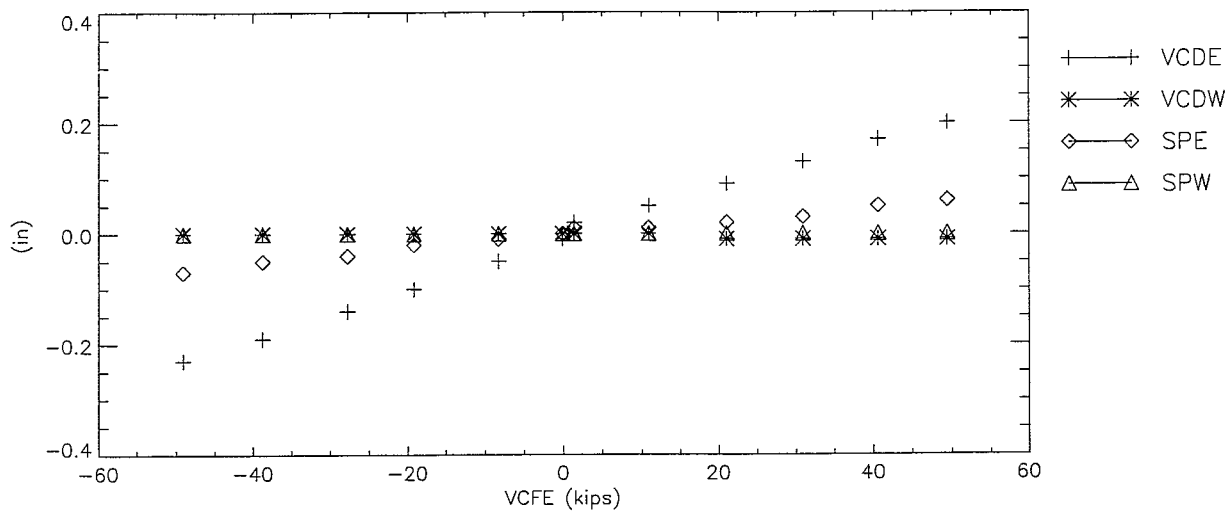
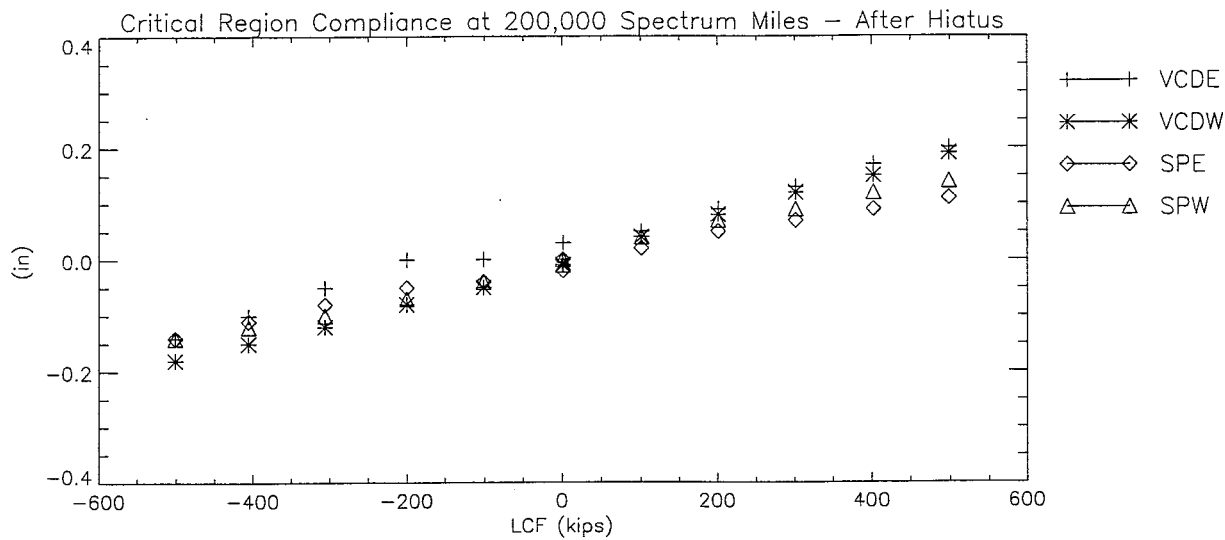


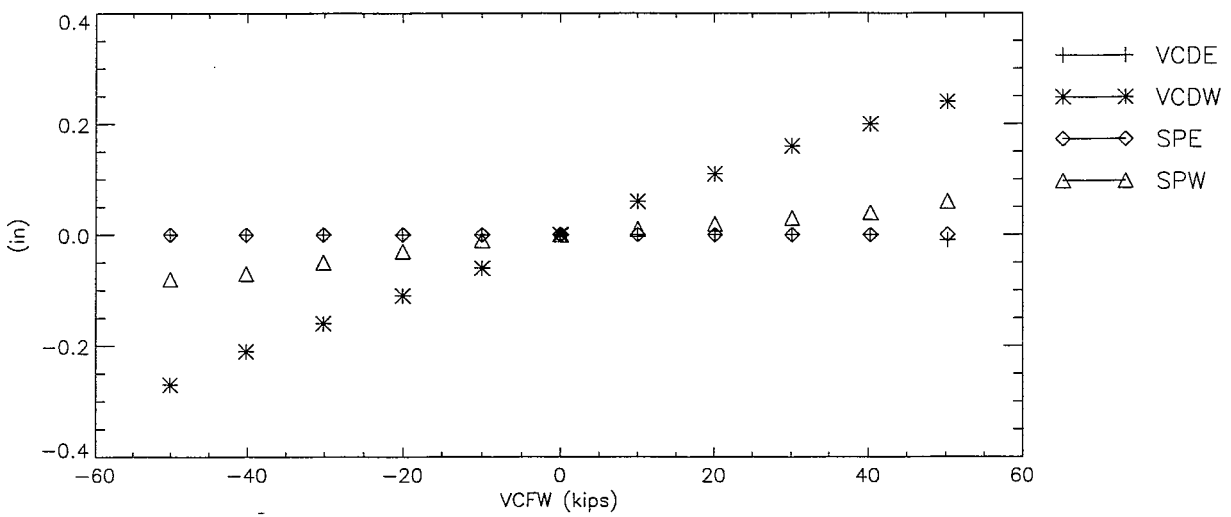
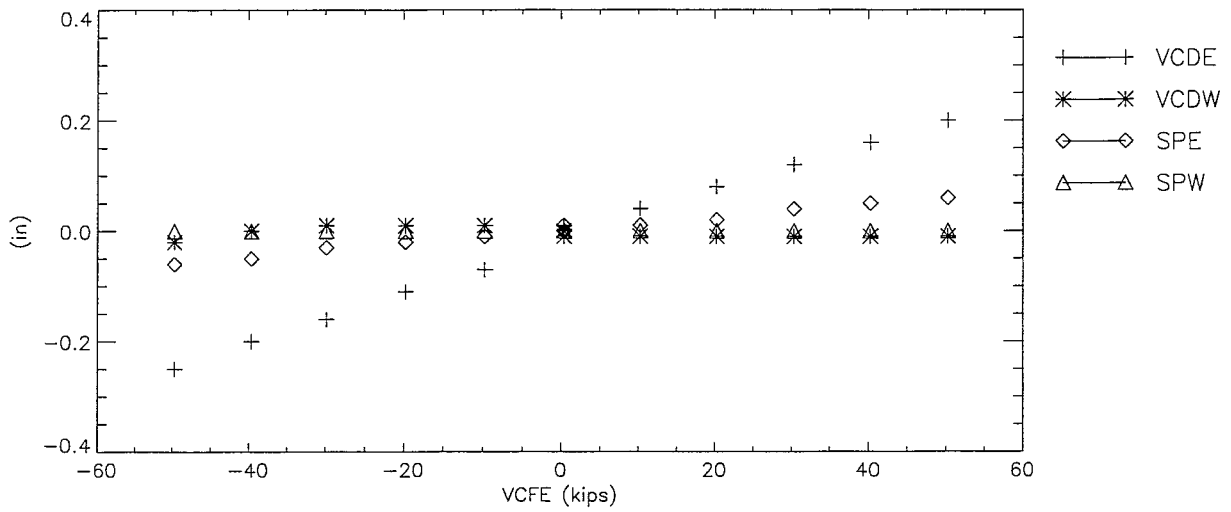
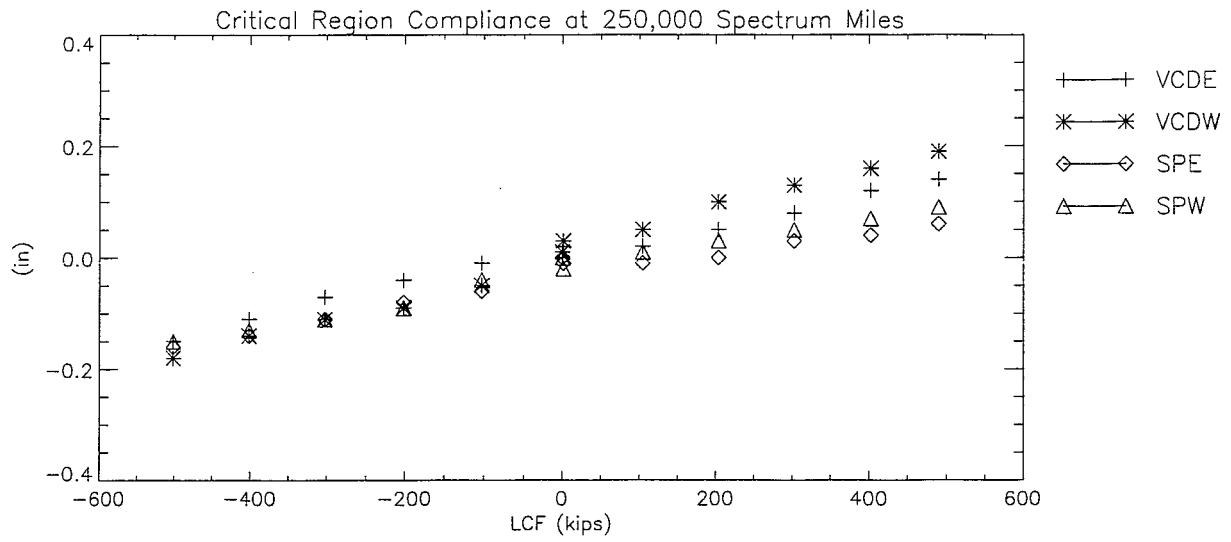


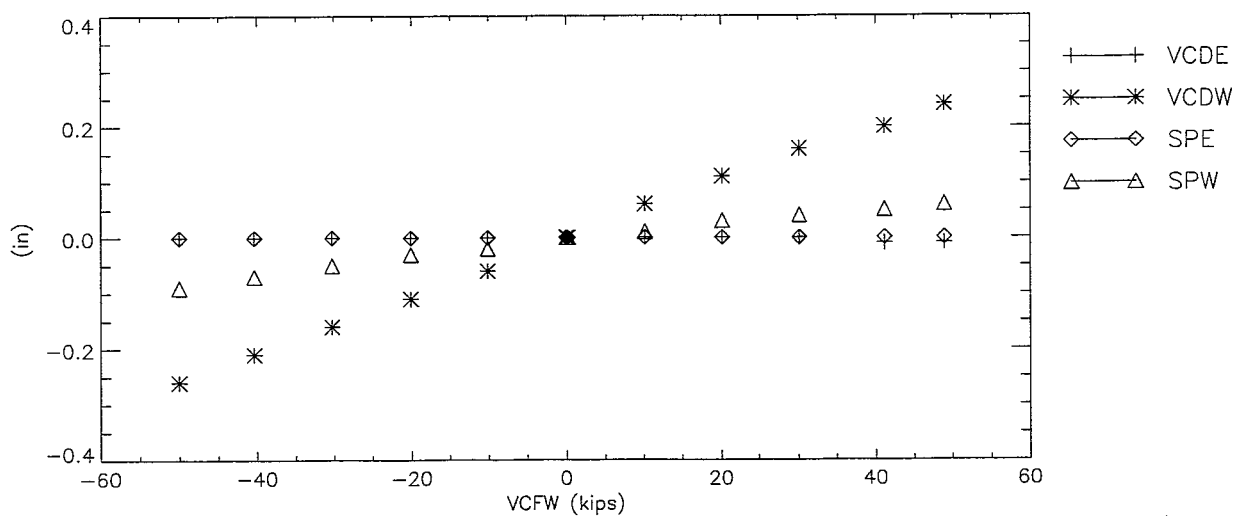
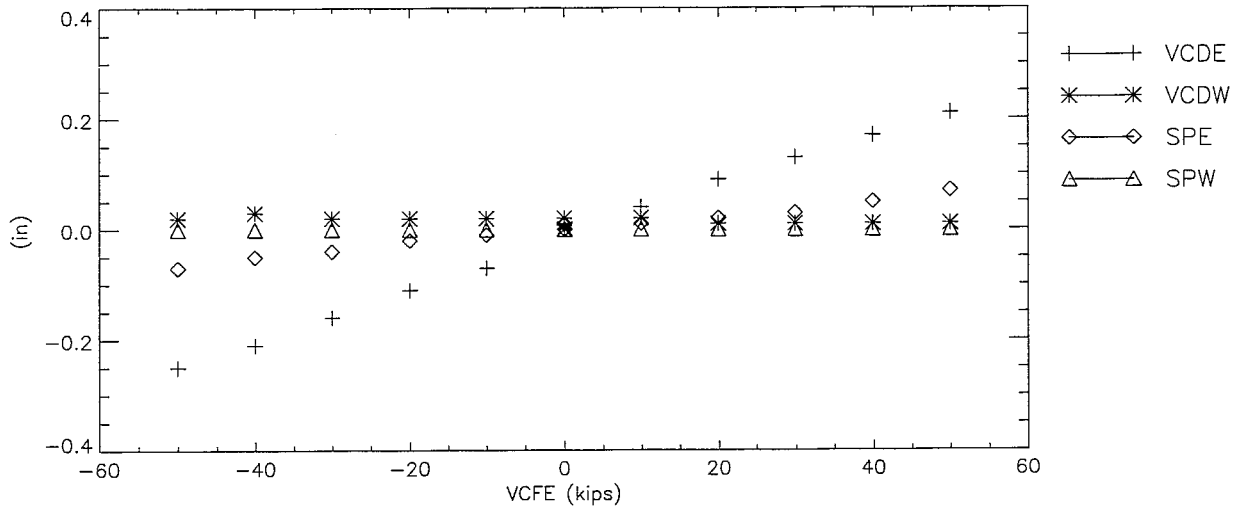
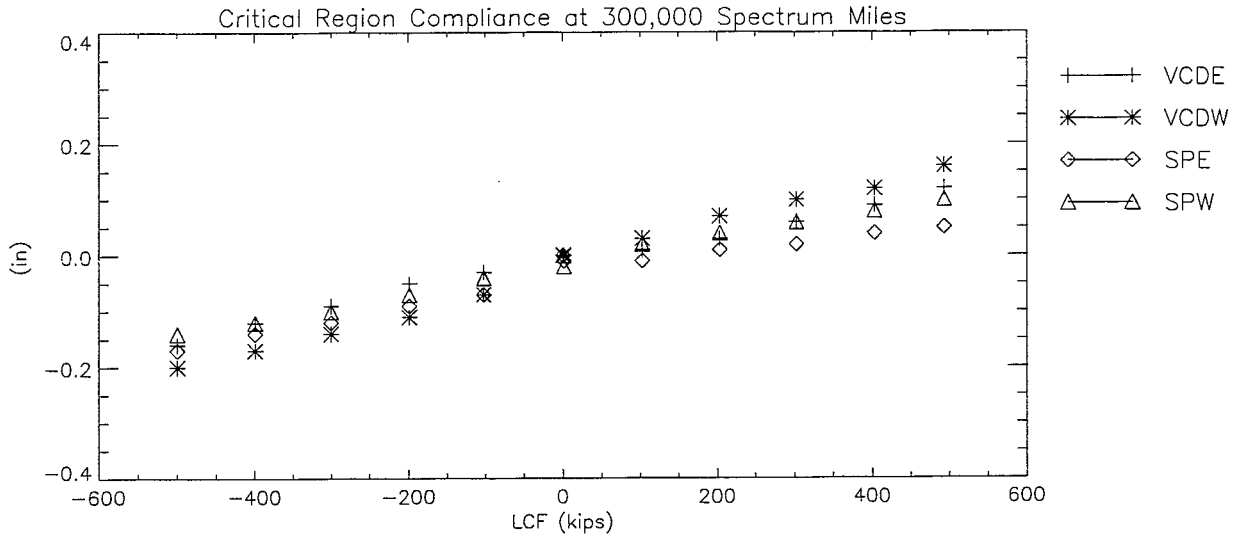






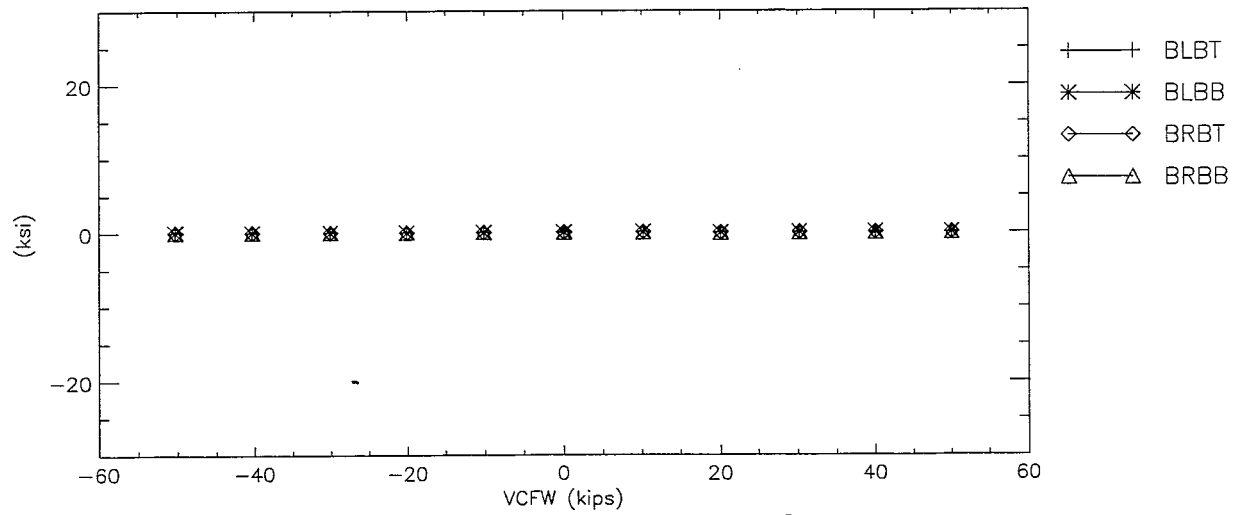
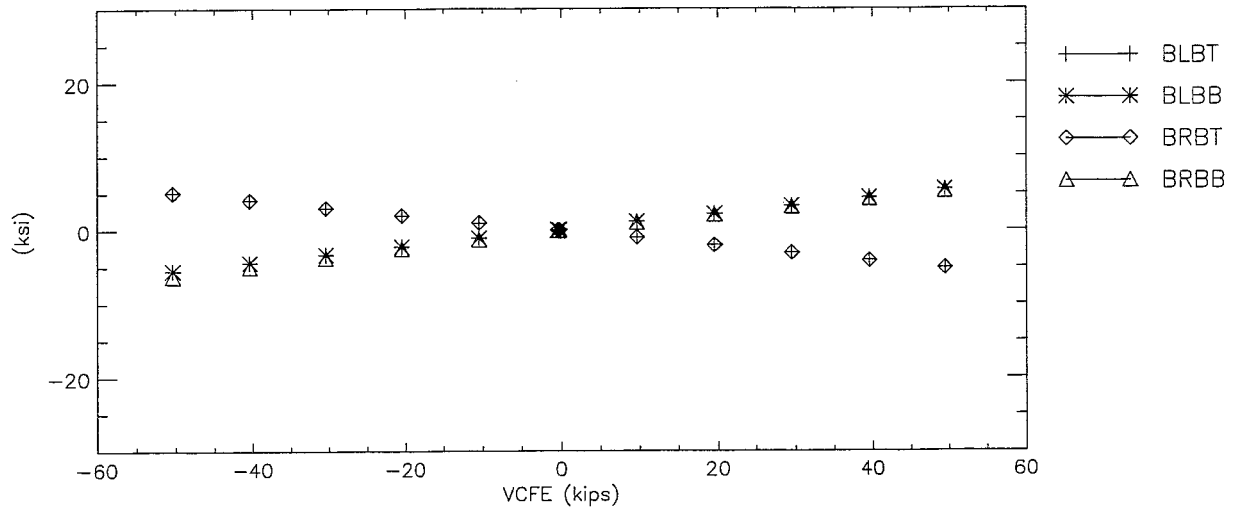
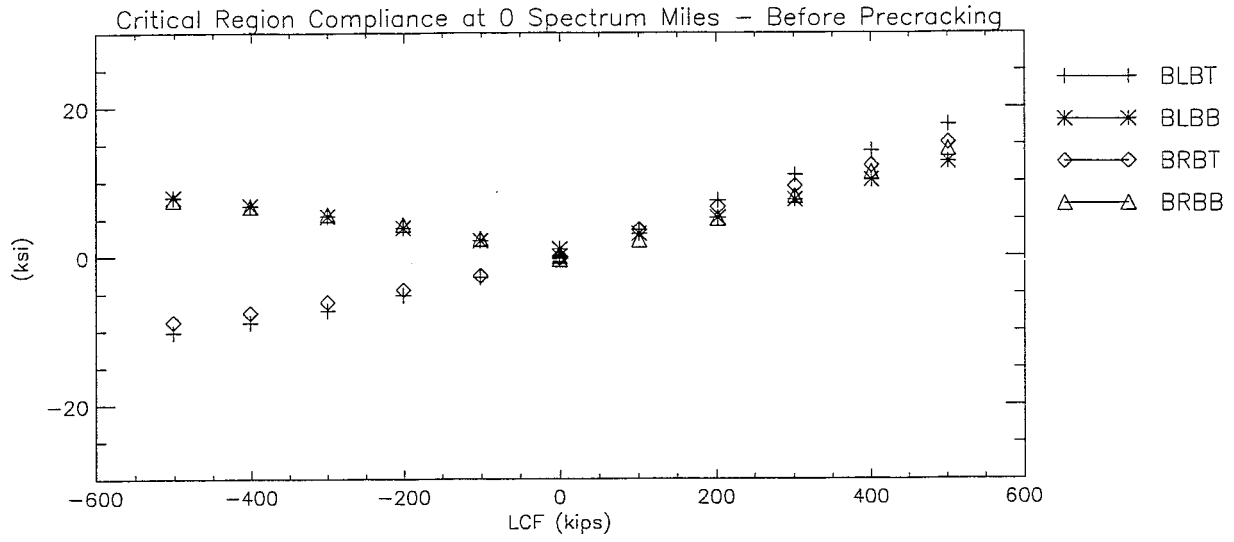


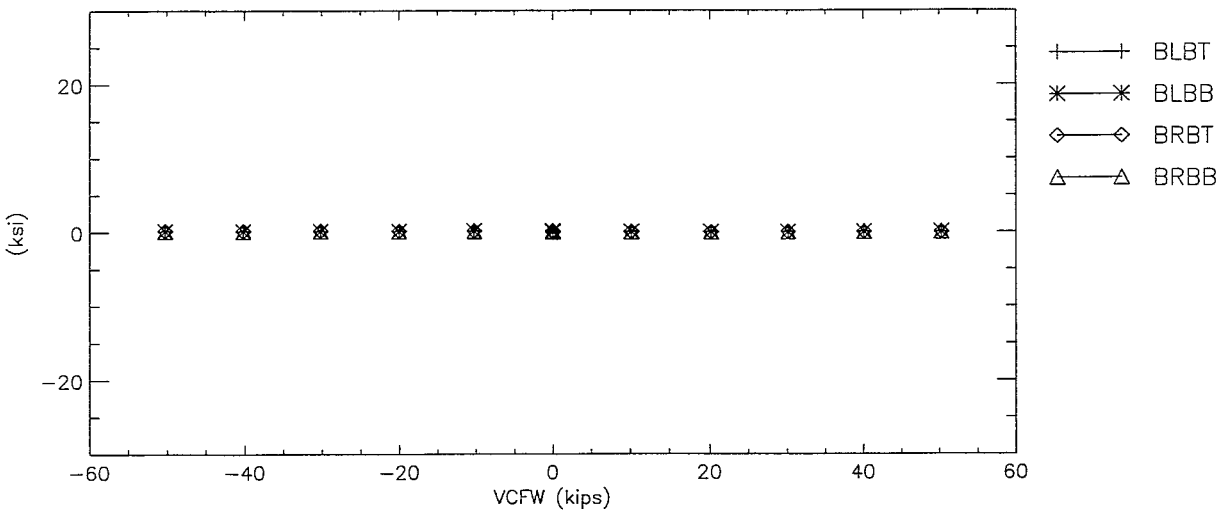
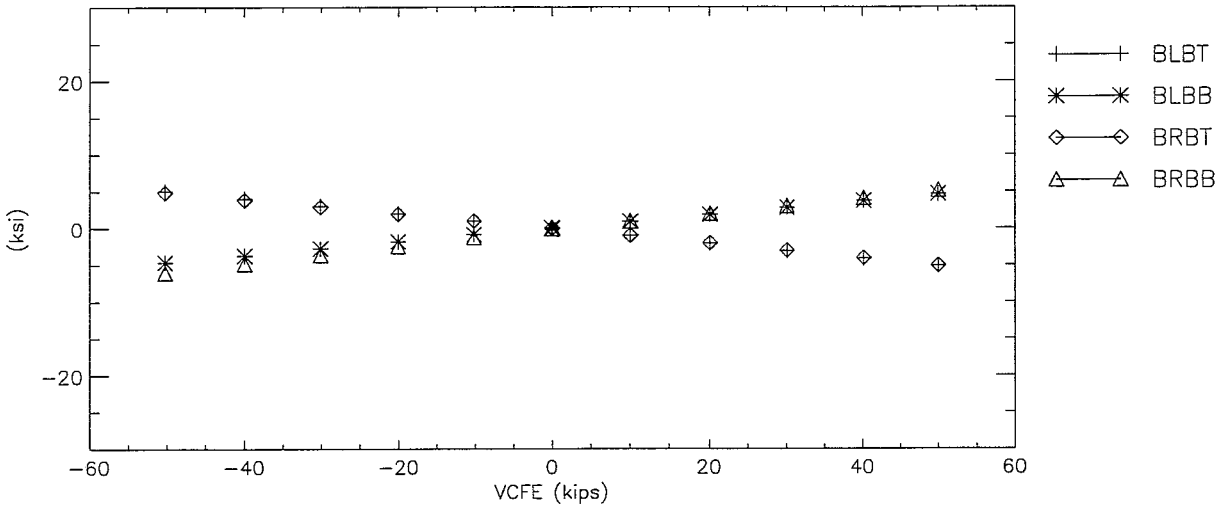
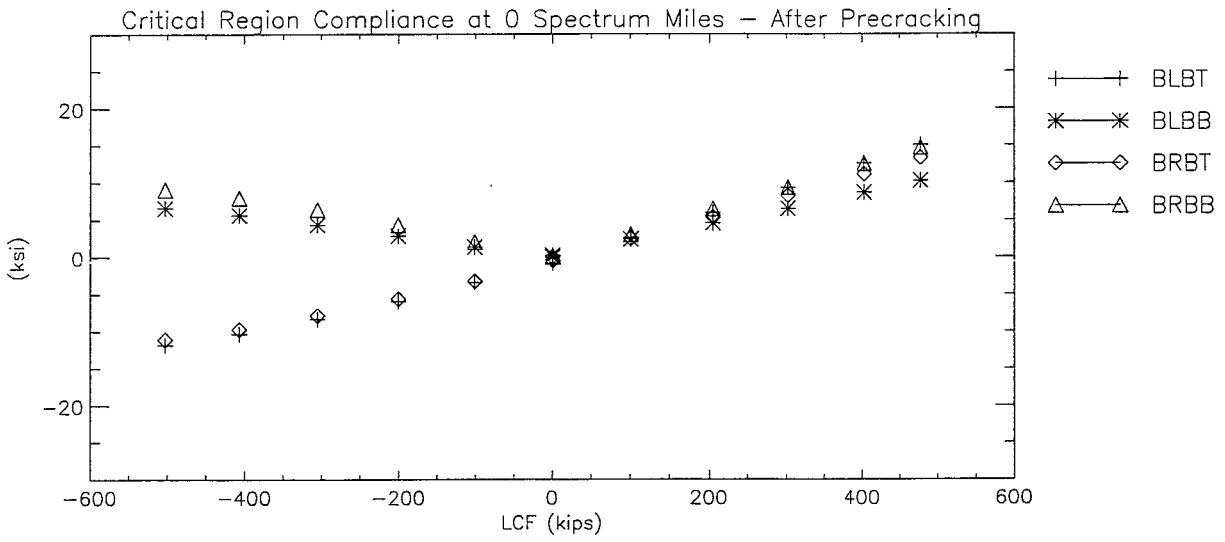


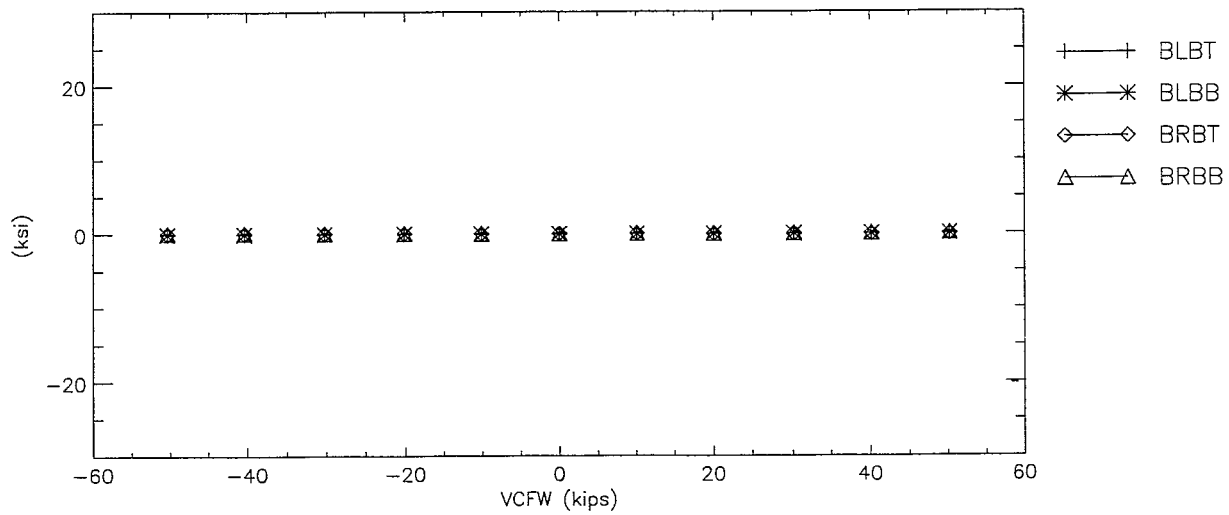
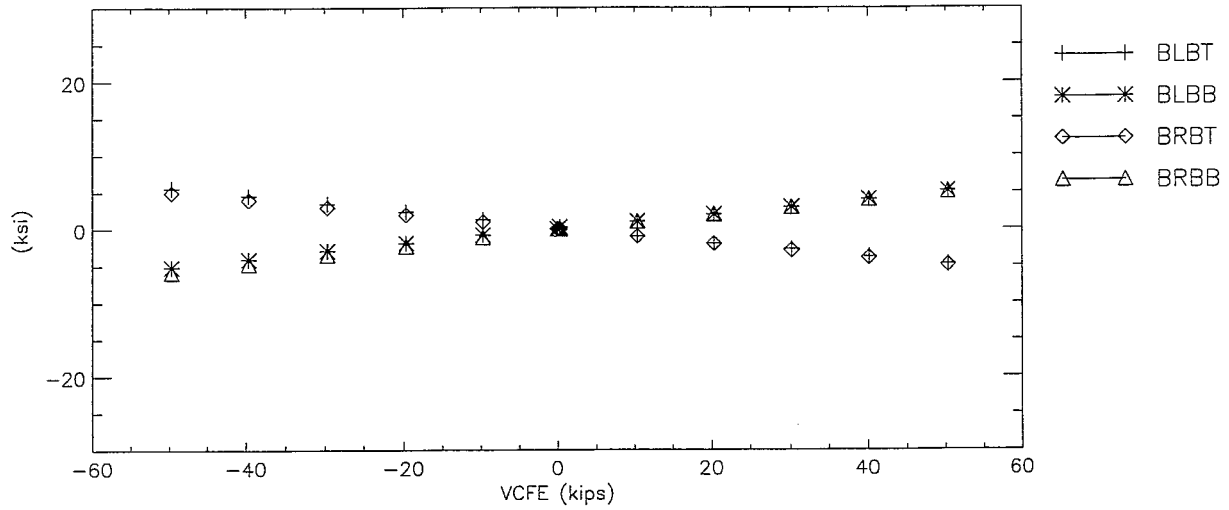
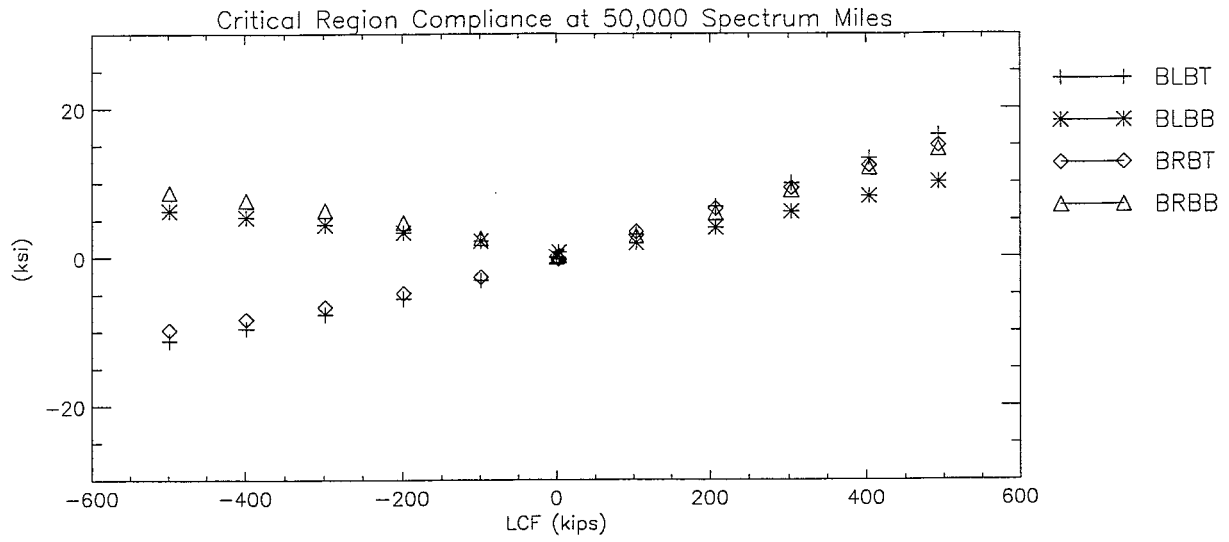


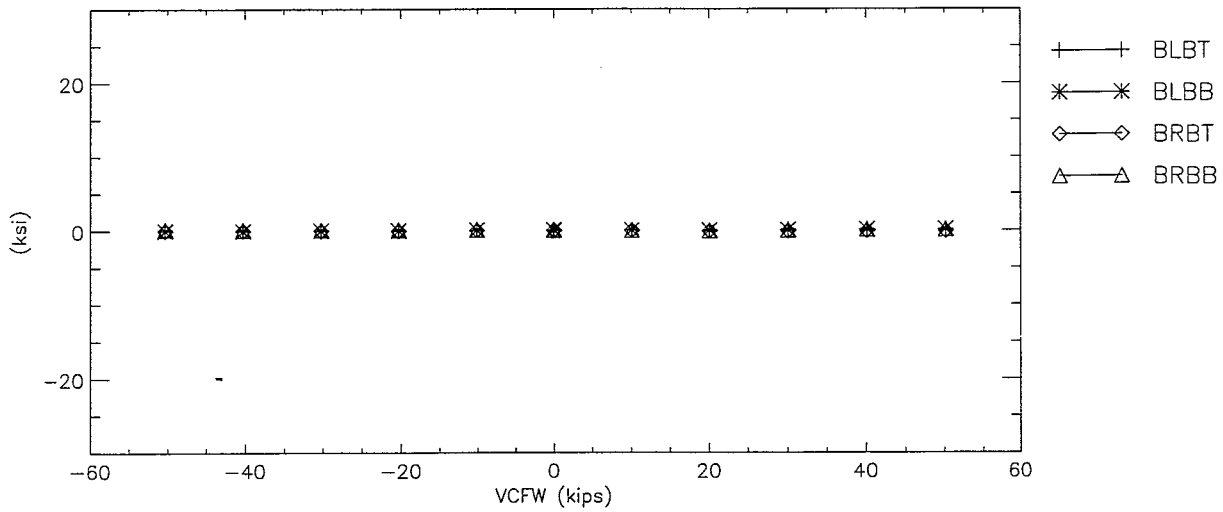
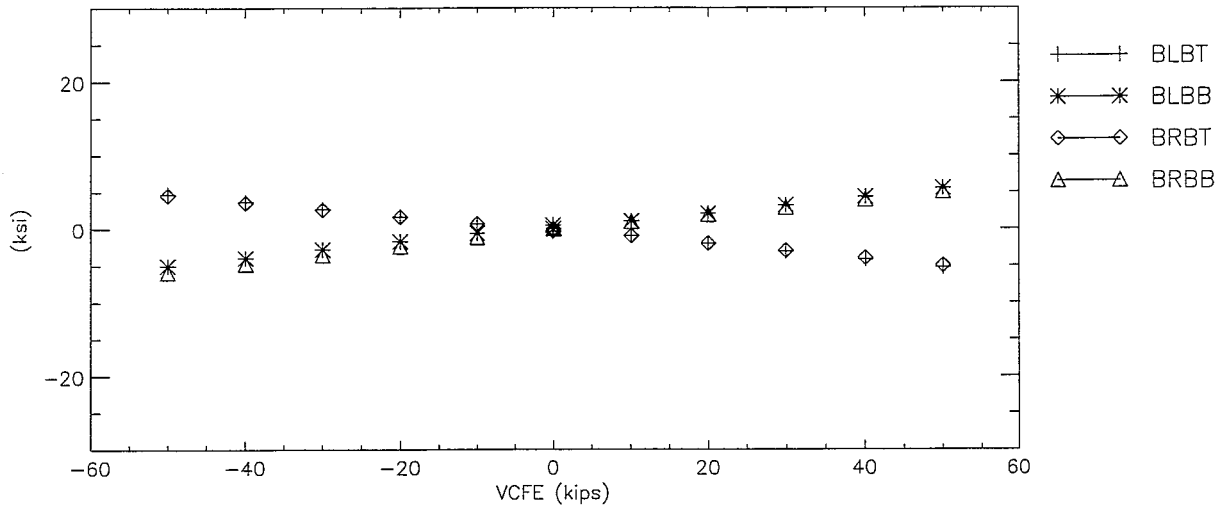
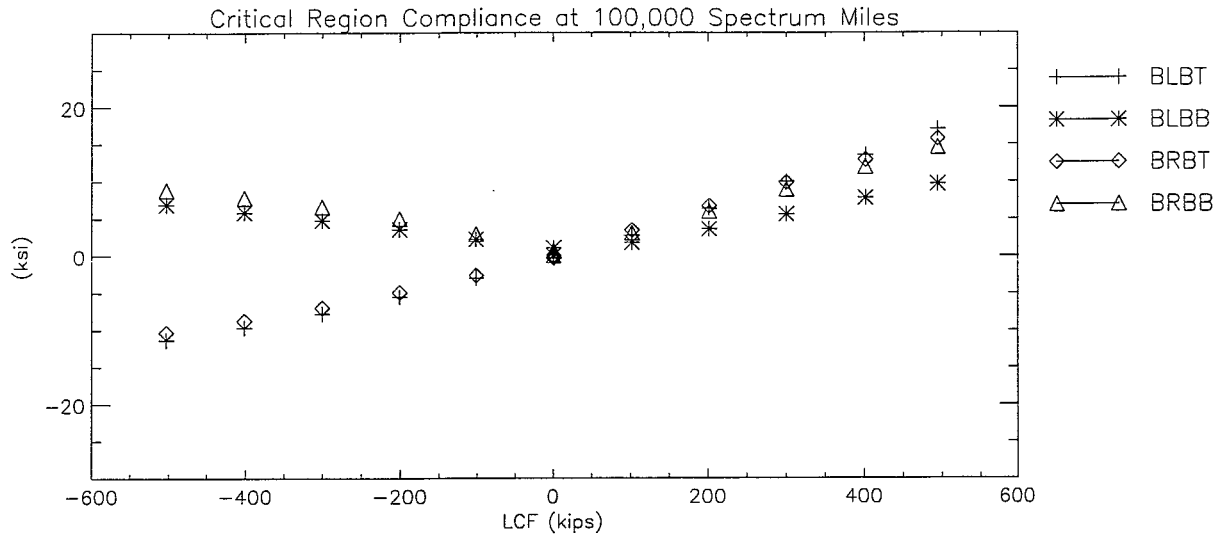
FINAL DRAFT

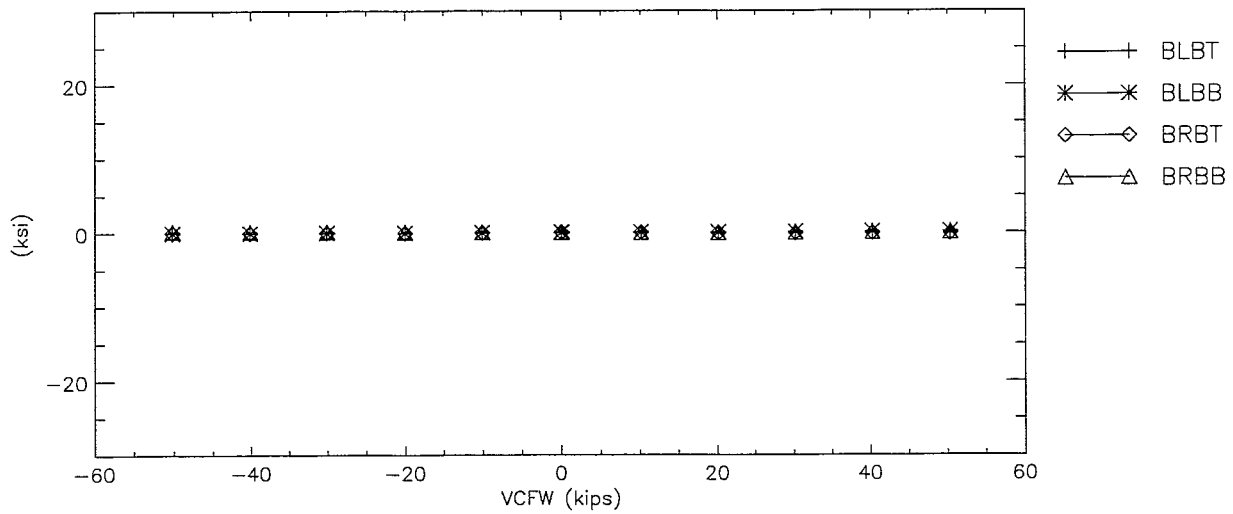
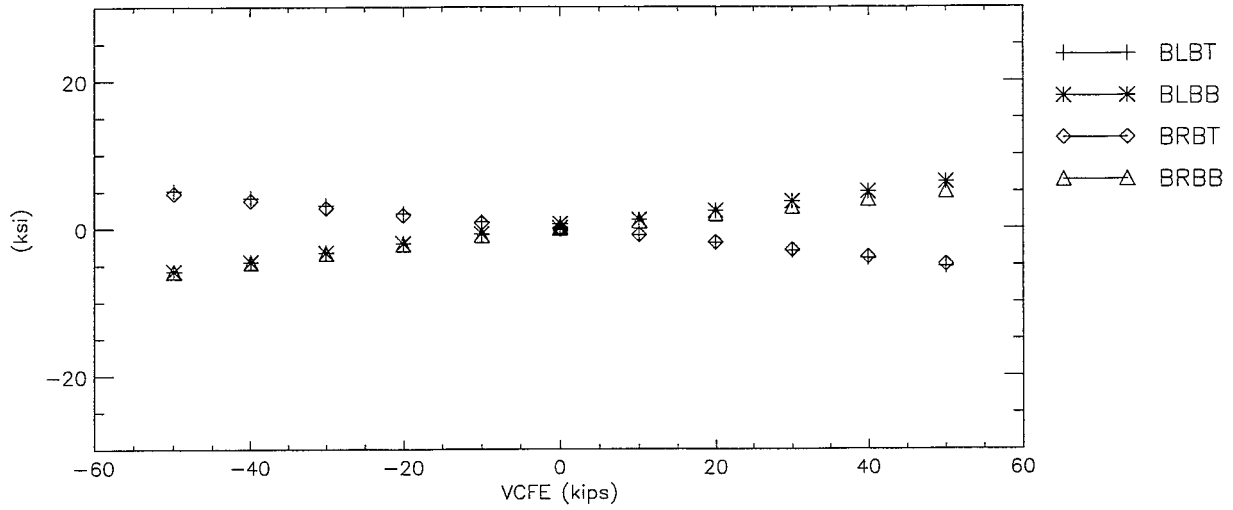
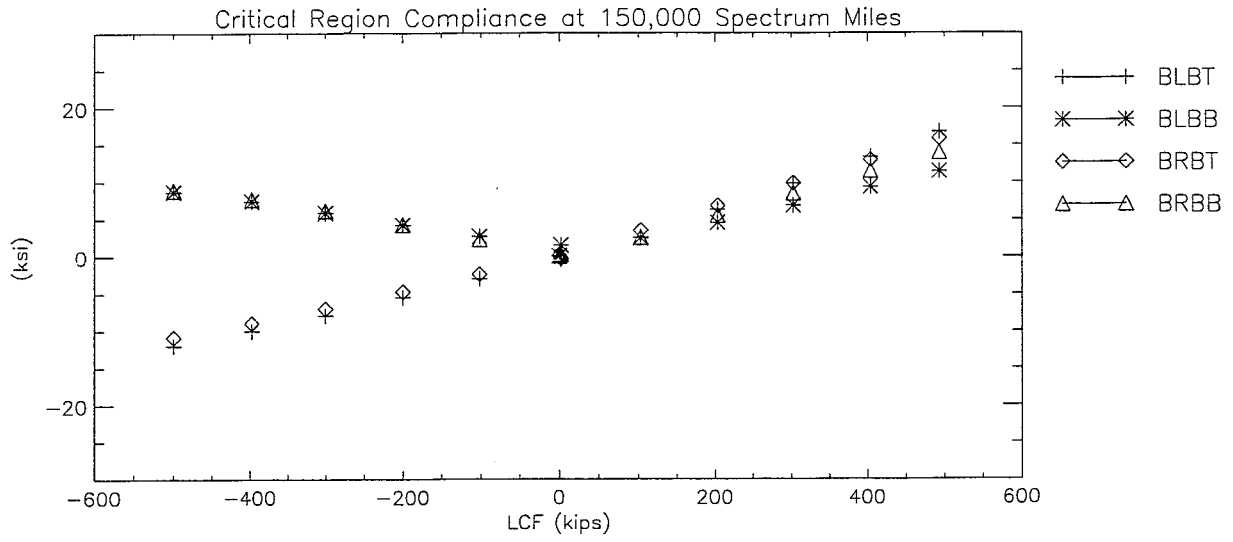
Section C-II: B-End Sill Bending Stresses

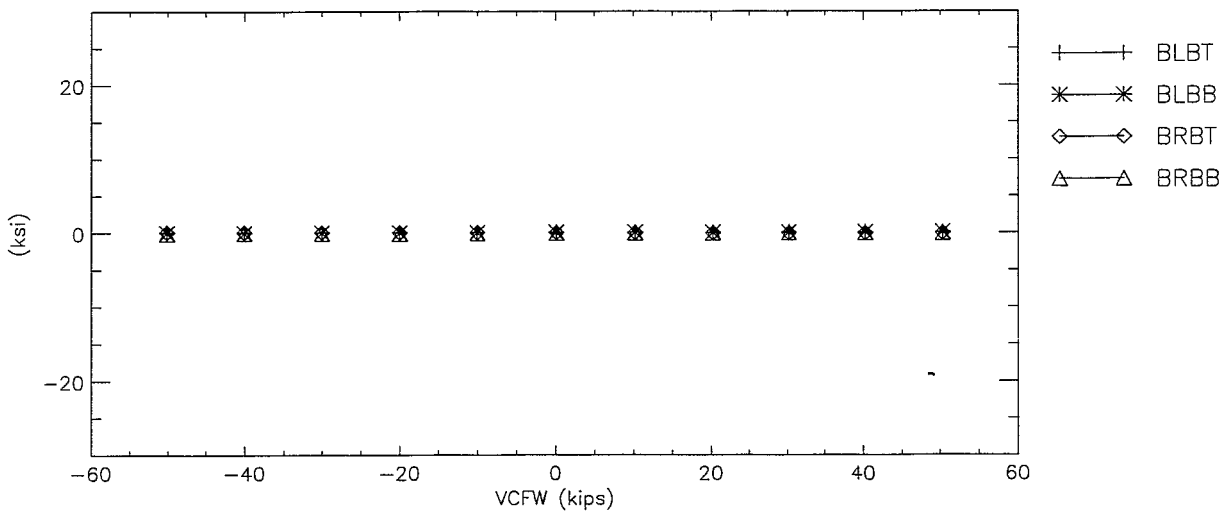
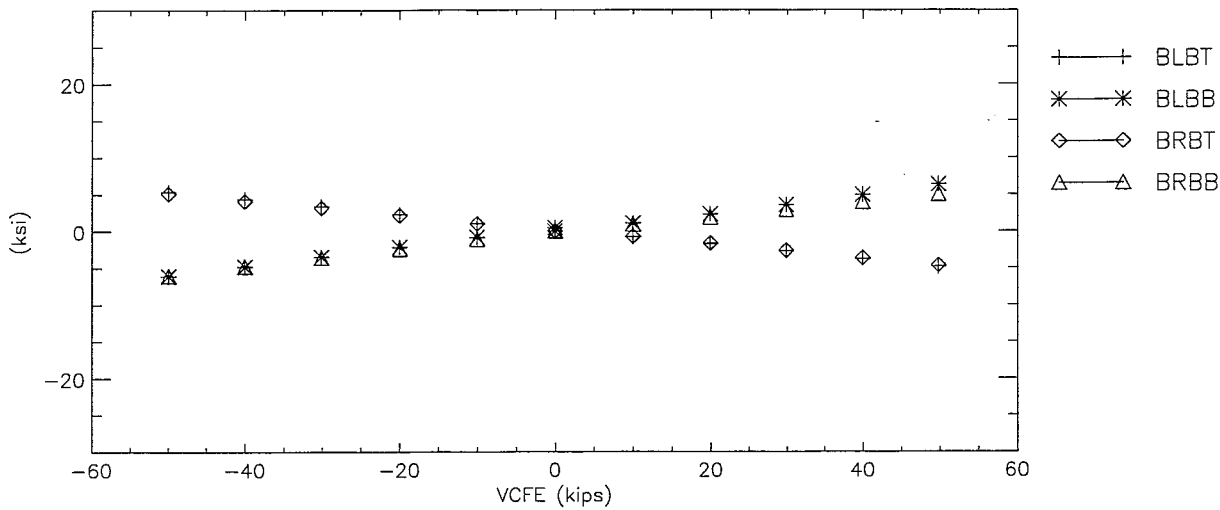
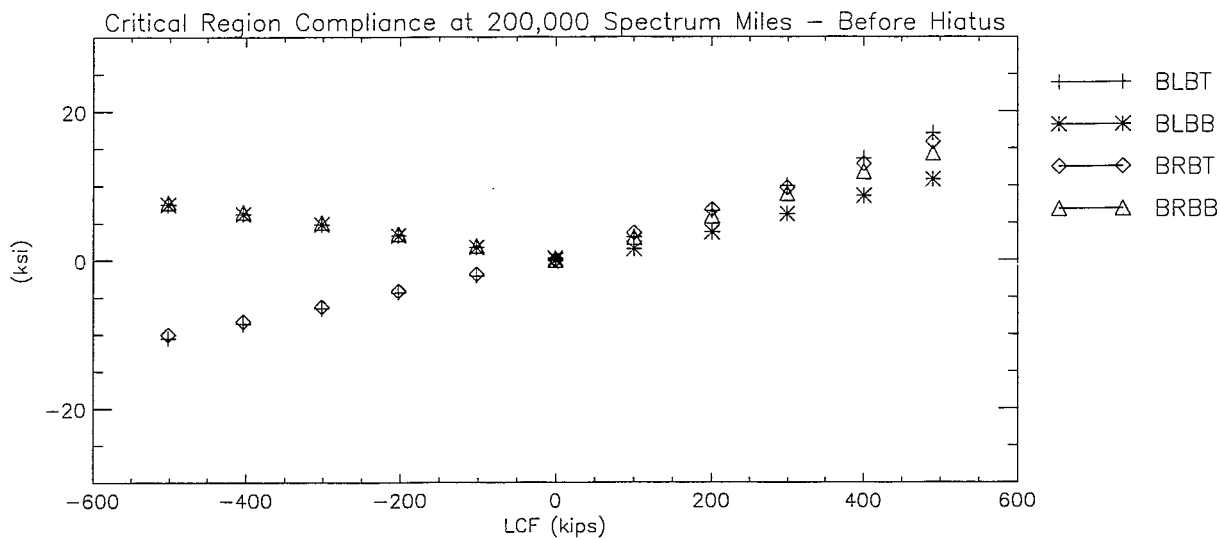


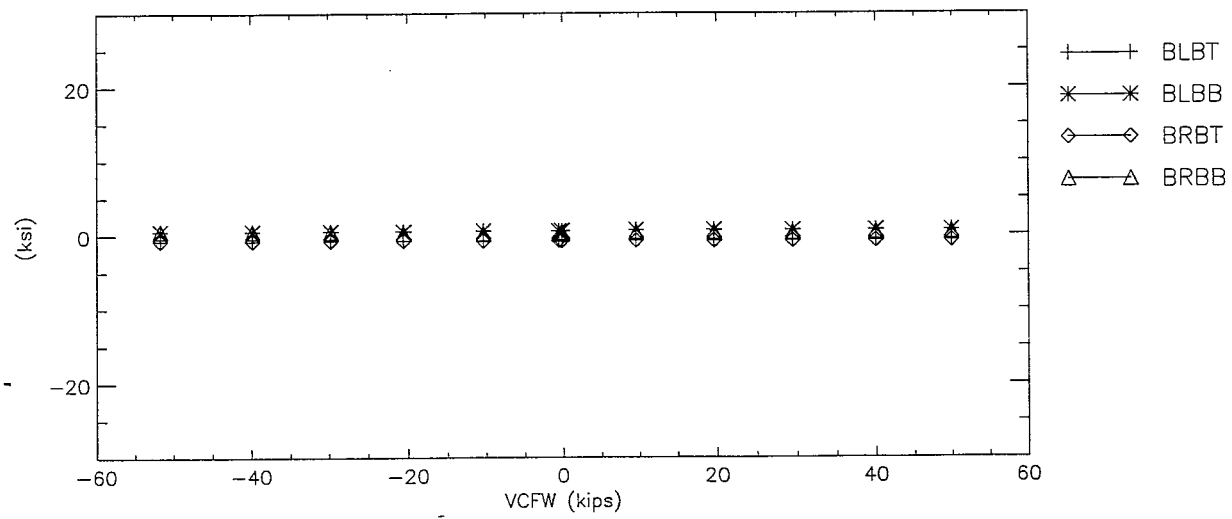
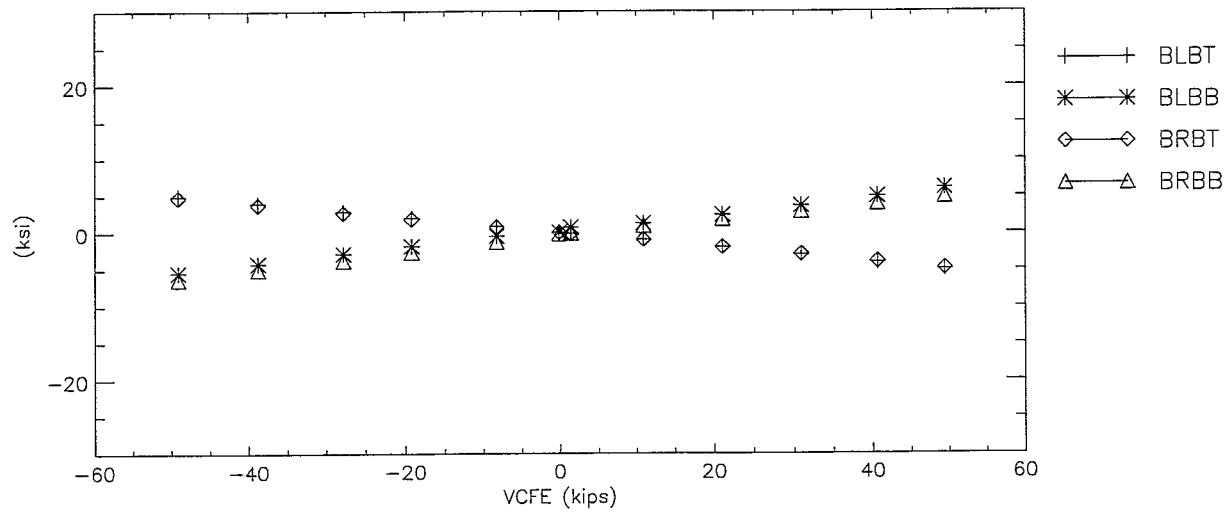
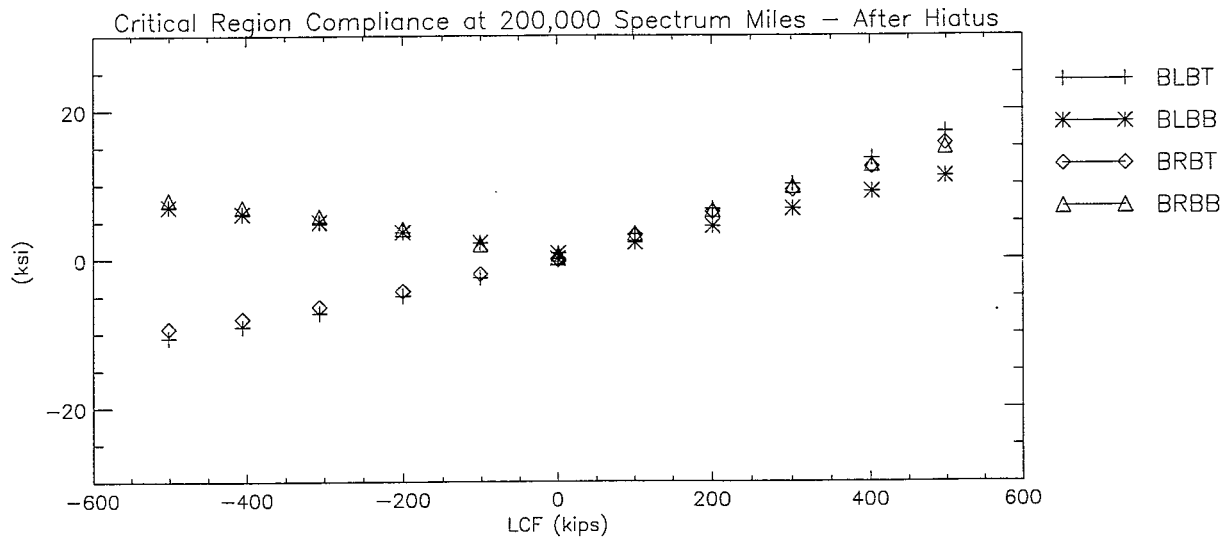


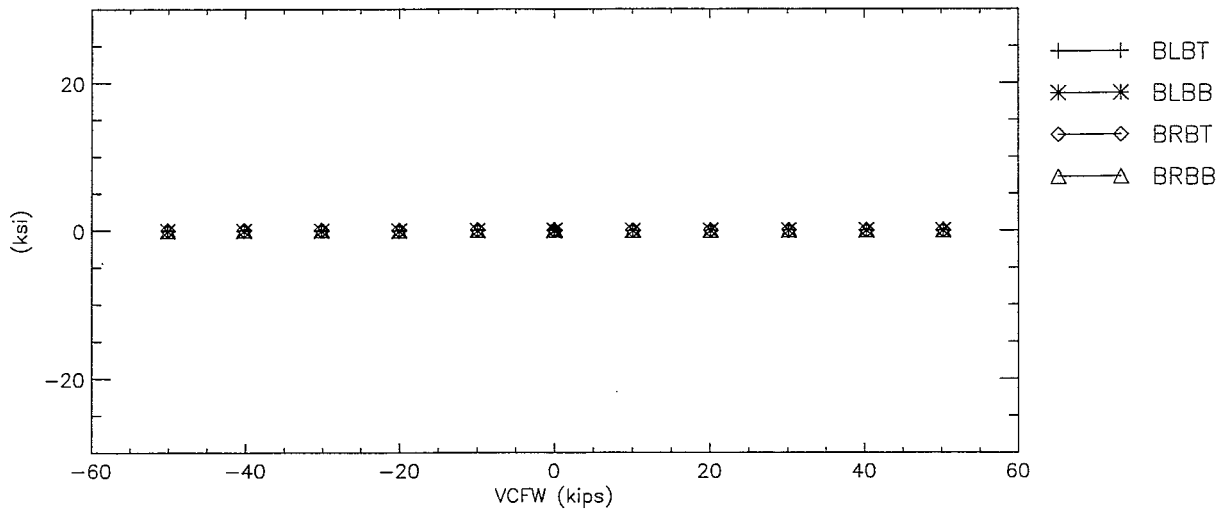
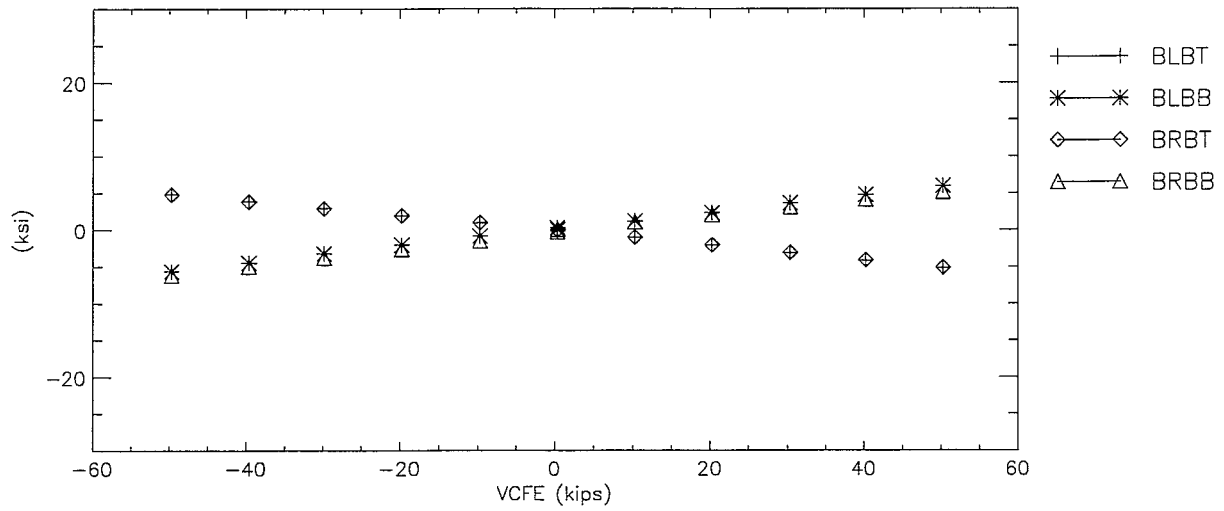
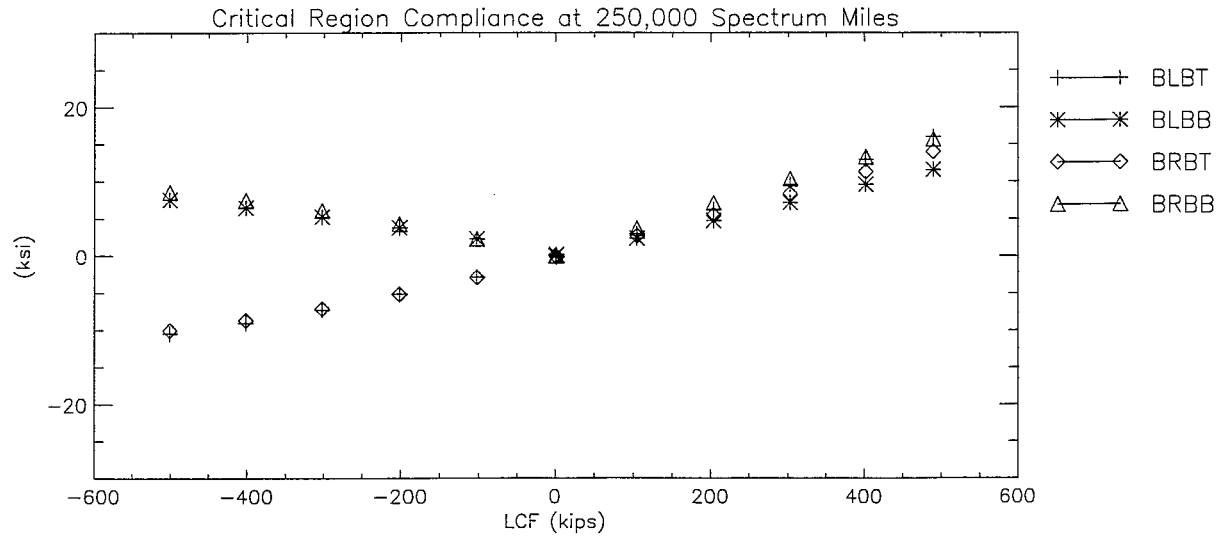


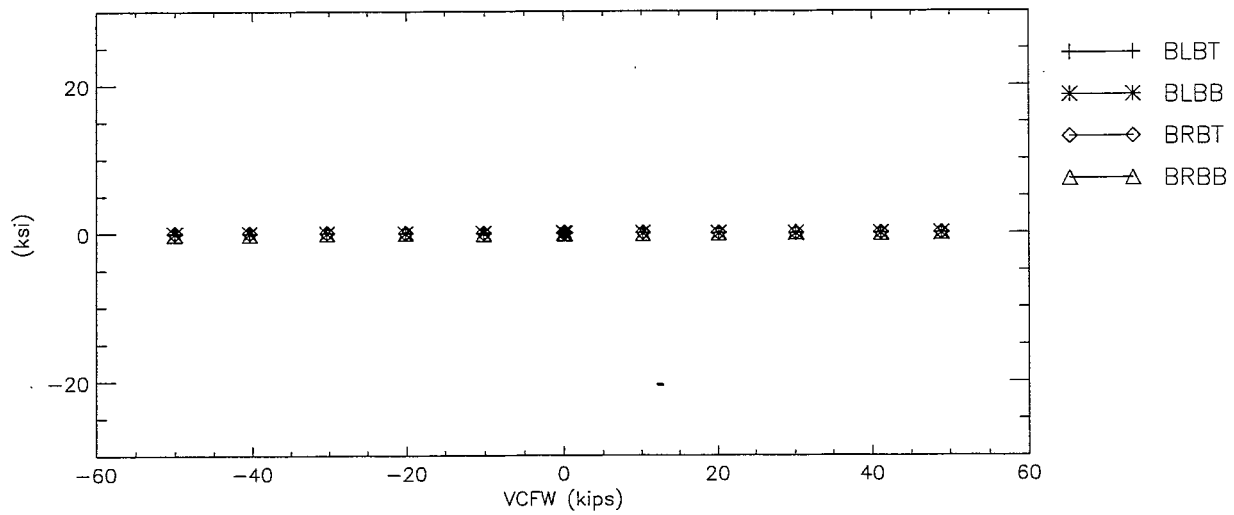
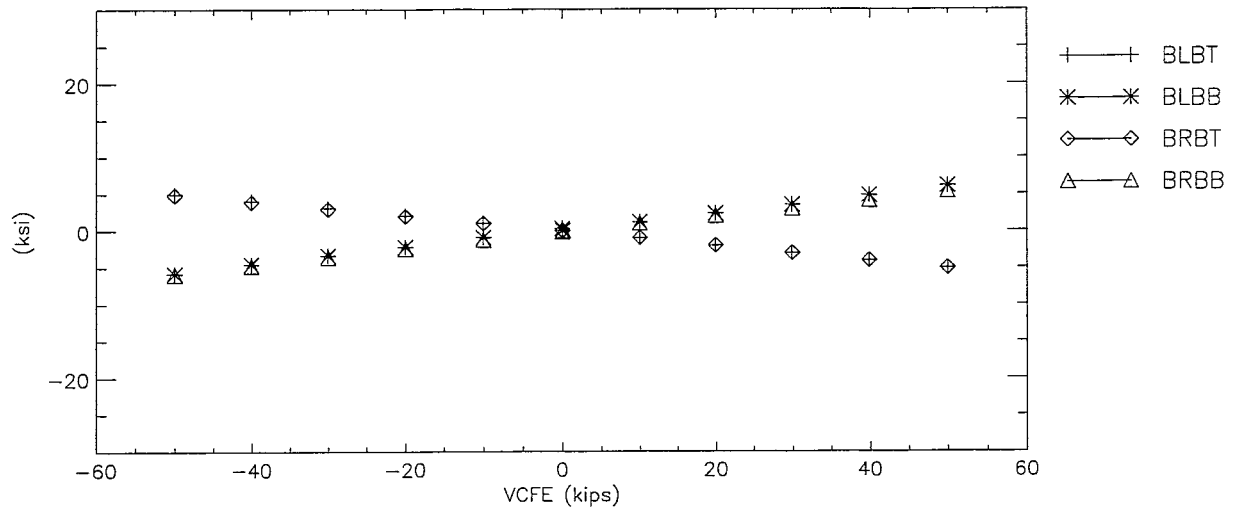
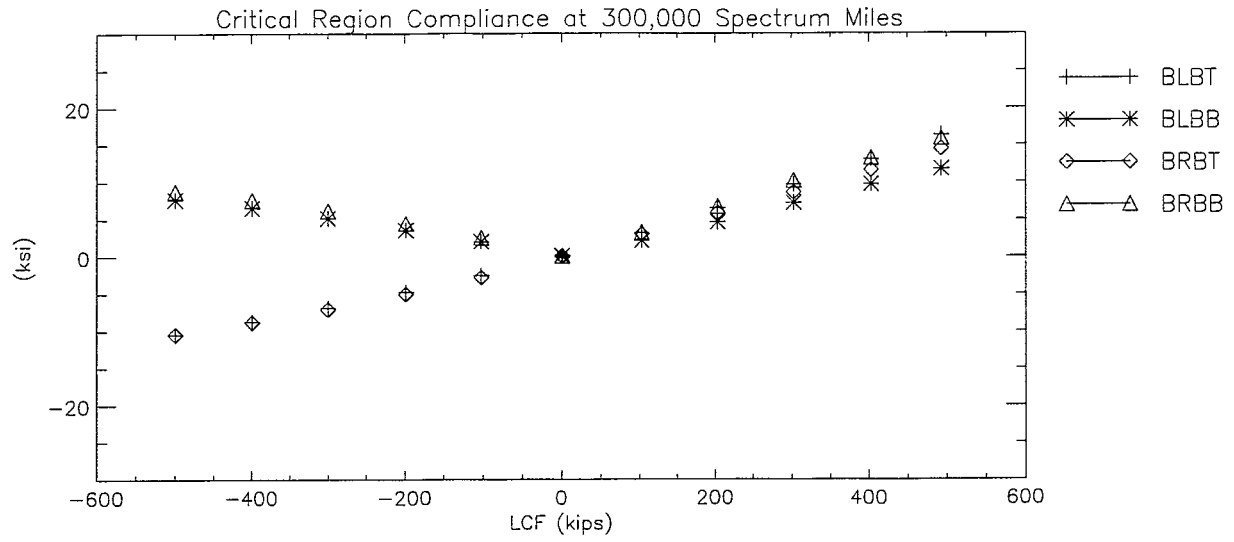






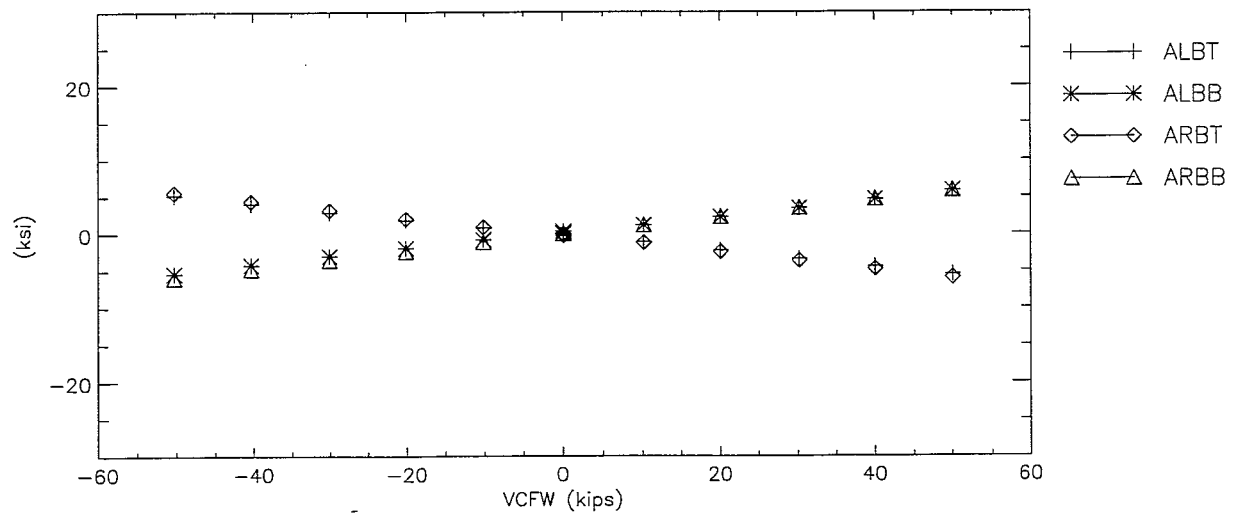
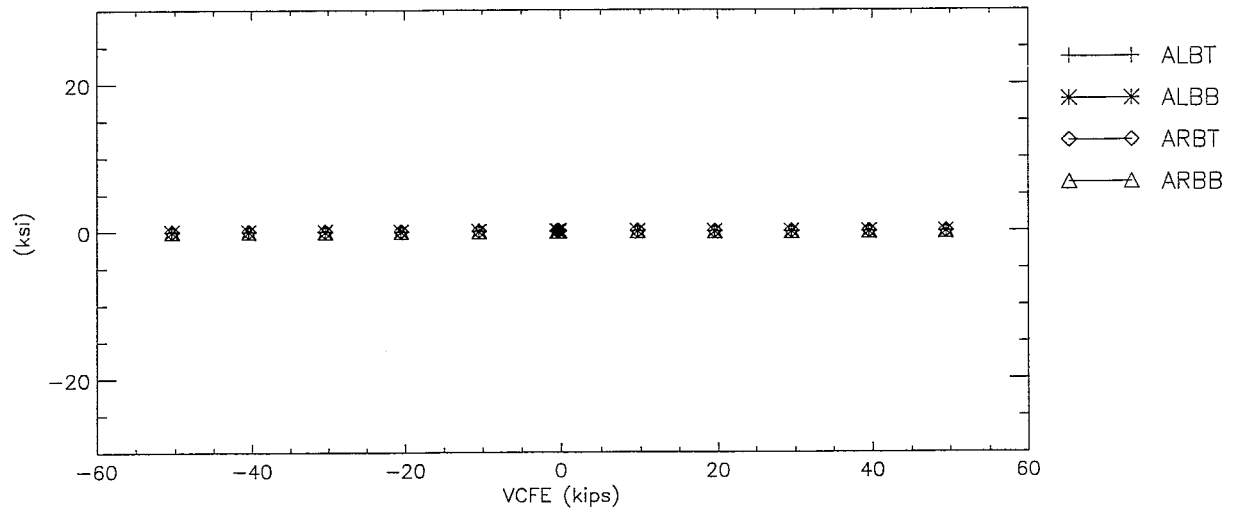
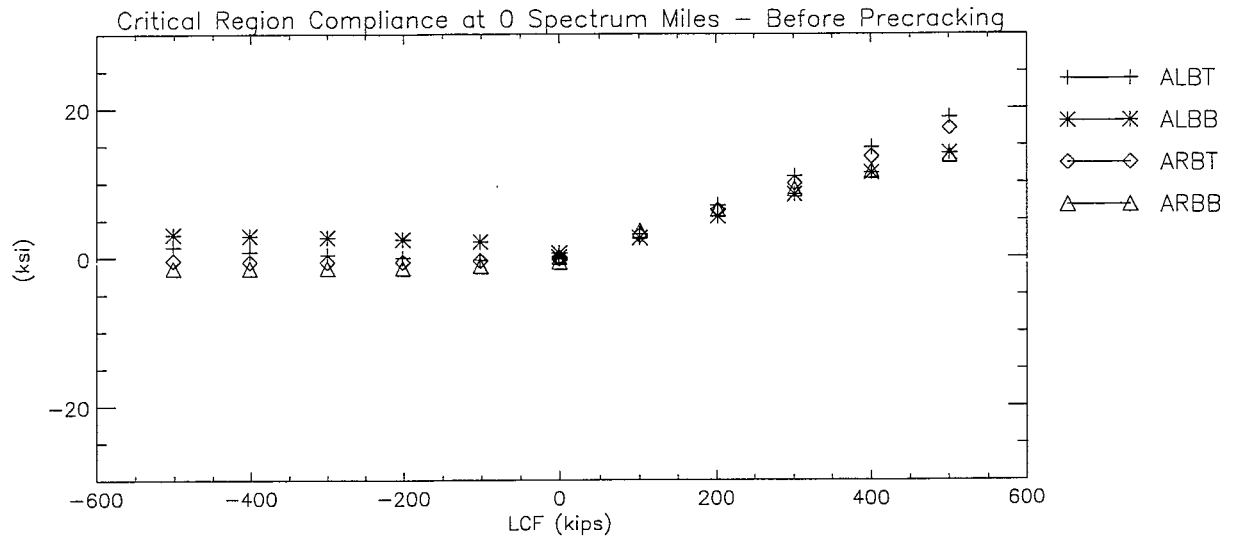


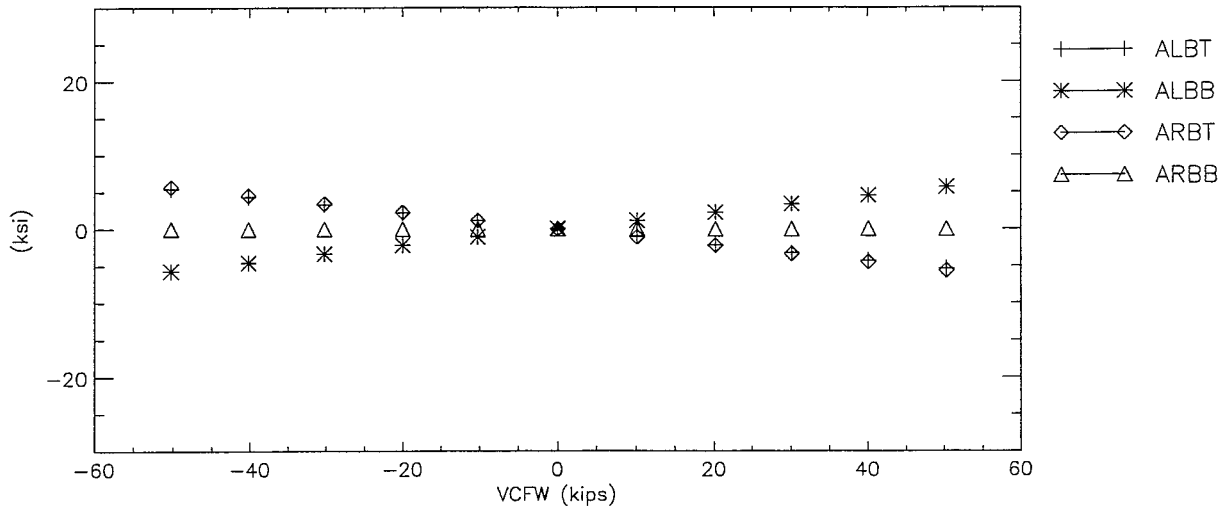
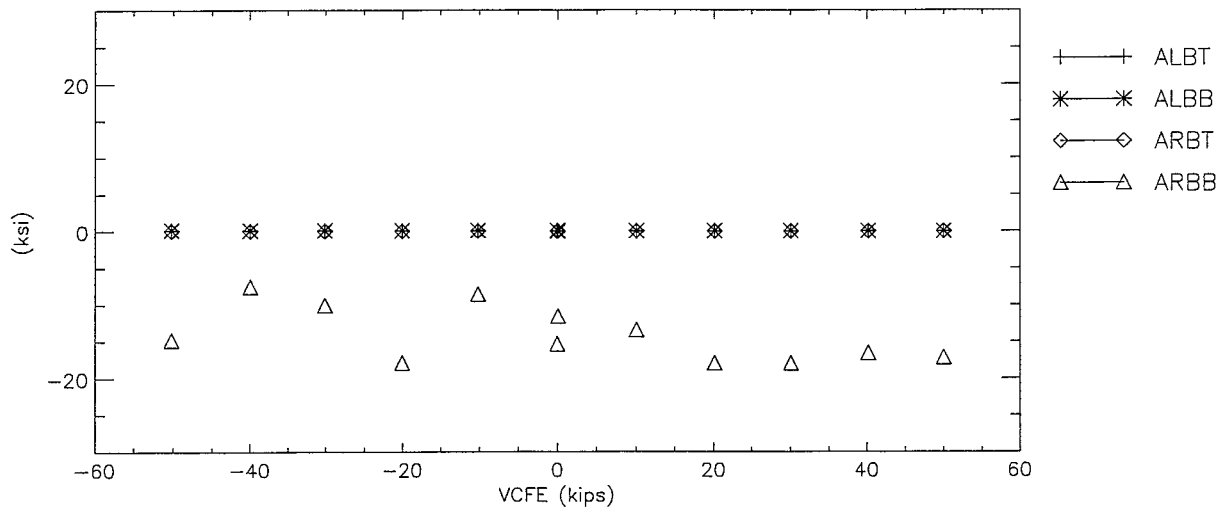
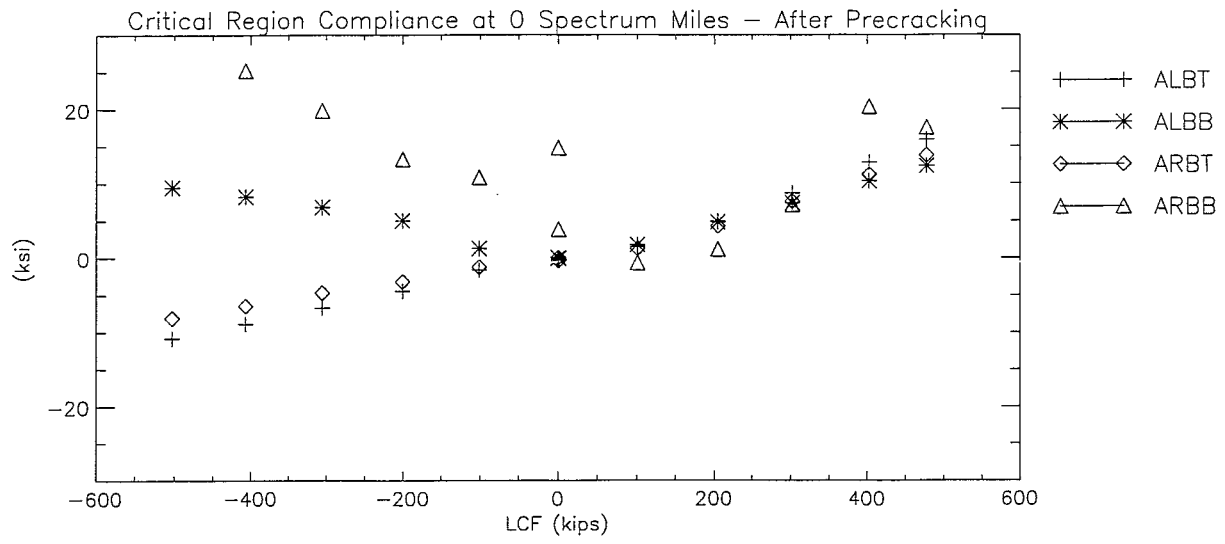


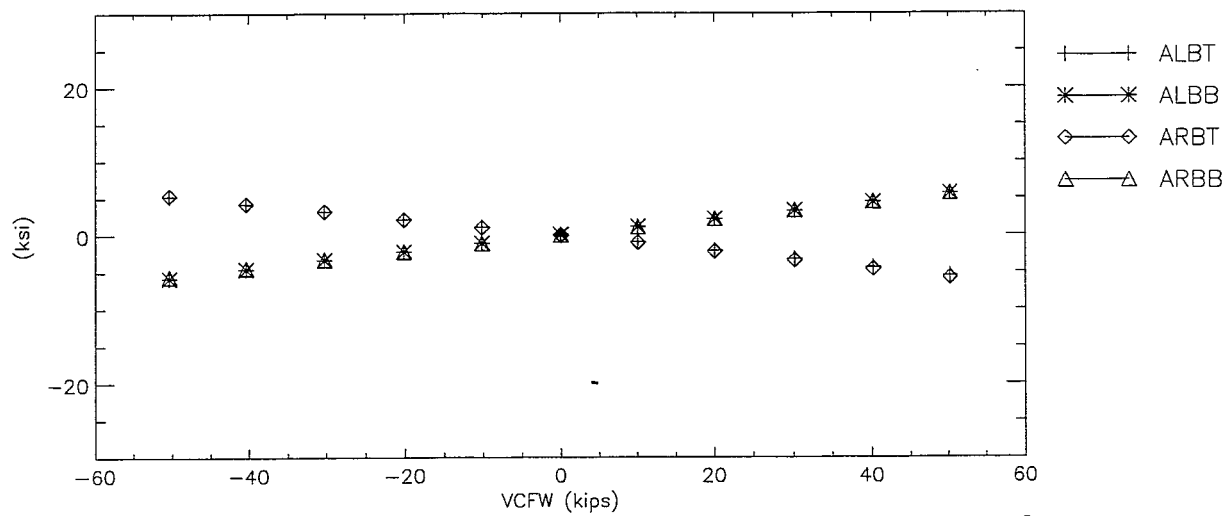
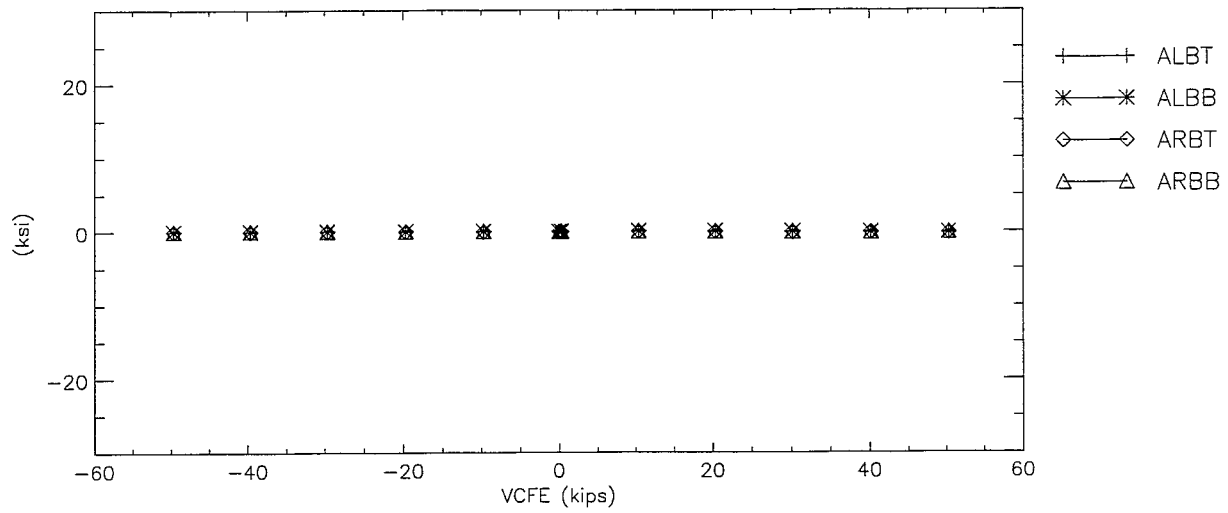
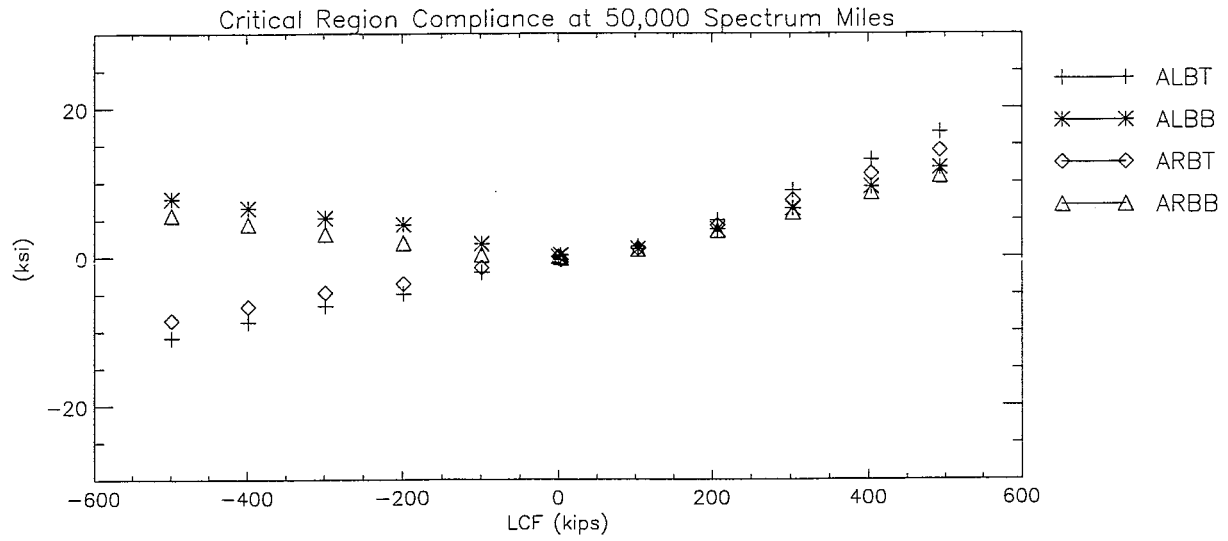


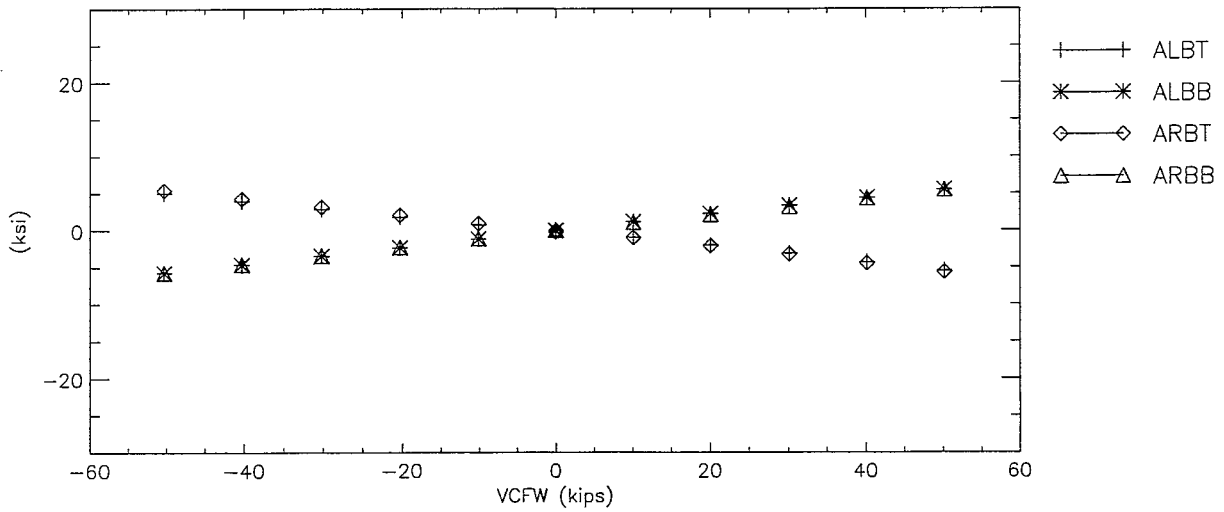
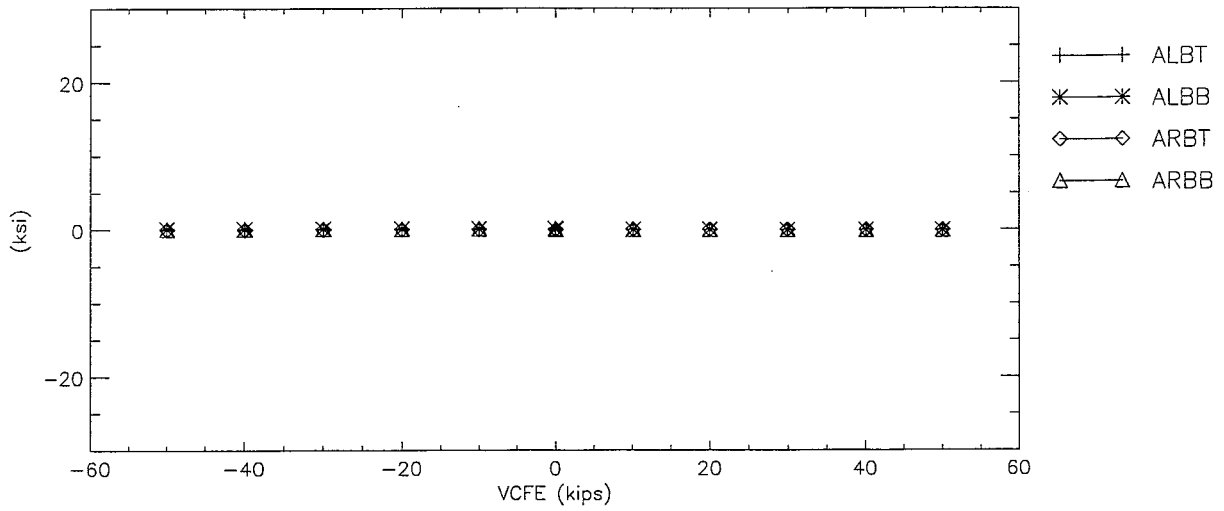
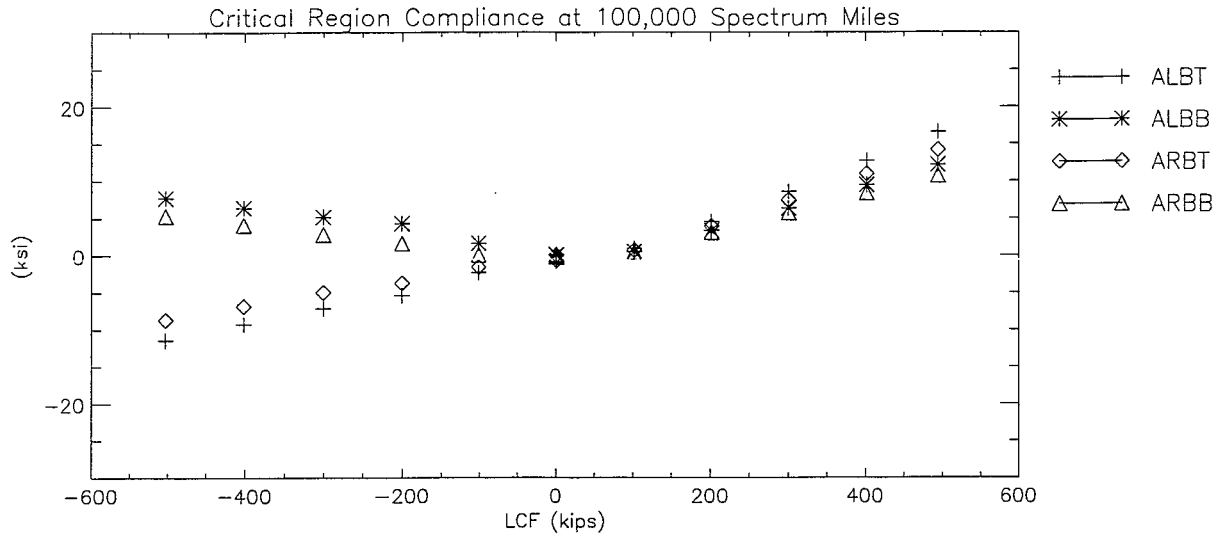
FINAL DRAFT

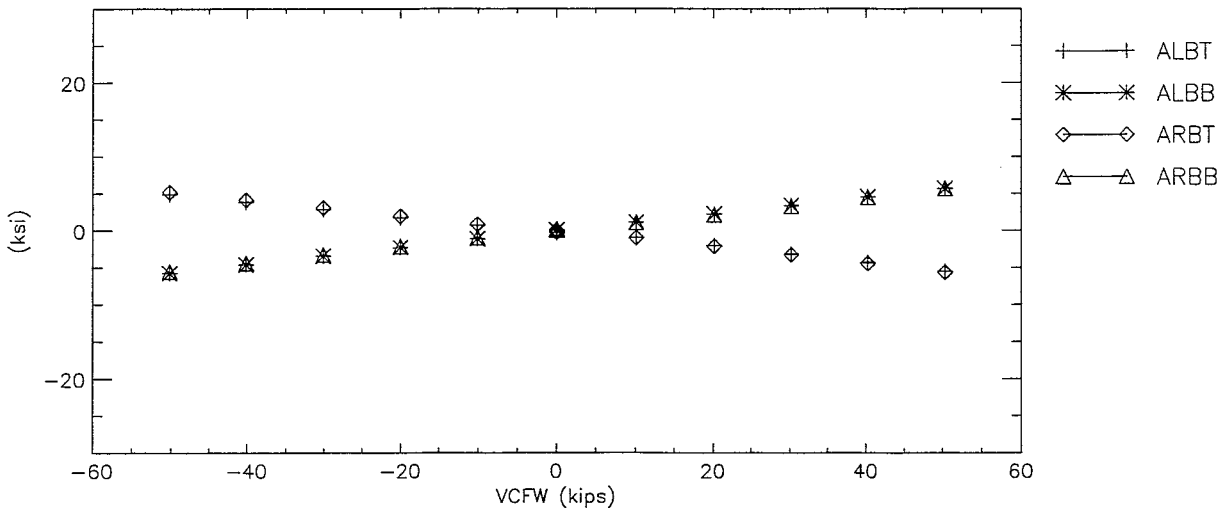
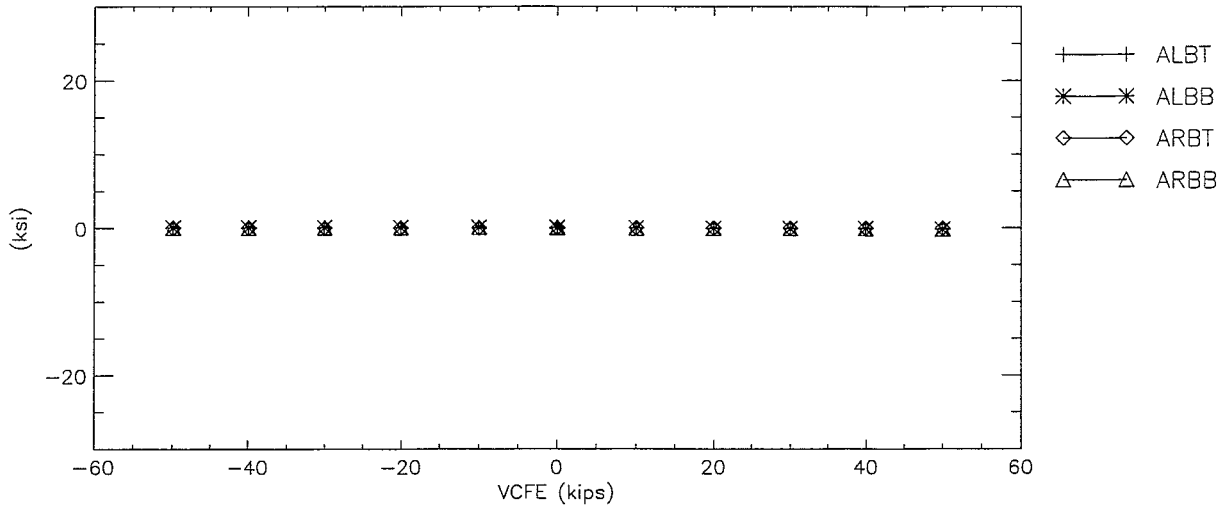
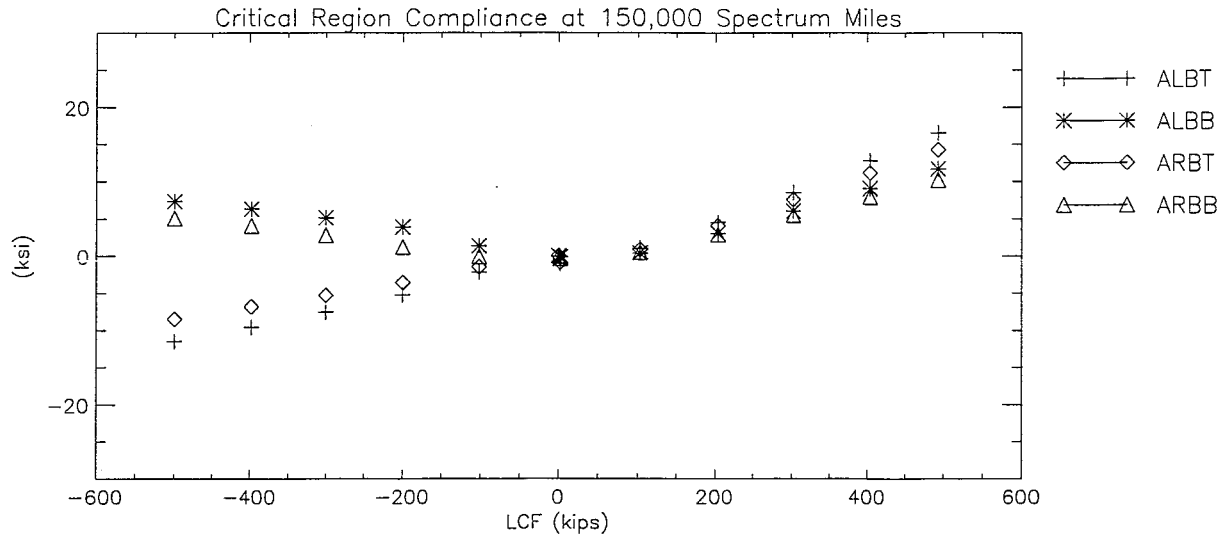
Section C-III: A-End Sill Bending Stresses

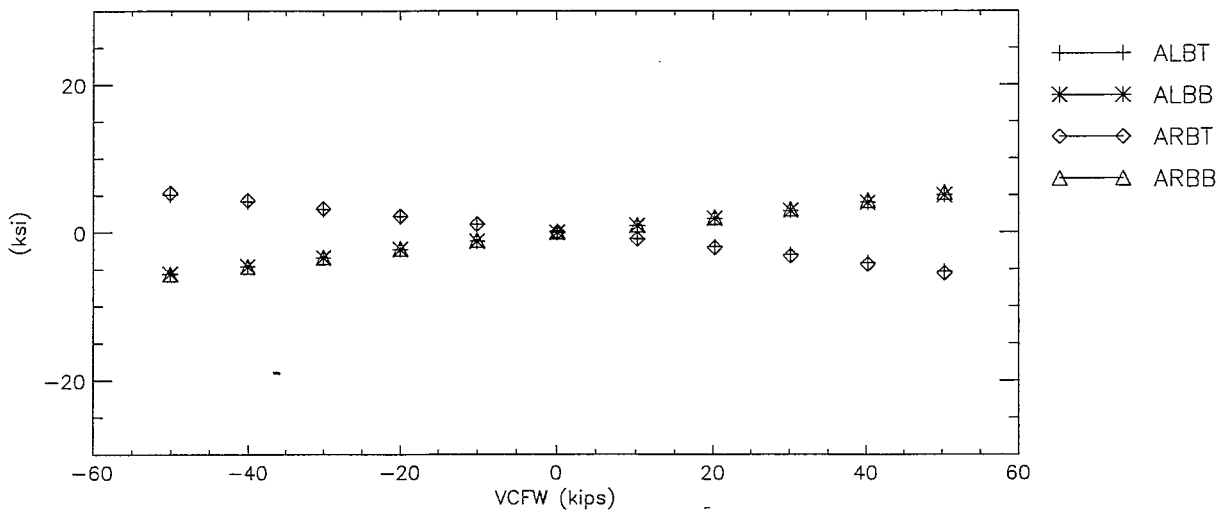
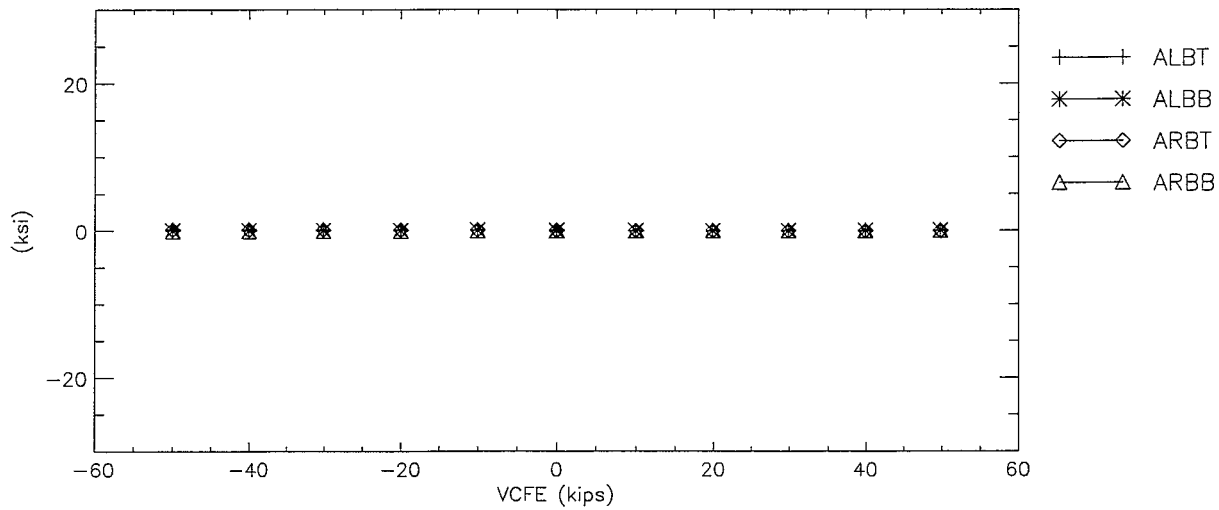
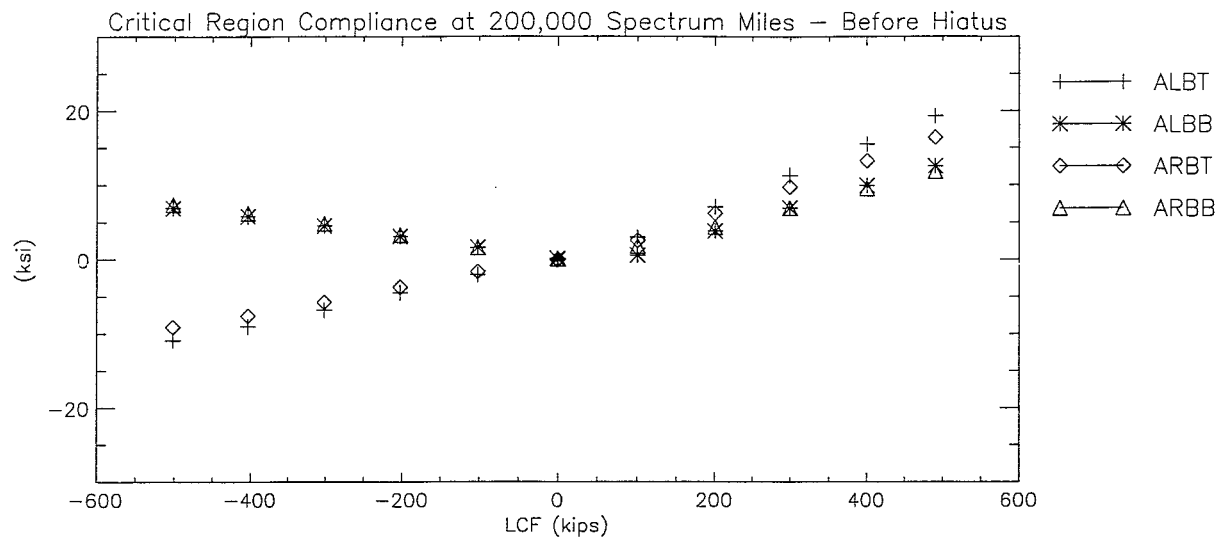


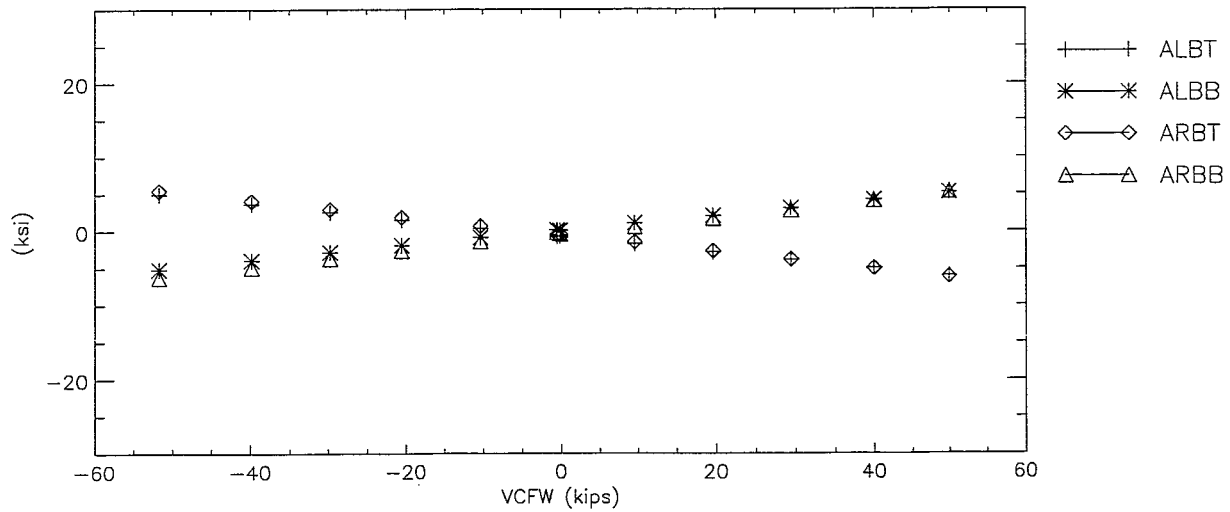
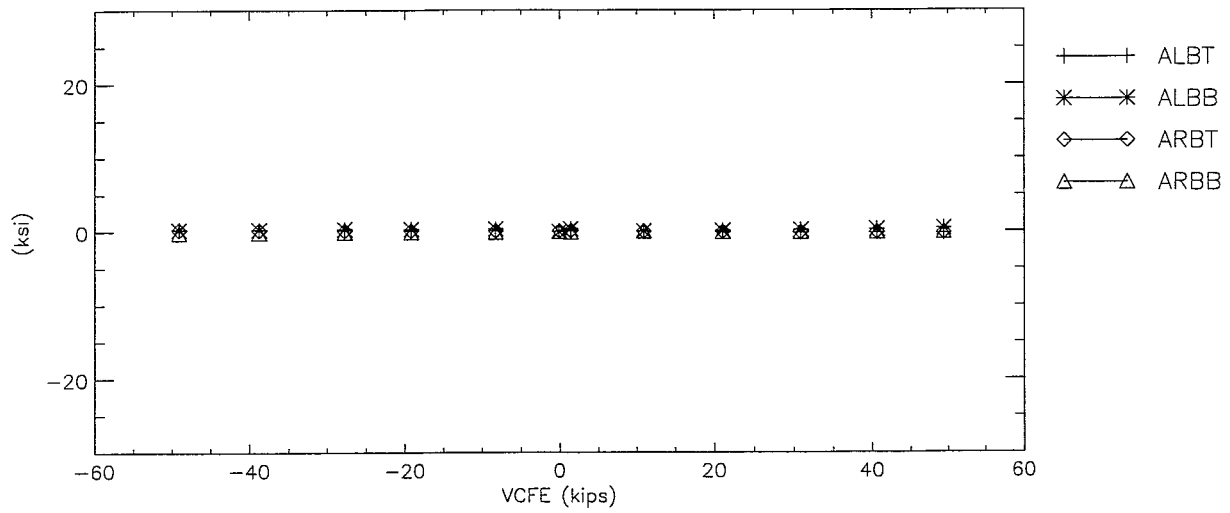
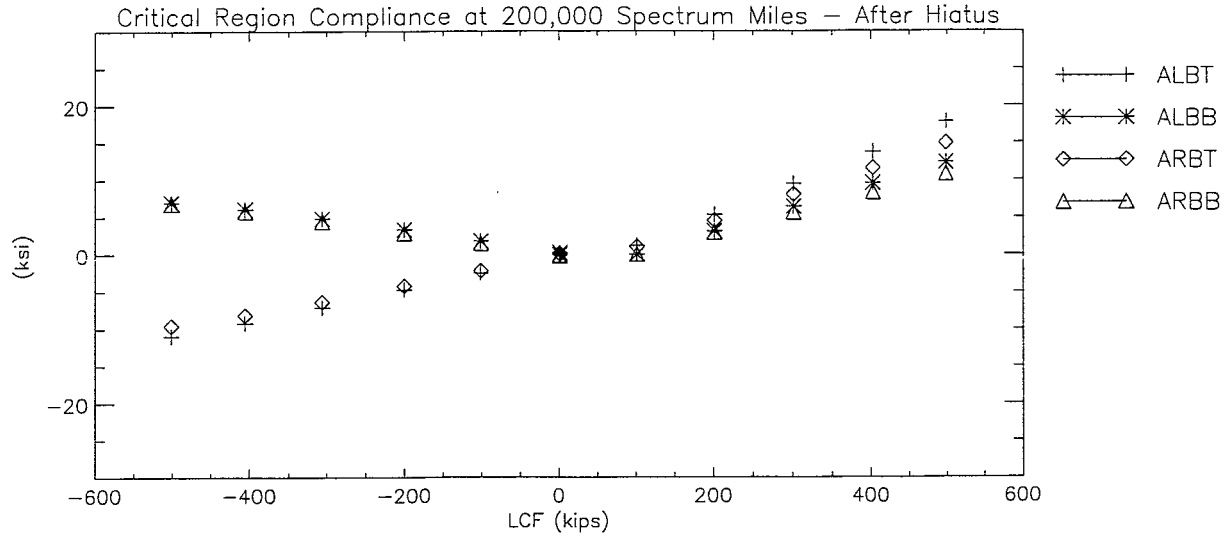


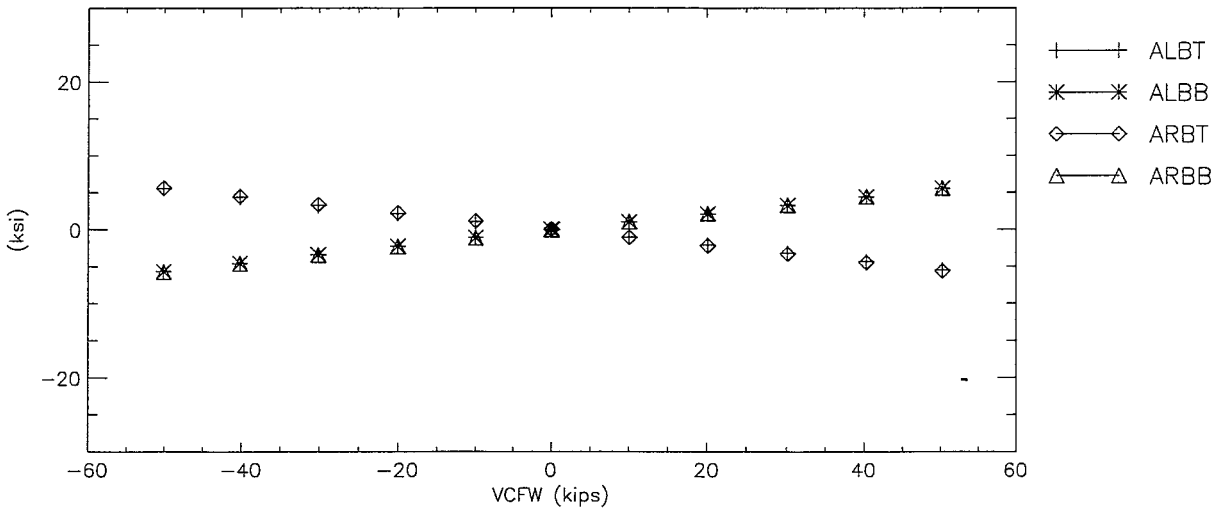
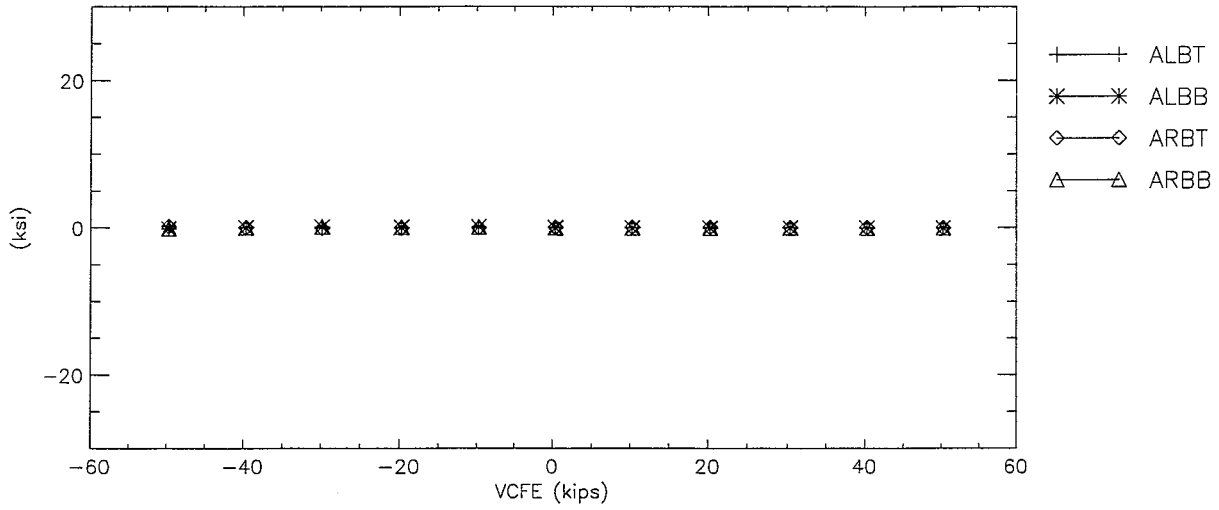
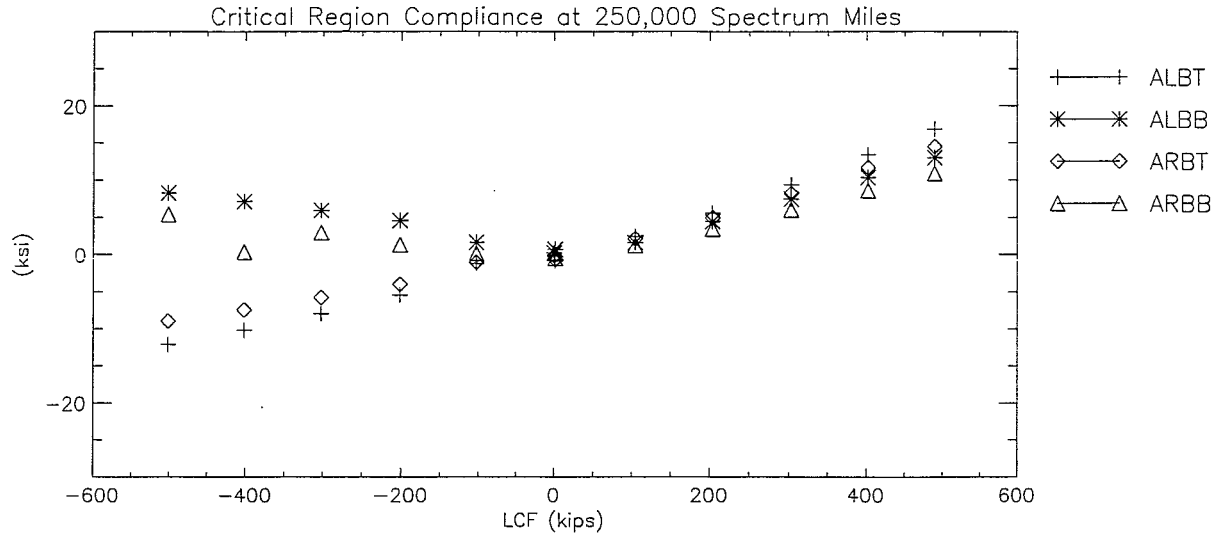


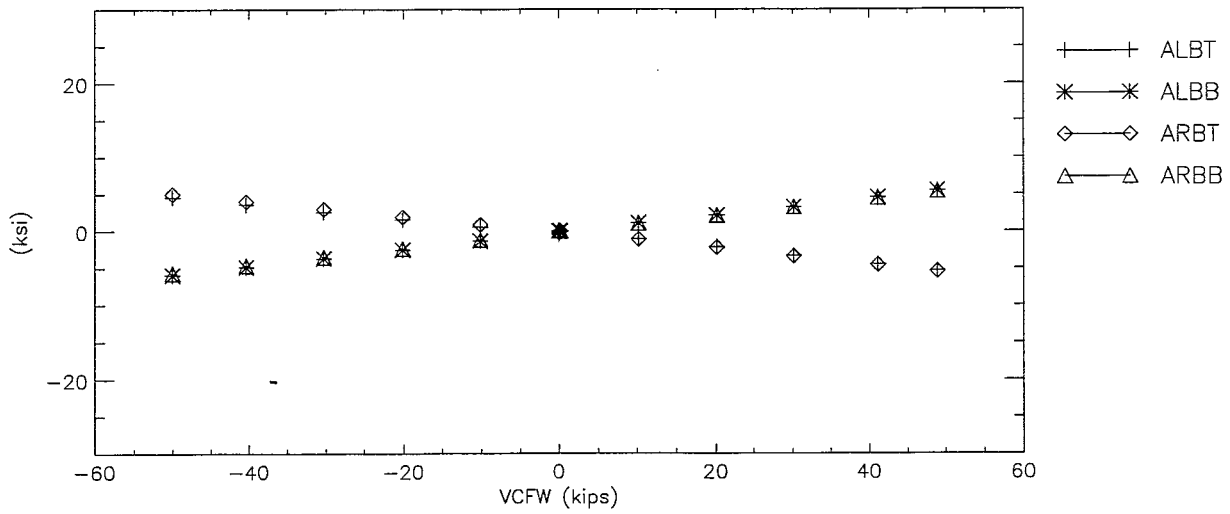
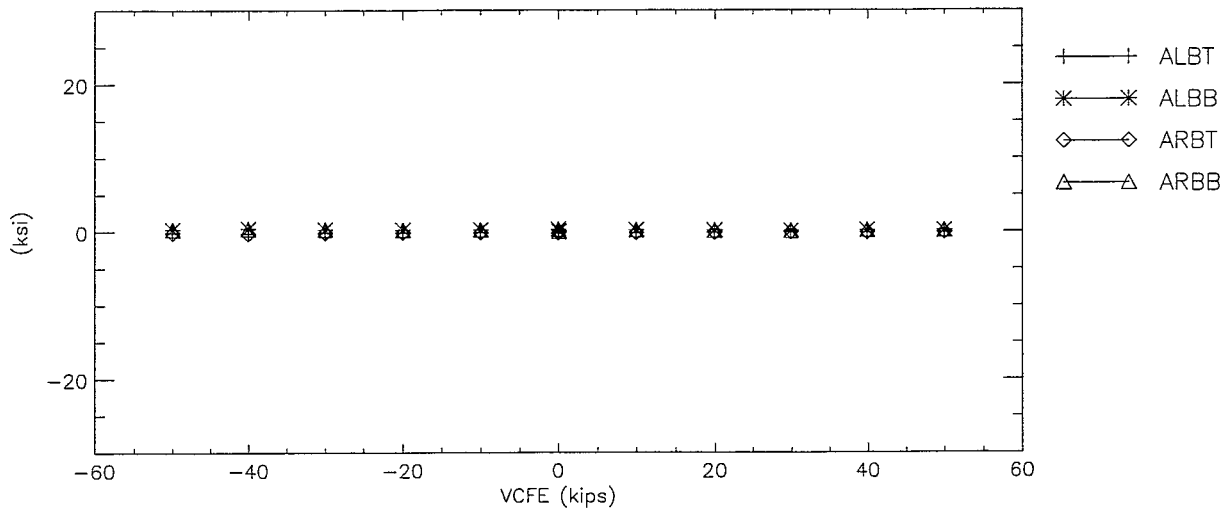
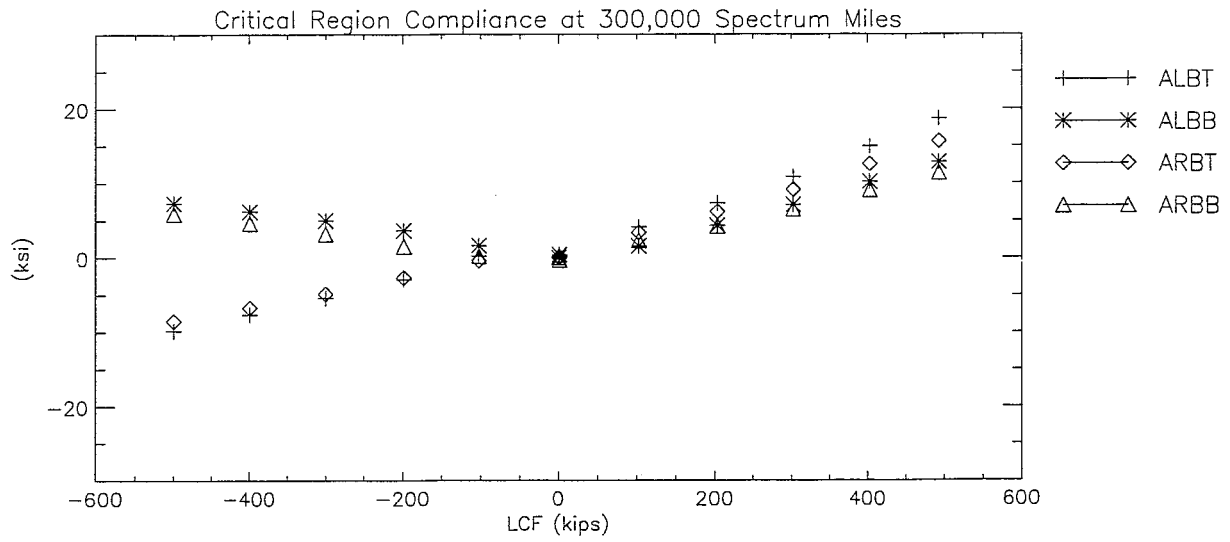








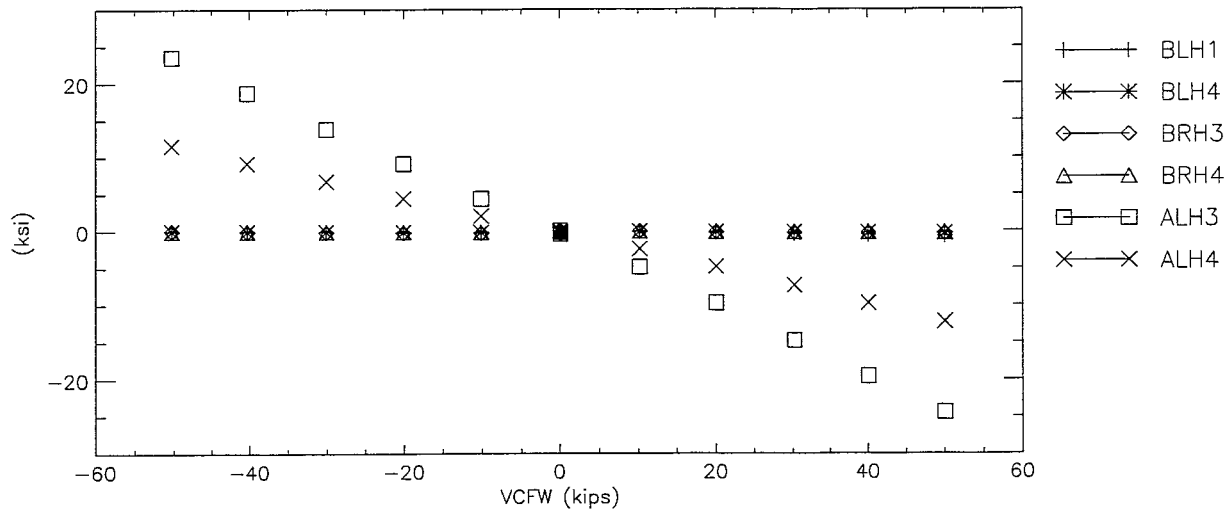
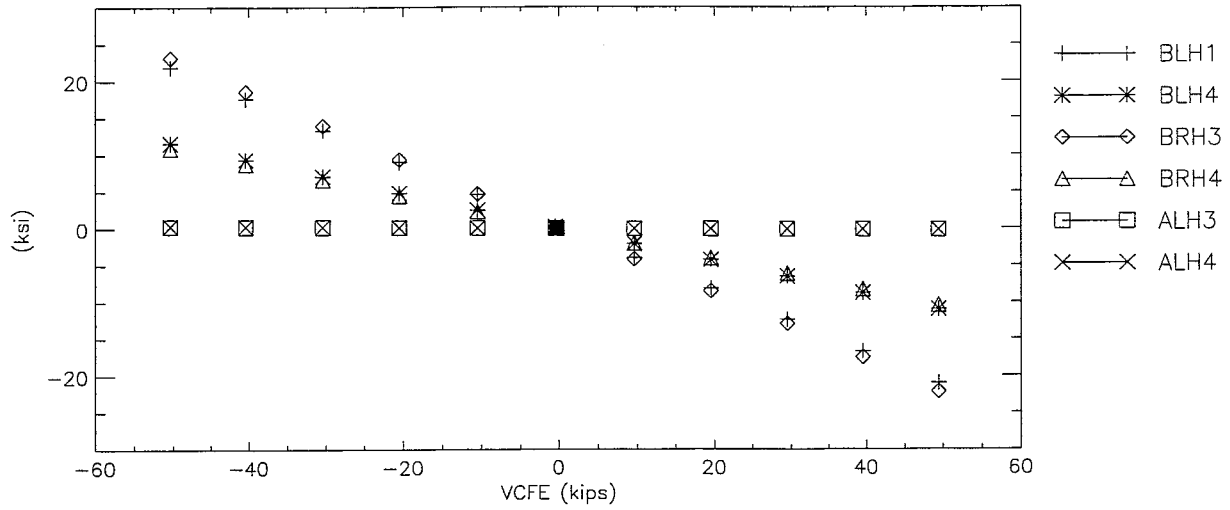
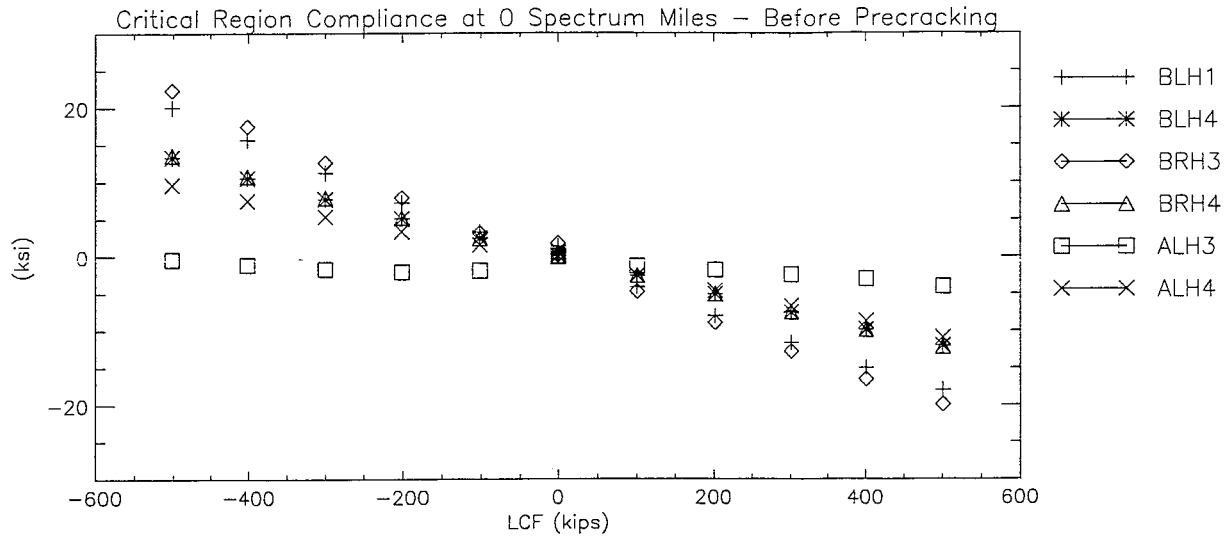


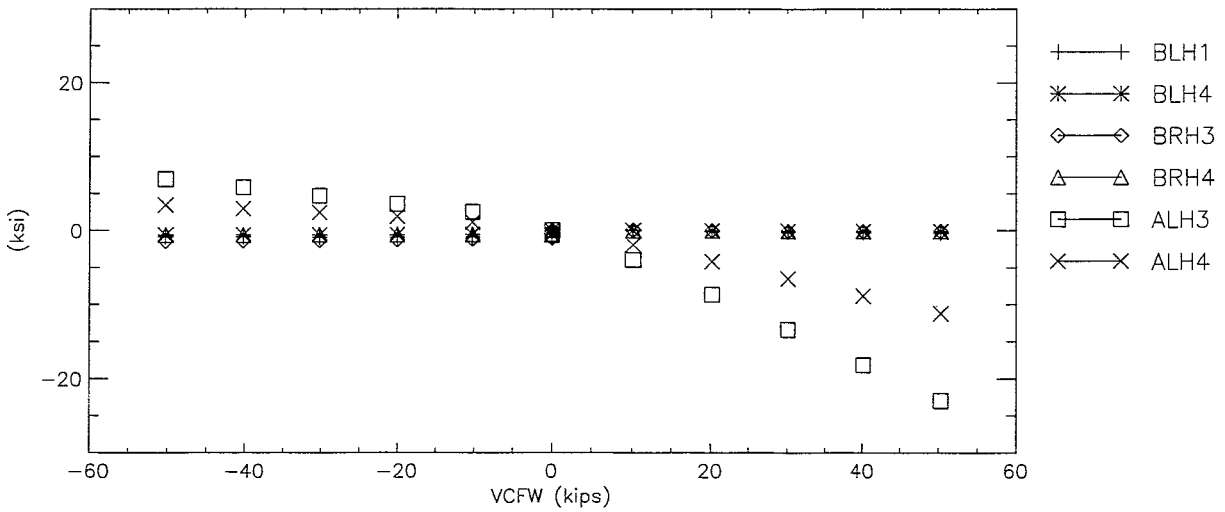
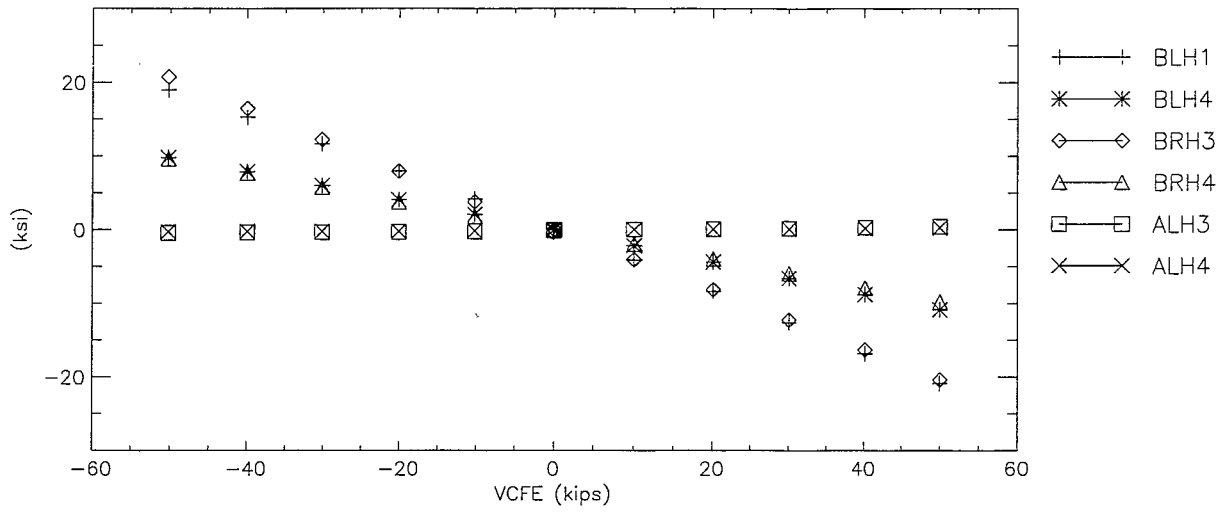
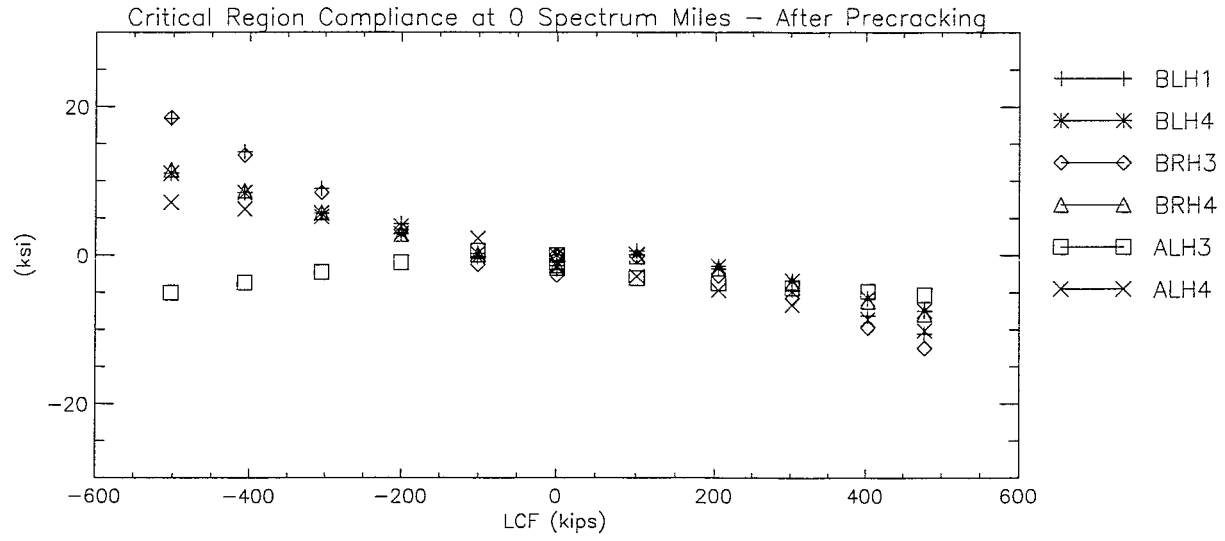


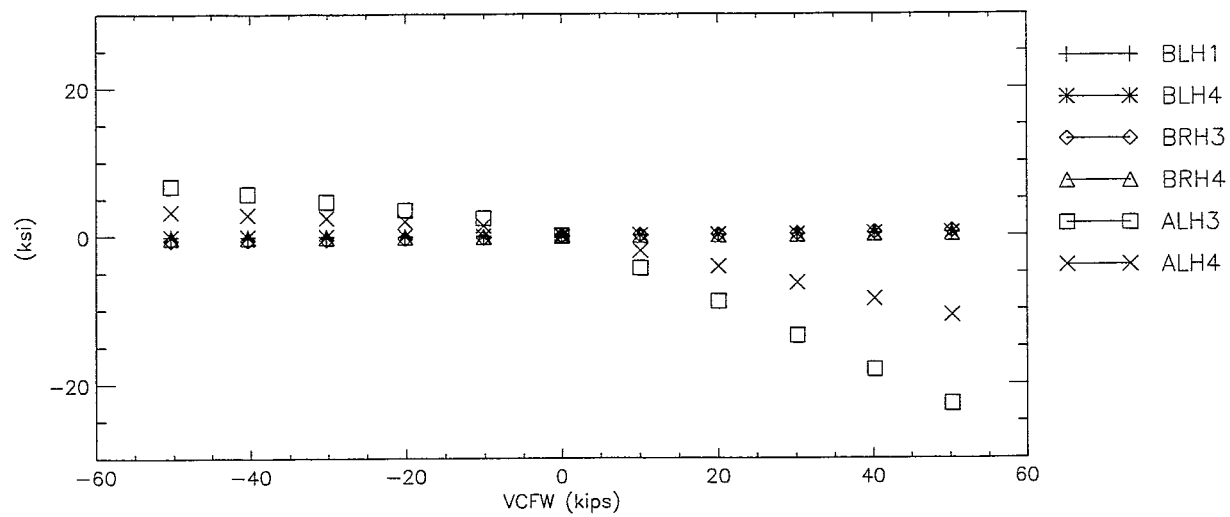
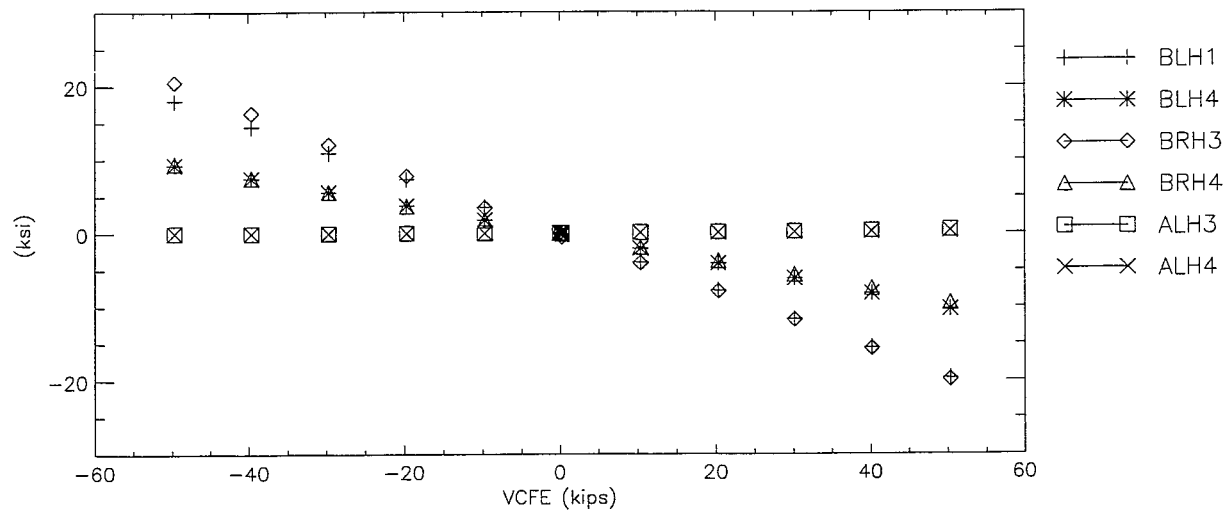
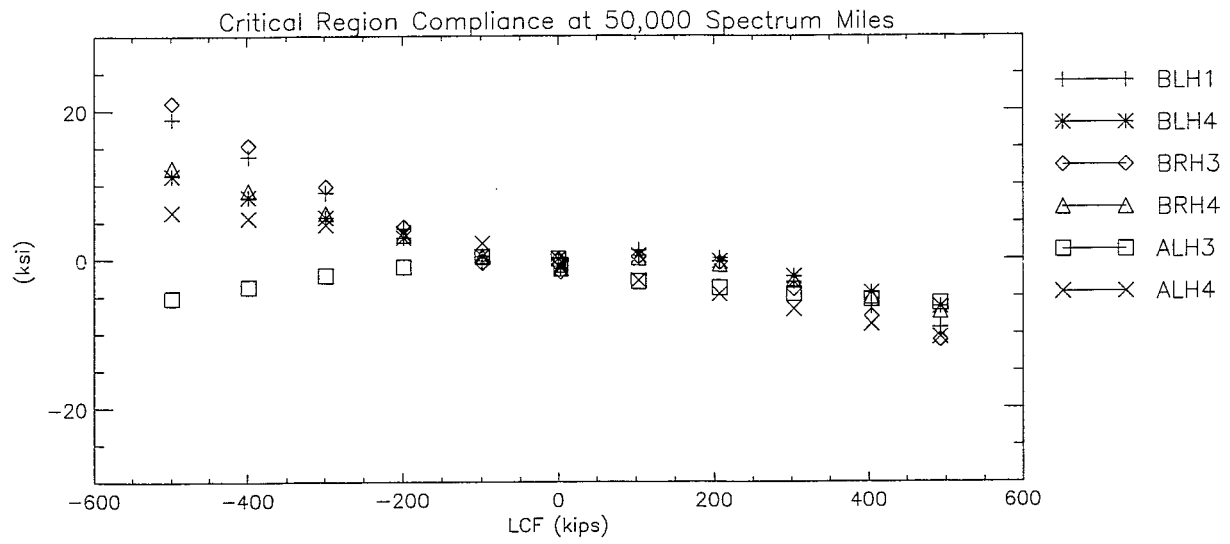
FINAL DRAFT

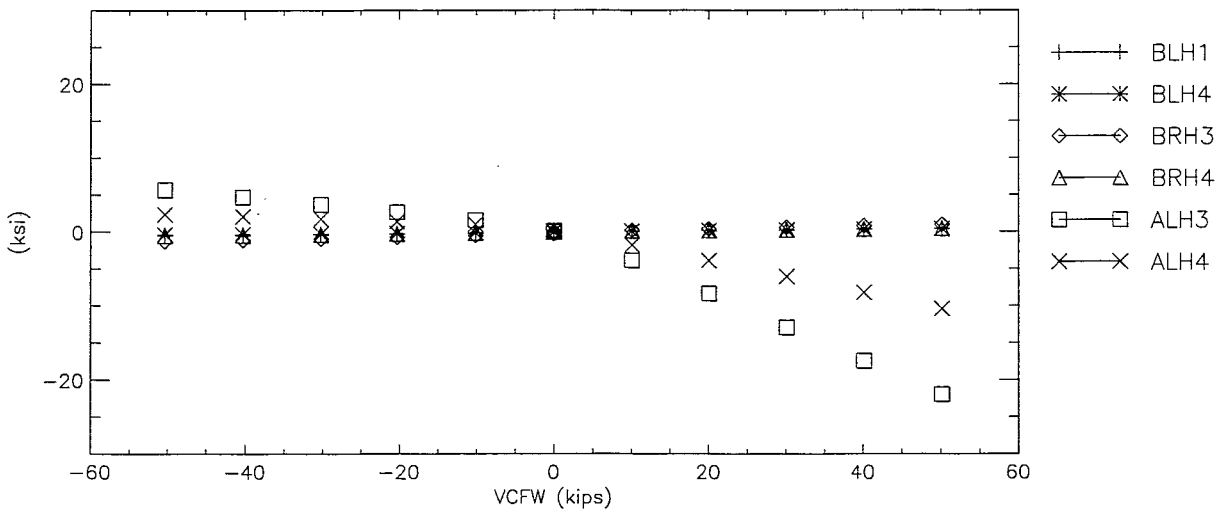
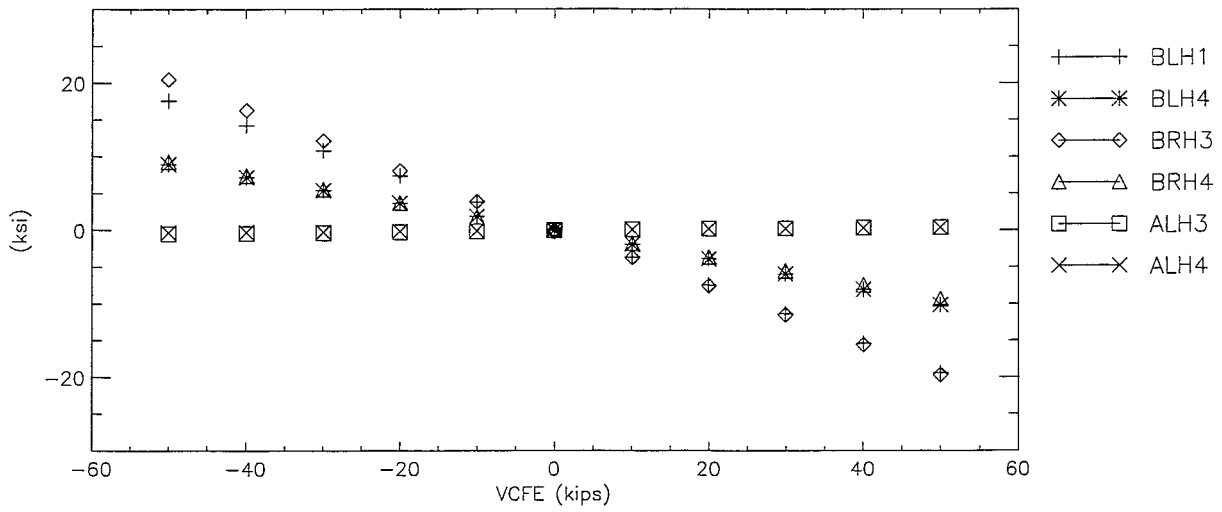
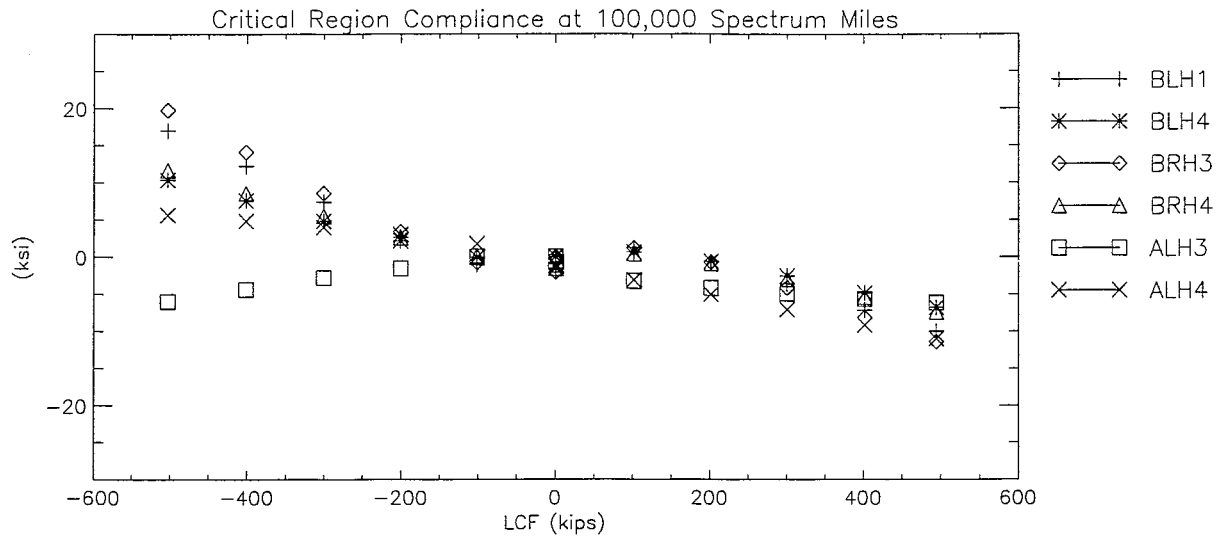
Section C-IV: Vertical Head Stresses (BL, BR and AL)

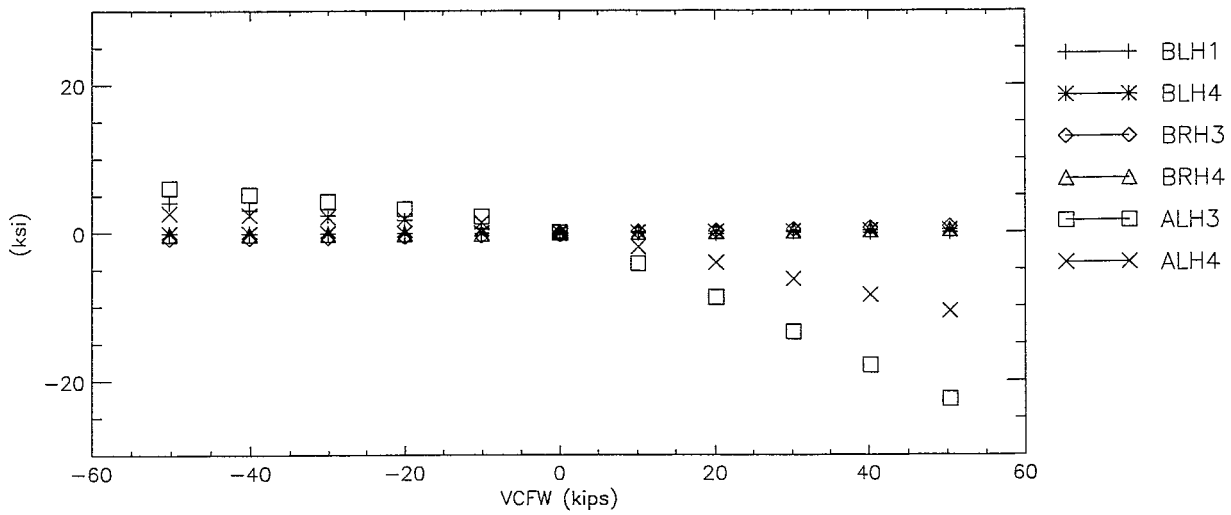
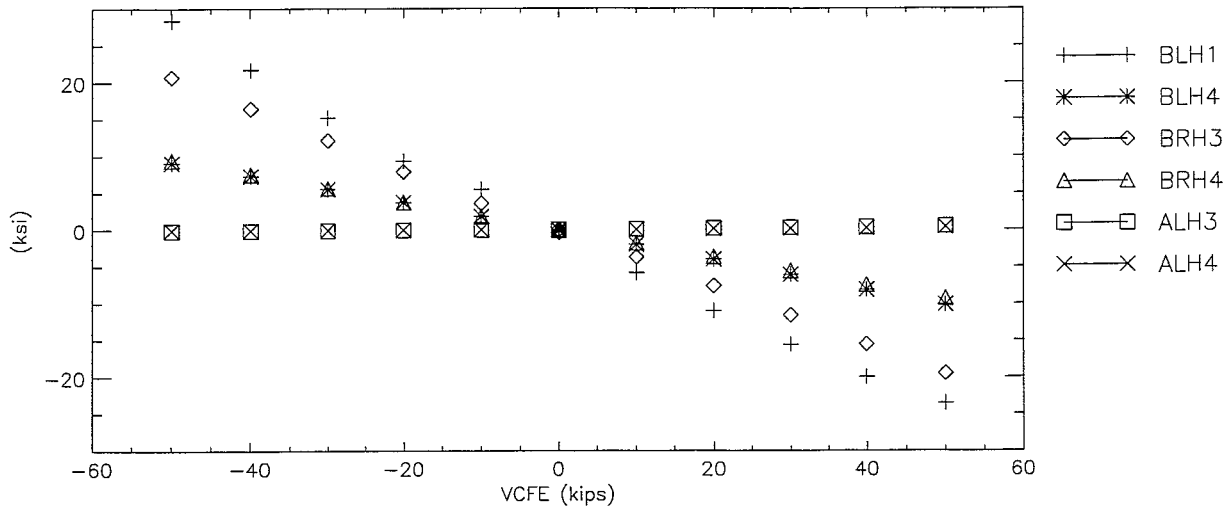
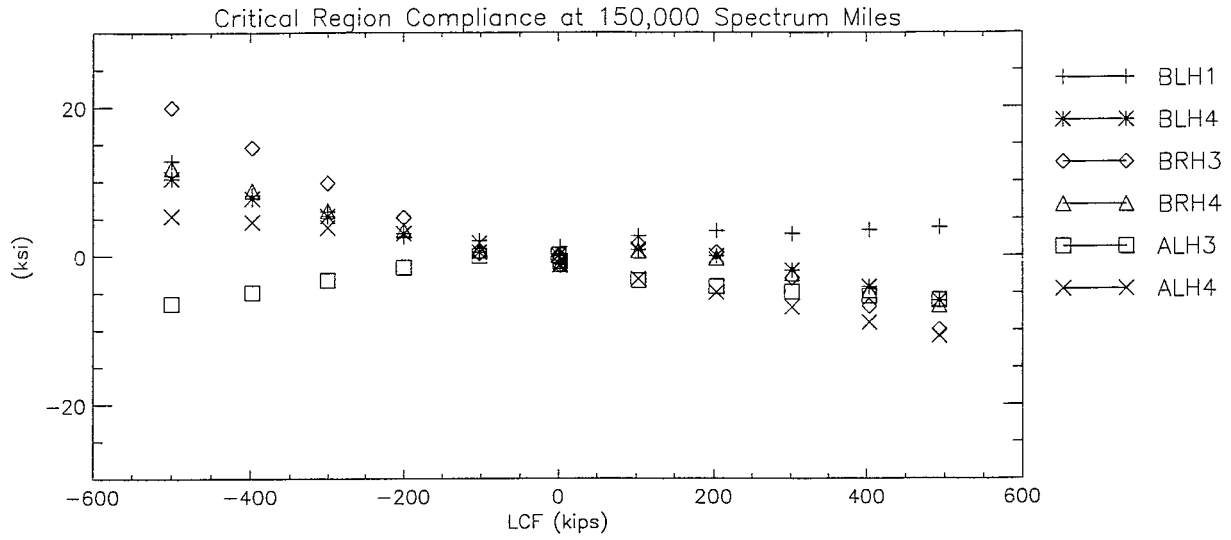
FINAL DRAFT

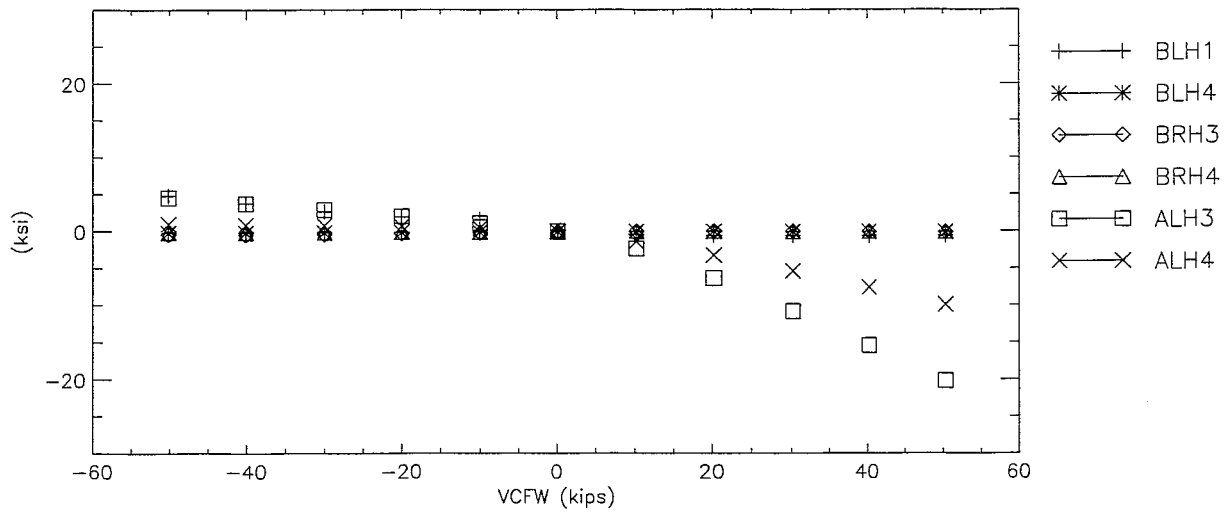
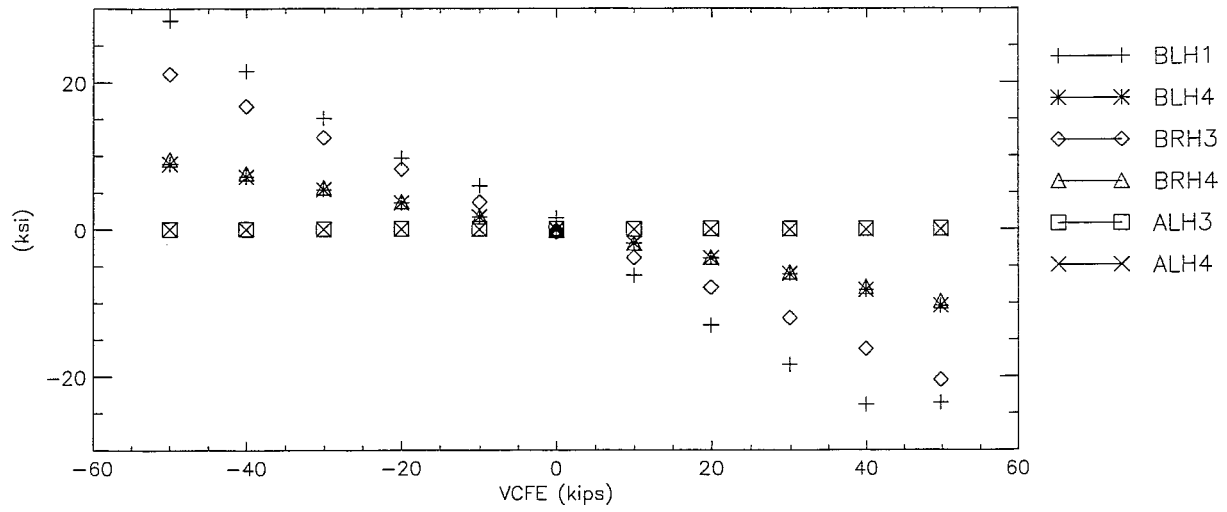
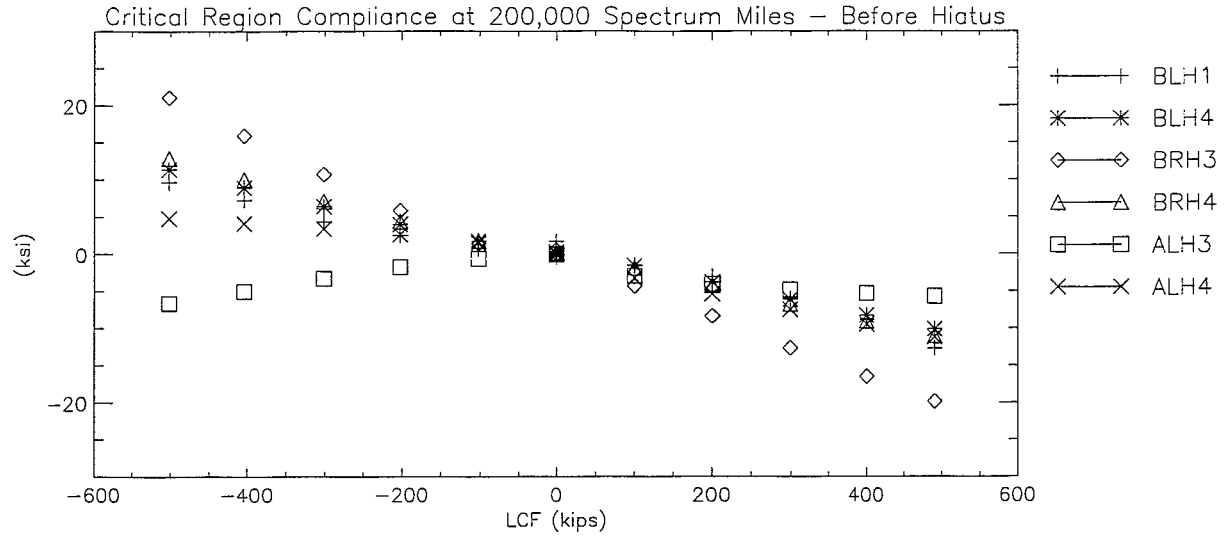


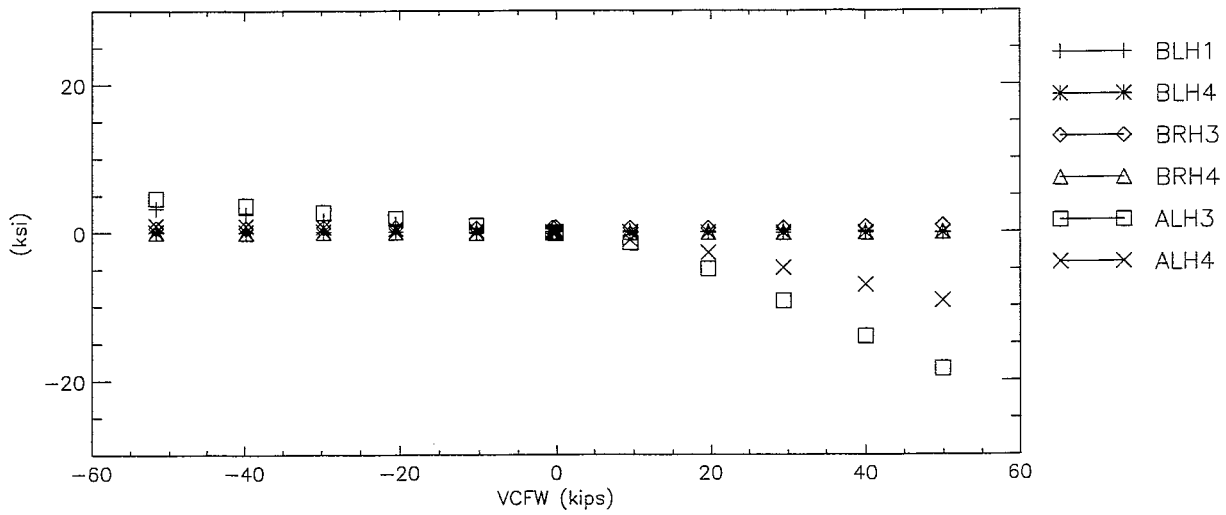
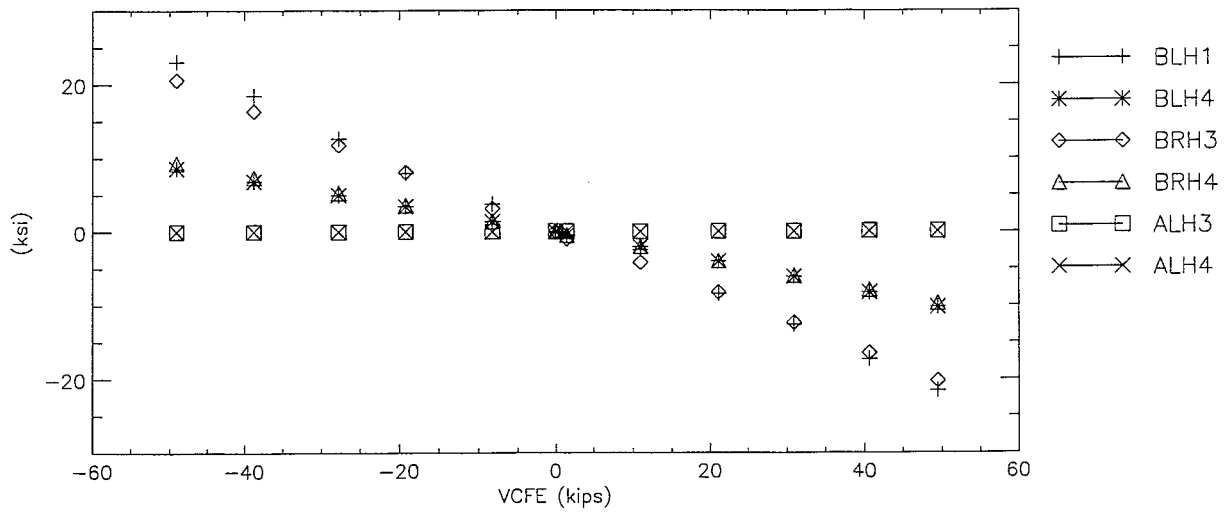
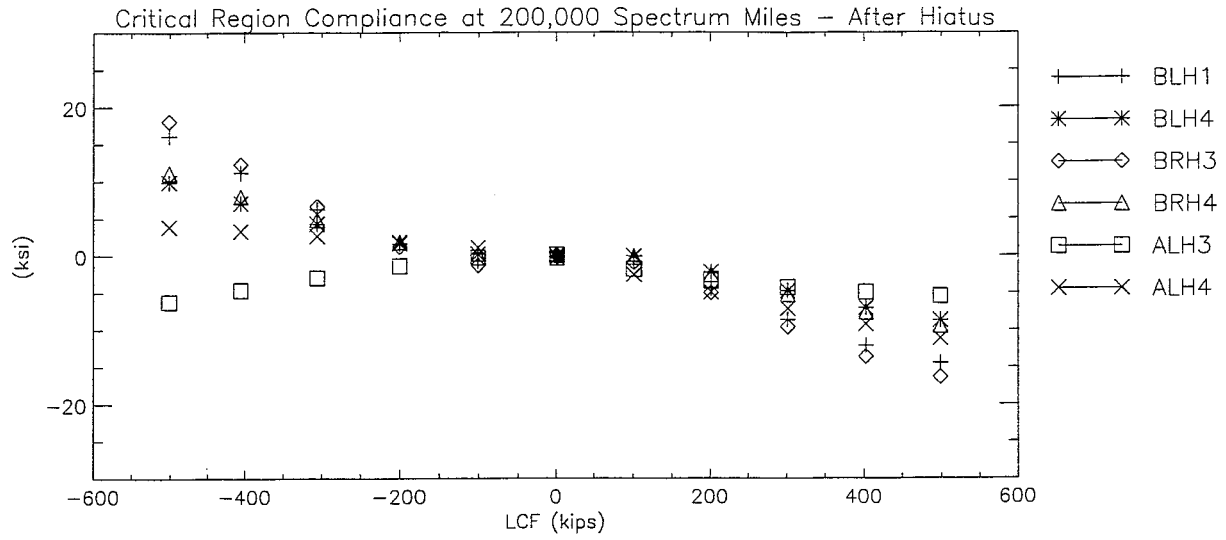


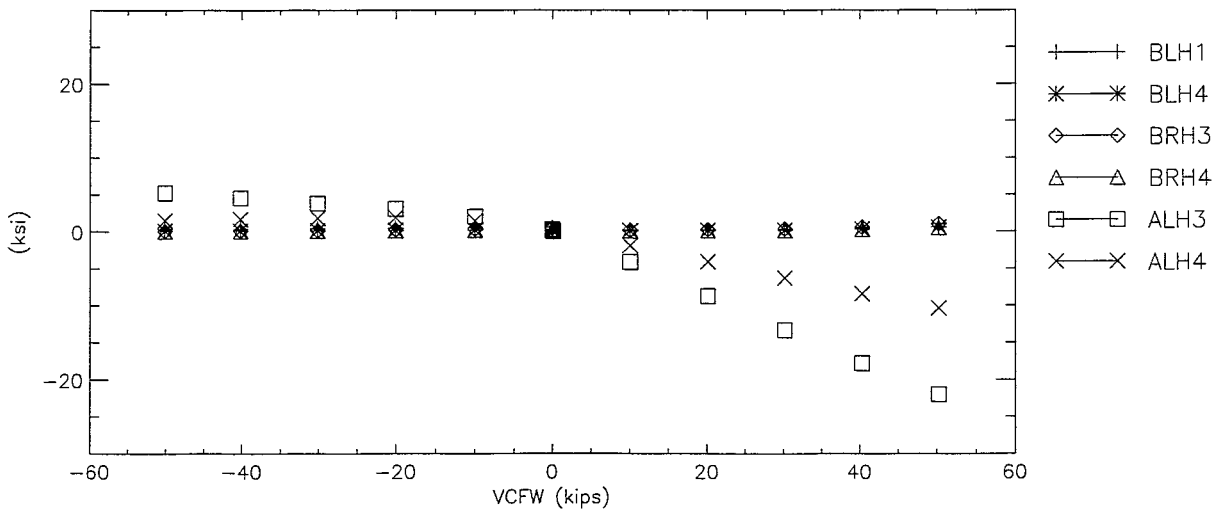
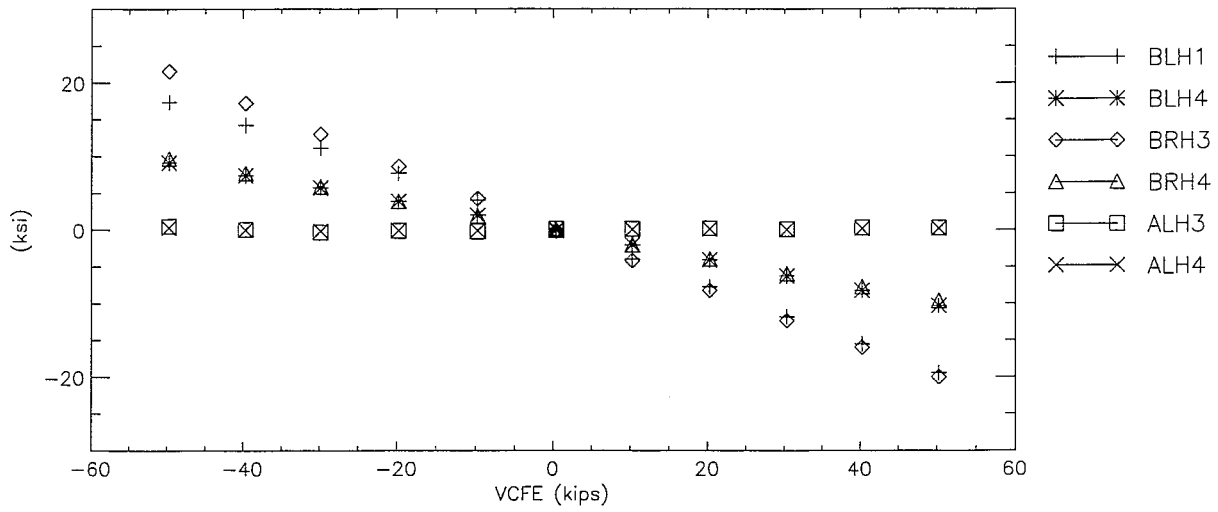
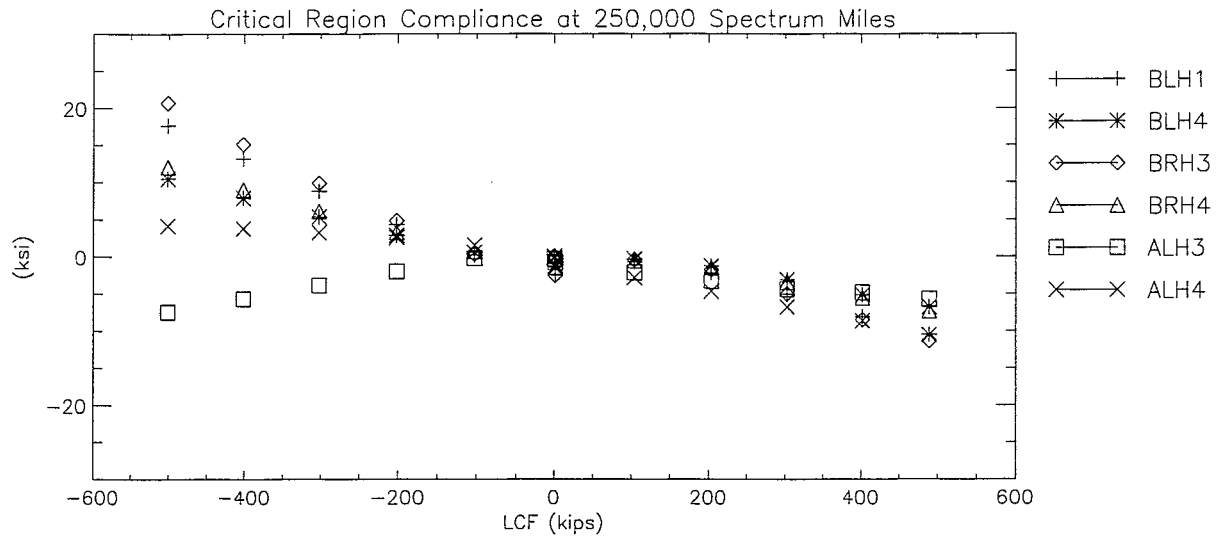


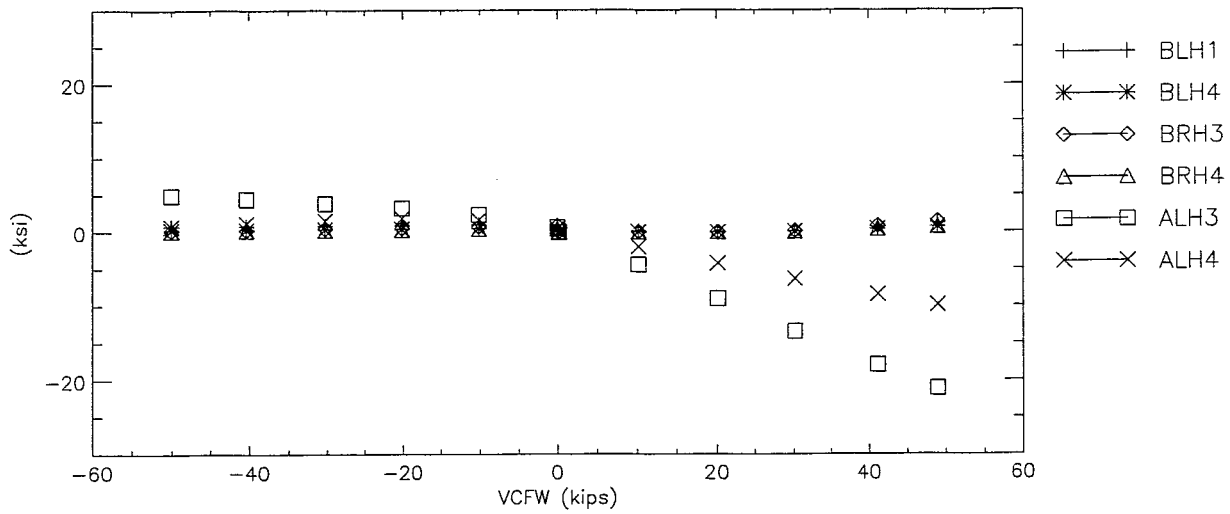
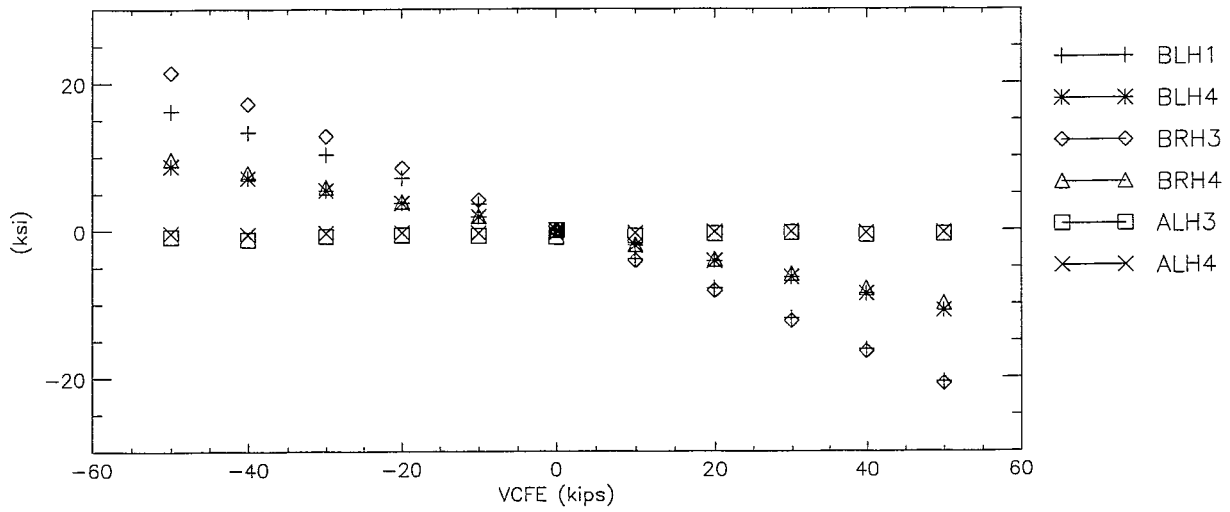
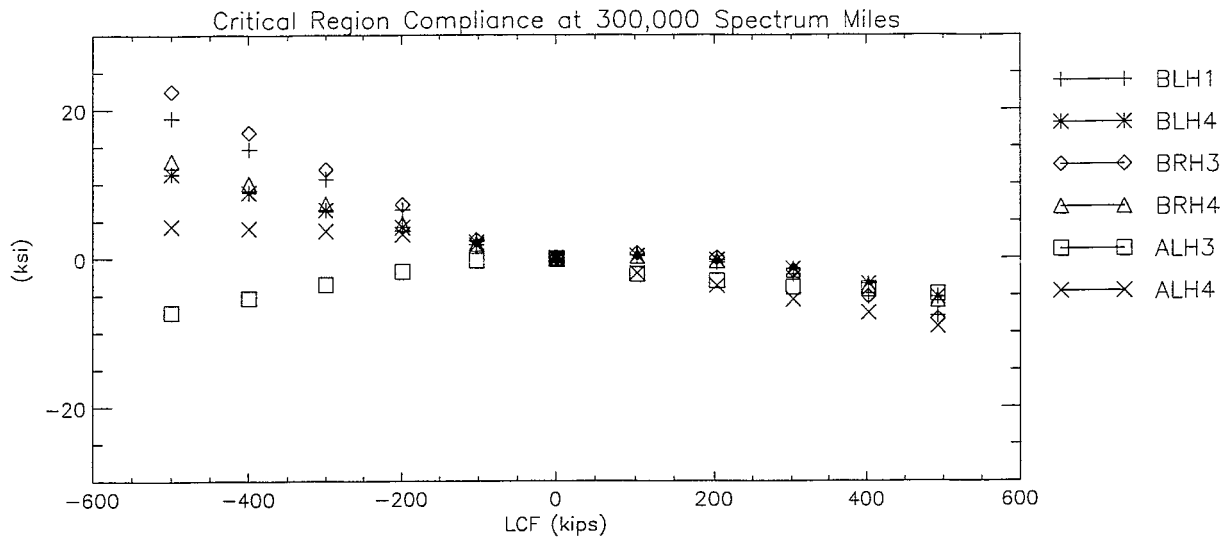








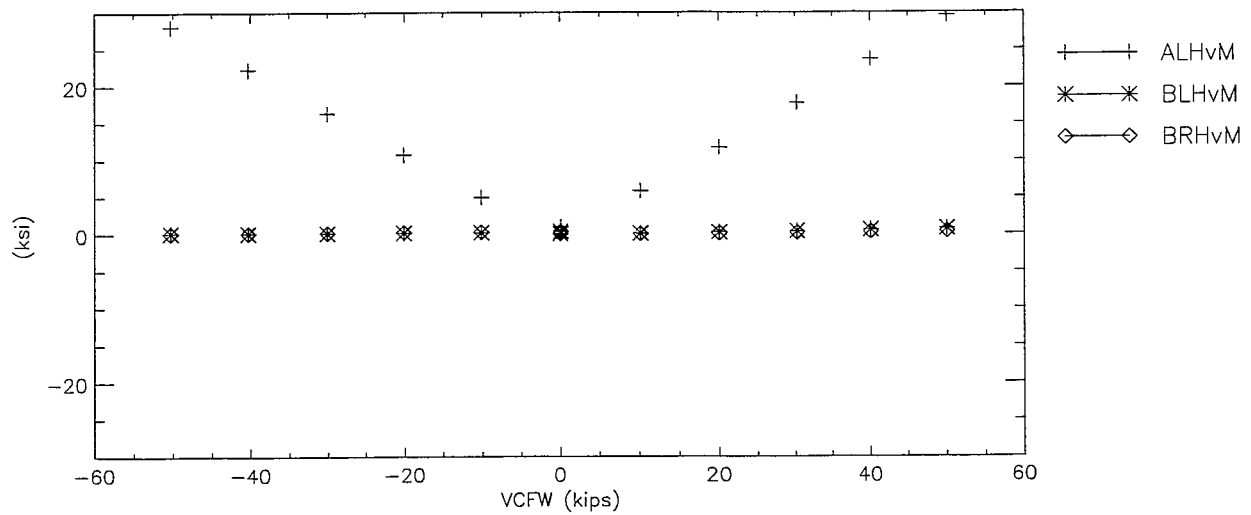
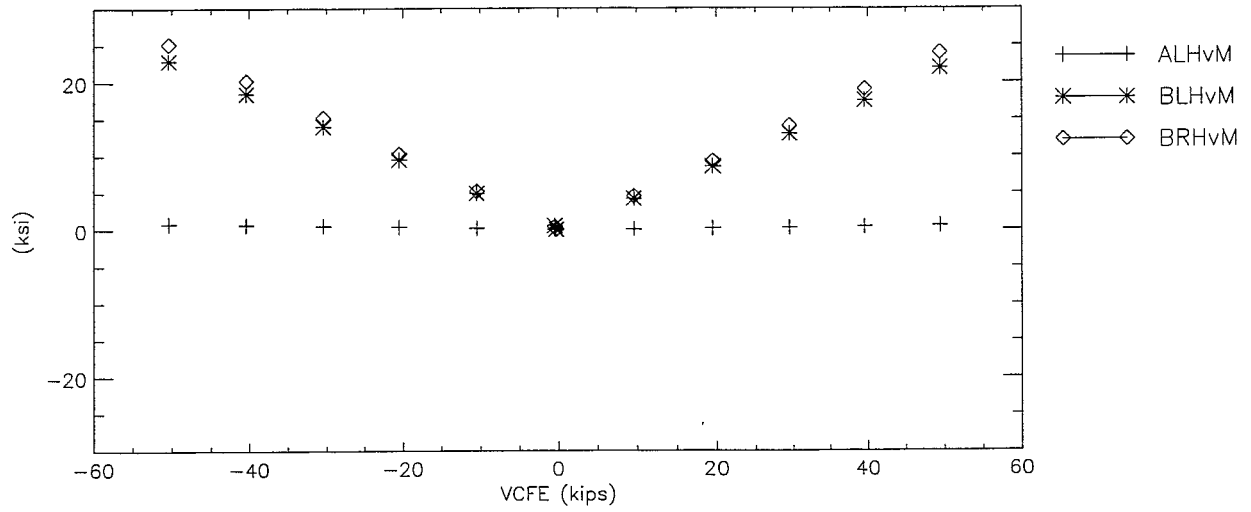
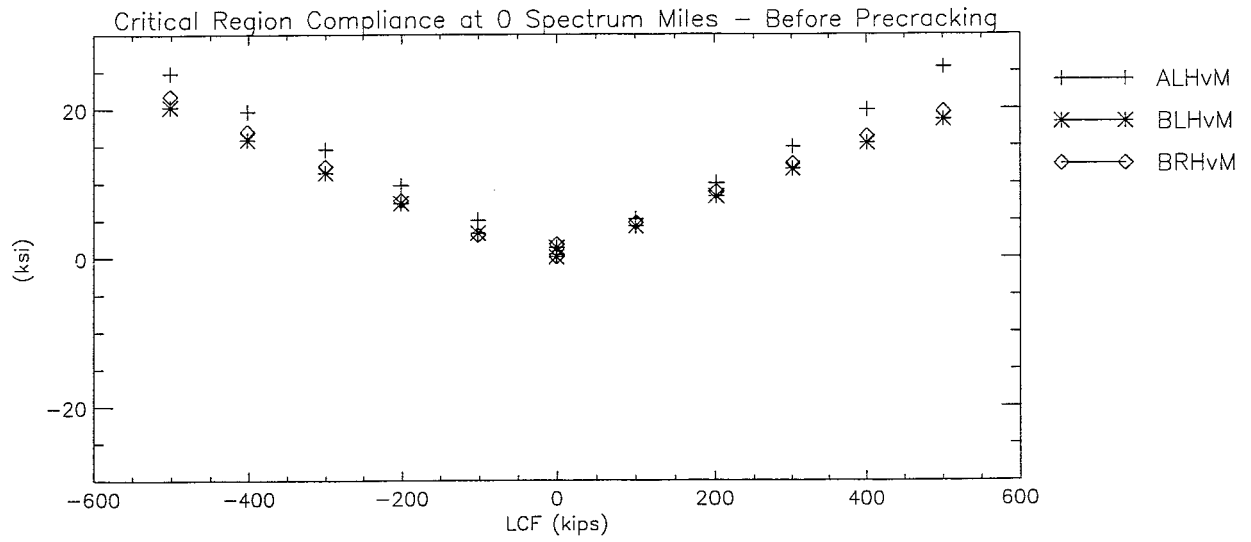


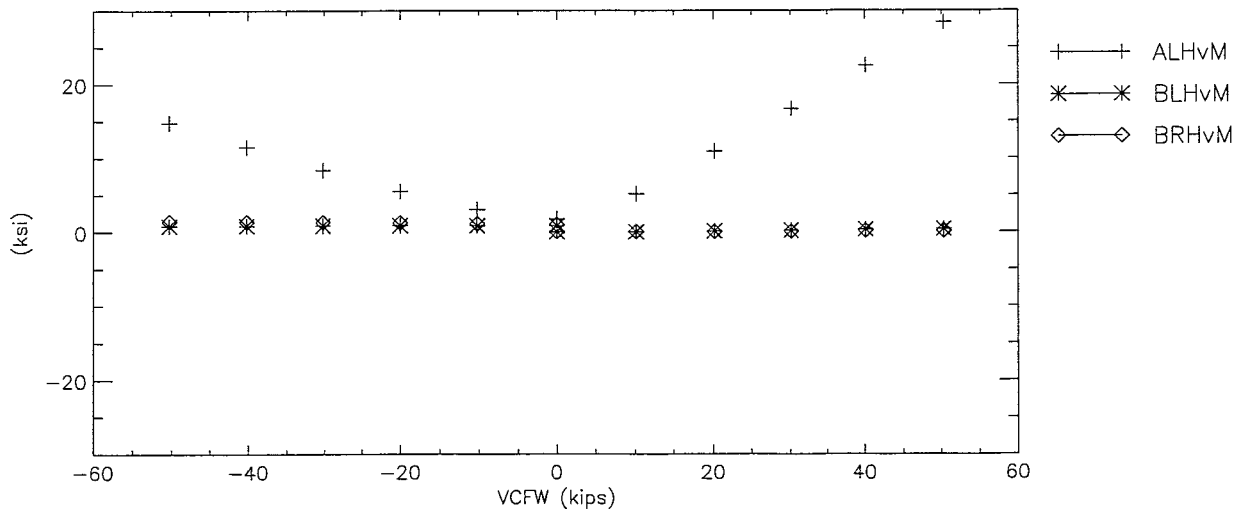
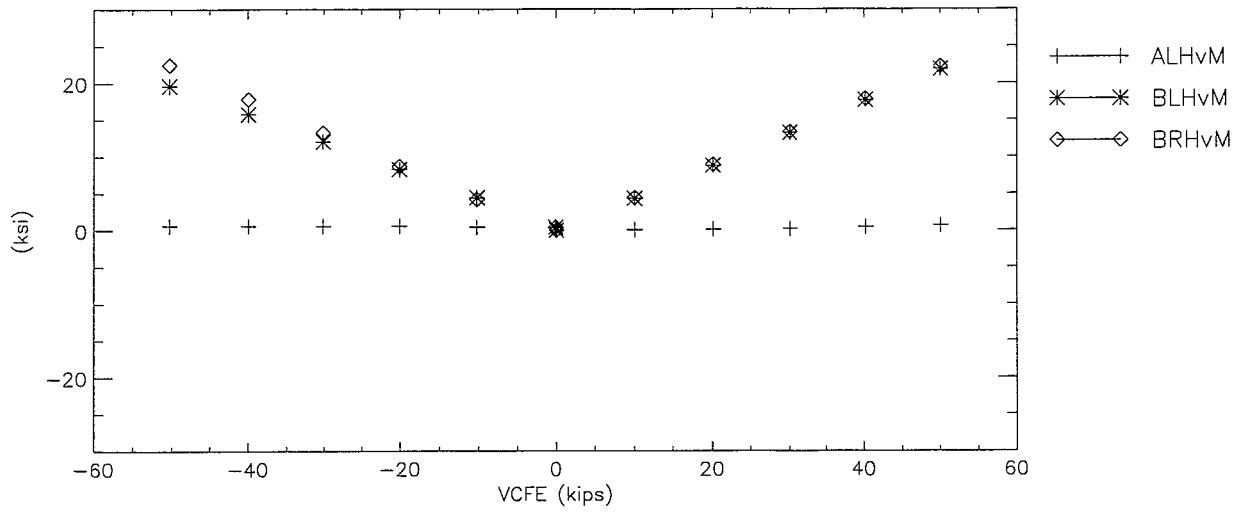
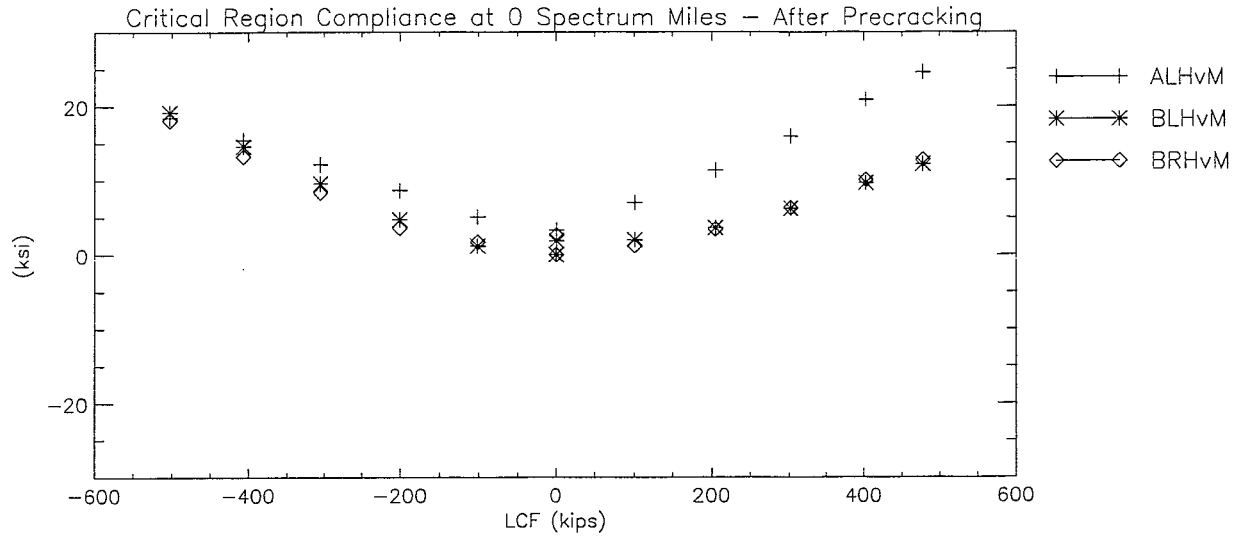


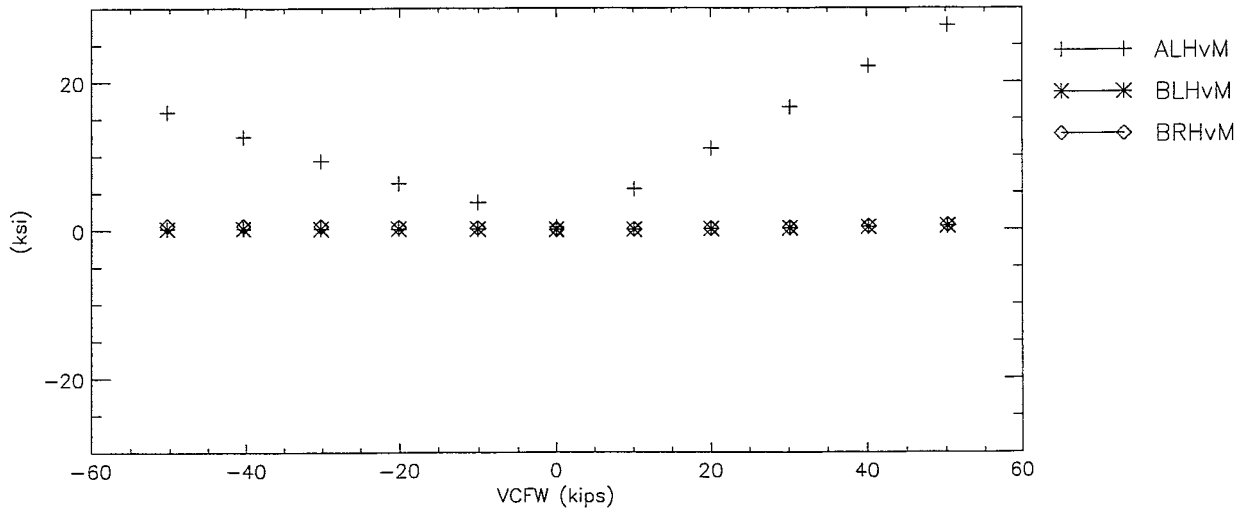
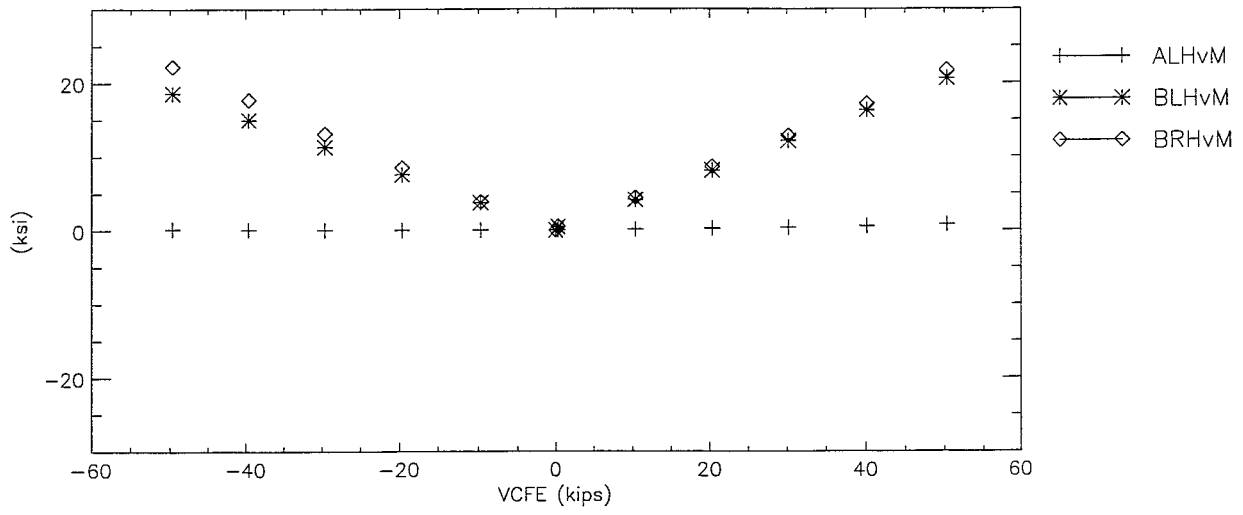
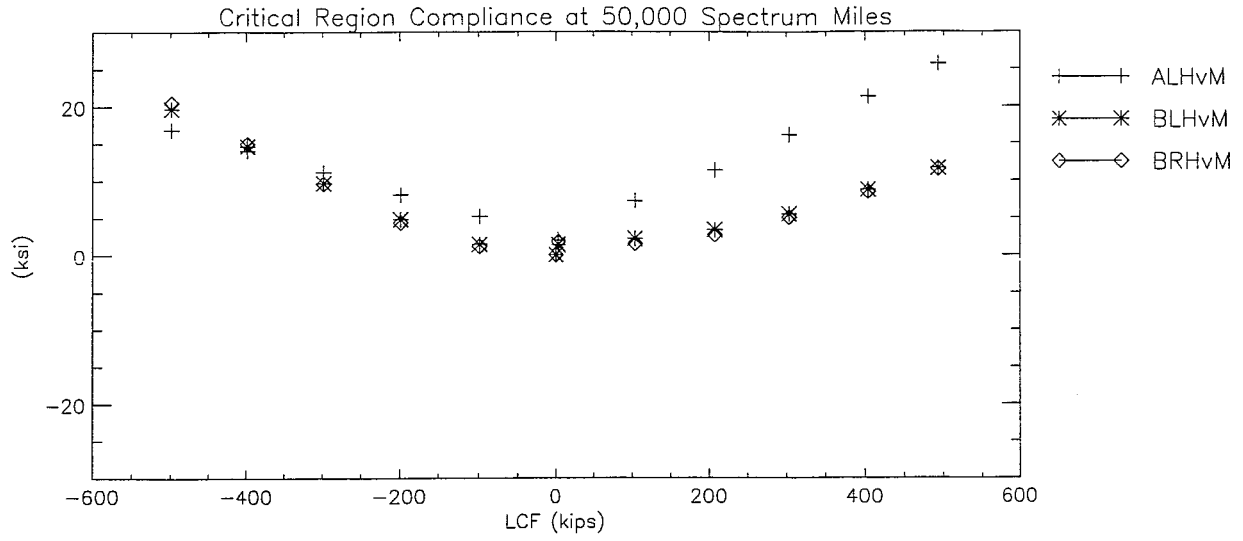
FINAL DRAFT

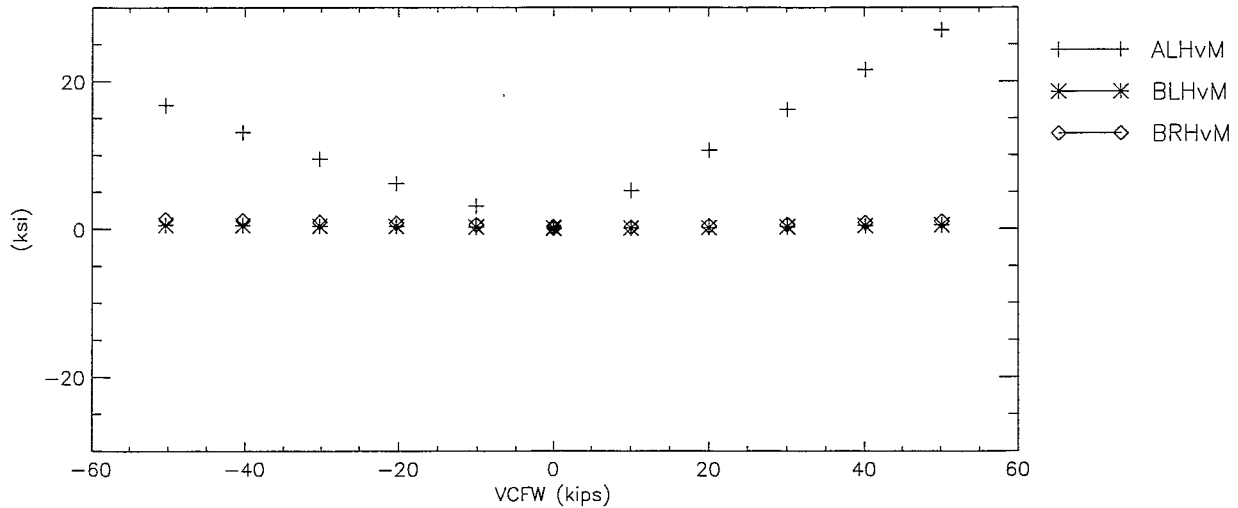
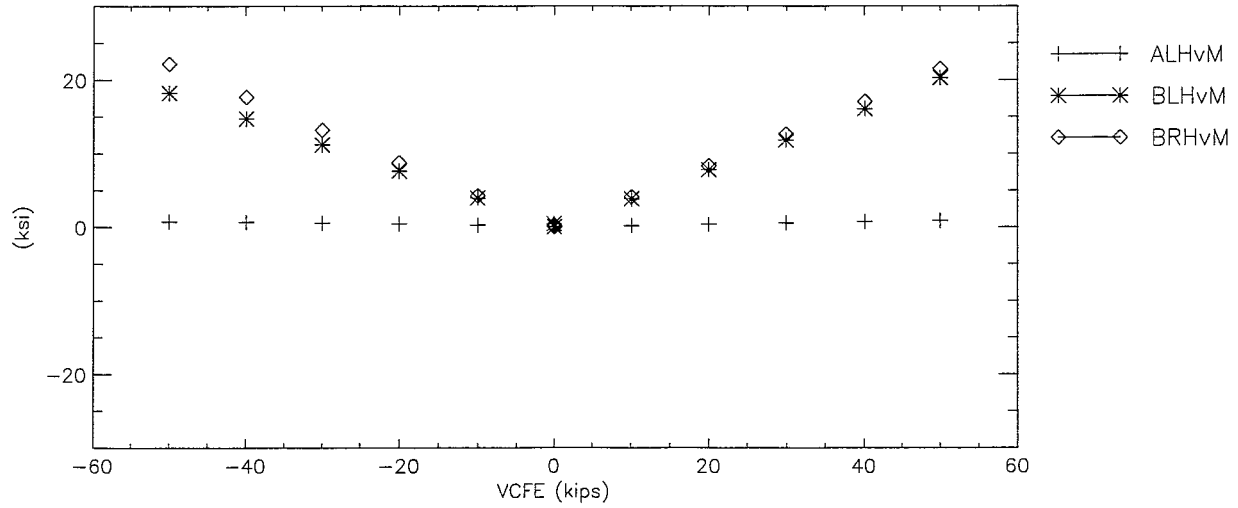
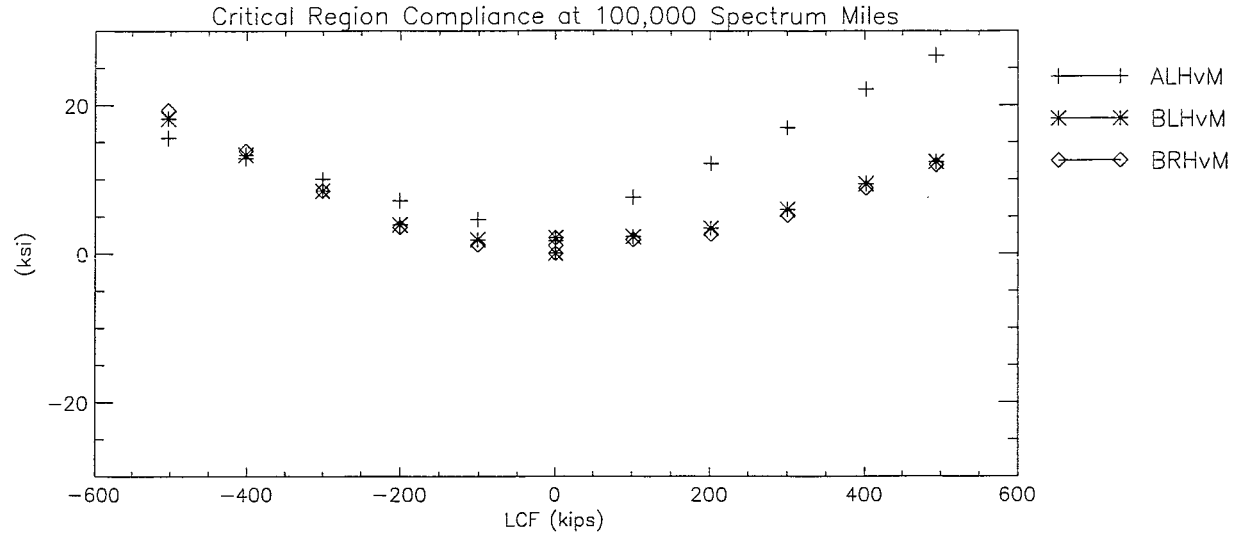
Section C-V: Von Mises Head Stresses (AL, BL and BR)

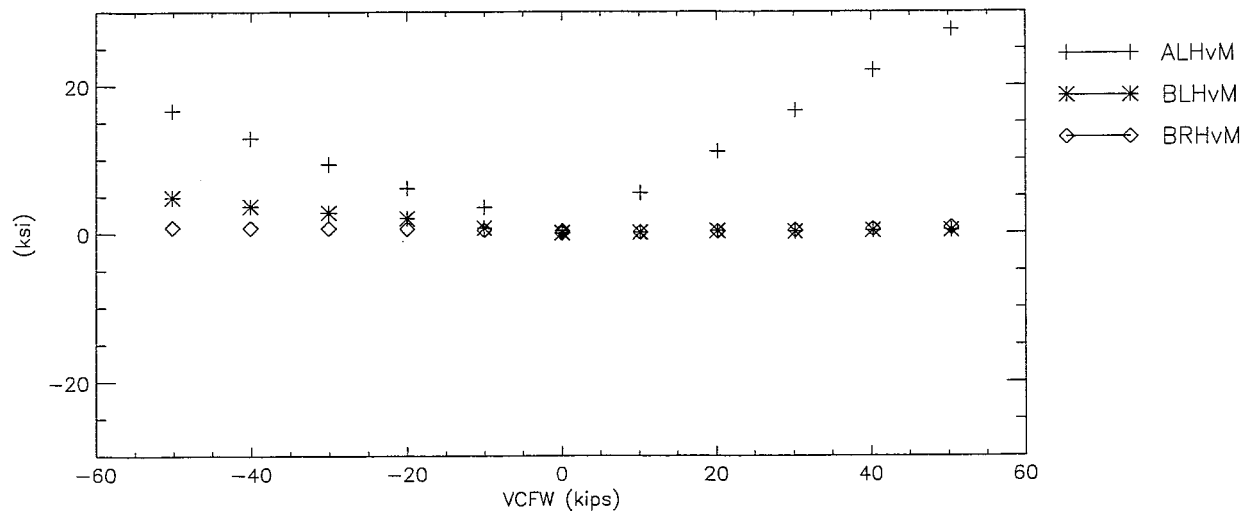
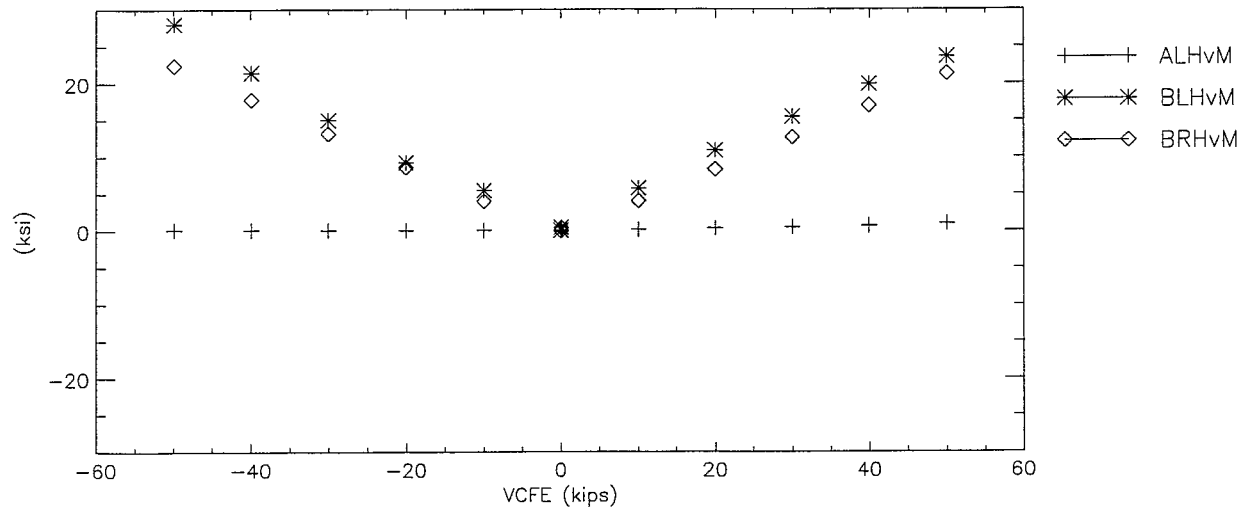
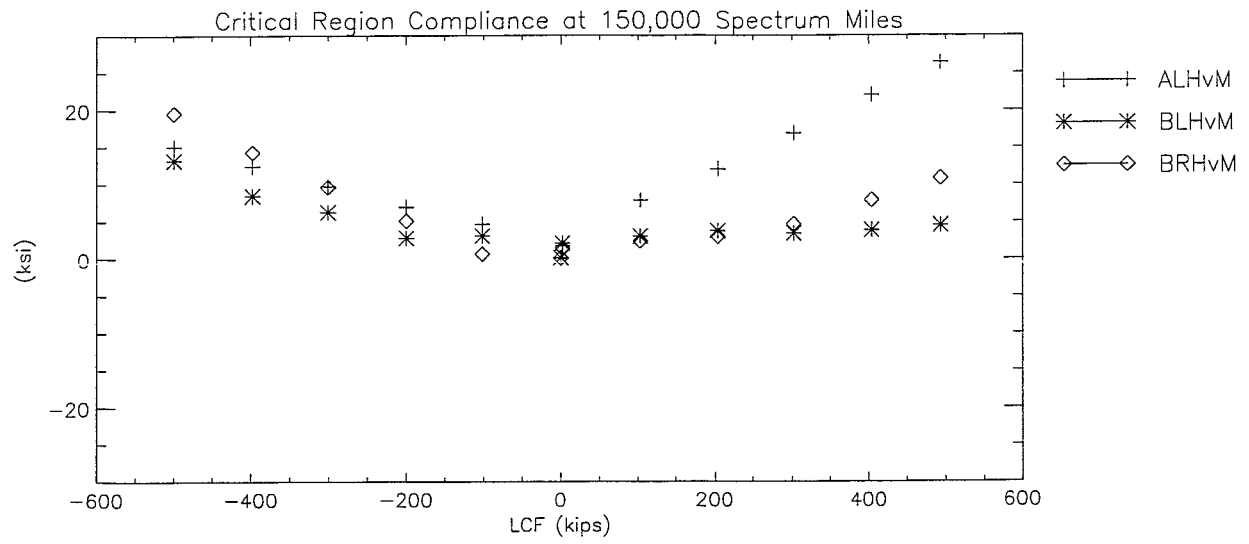
FINAL DRAFT

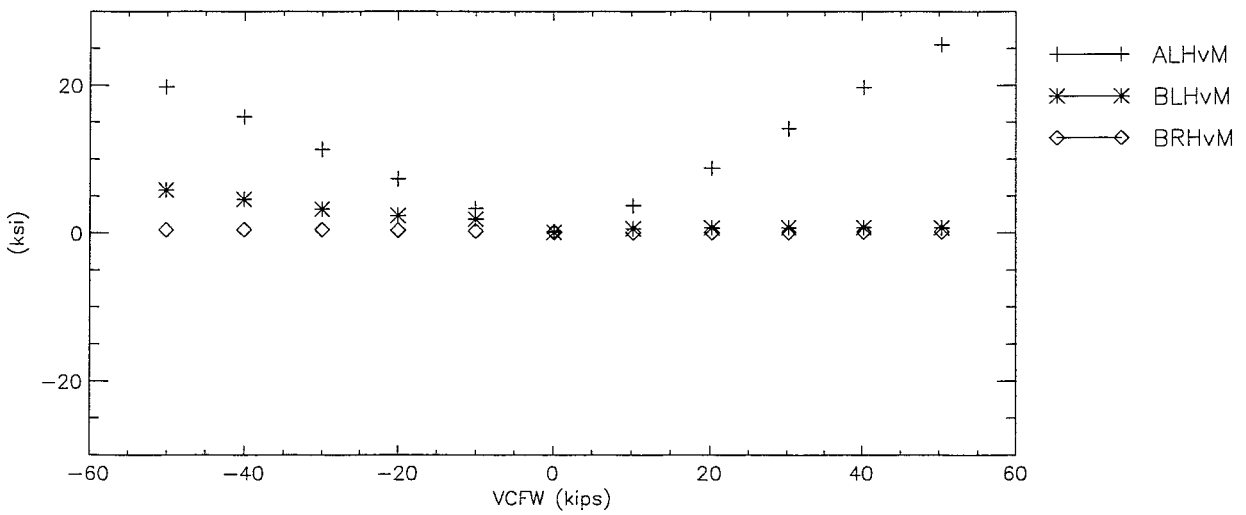
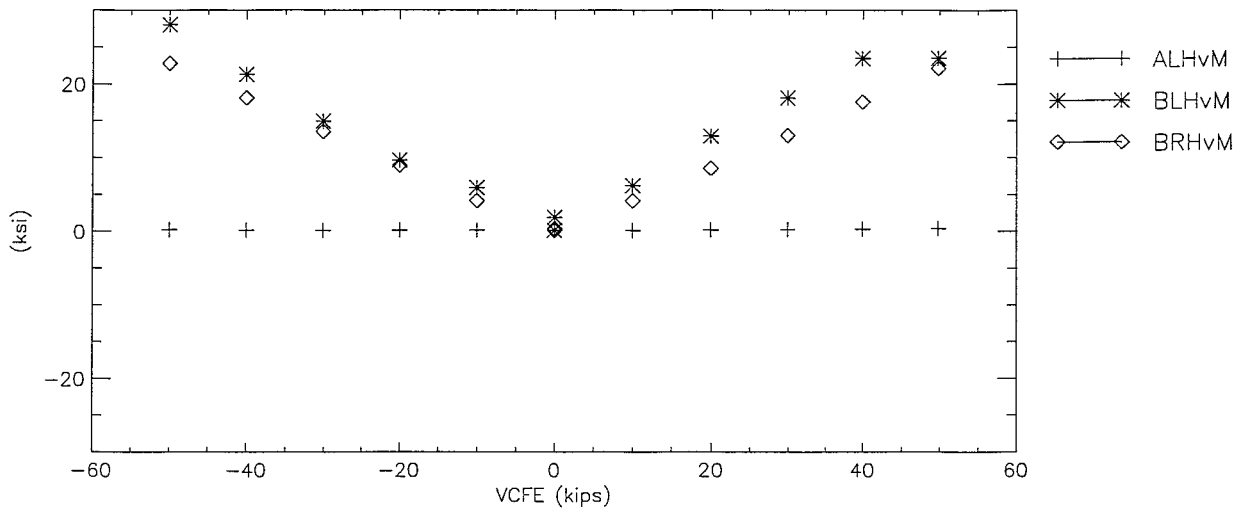
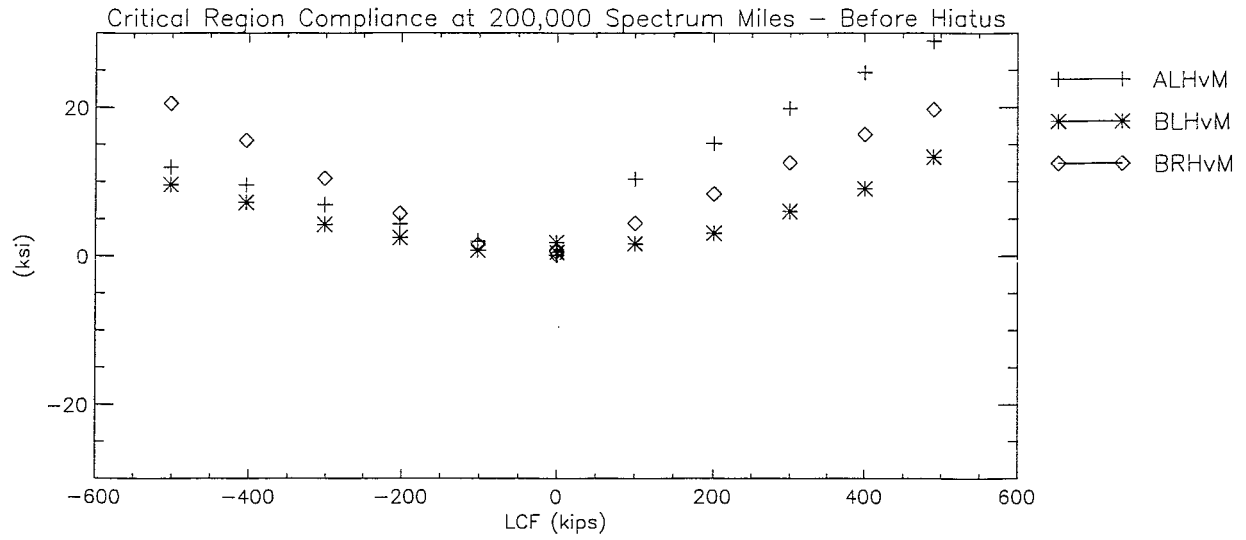


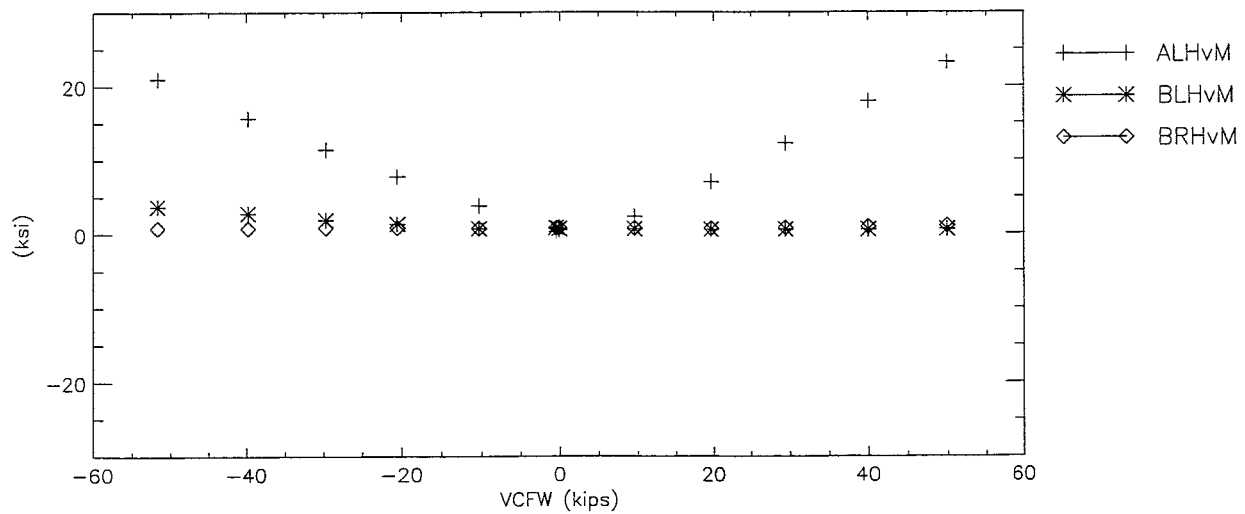
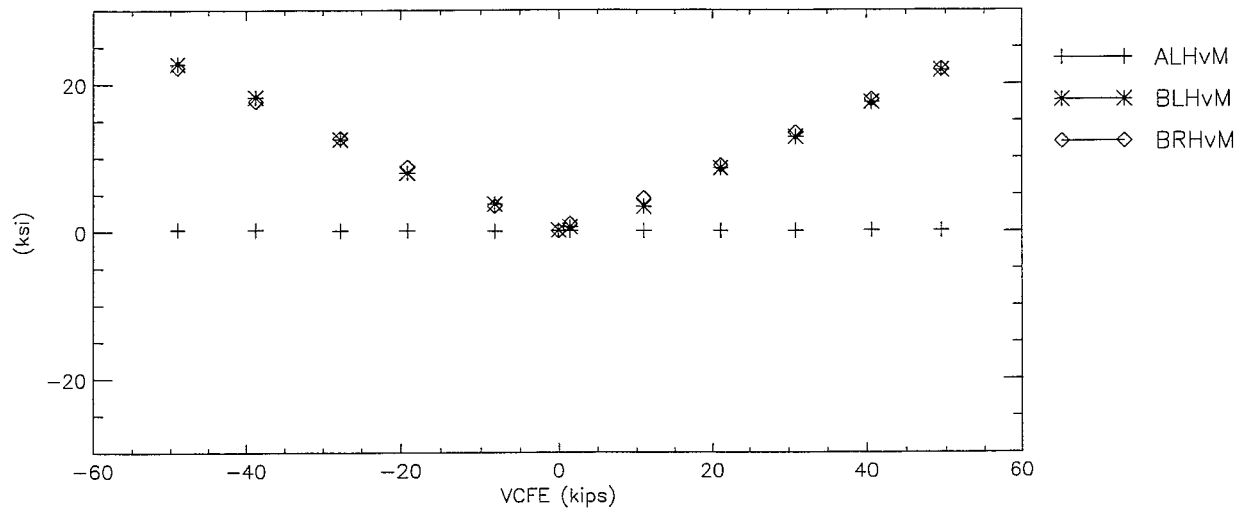
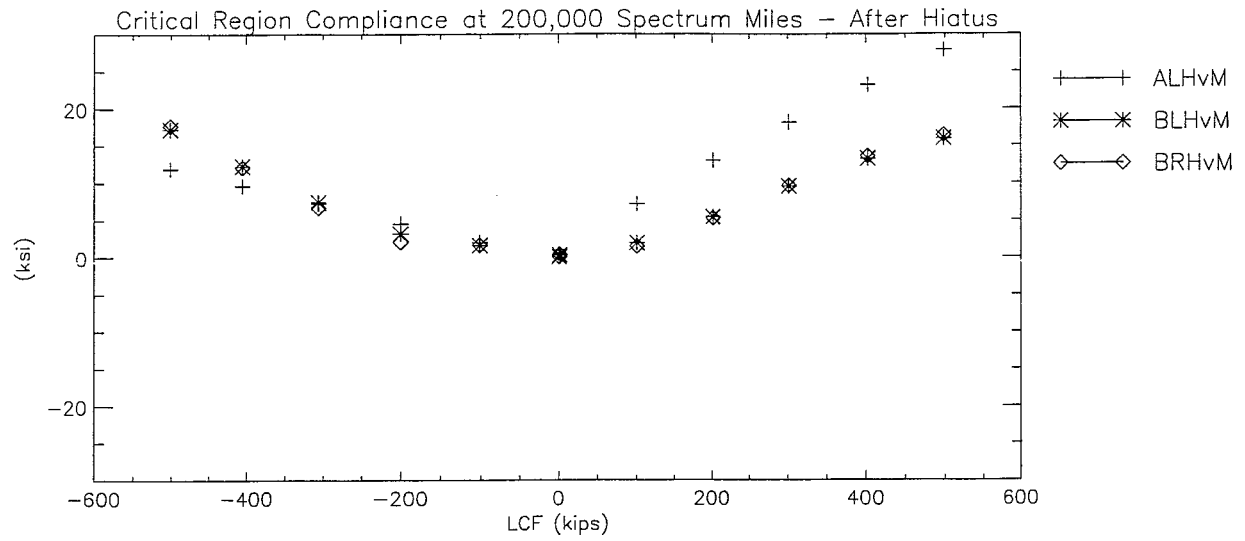


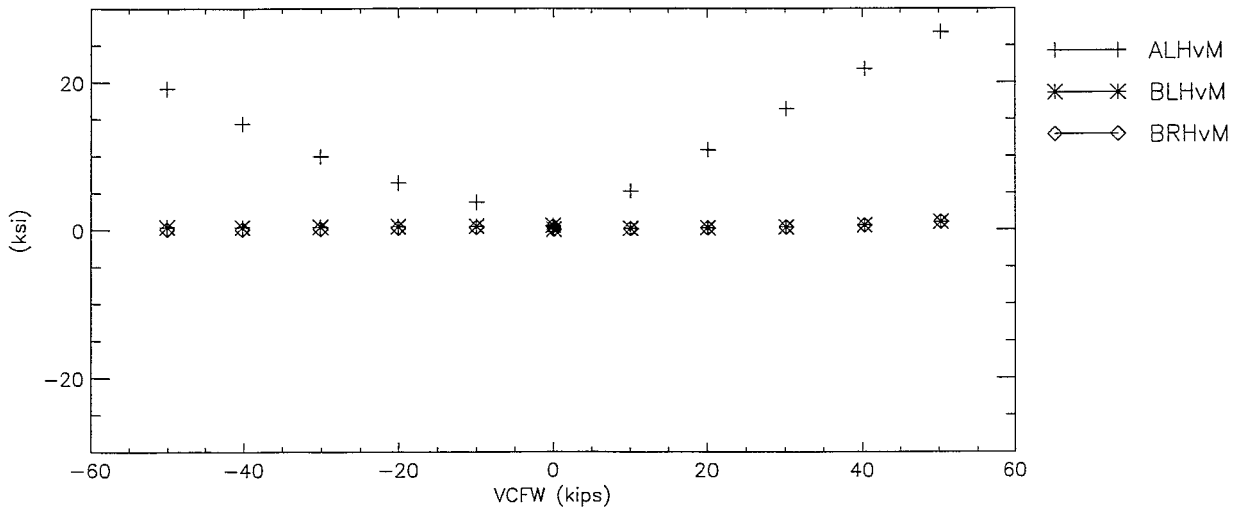
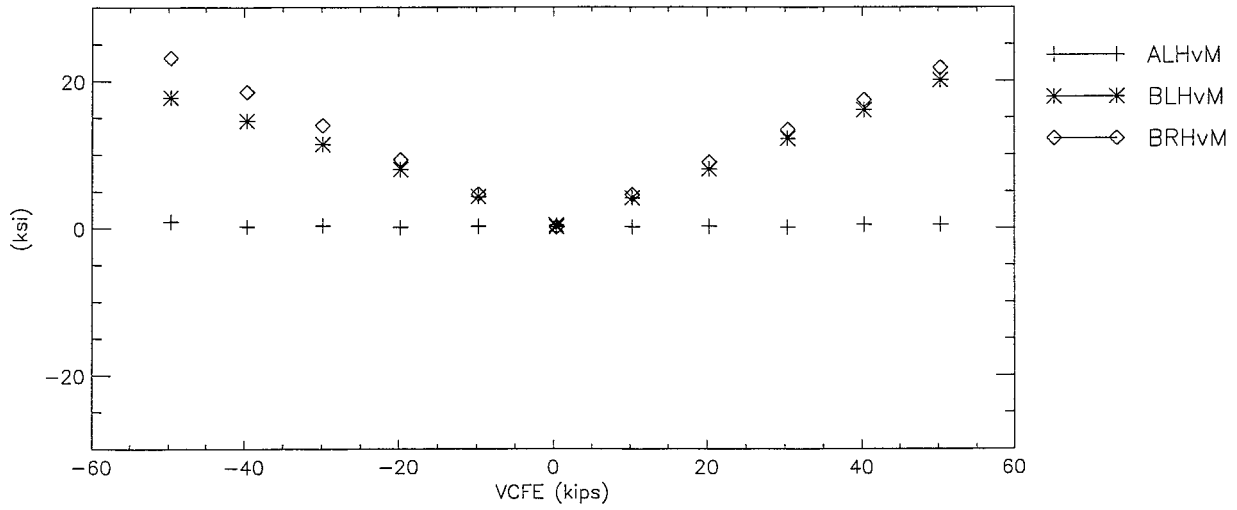
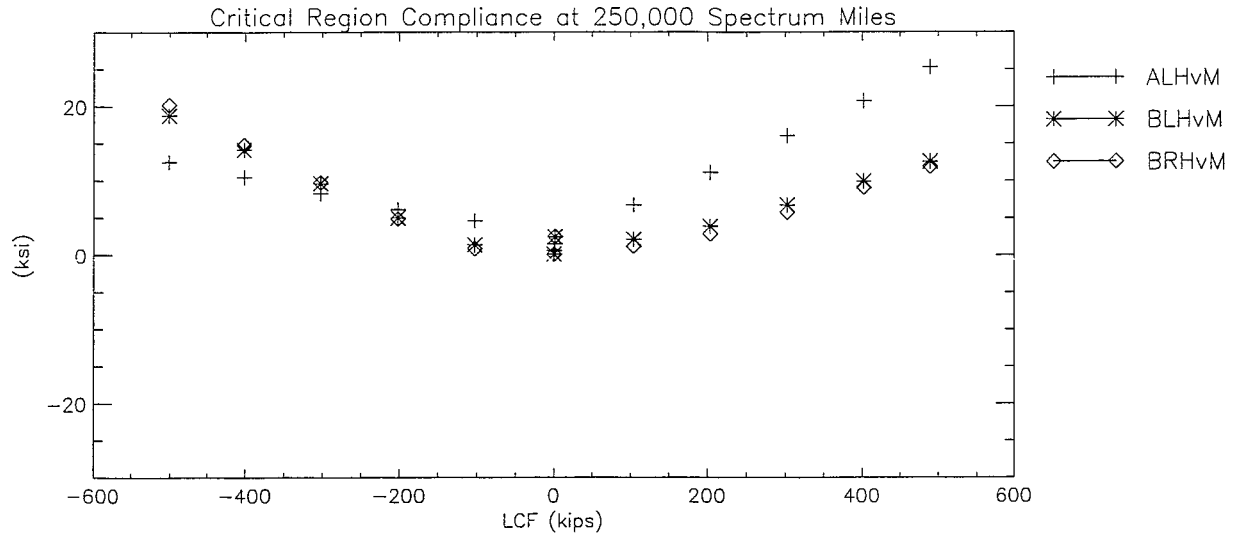


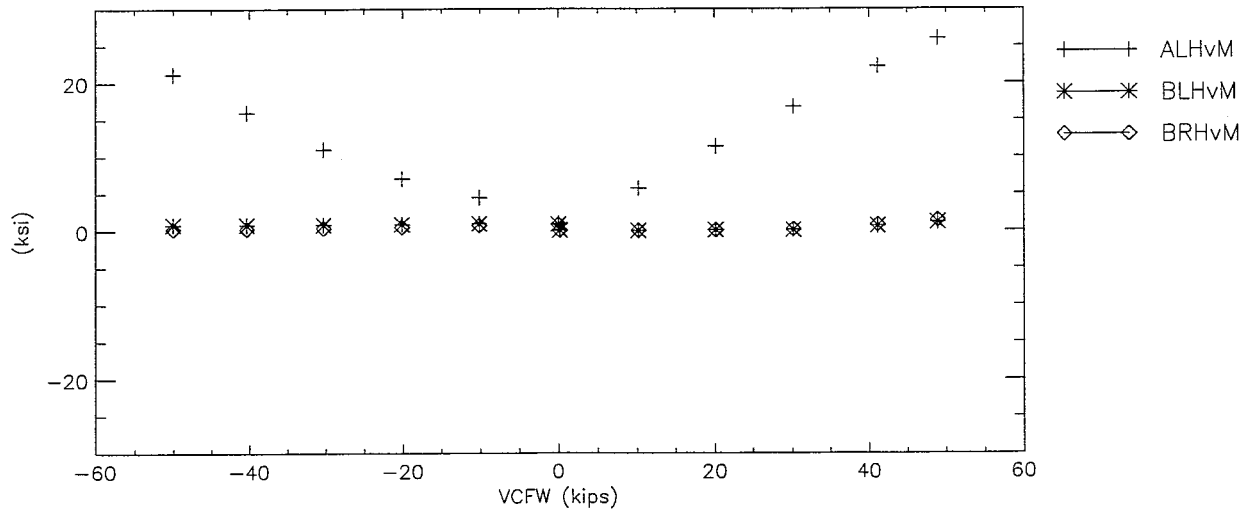
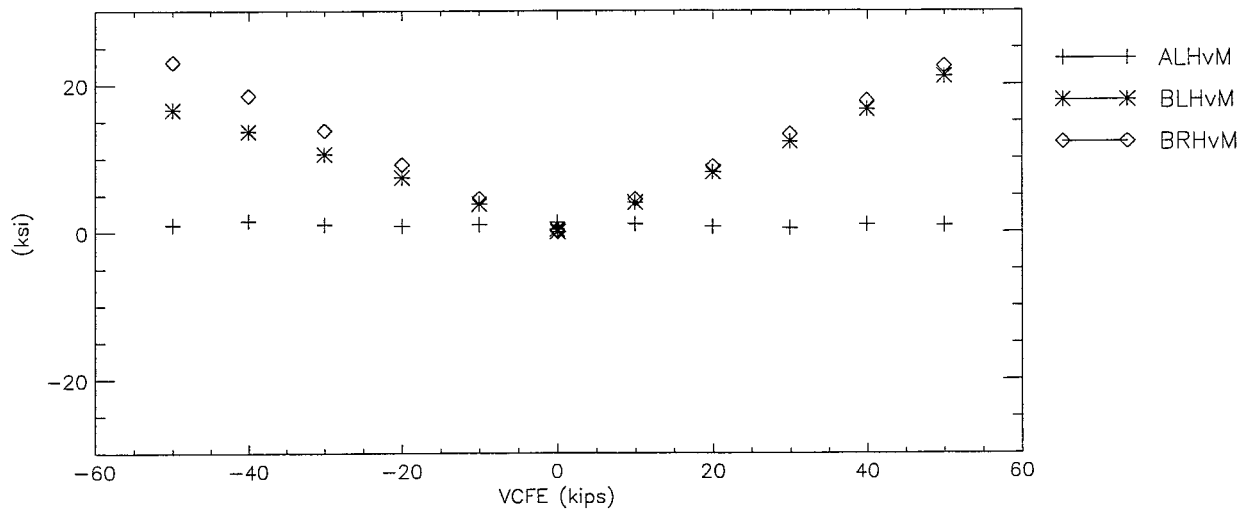
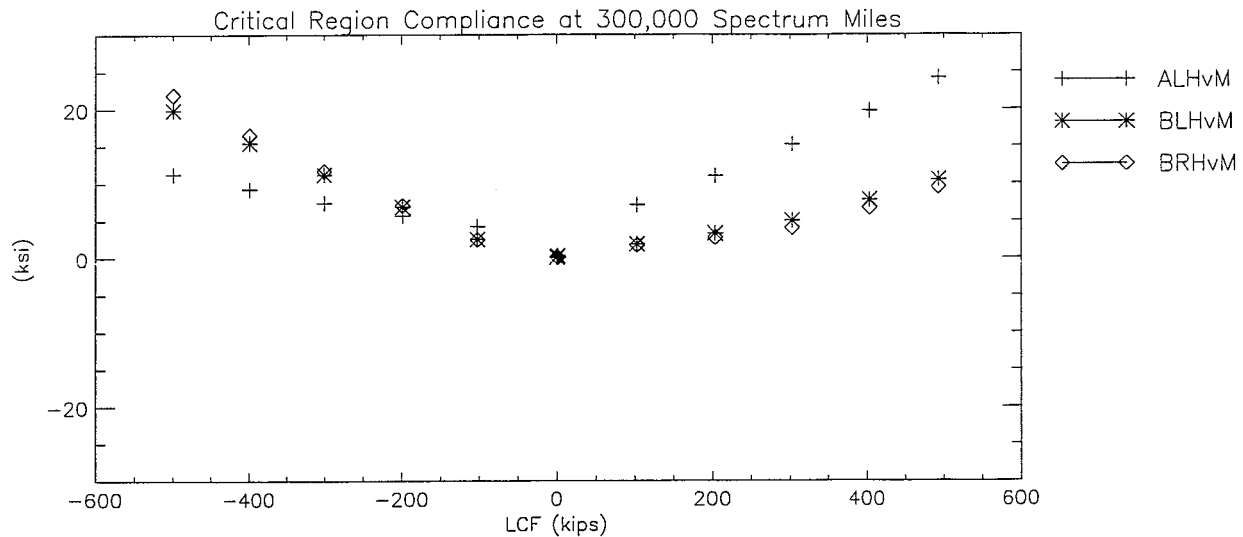








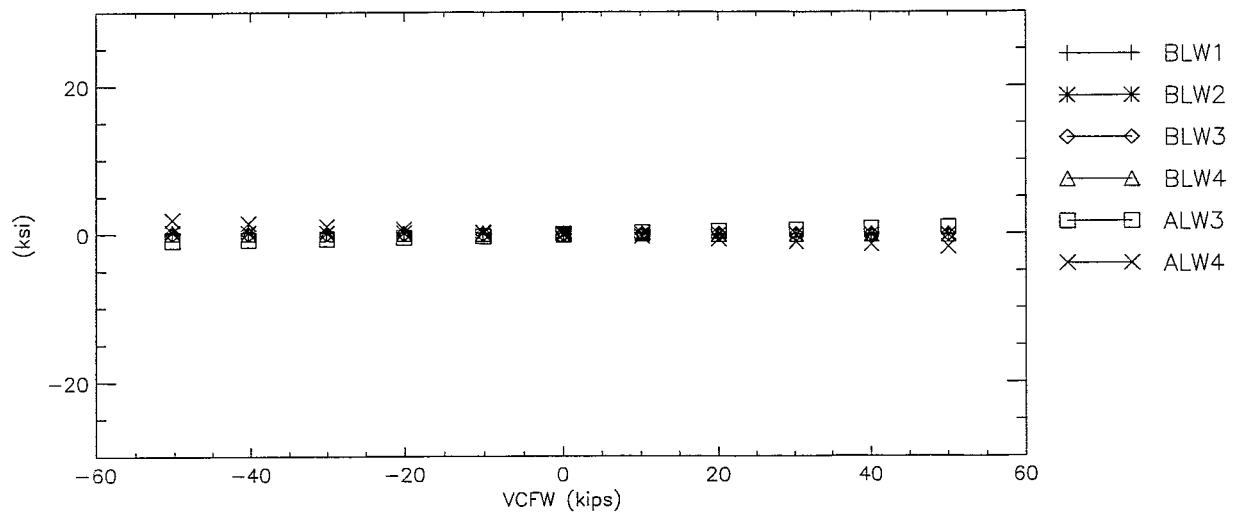
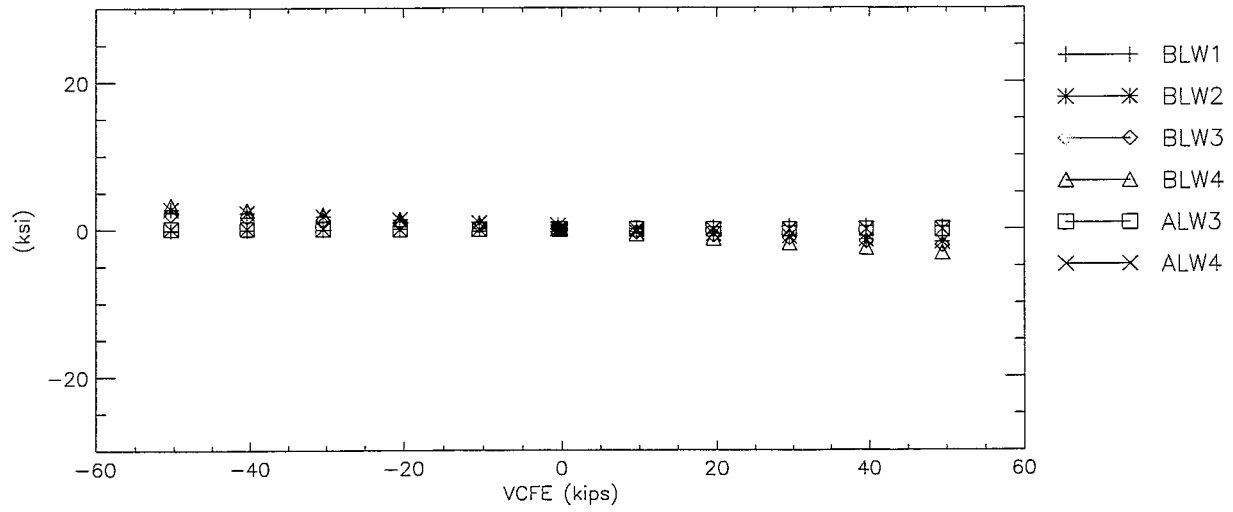
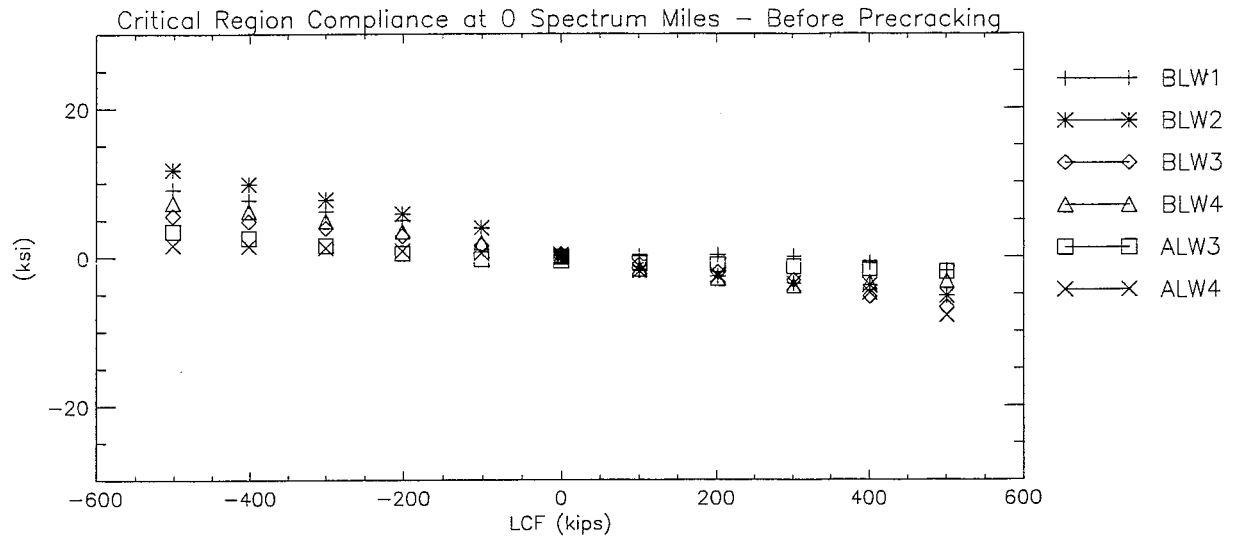


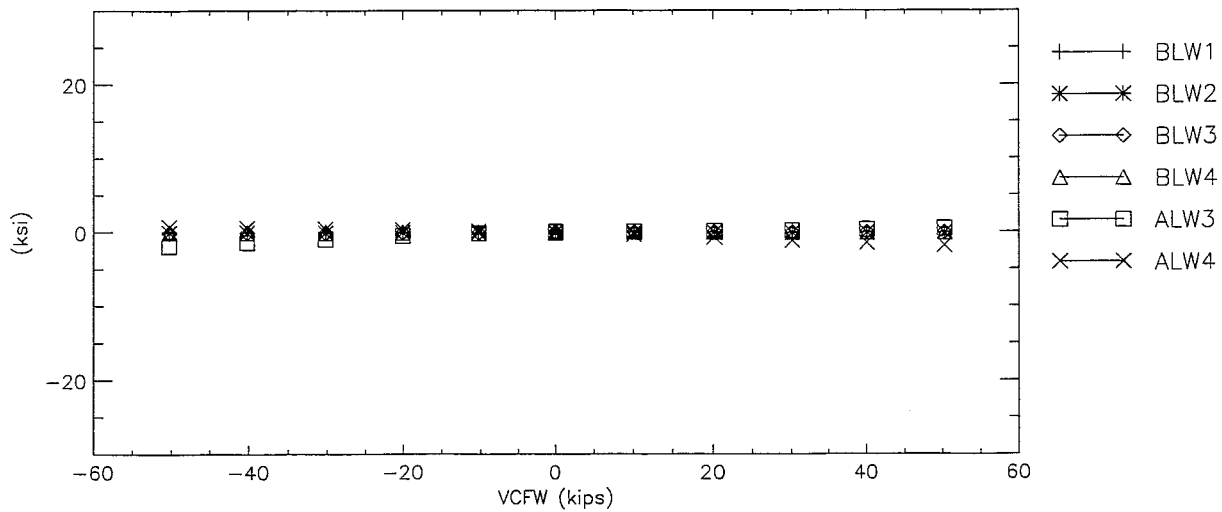
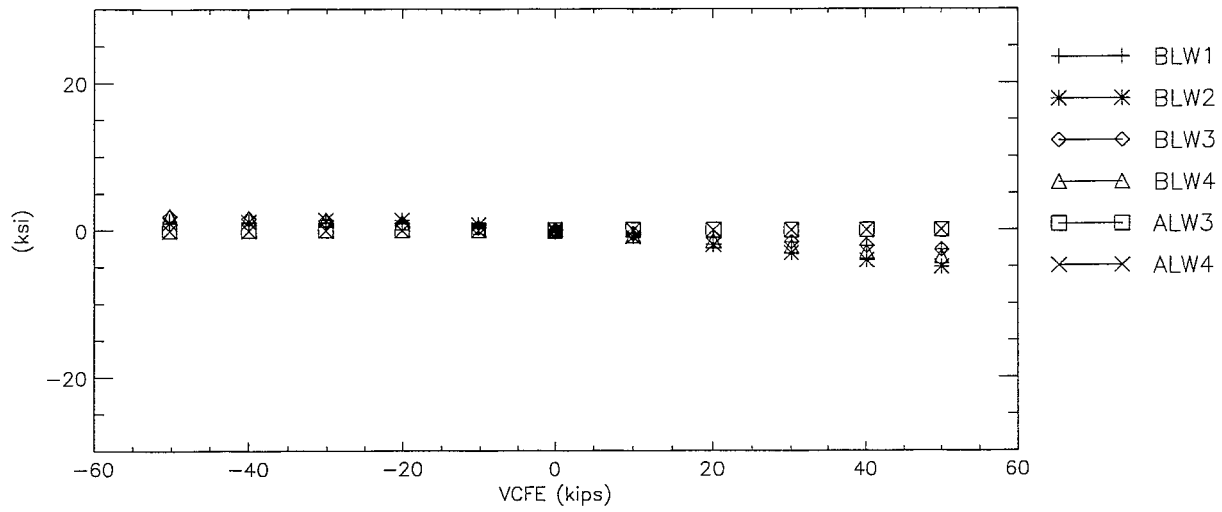
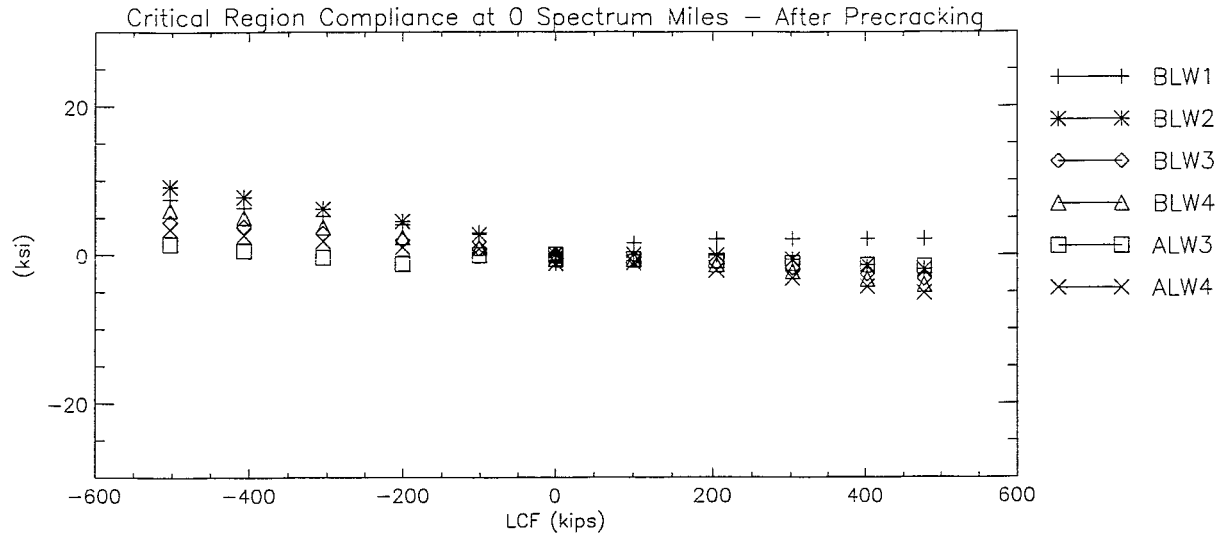


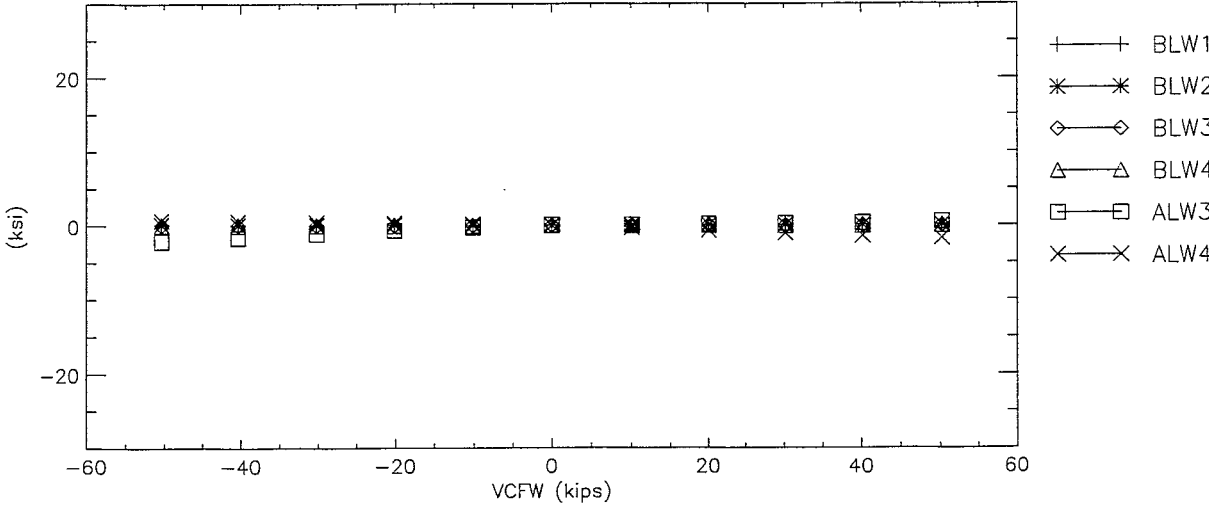
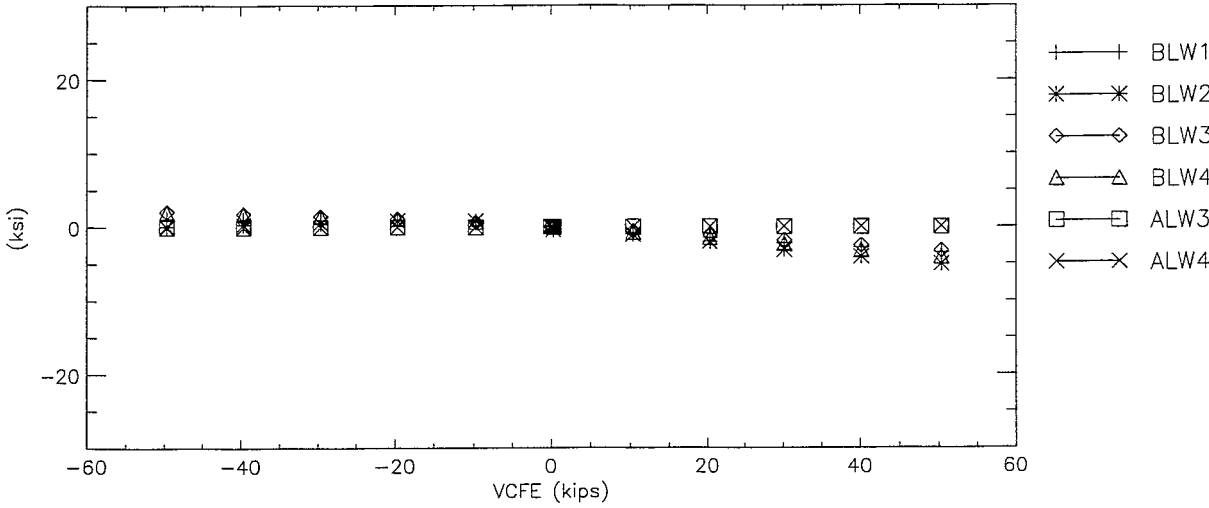
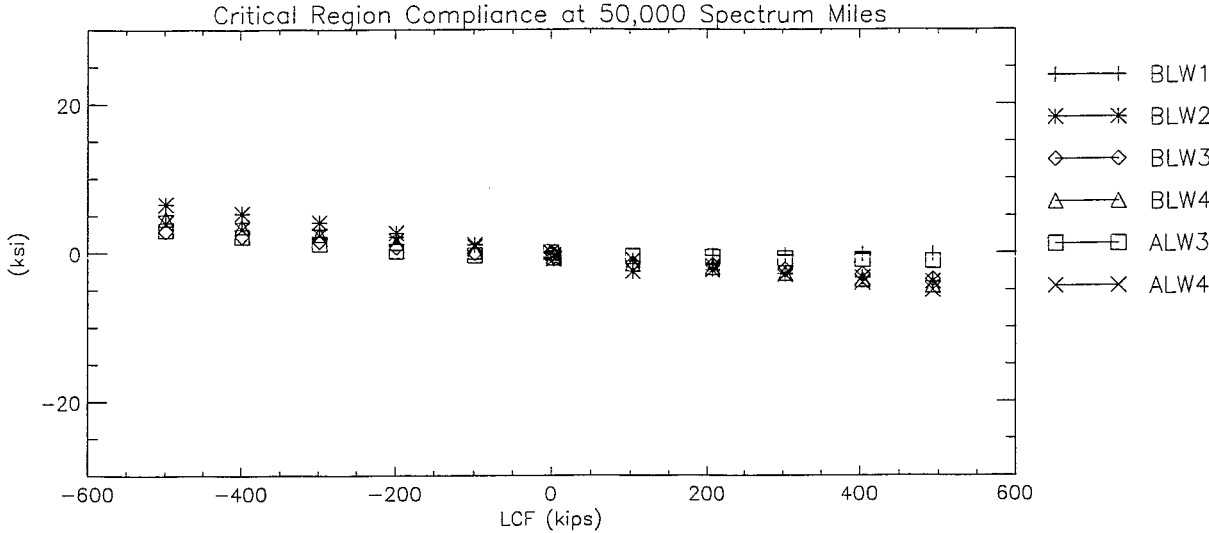
FINAL DRAFT

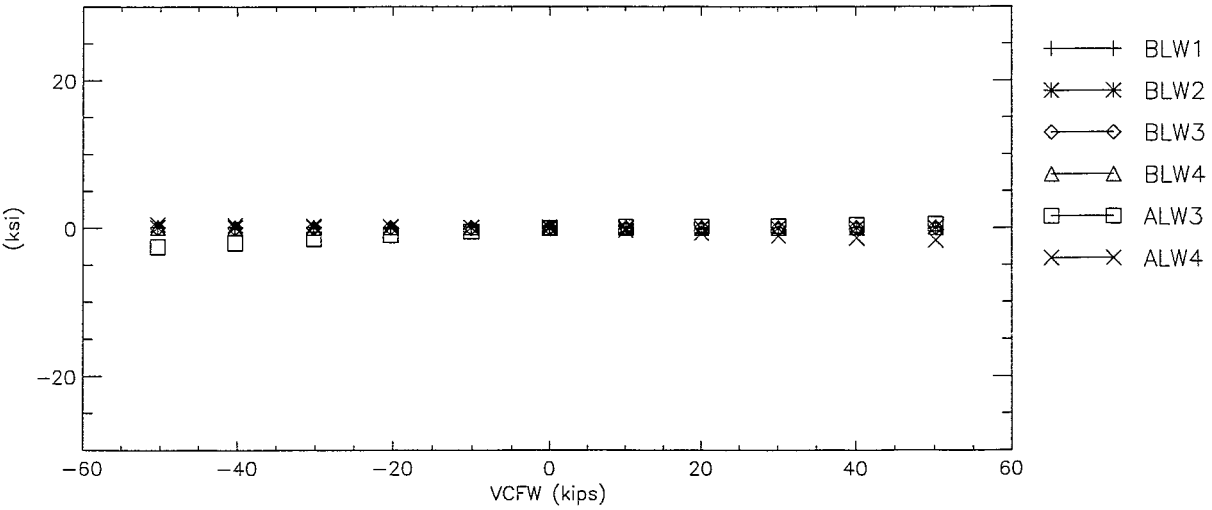
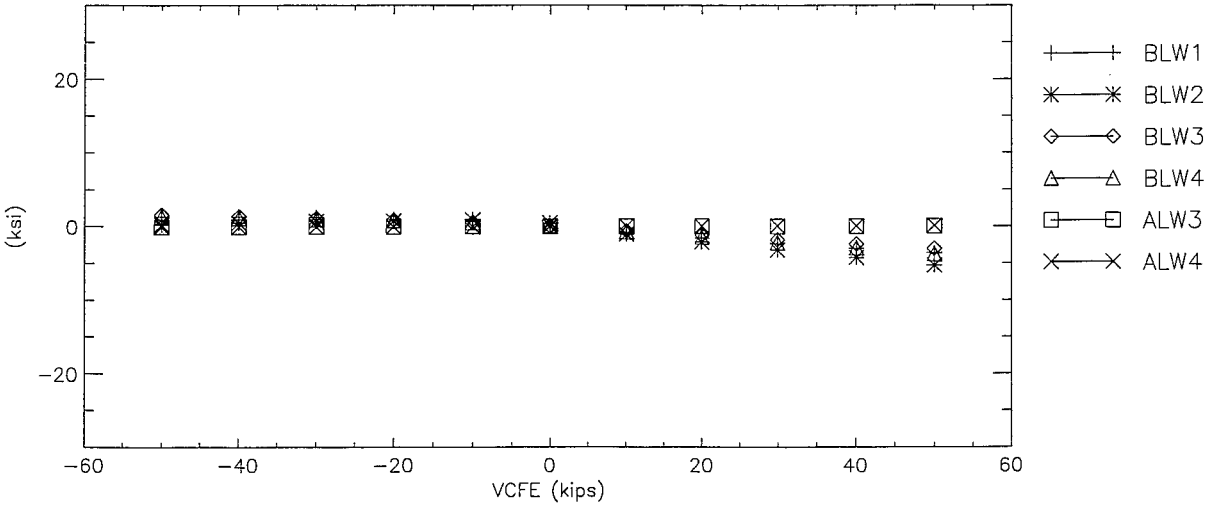
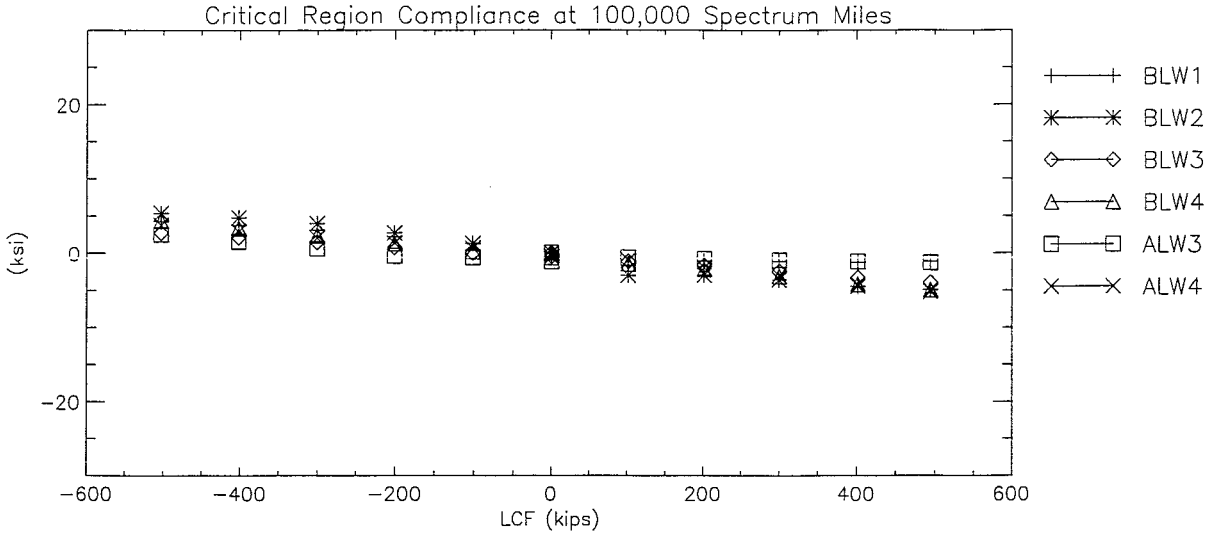
Section C-VI: Vertical Web Stresses (BL and AL)

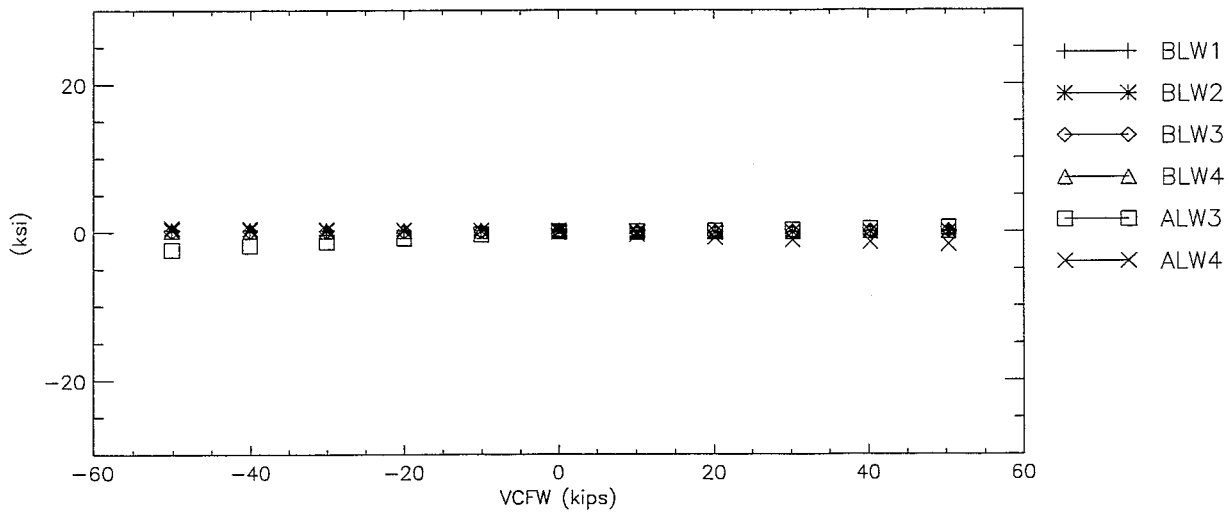
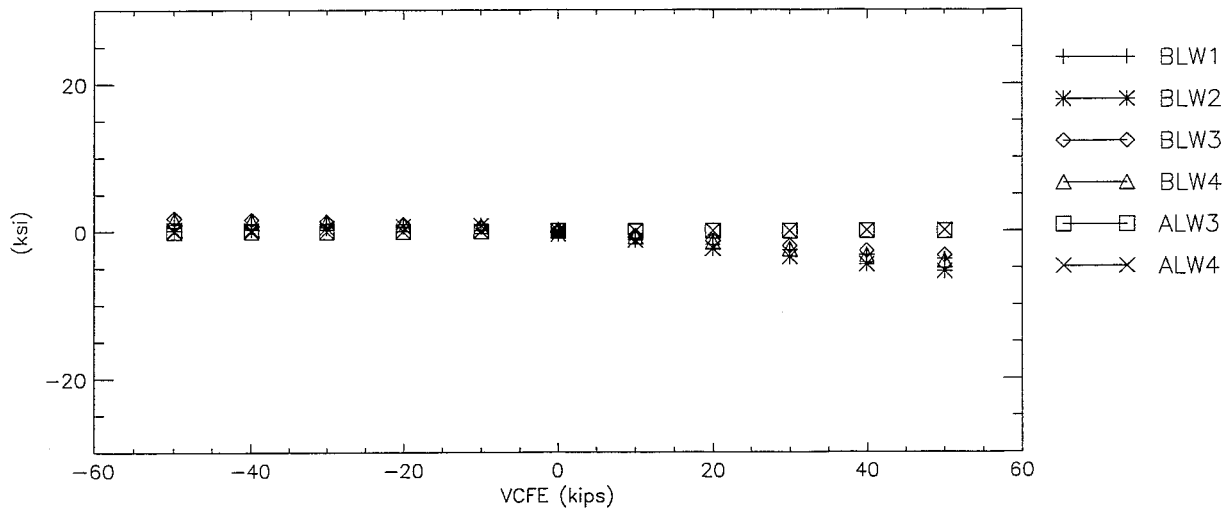
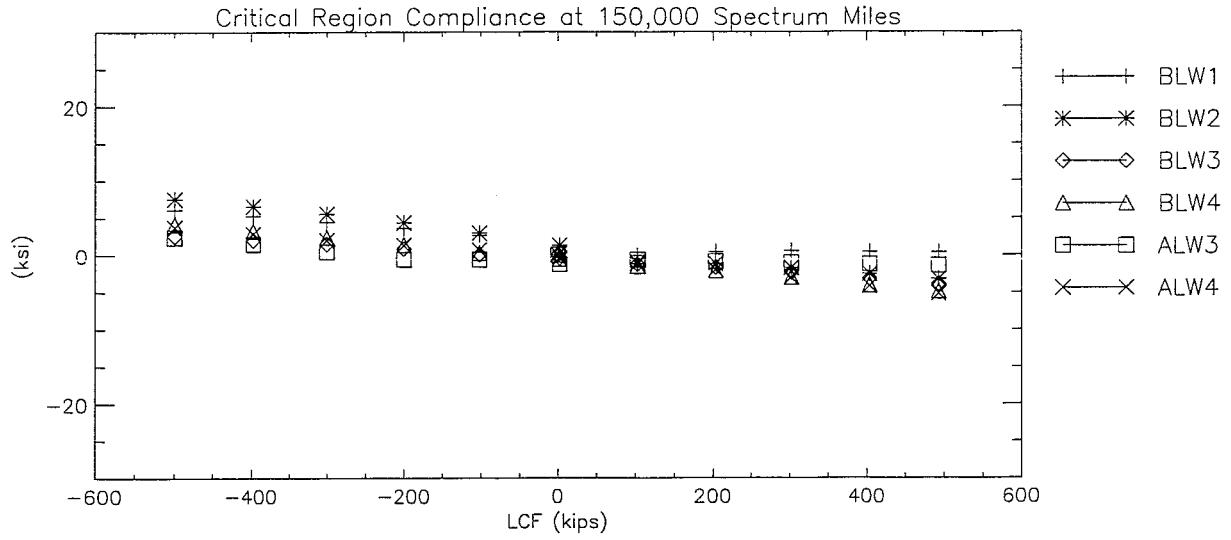
FINAL DRAFT

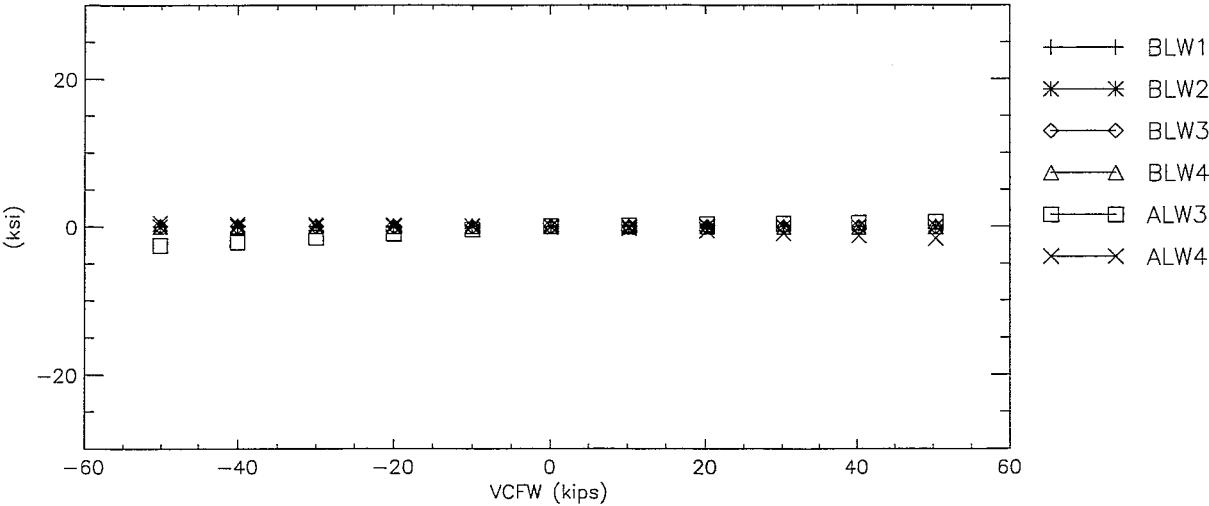
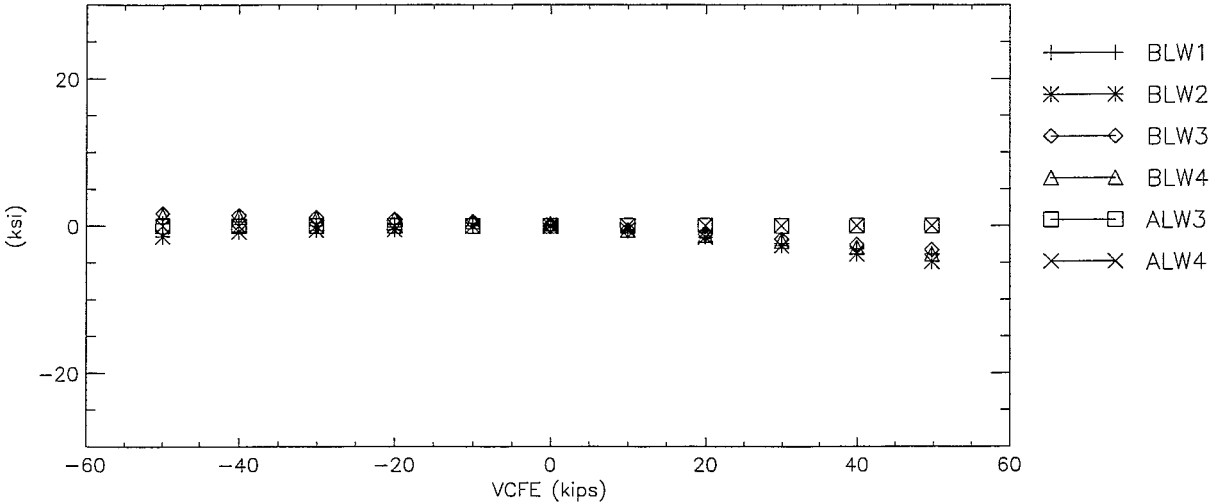
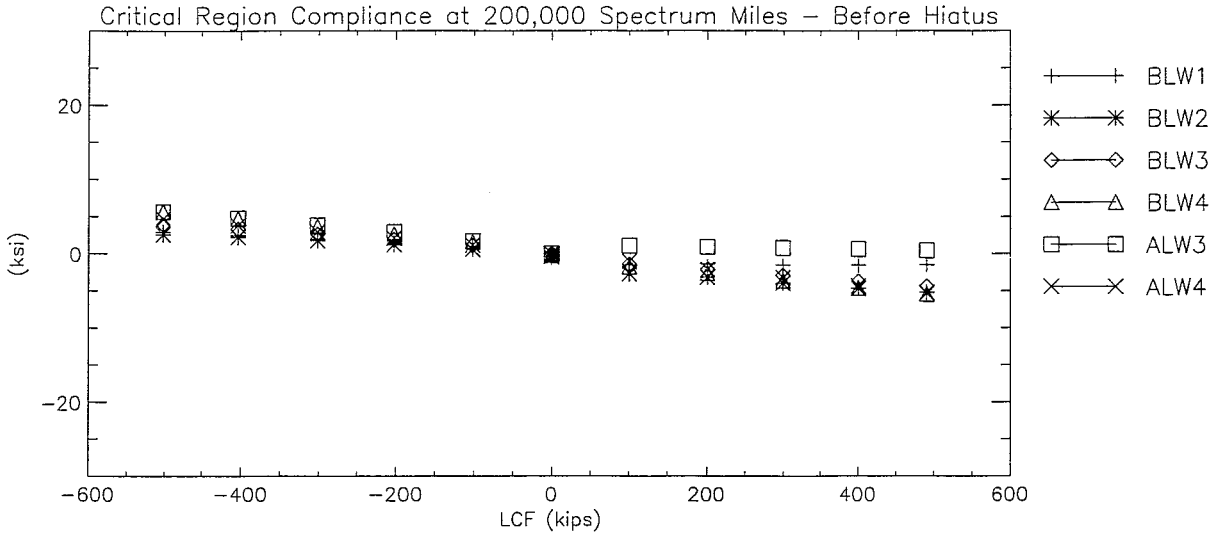


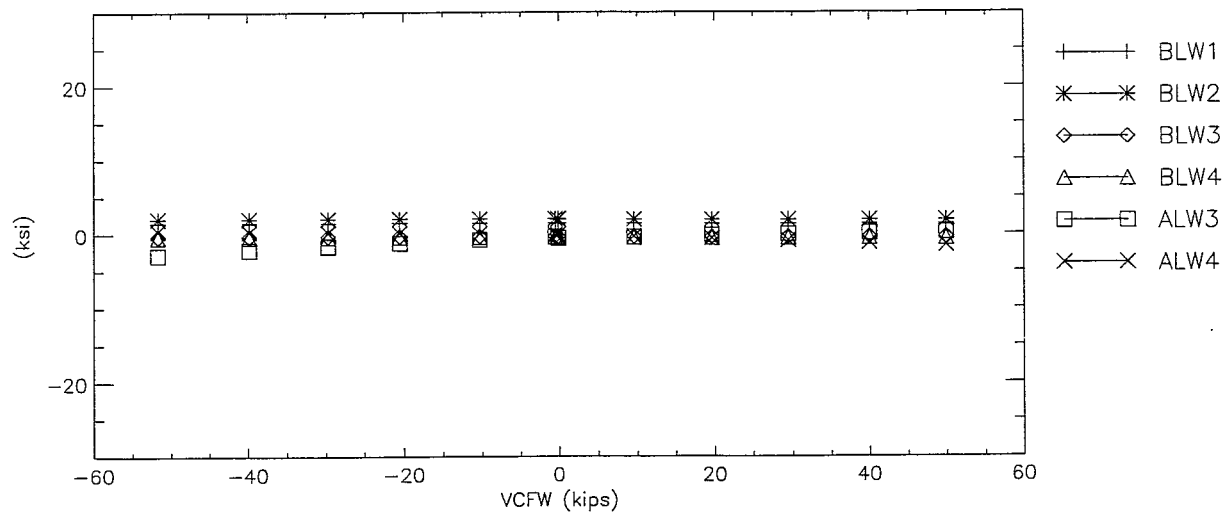
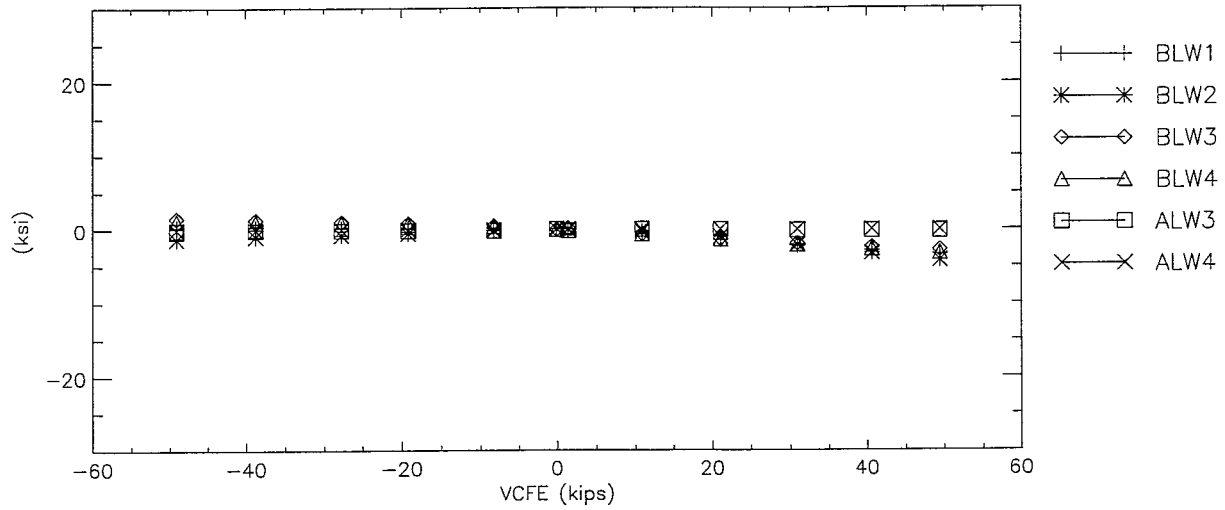
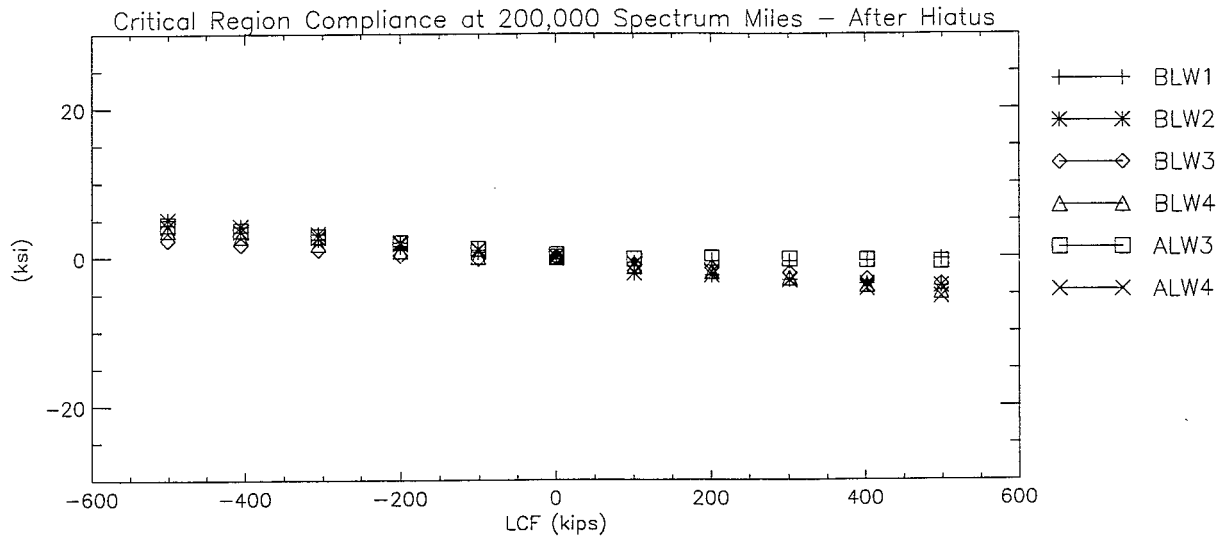


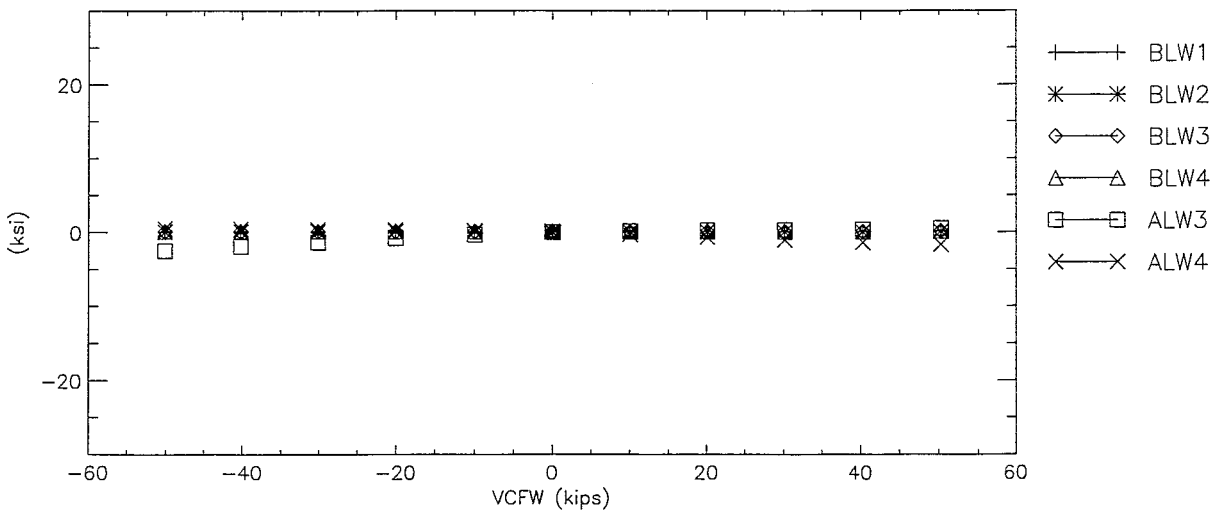
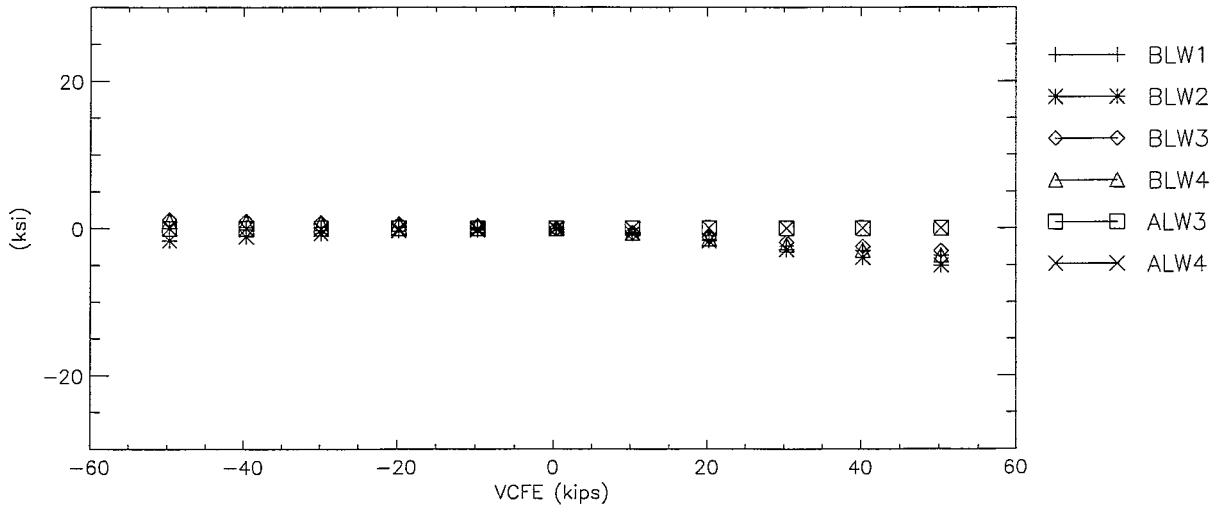
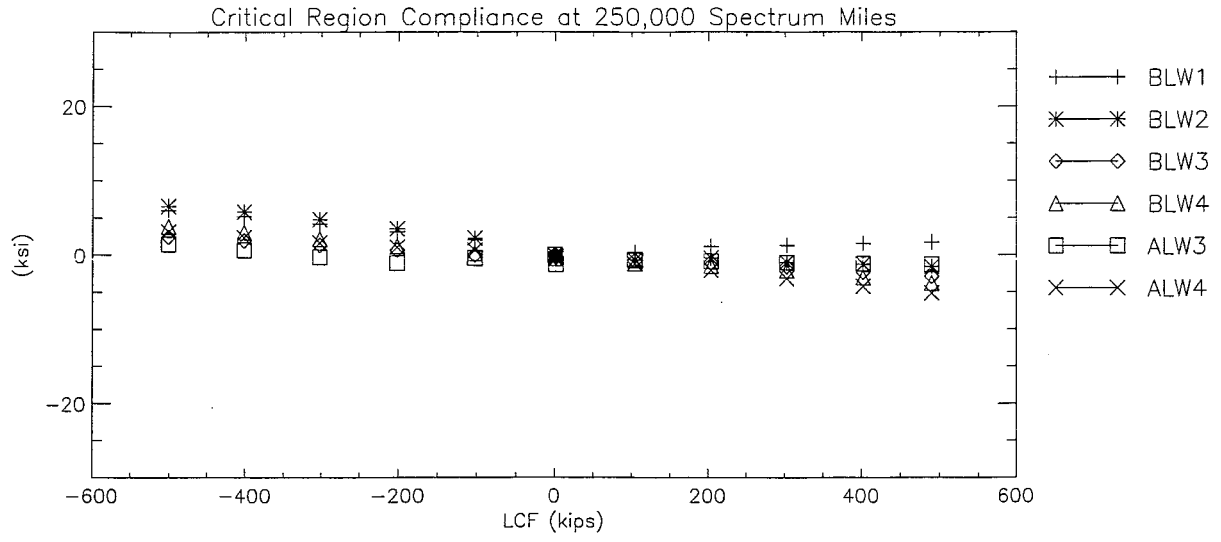


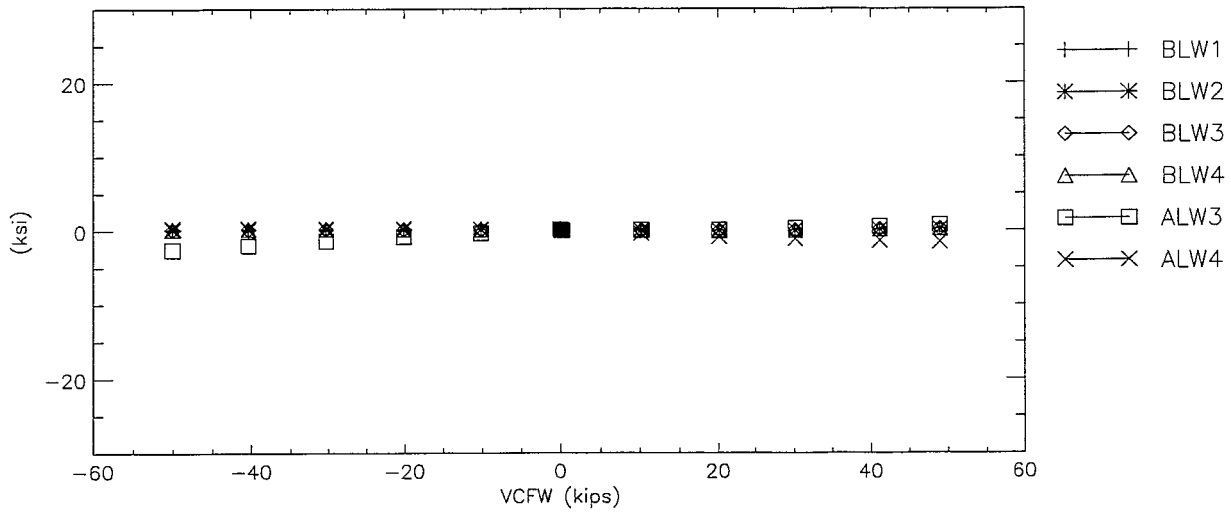
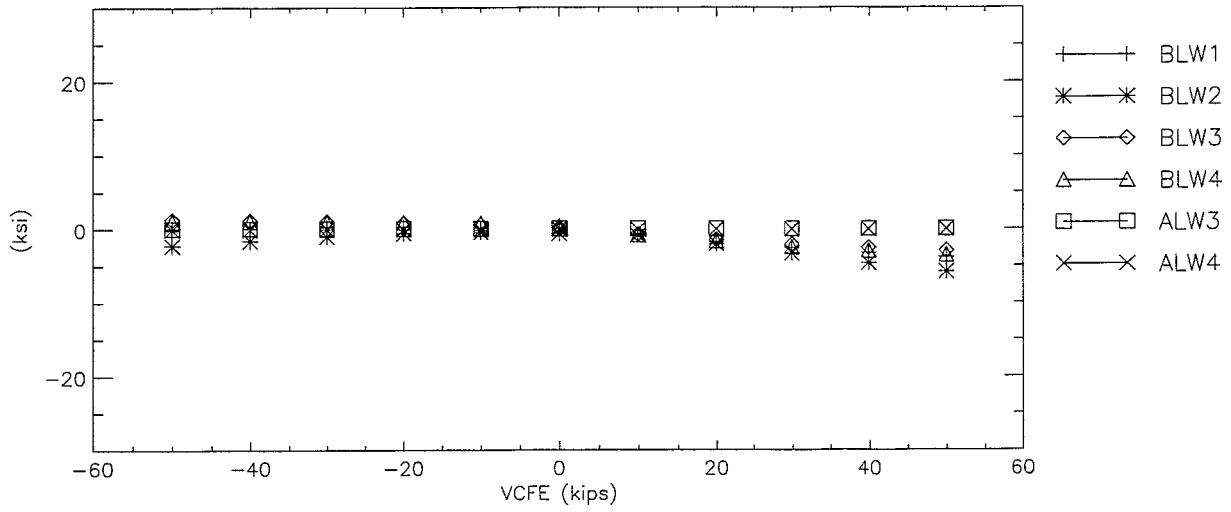
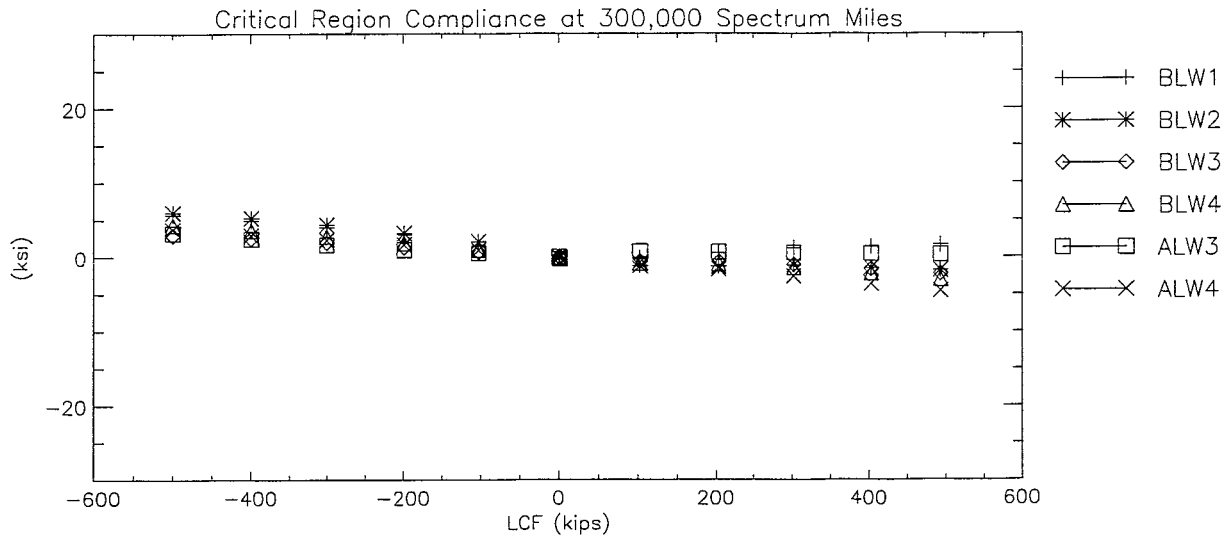






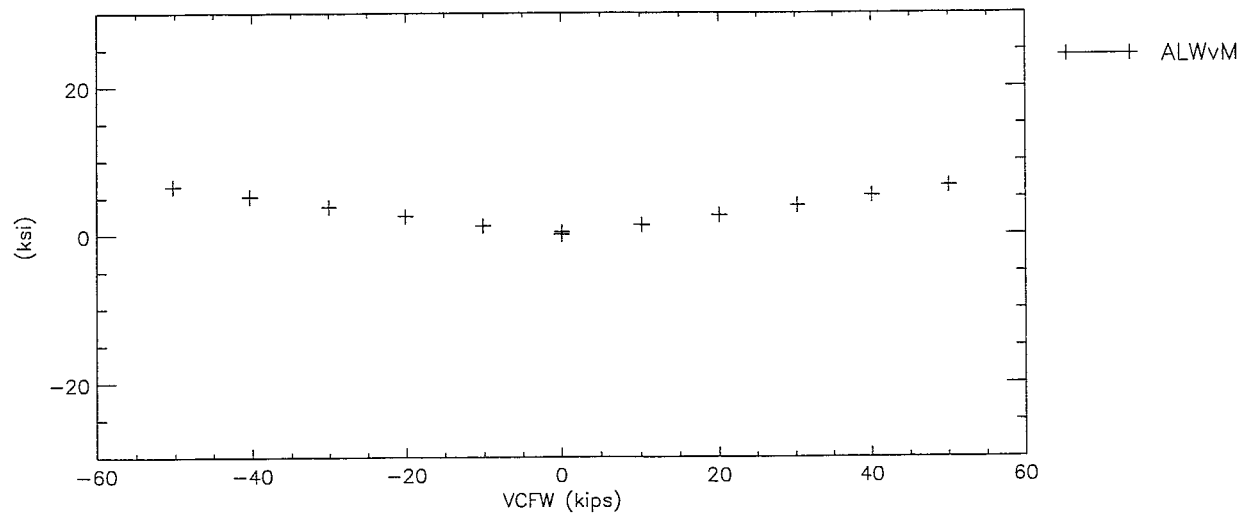
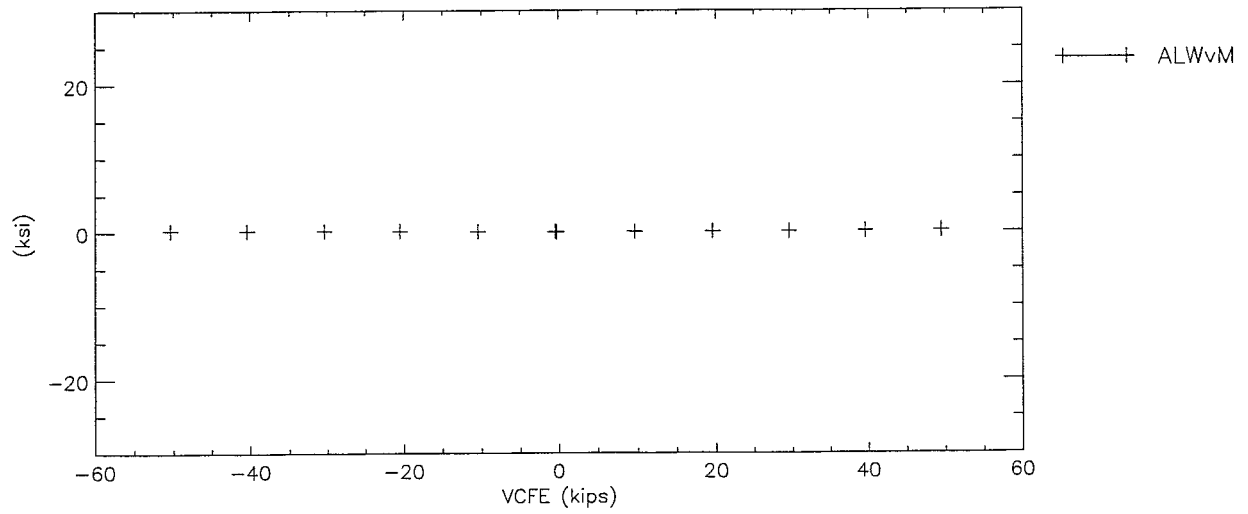
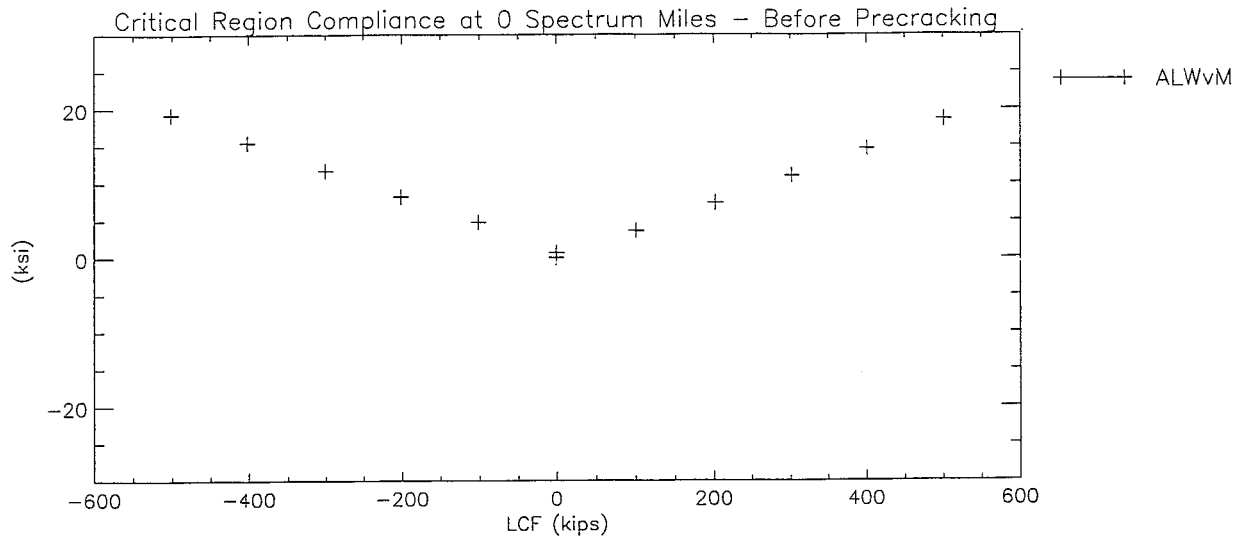


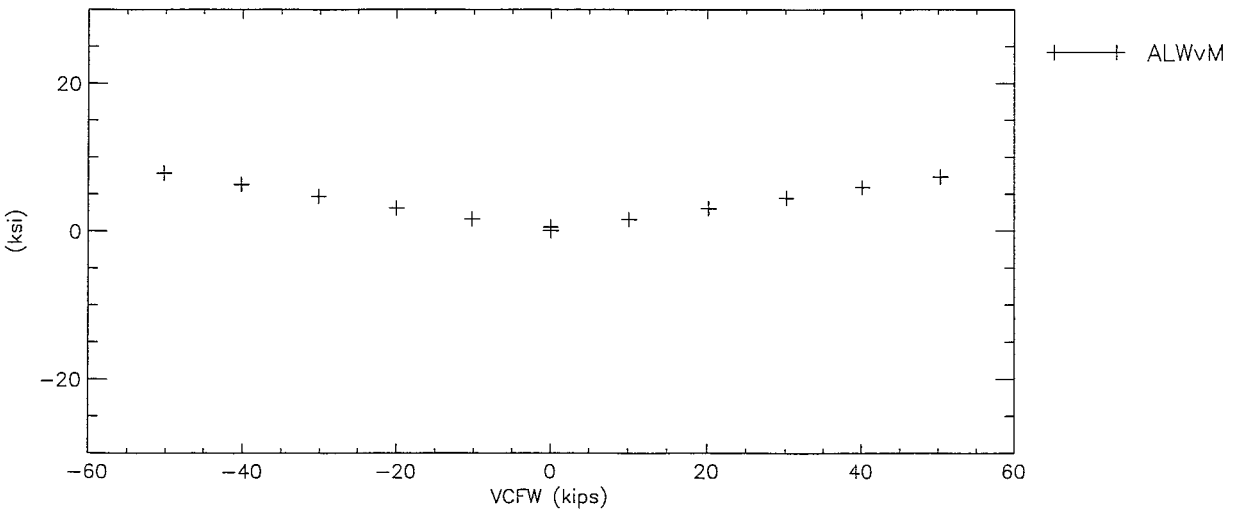
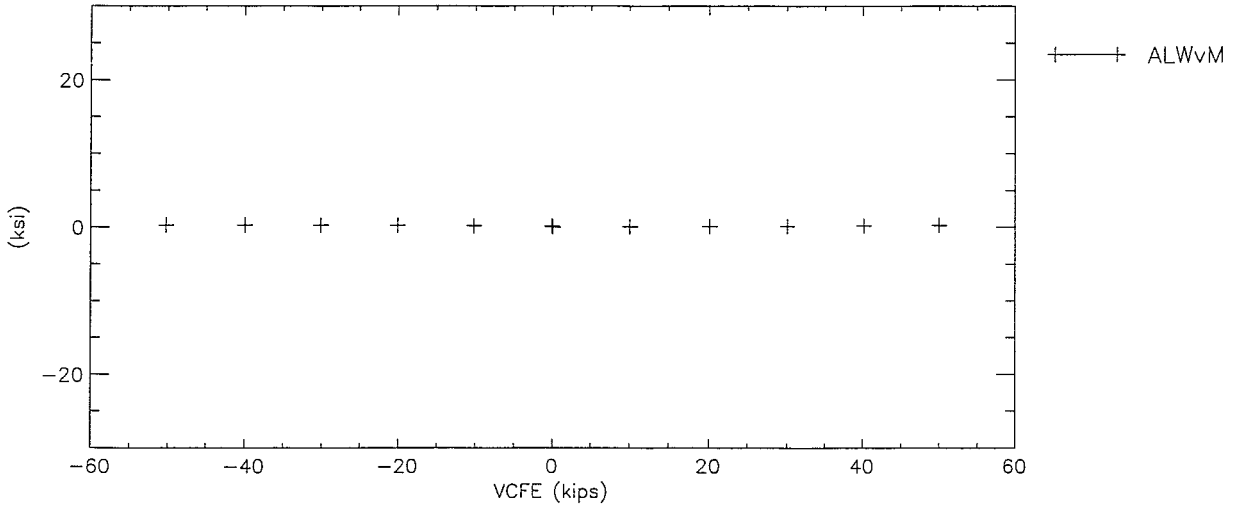
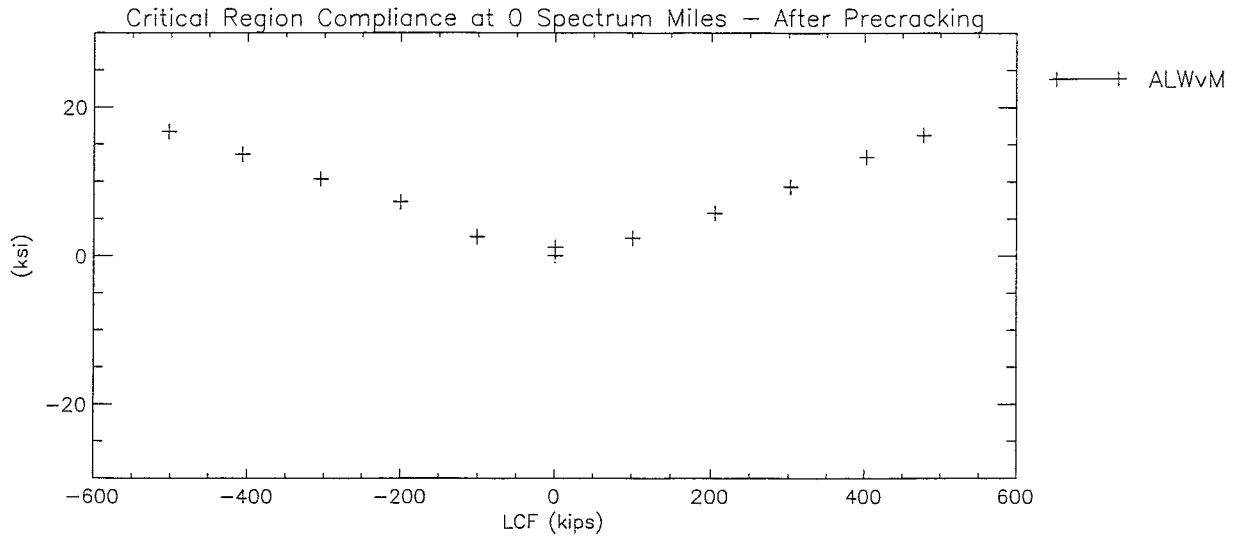


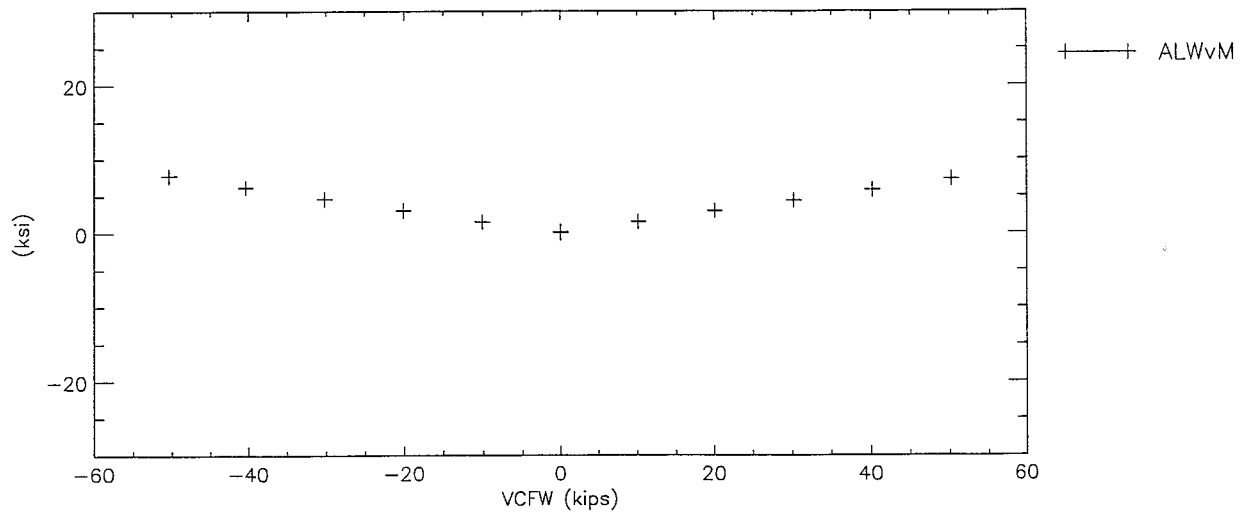
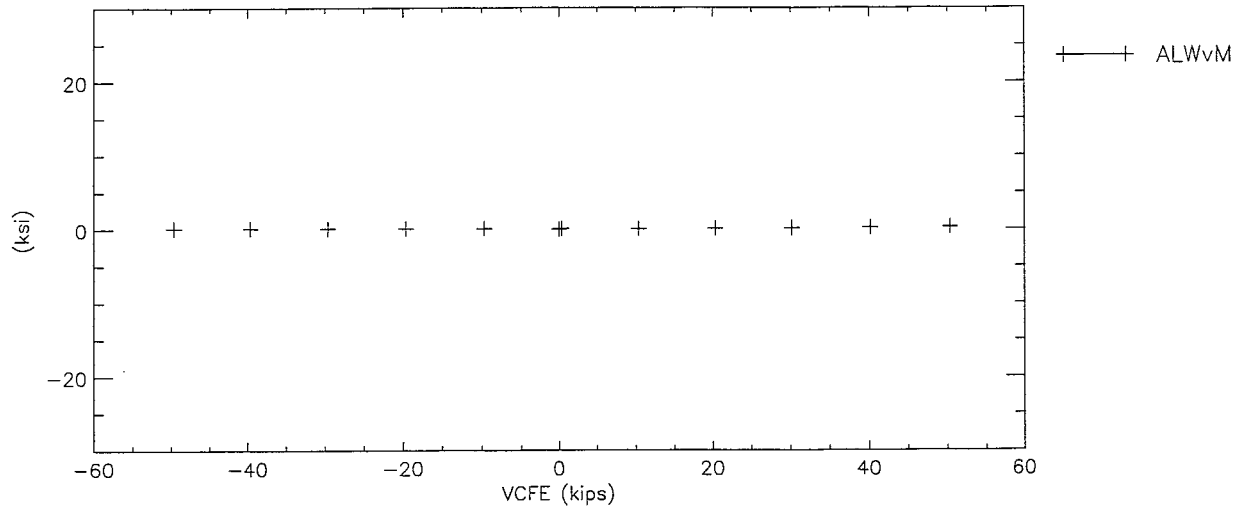
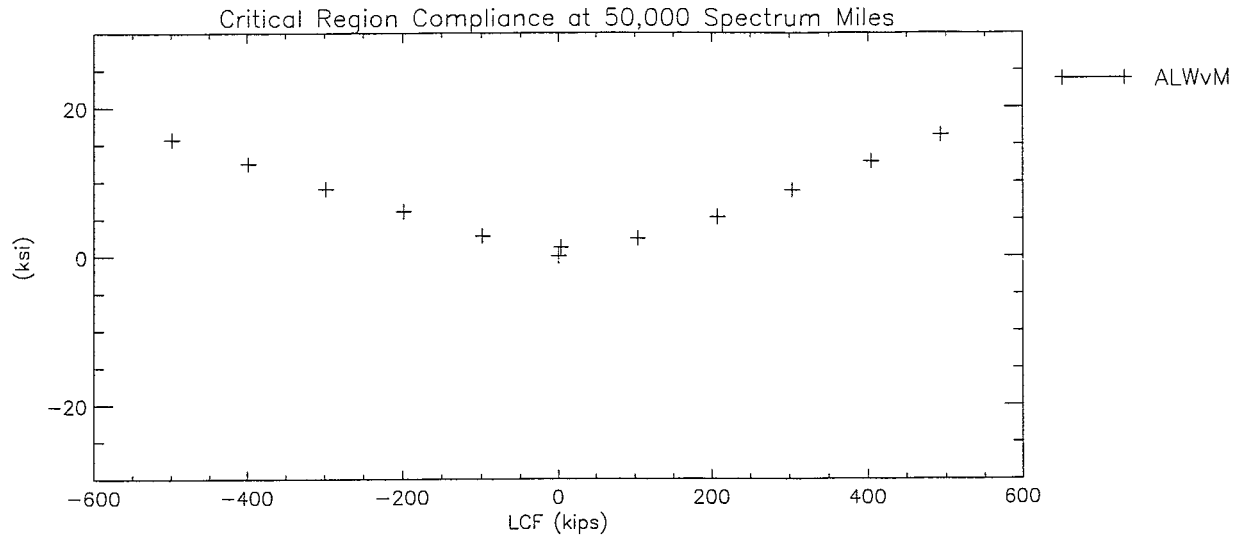


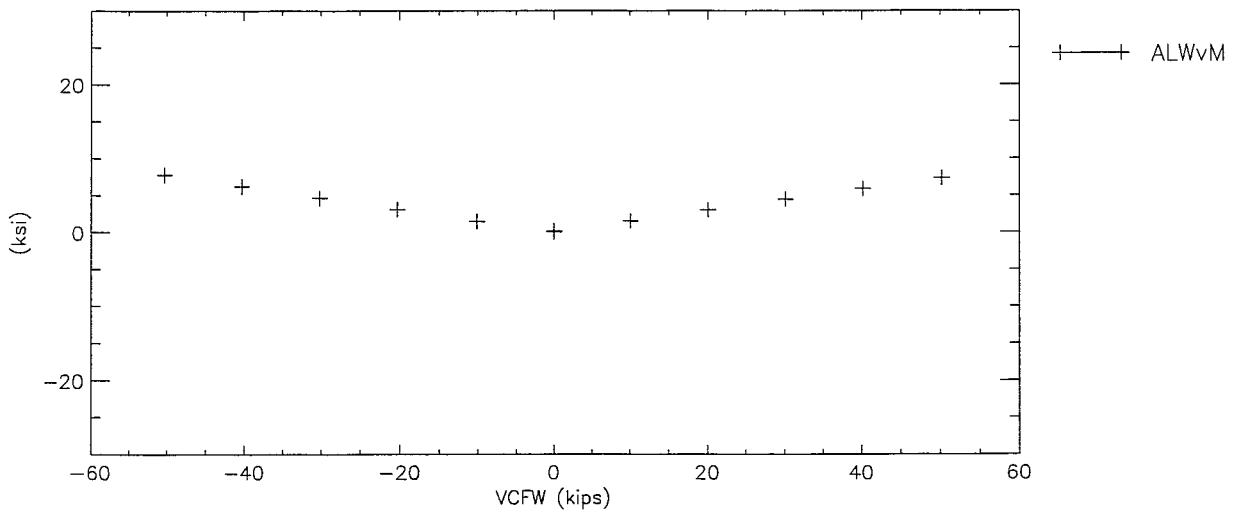
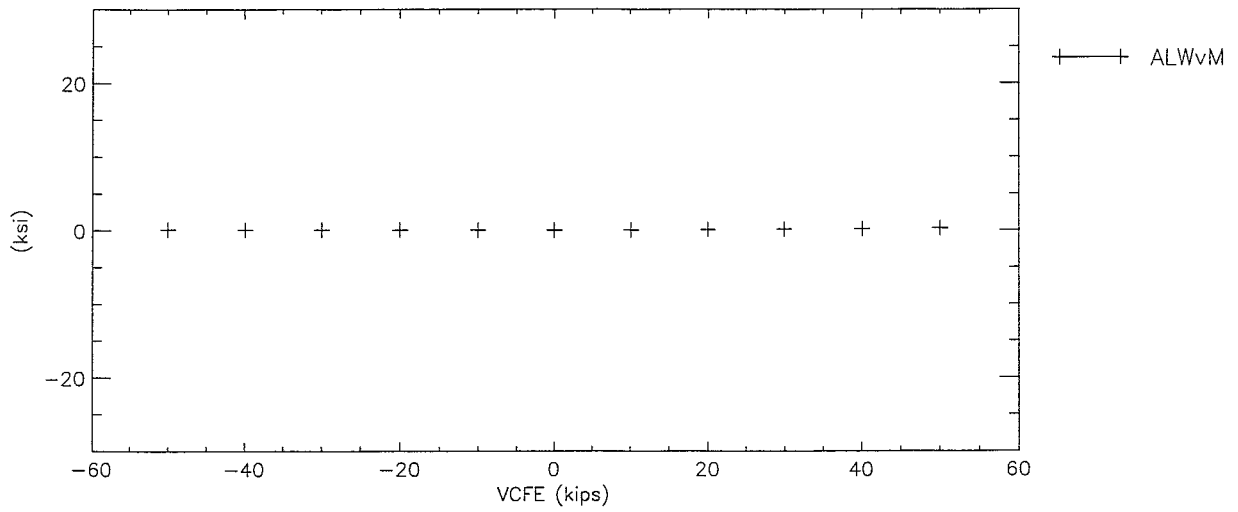
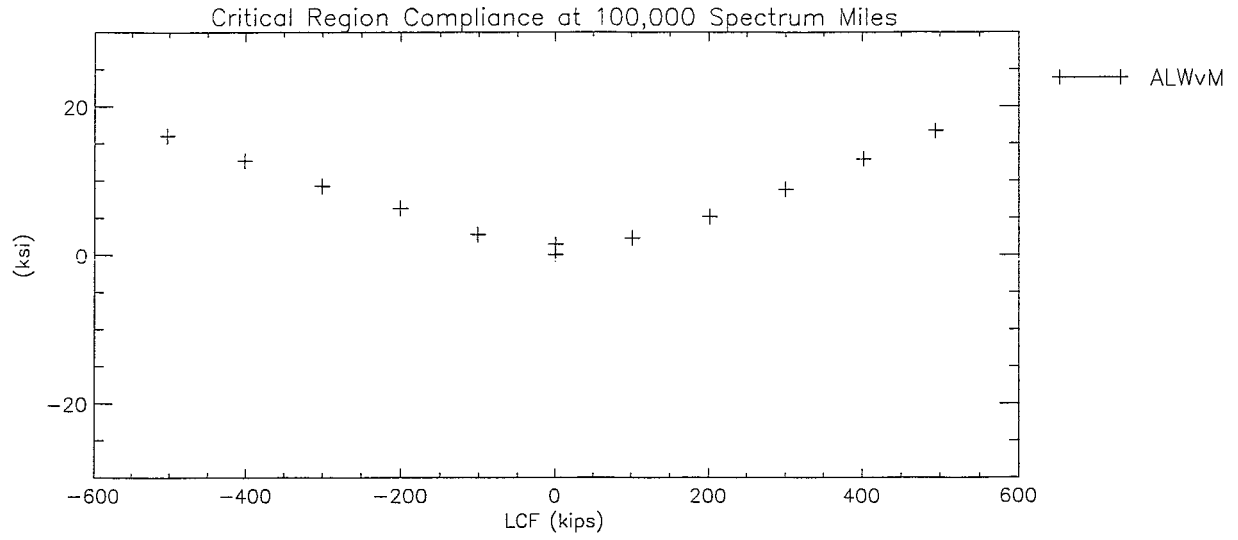
Section C-VII: A-End Left Von Mises Web Stress

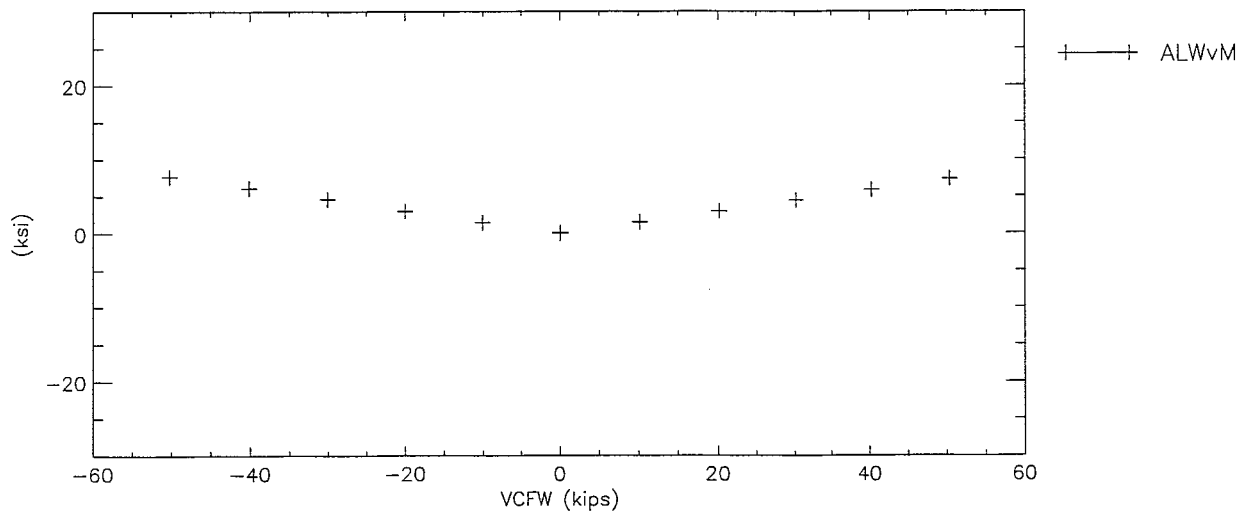
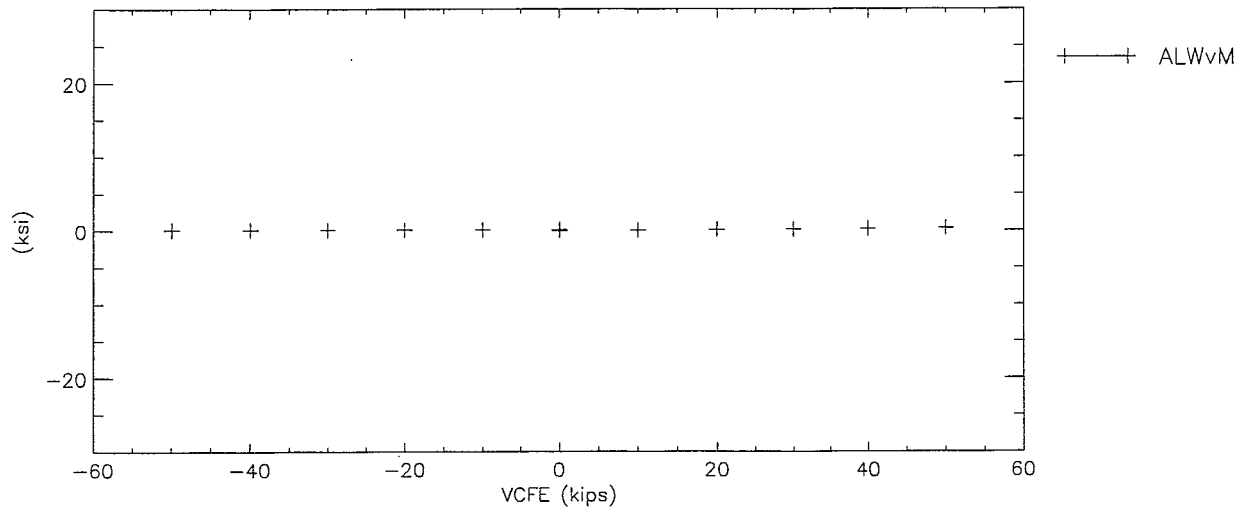
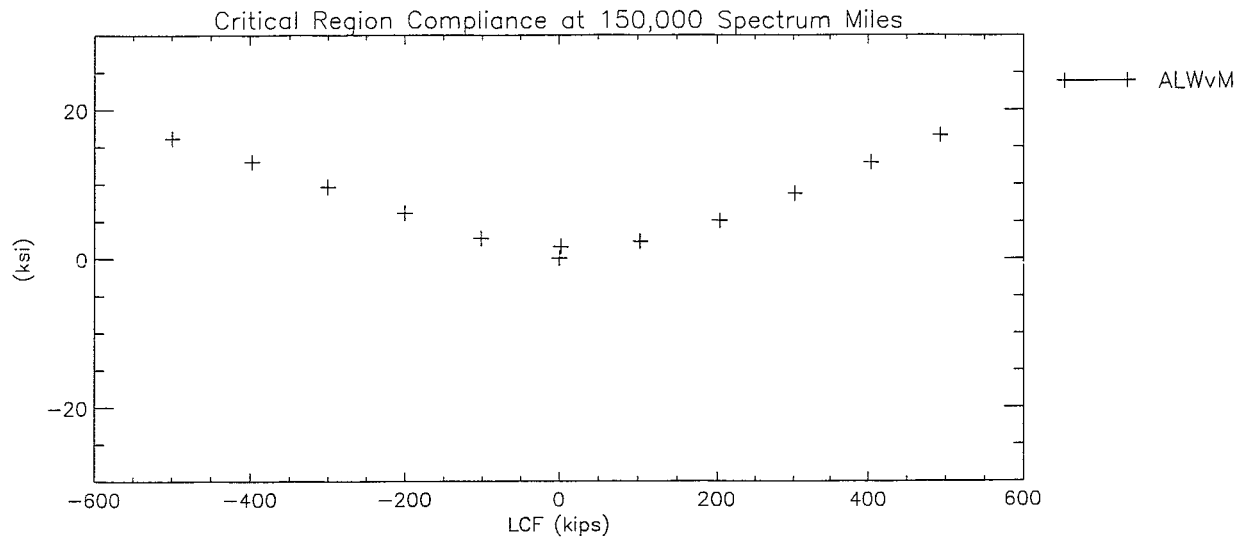
FINAL DRAFT

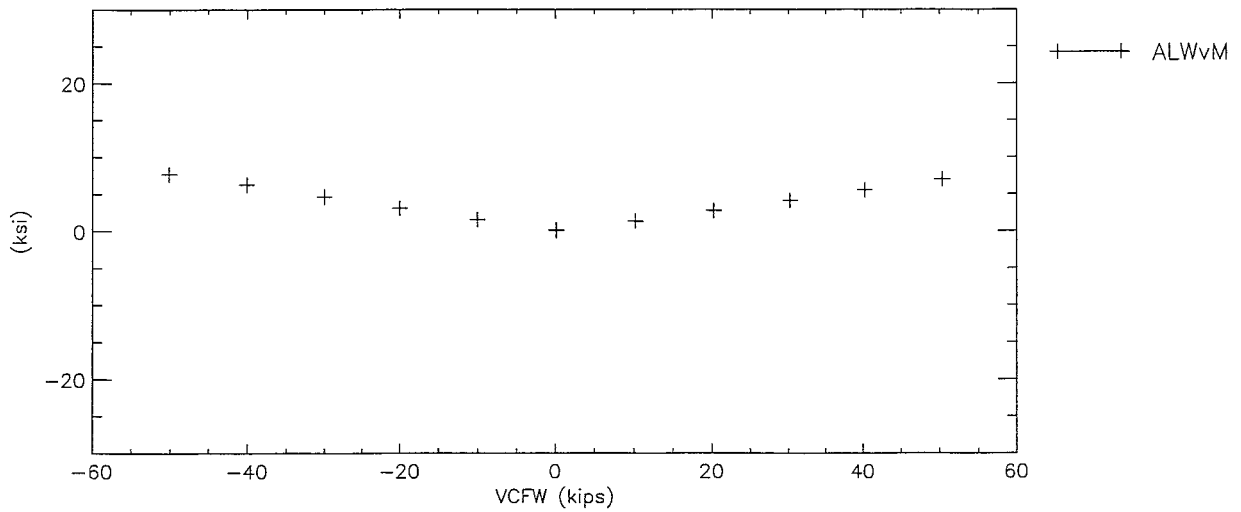
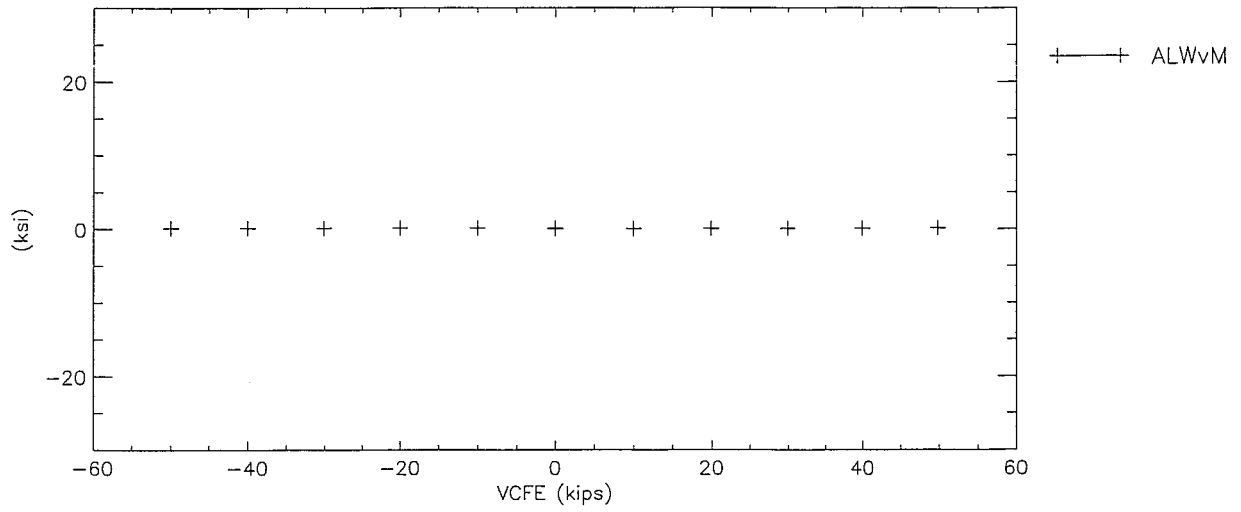
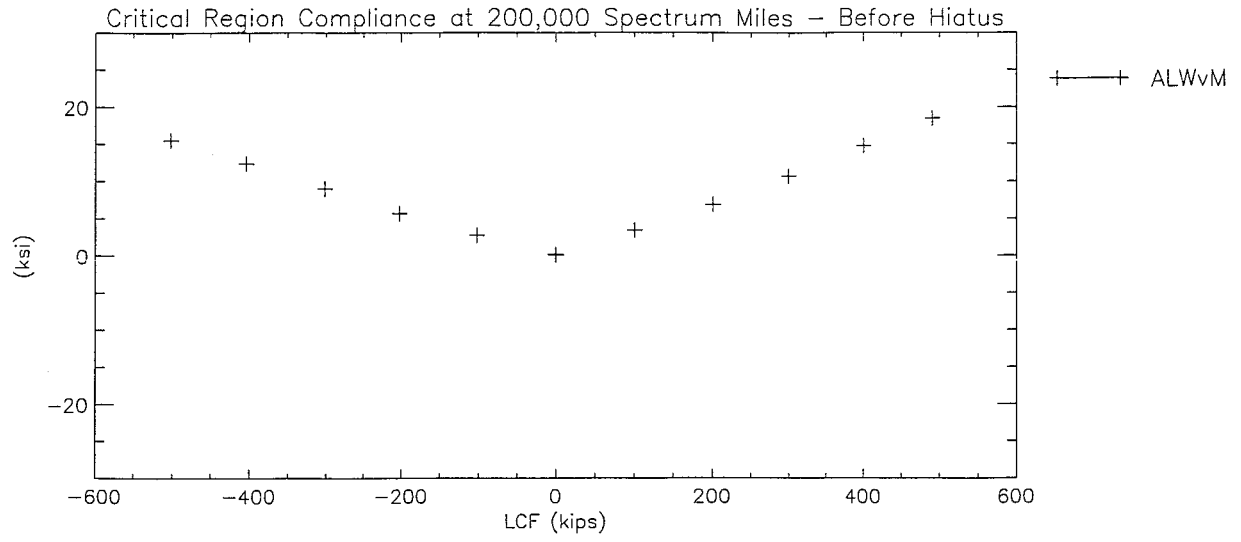


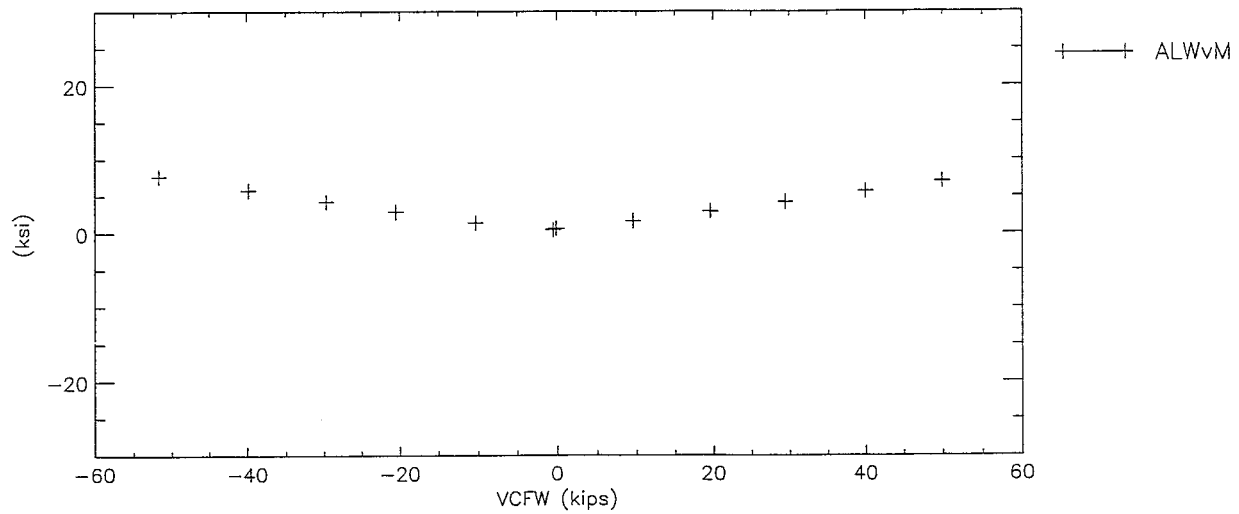
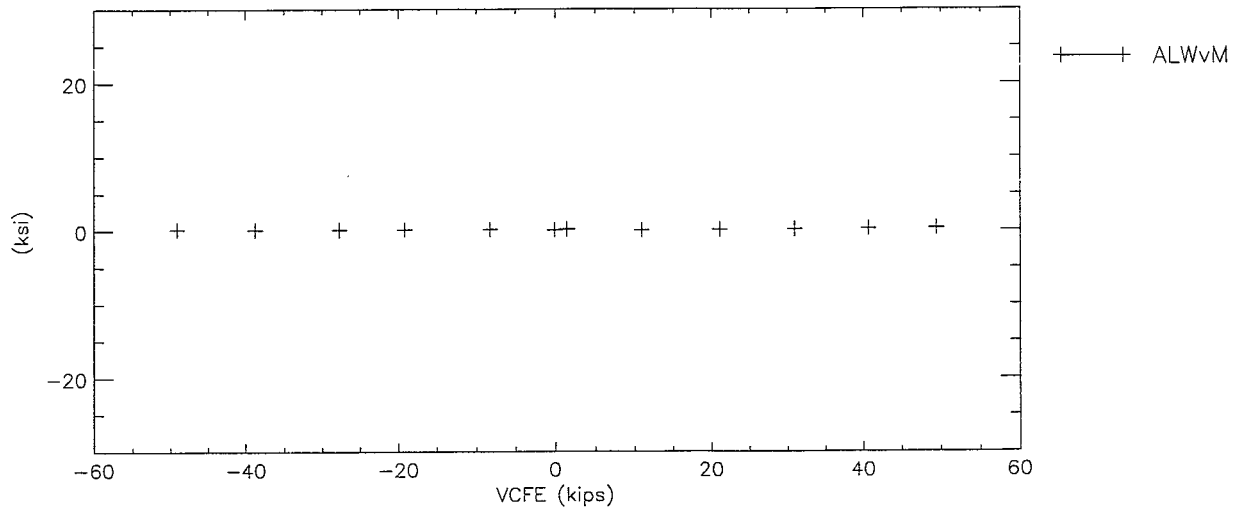
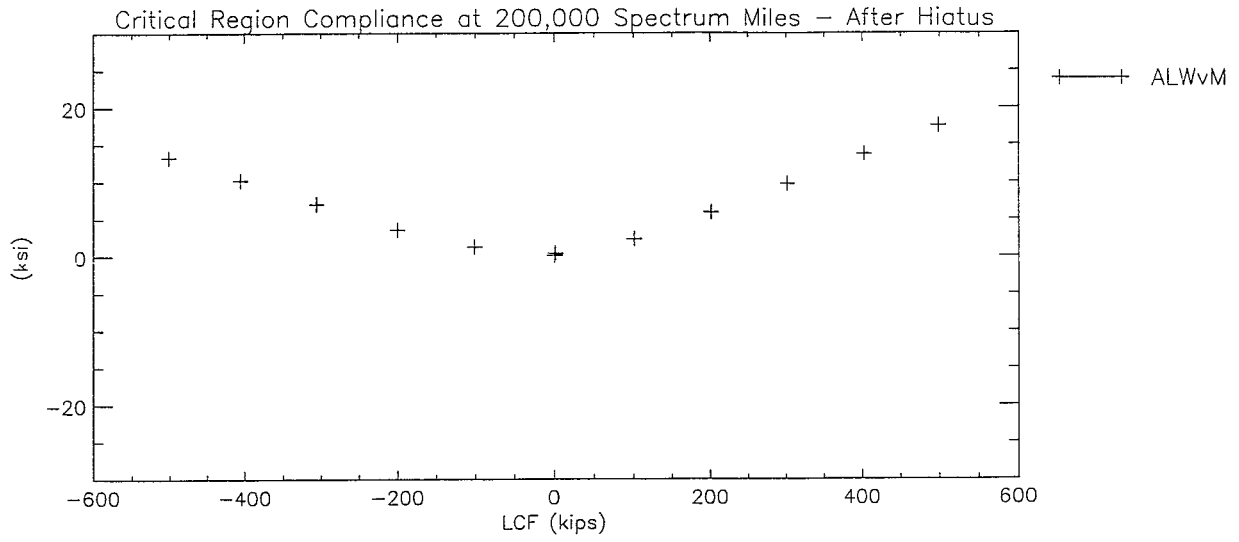


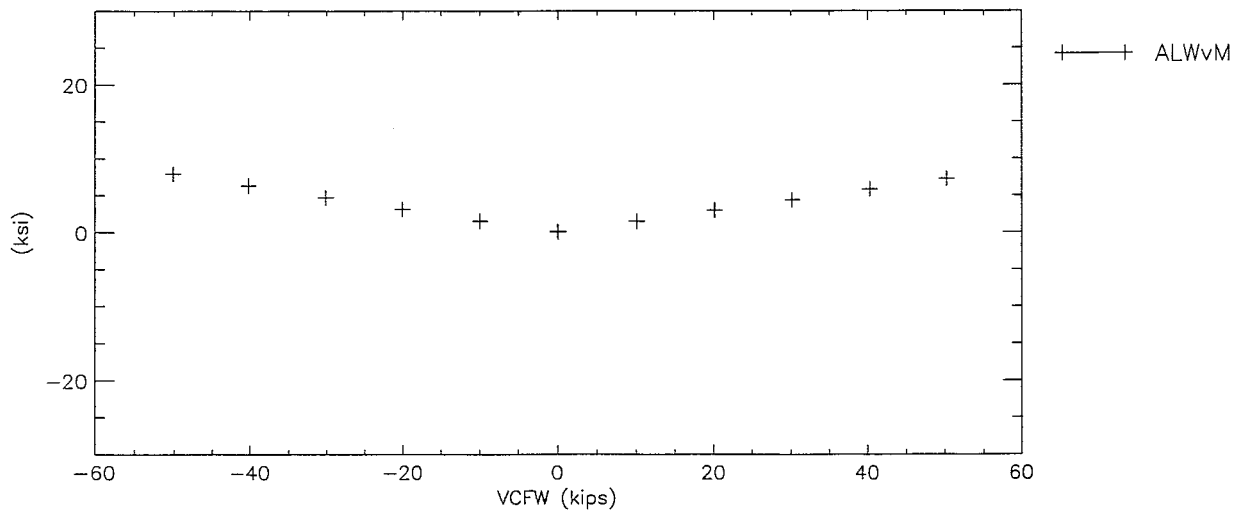
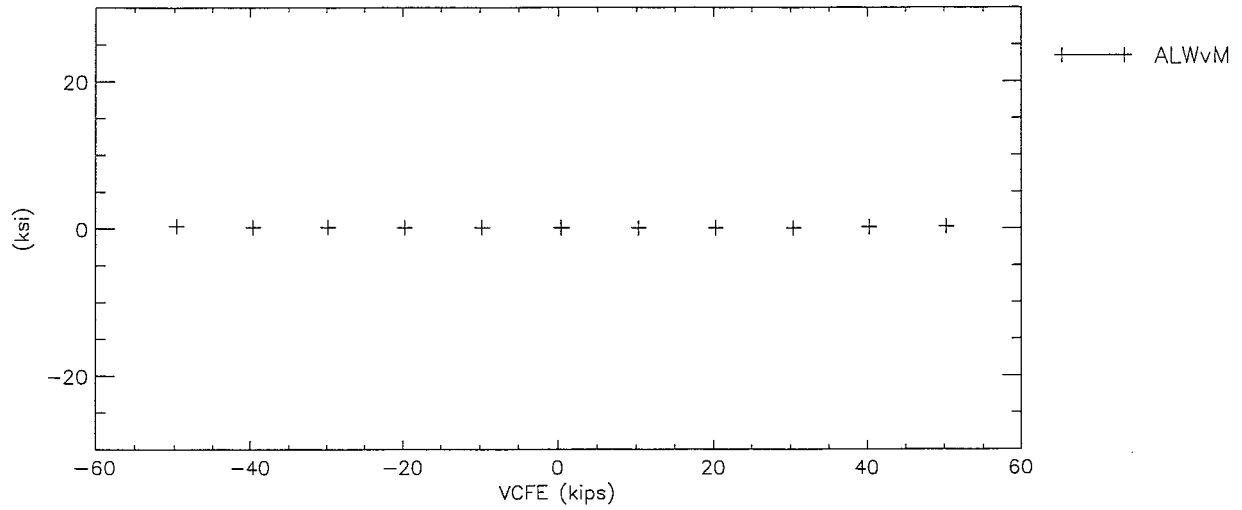
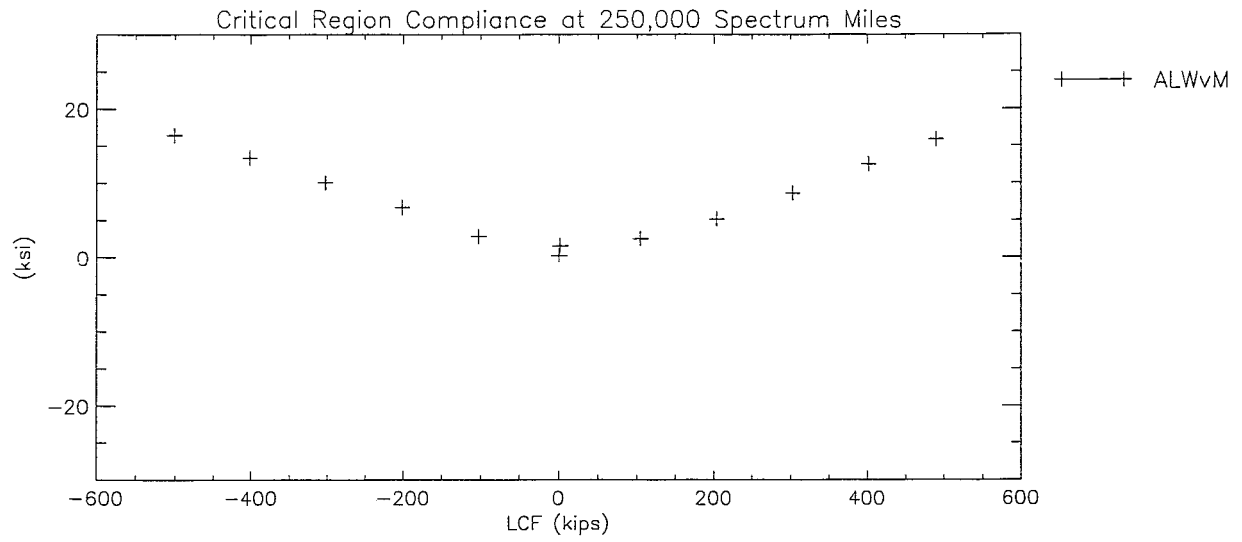


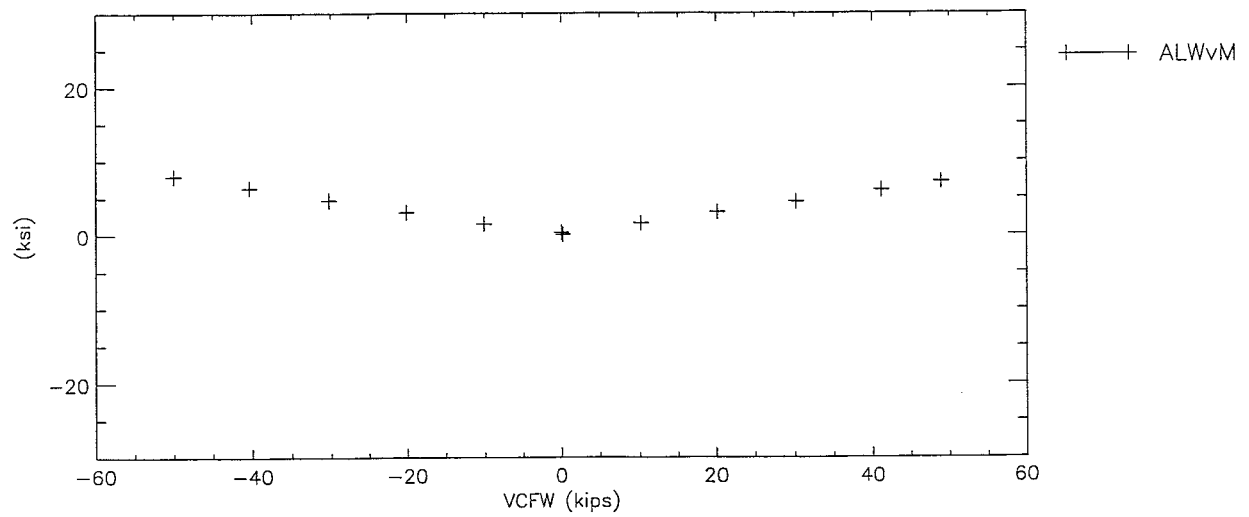
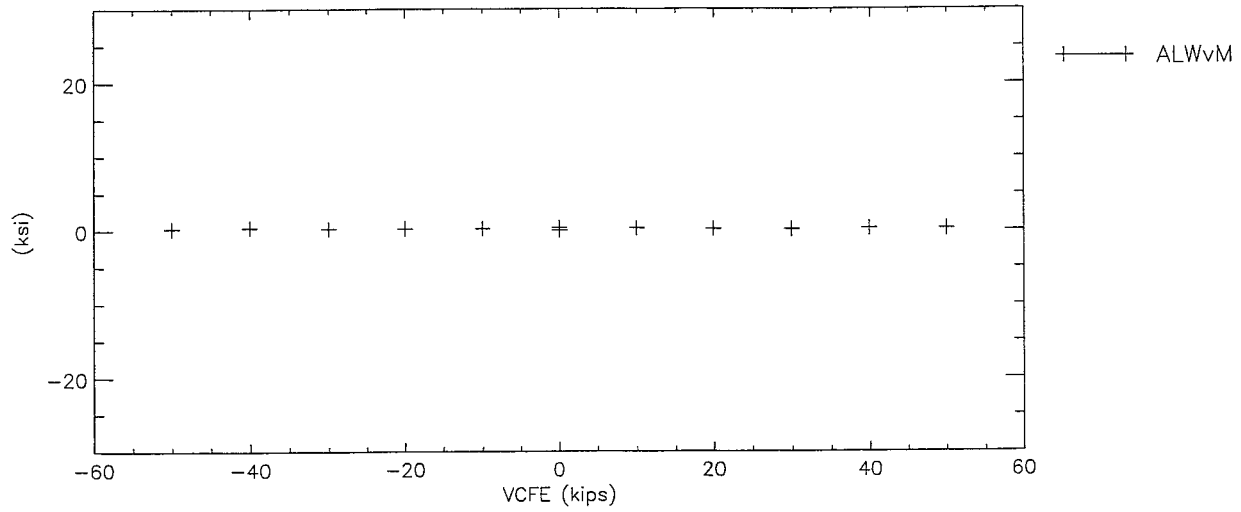
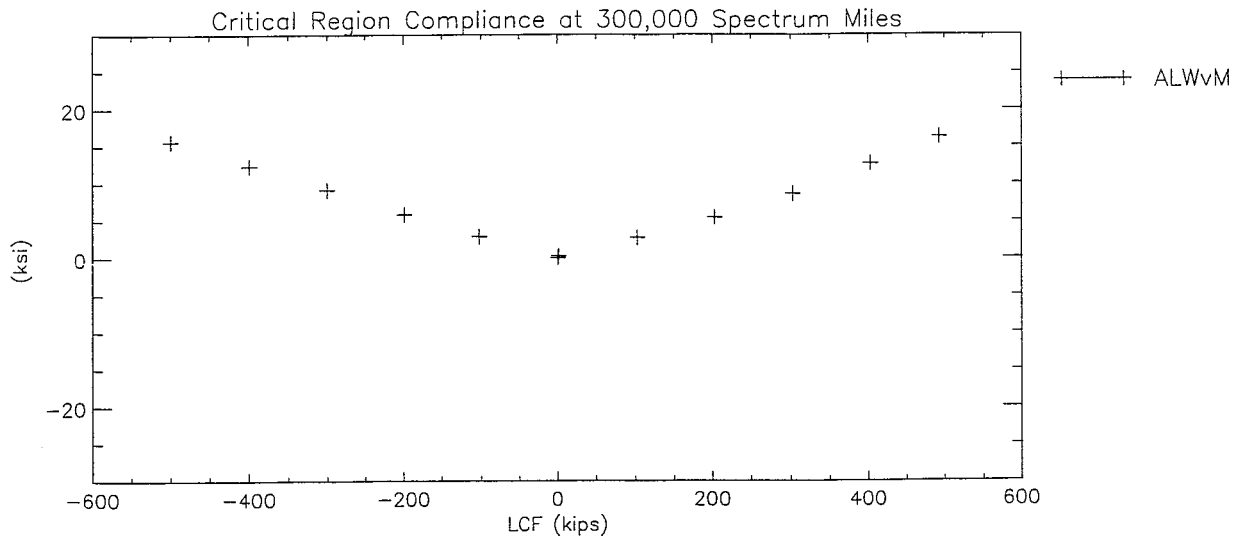








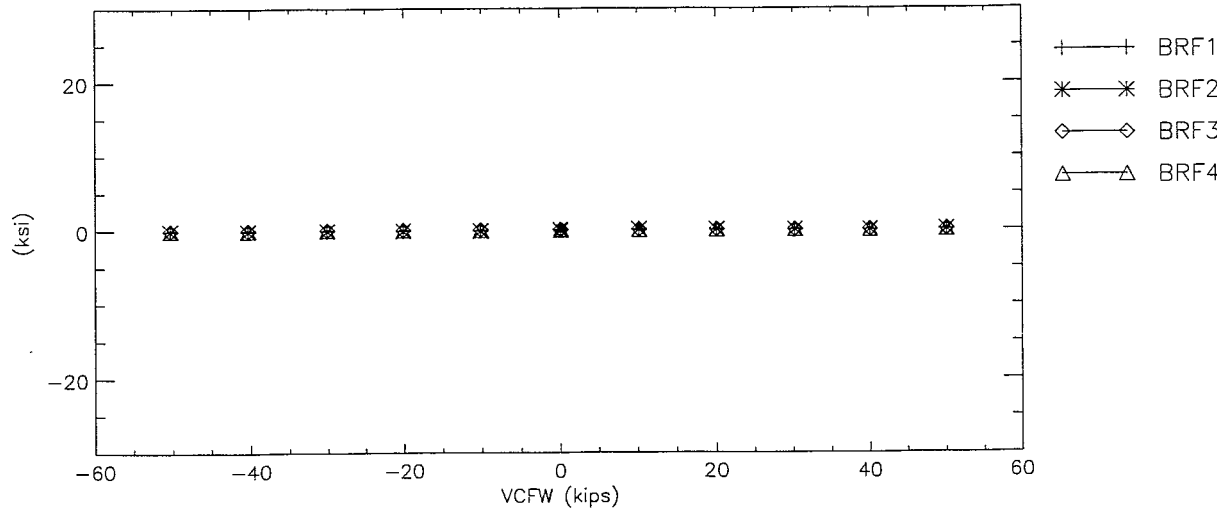
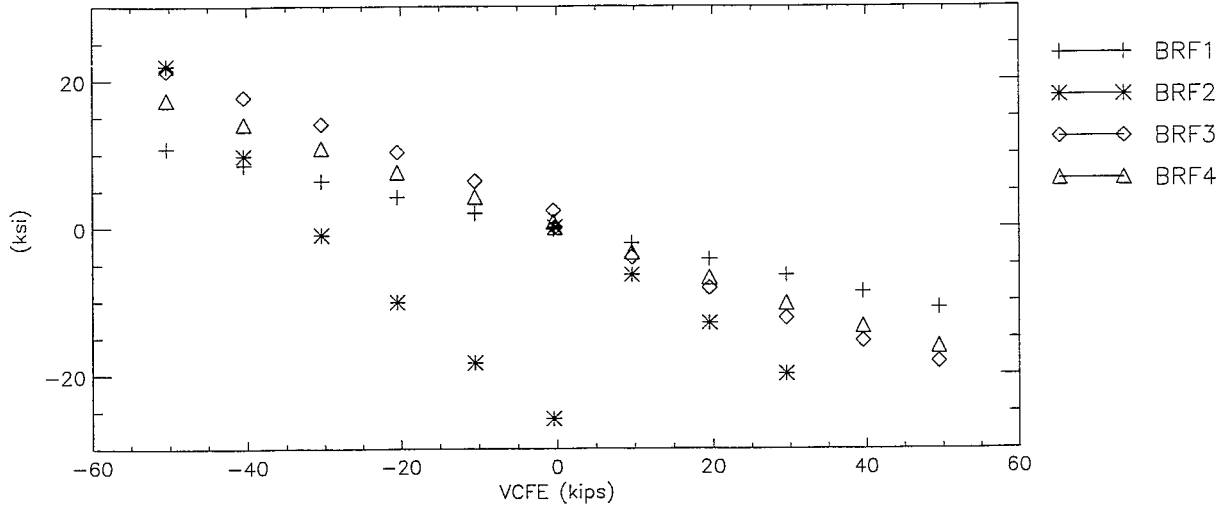
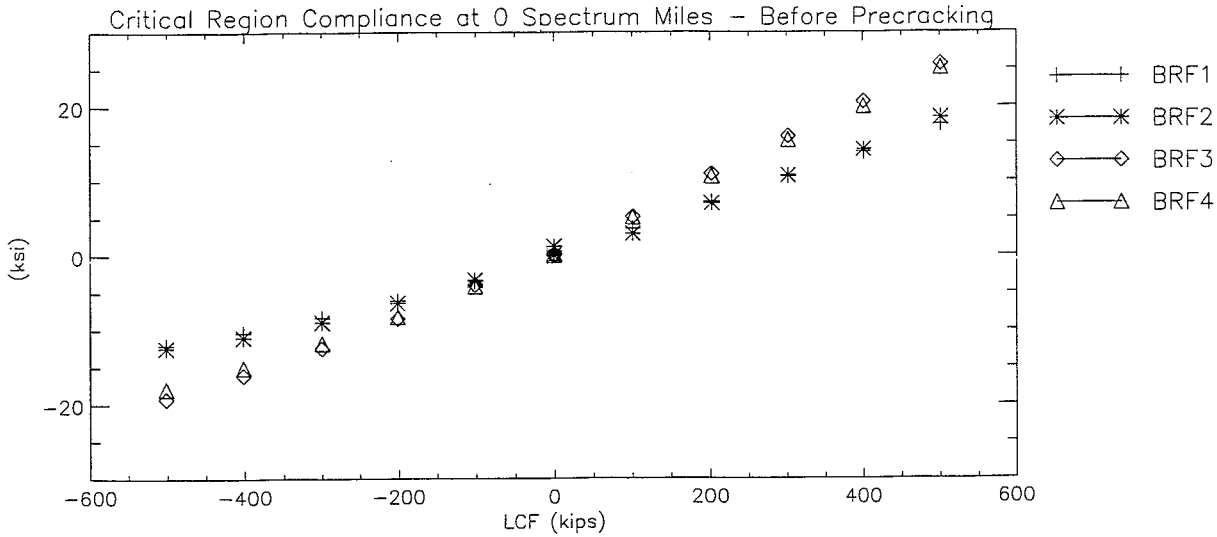


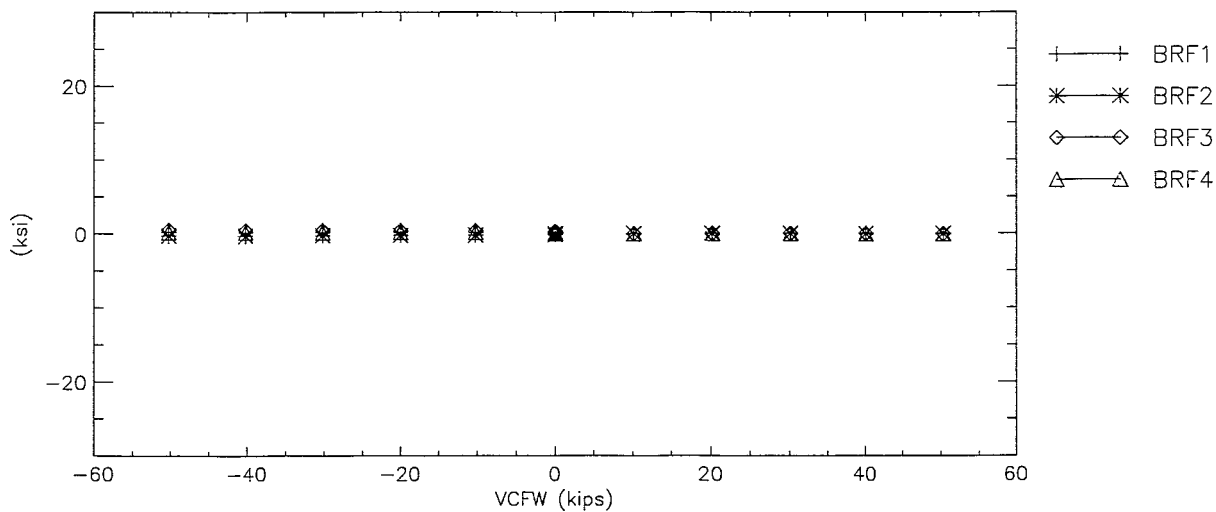
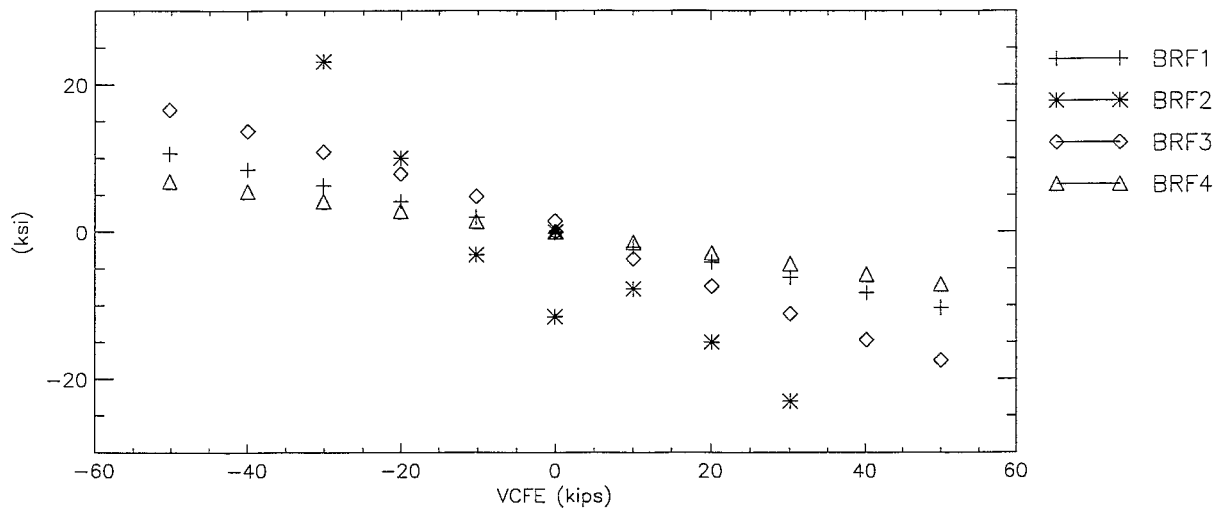
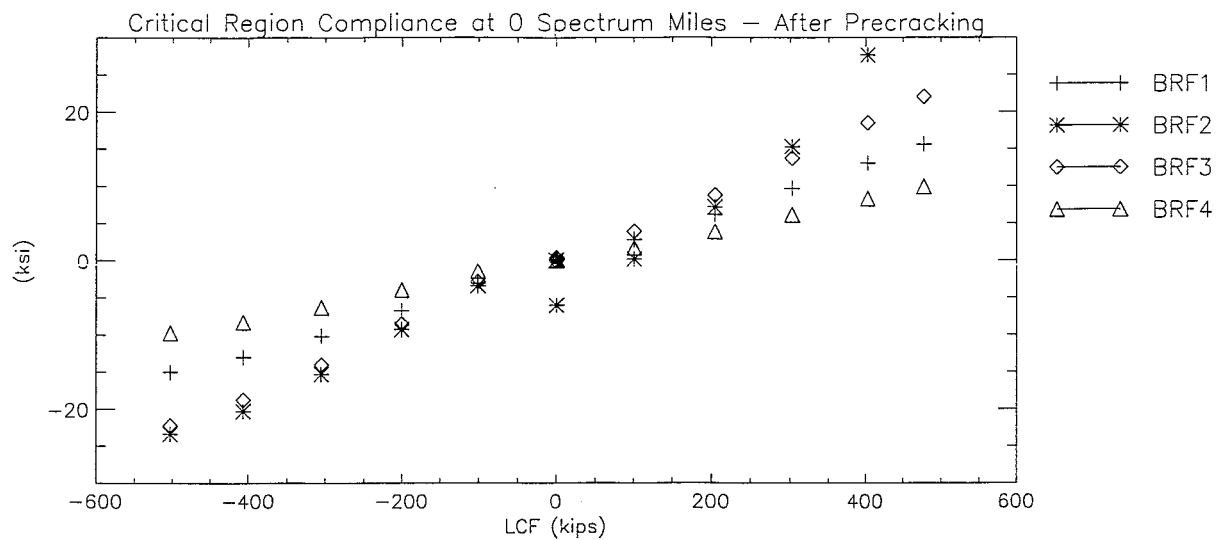


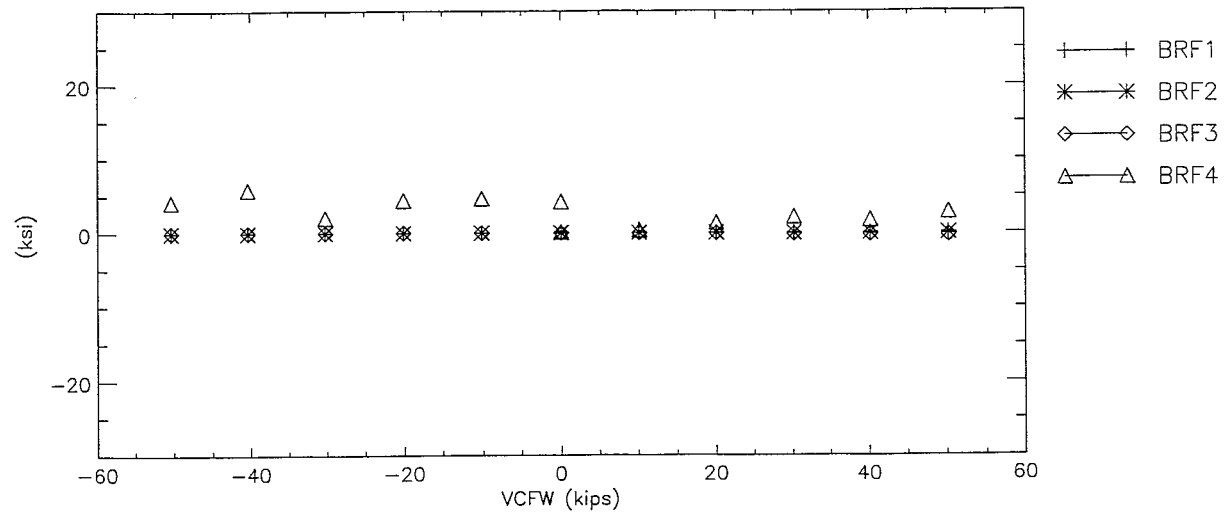
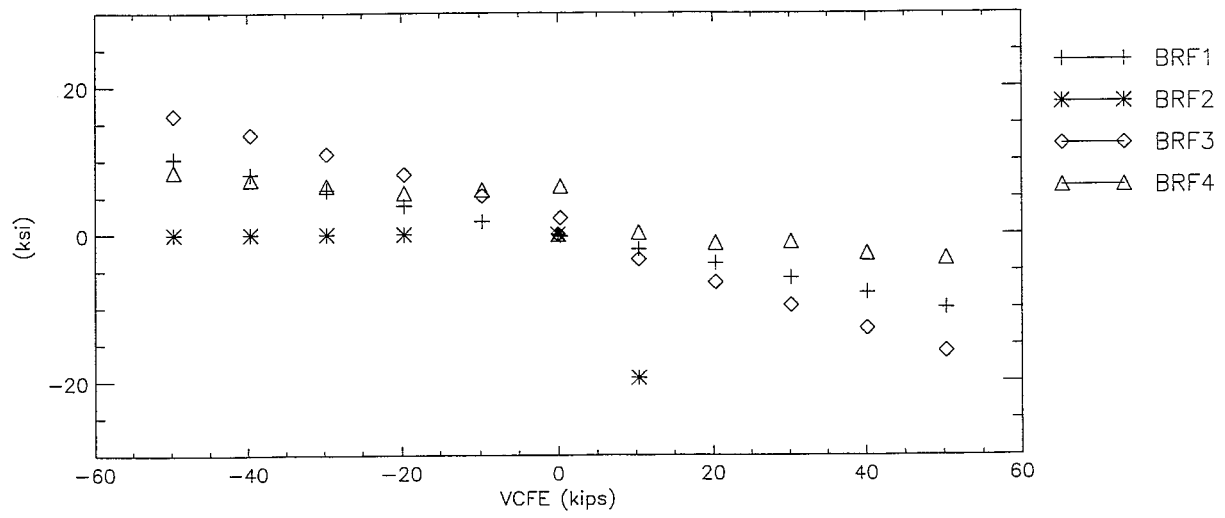
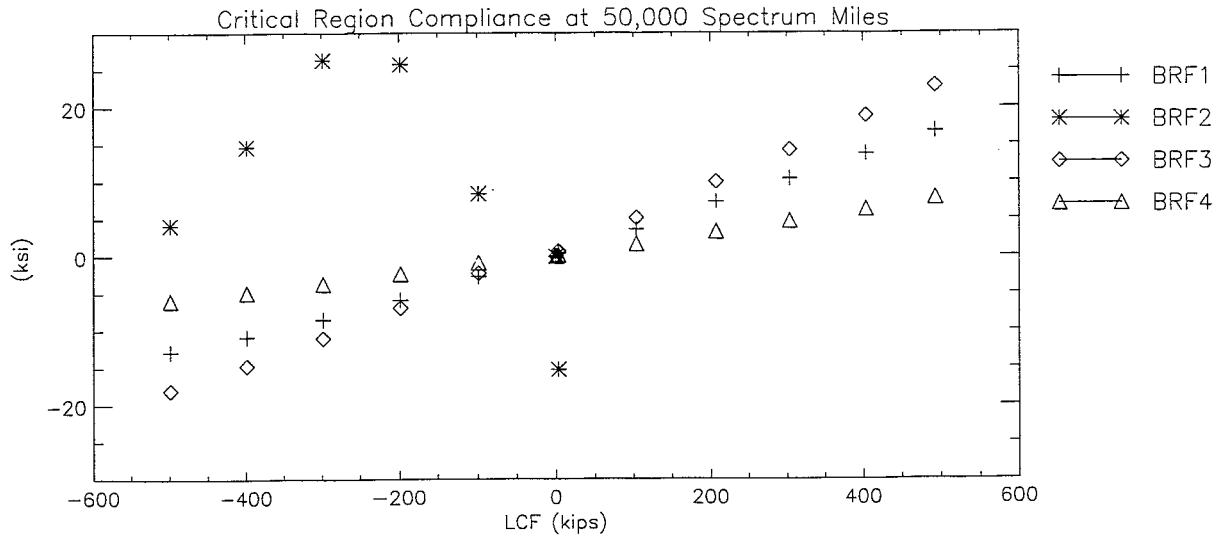
FINAL DRAFT

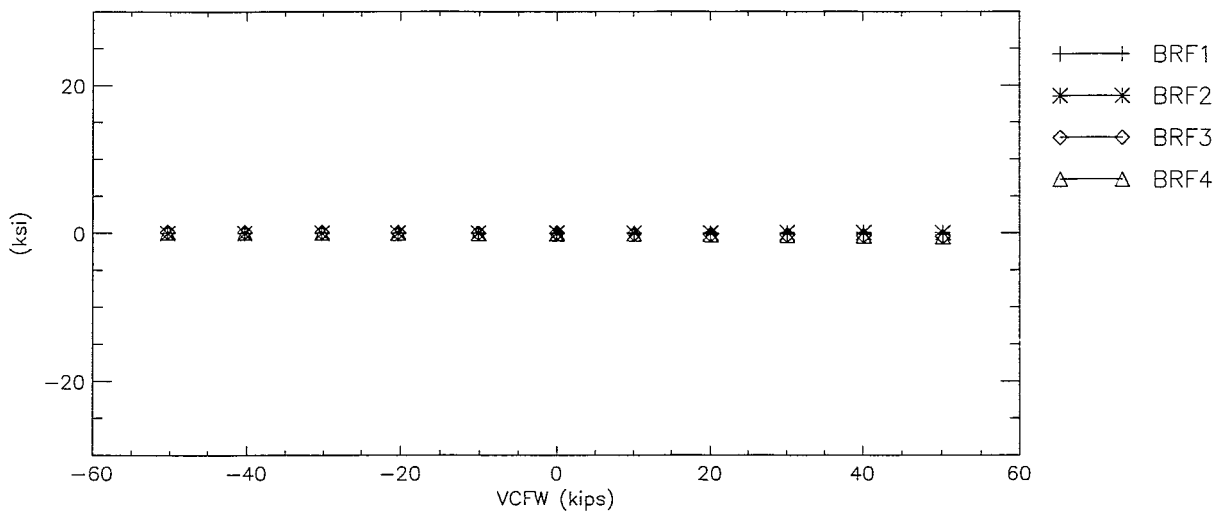
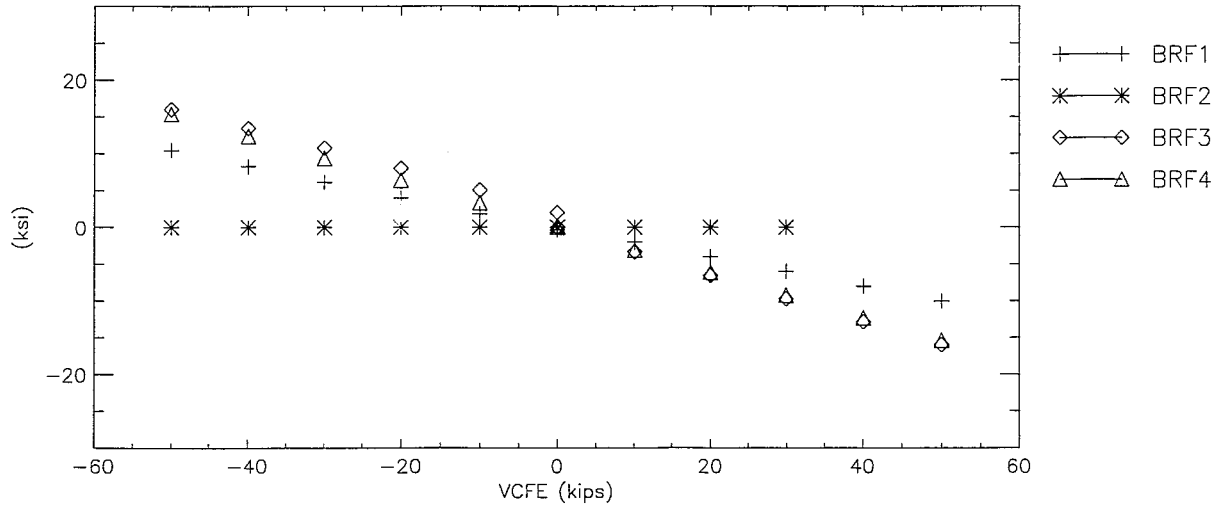
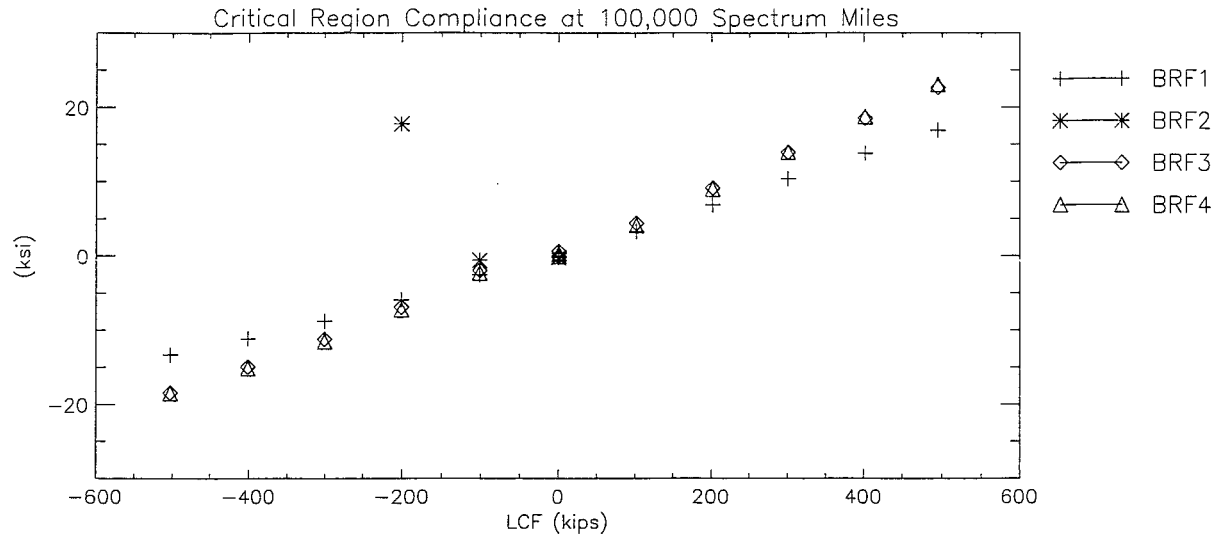
Section C-VIII: B-End Right Longitudinal Flange Stresses

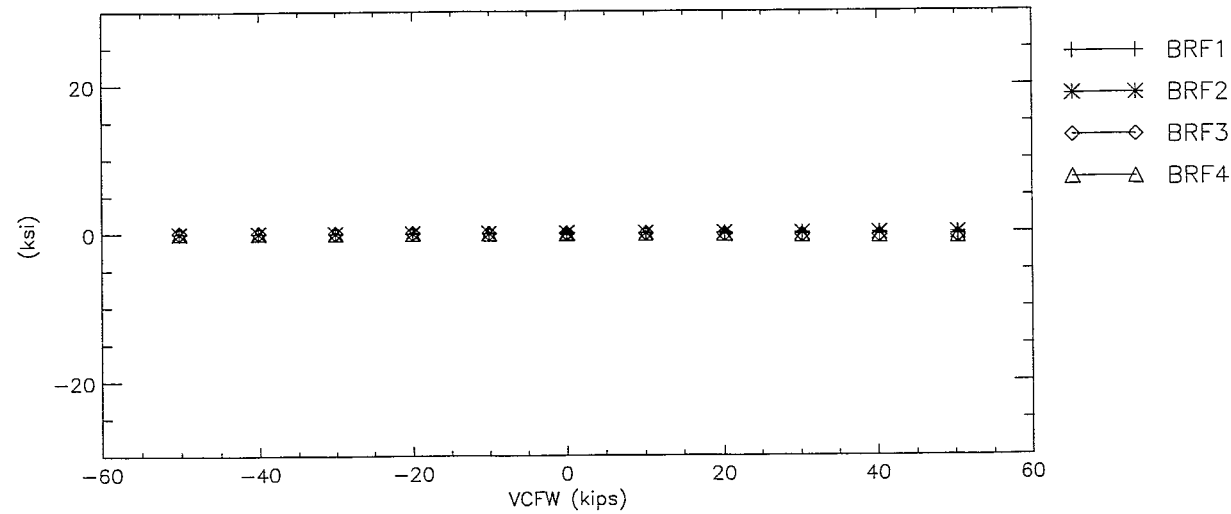
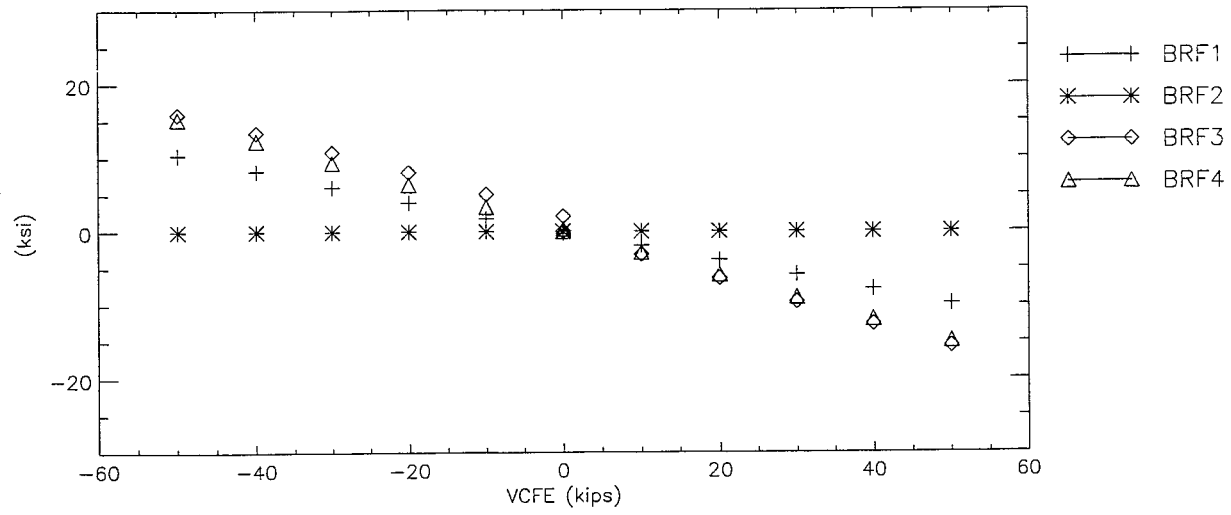
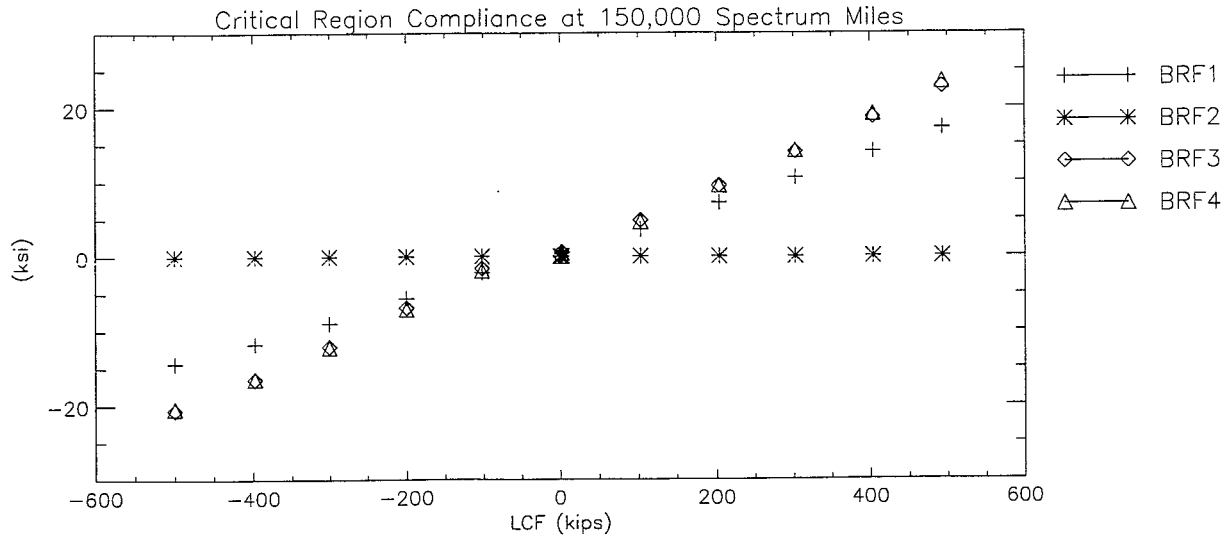
FINAL DRAFT

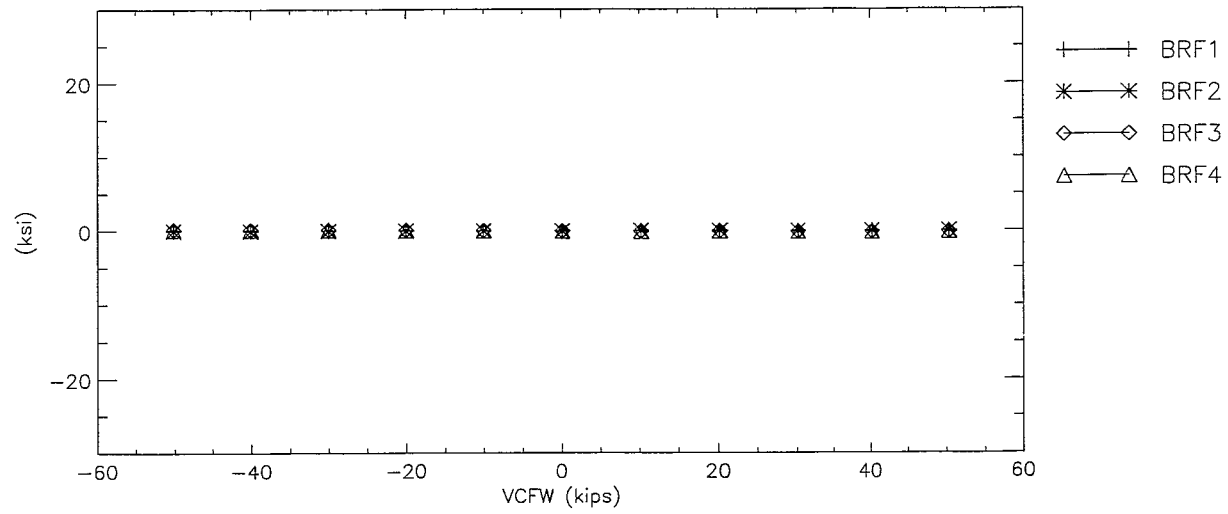
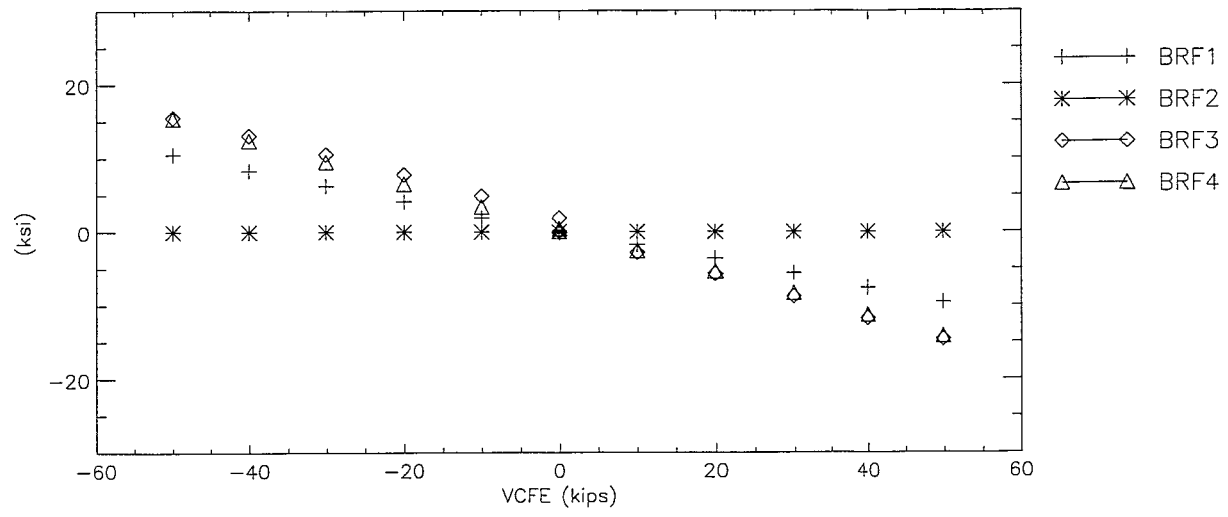
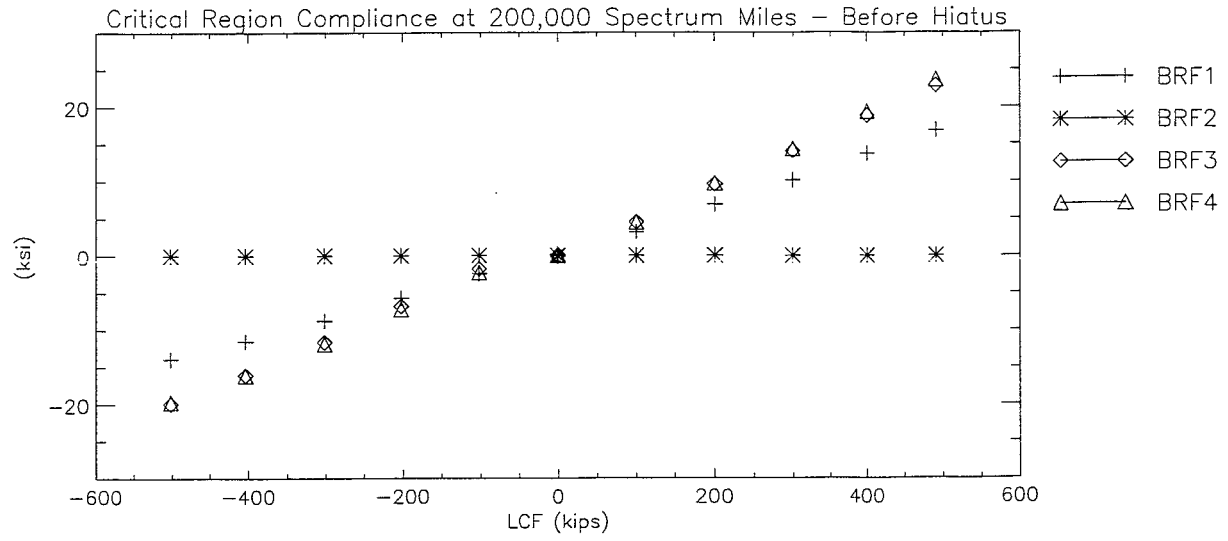


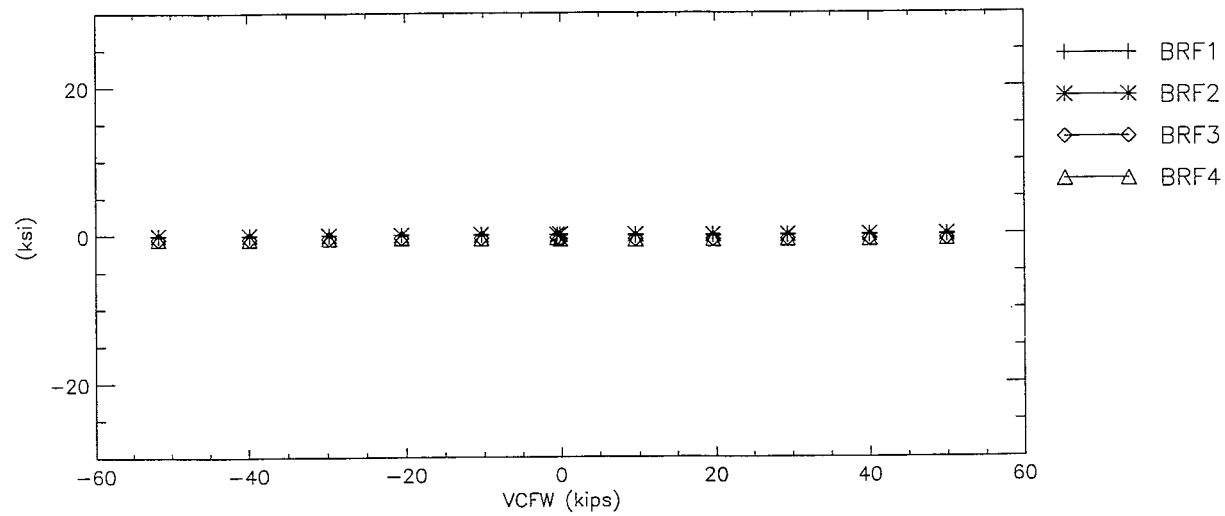
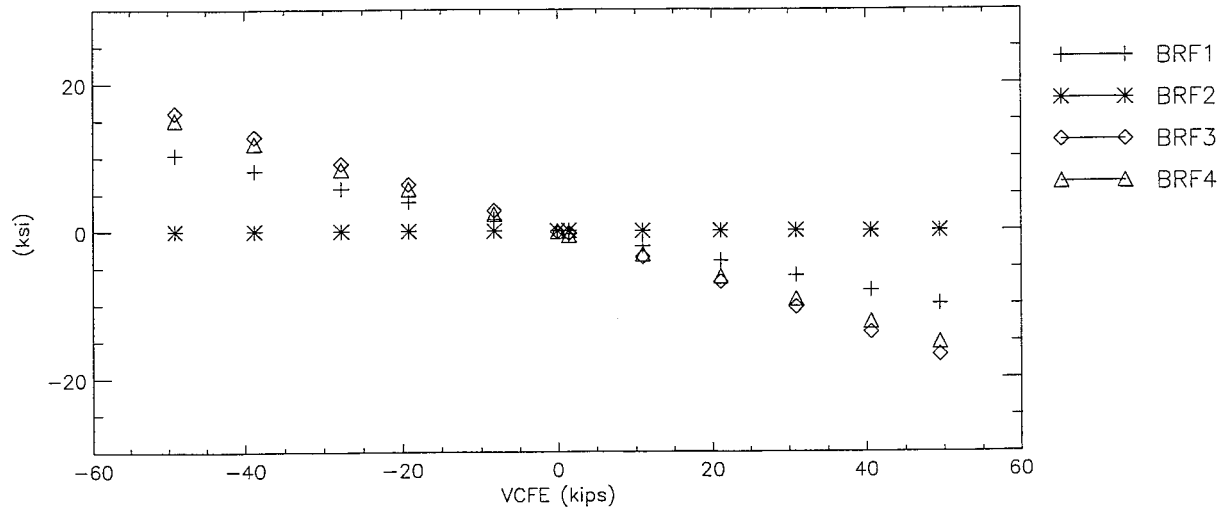
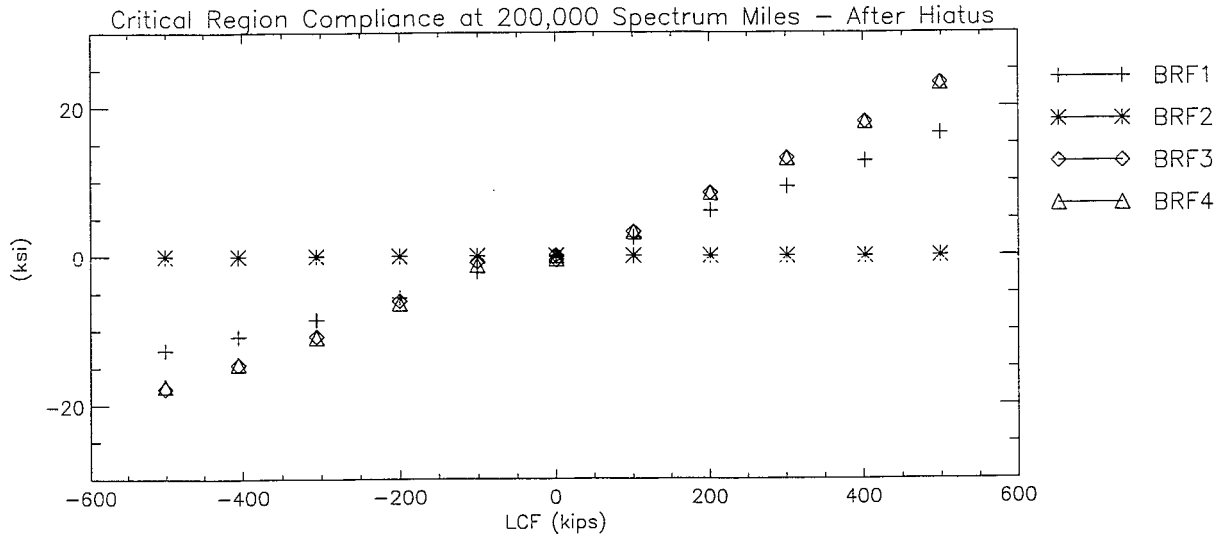


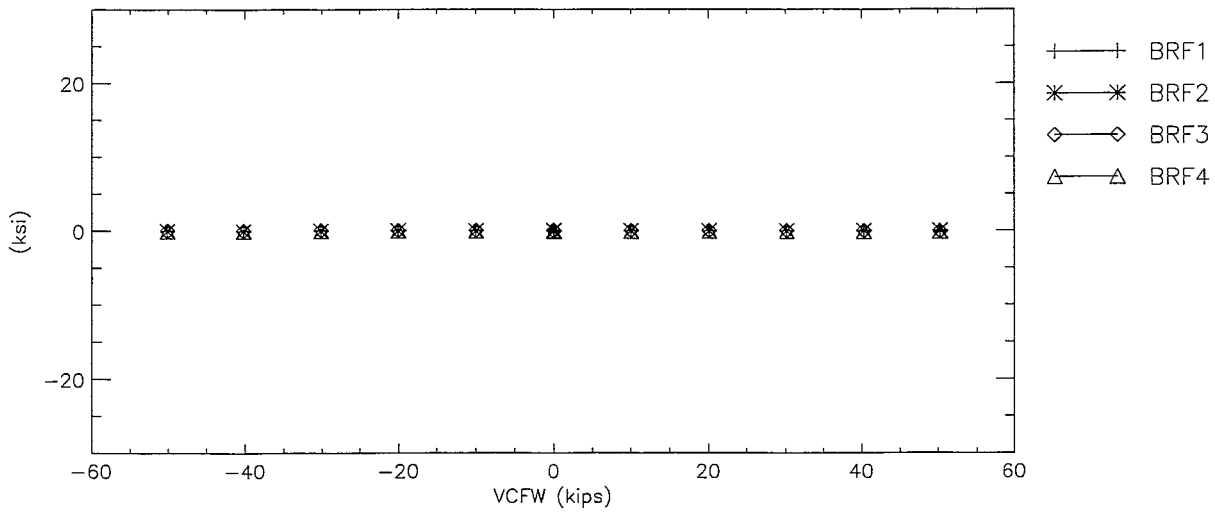
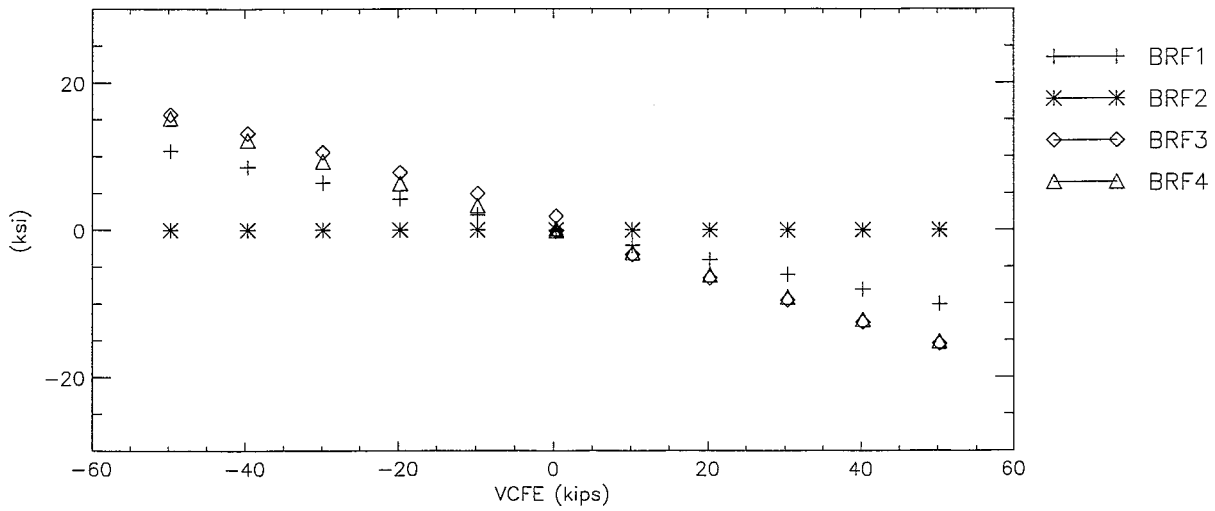
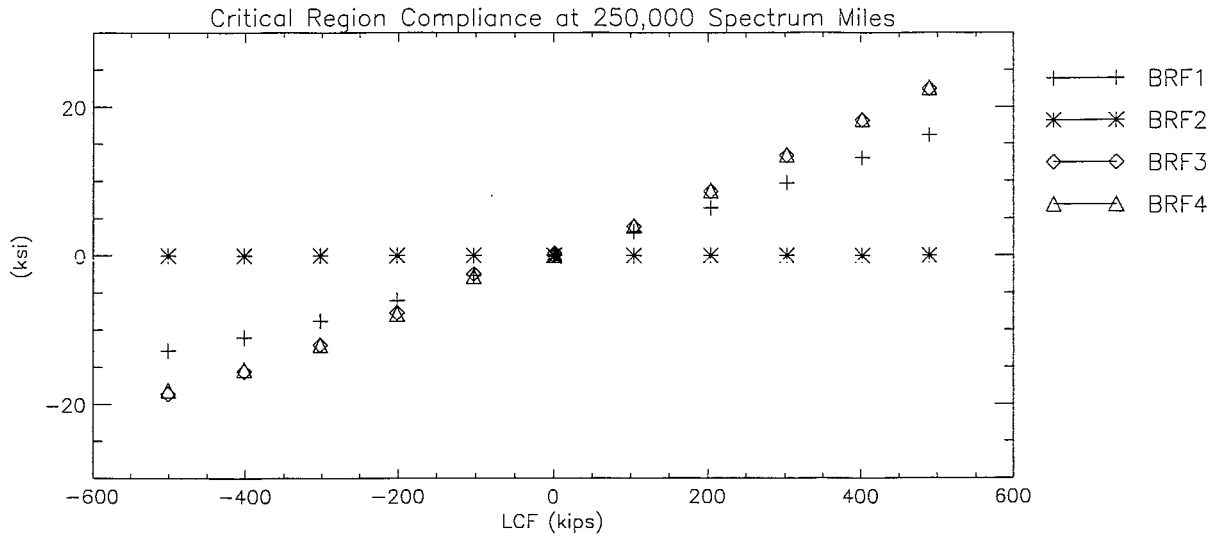


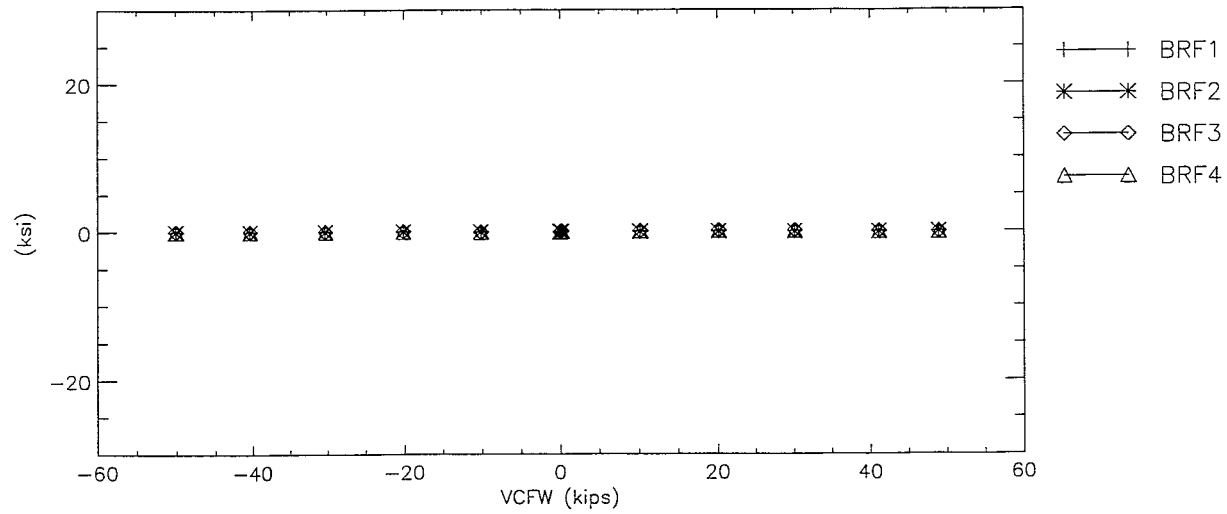
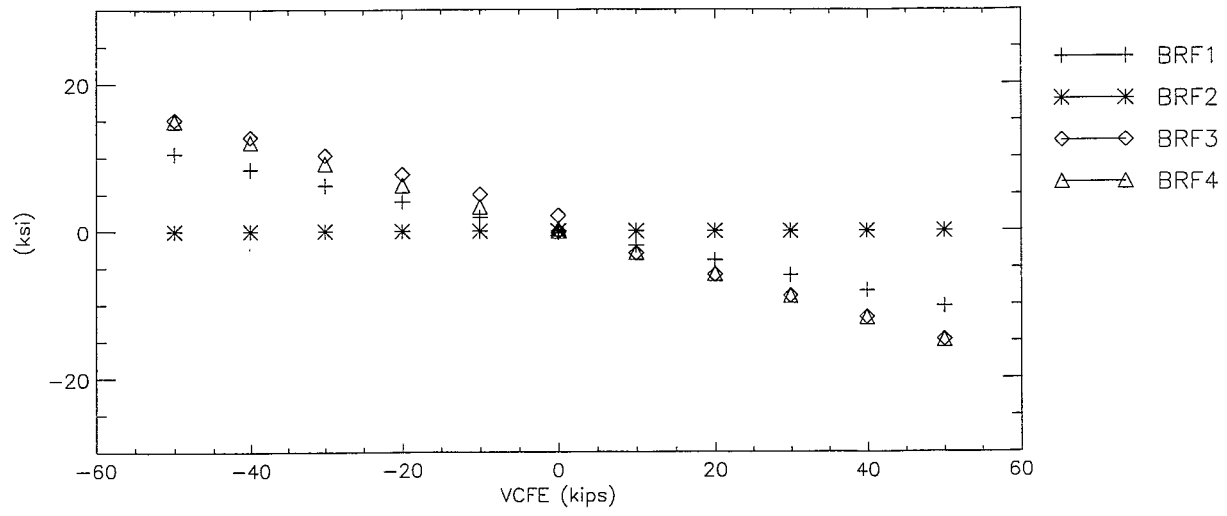
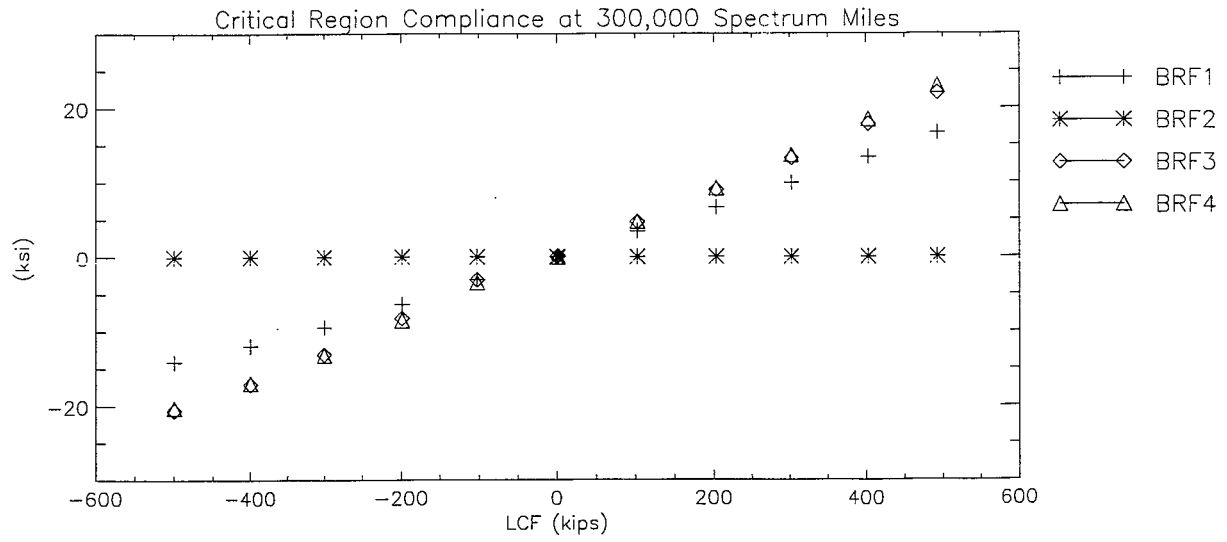








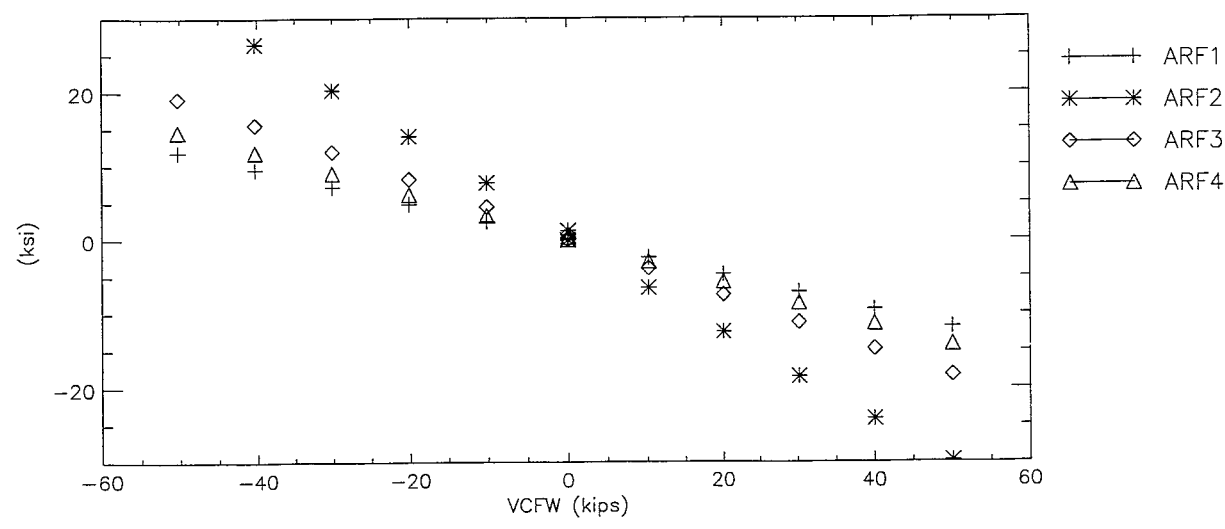
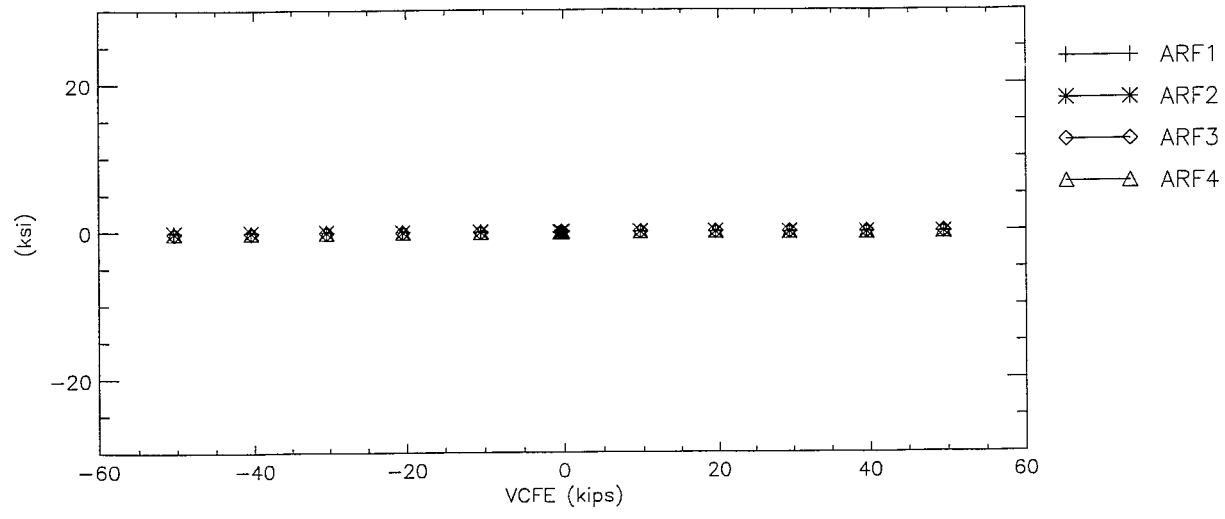
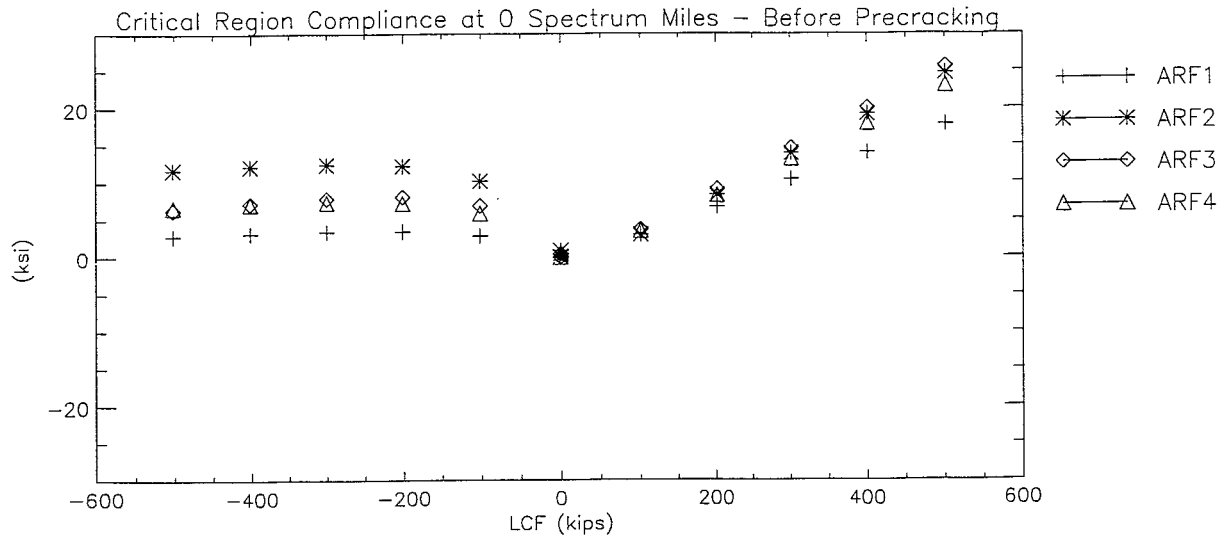


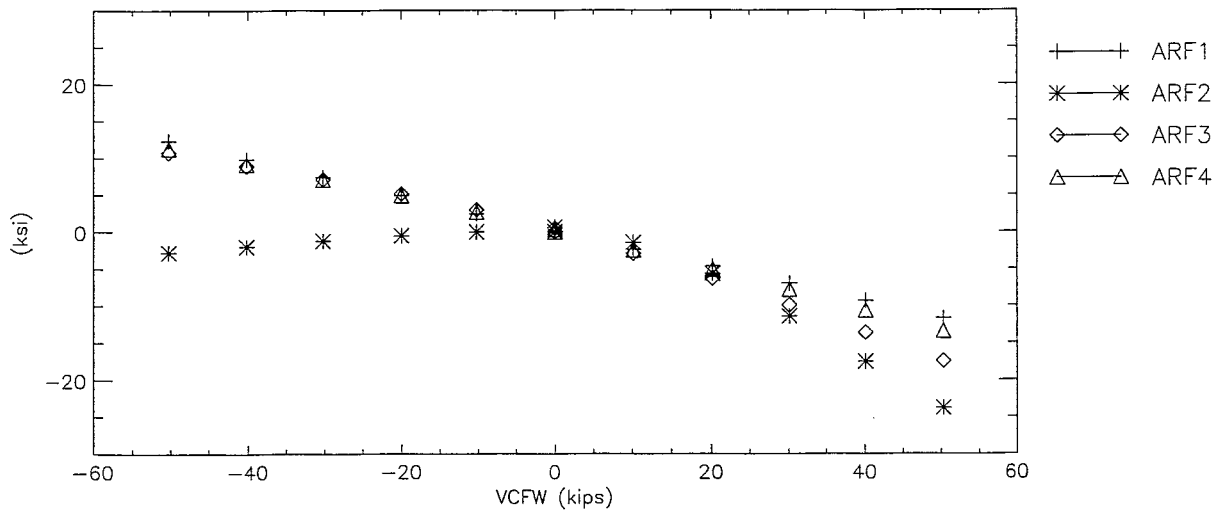
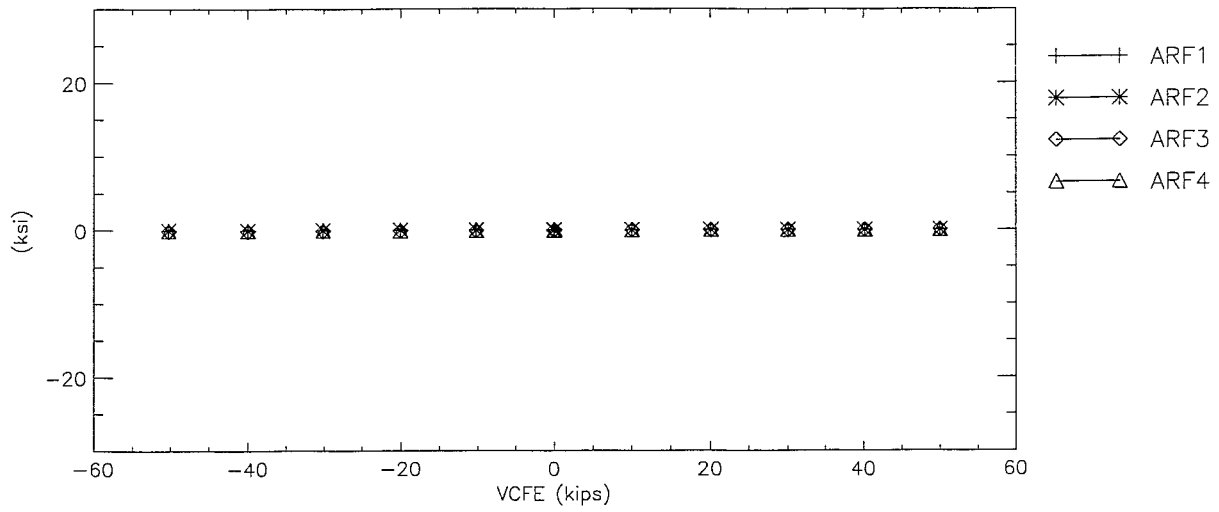
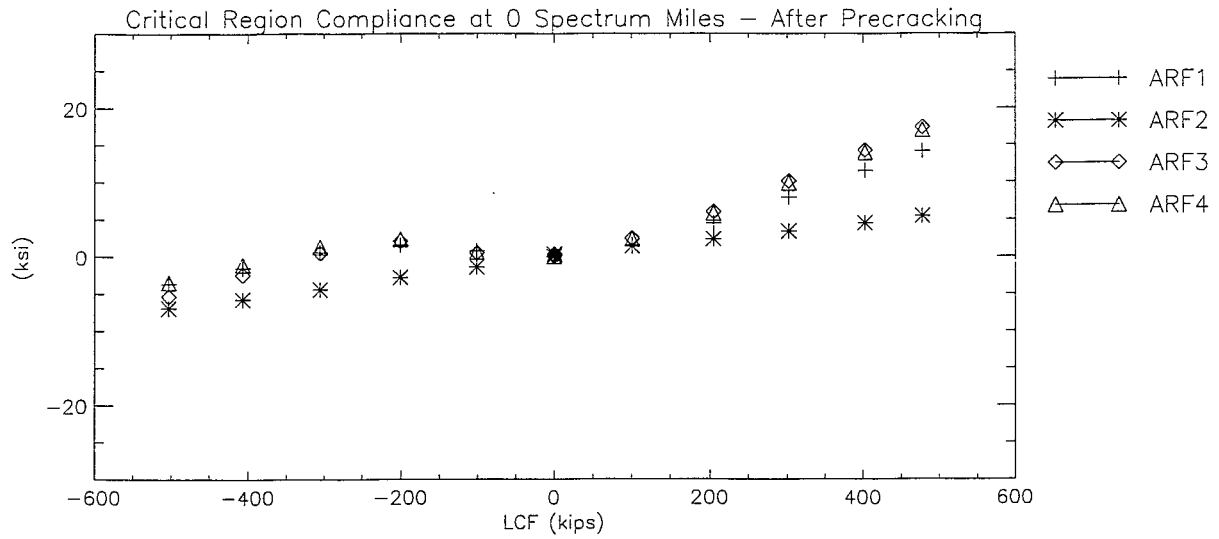


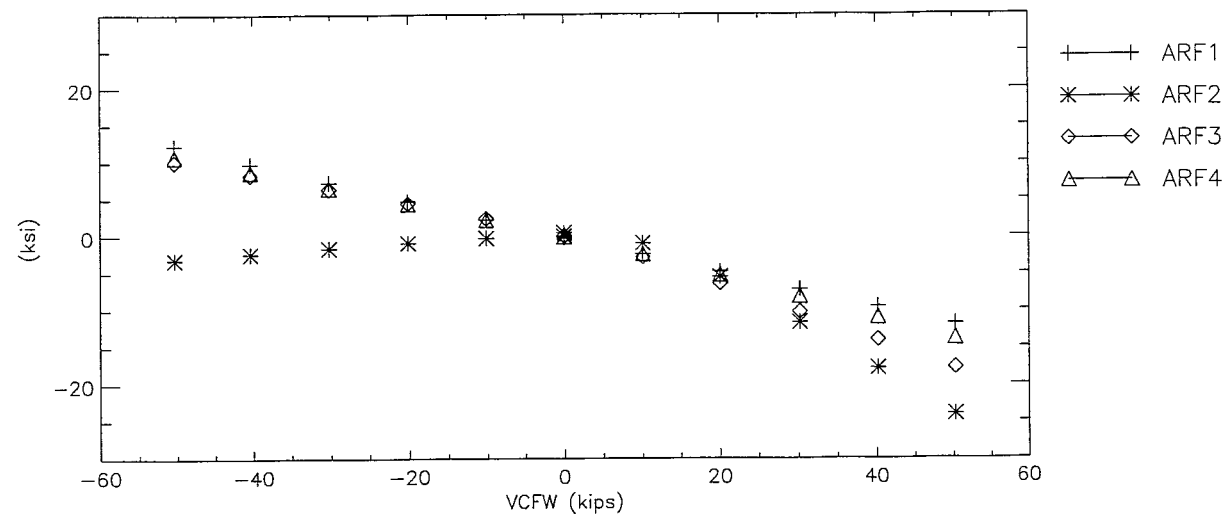
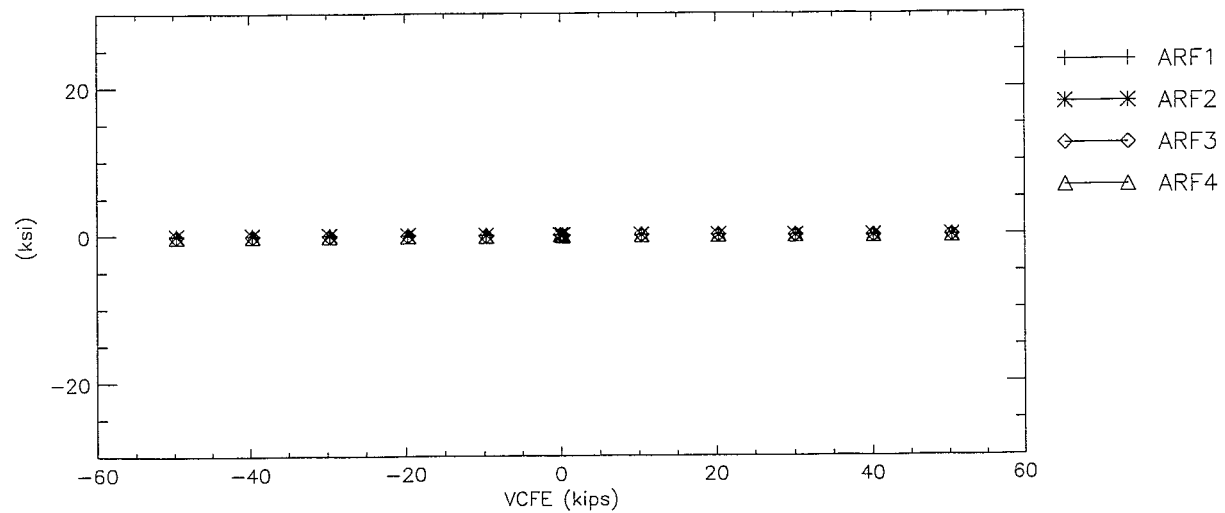
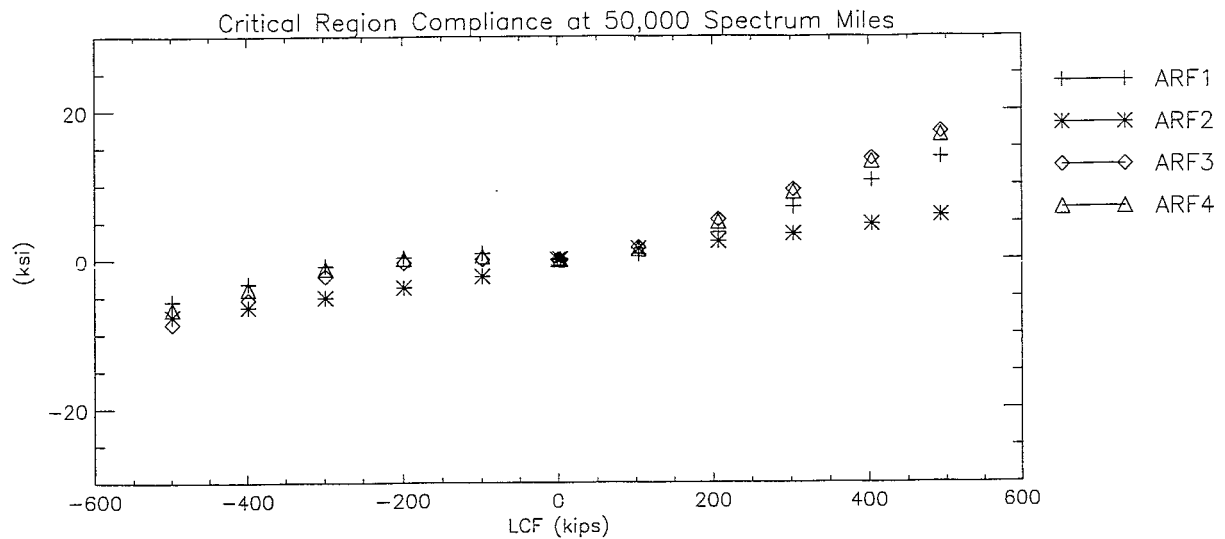
FINAL DRAFT

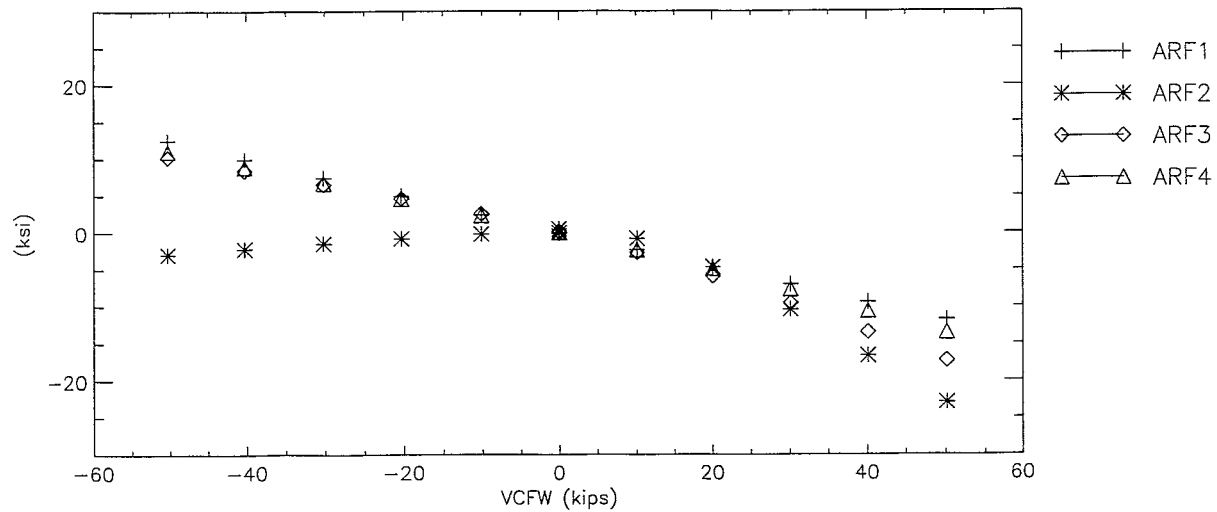
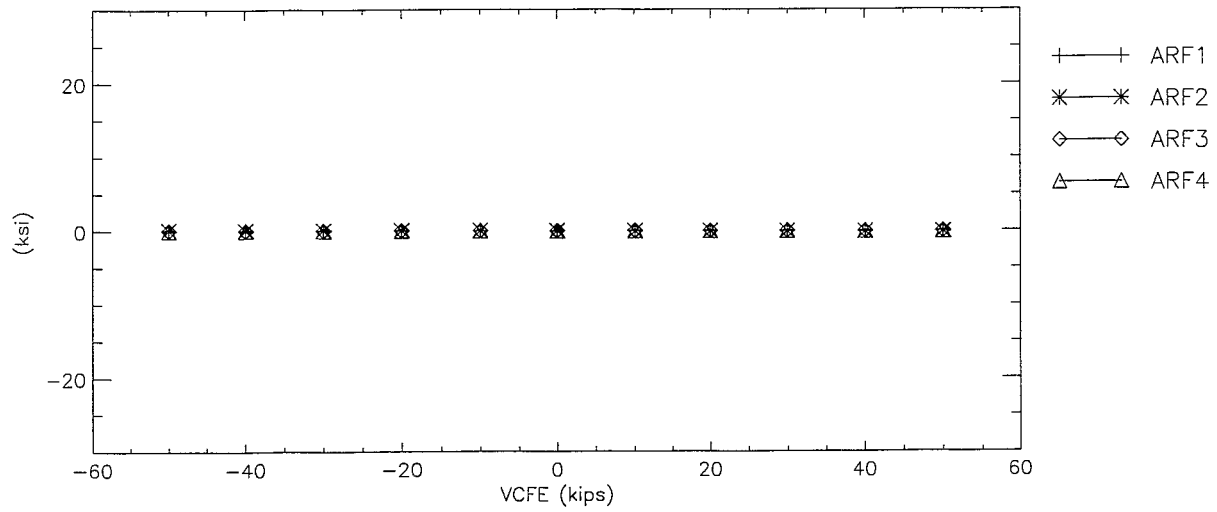
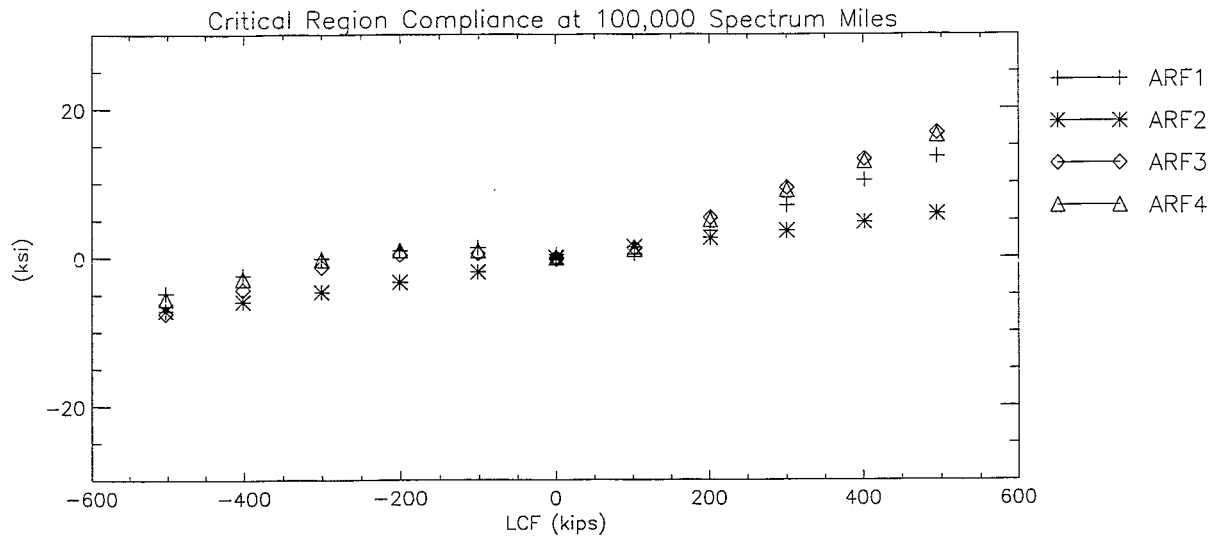
Section C-IX: A-End Right Longitudinal Flange Stresses

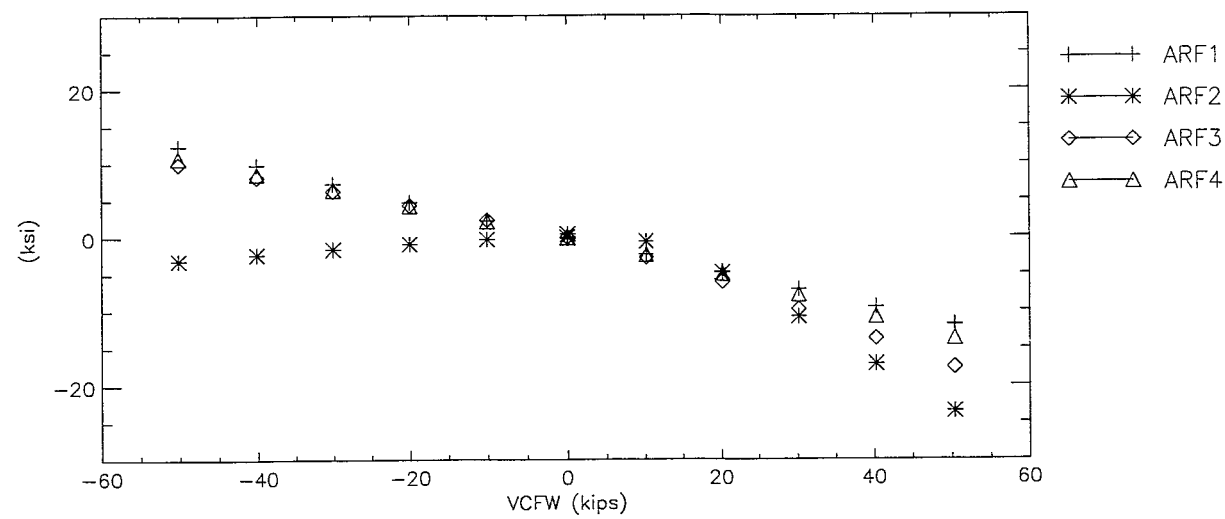
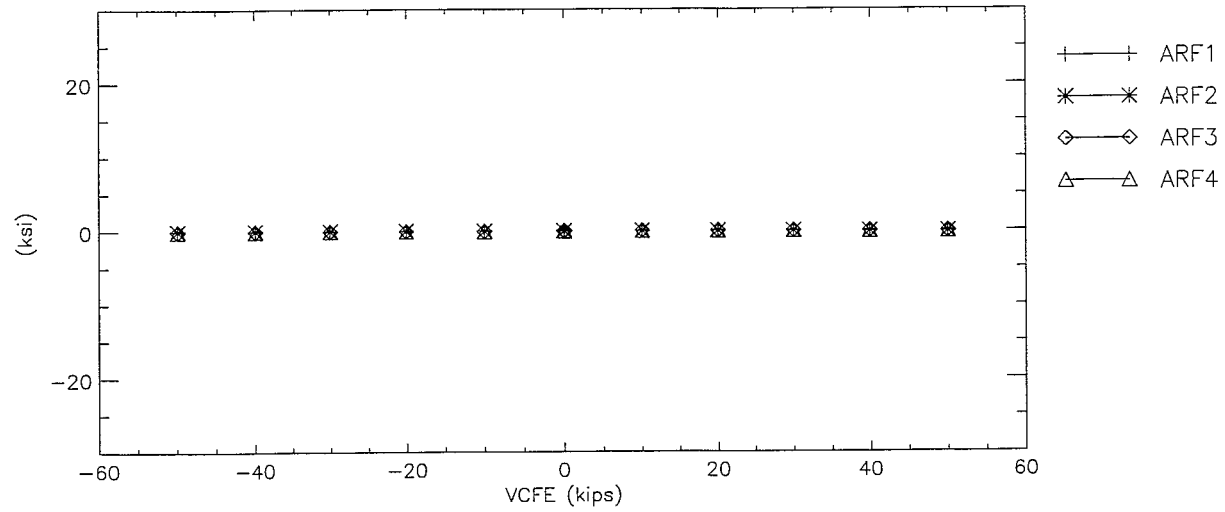
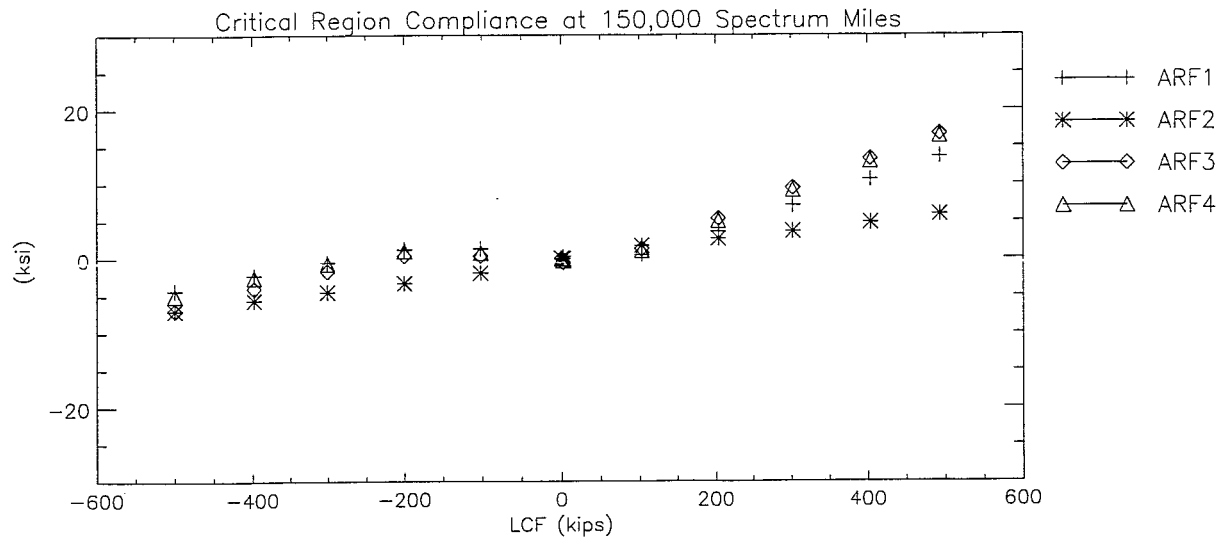
FINAL DRAFT

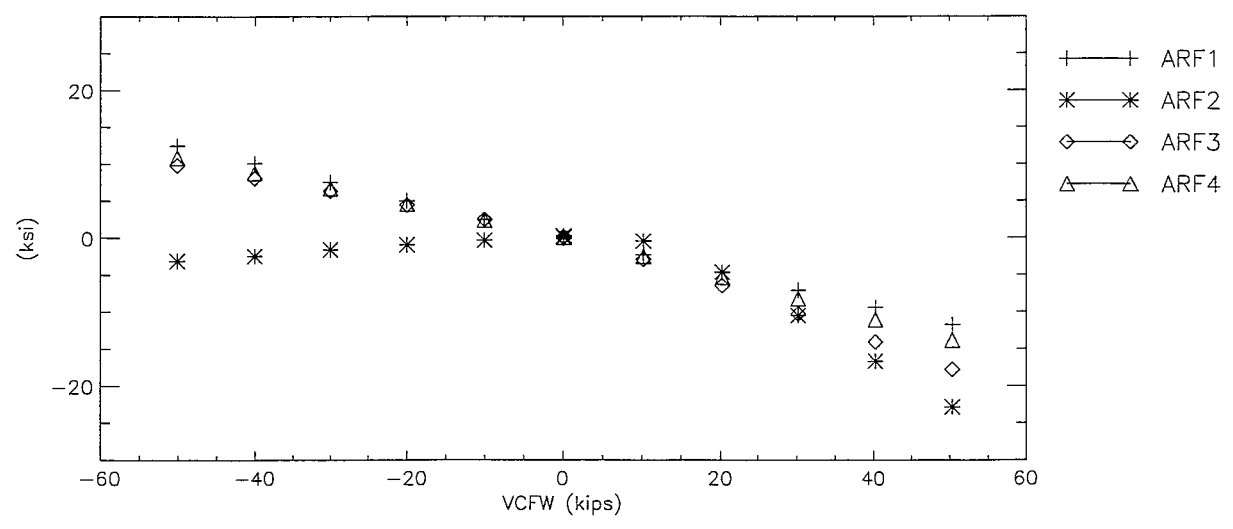
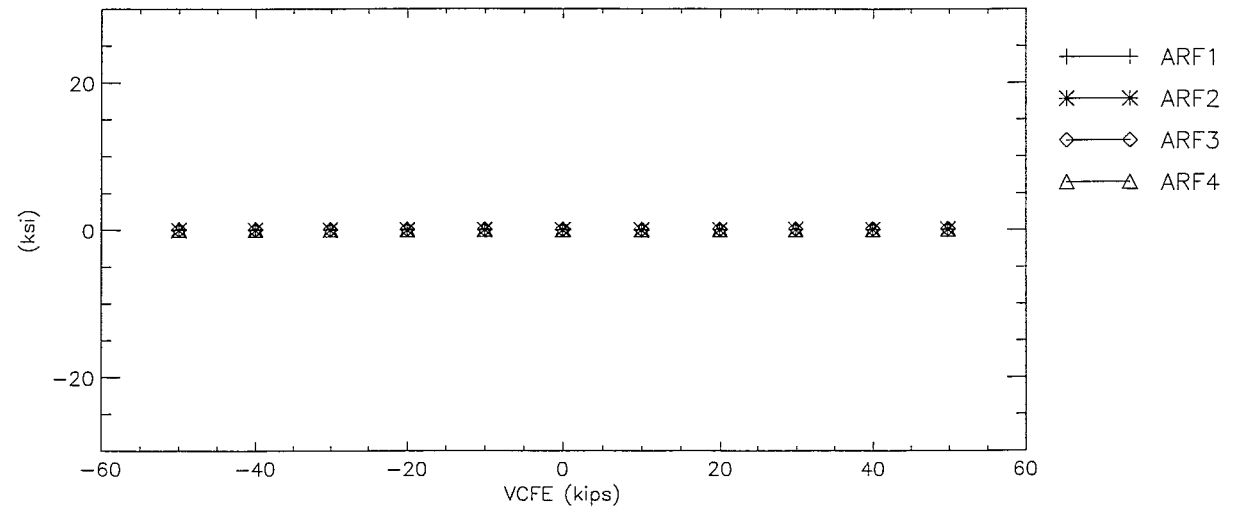
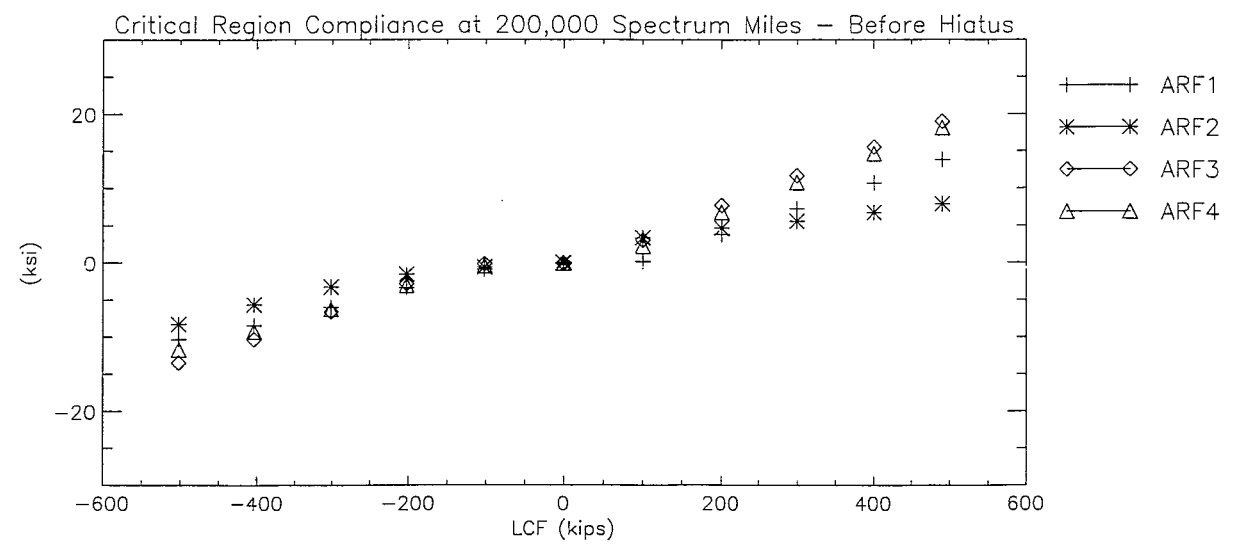


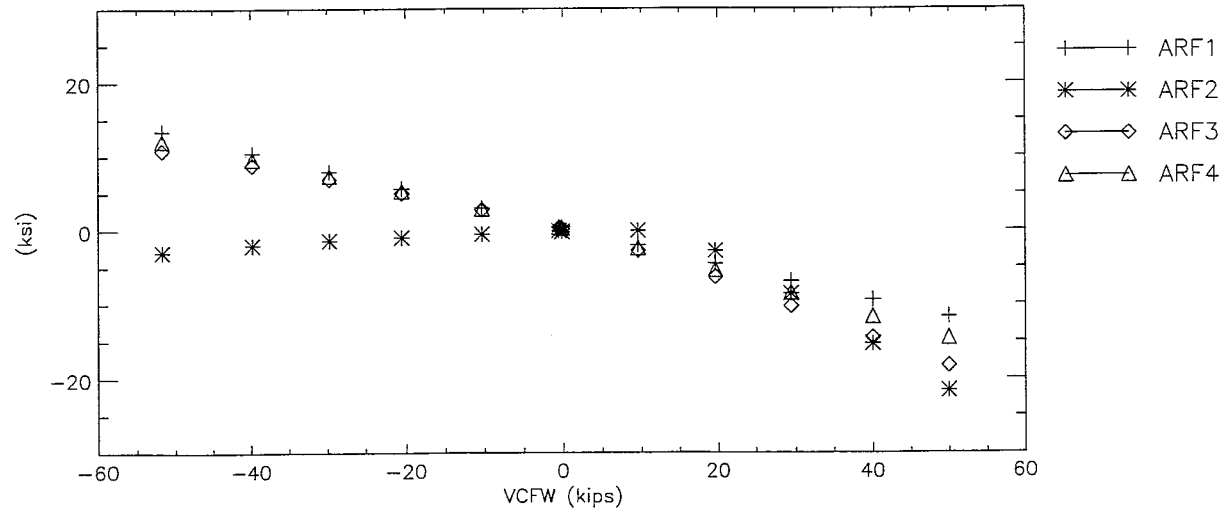
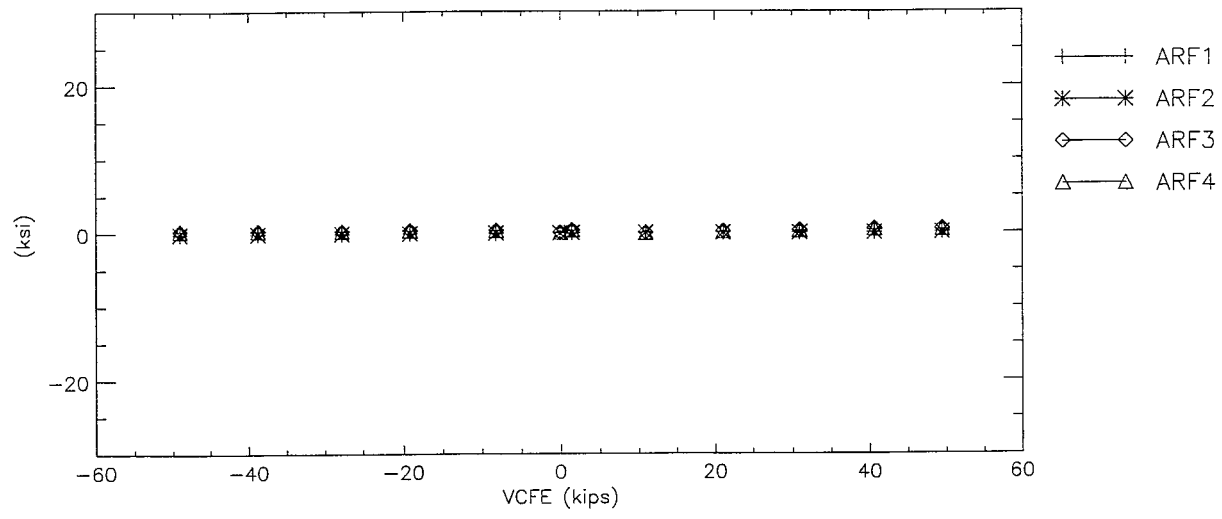
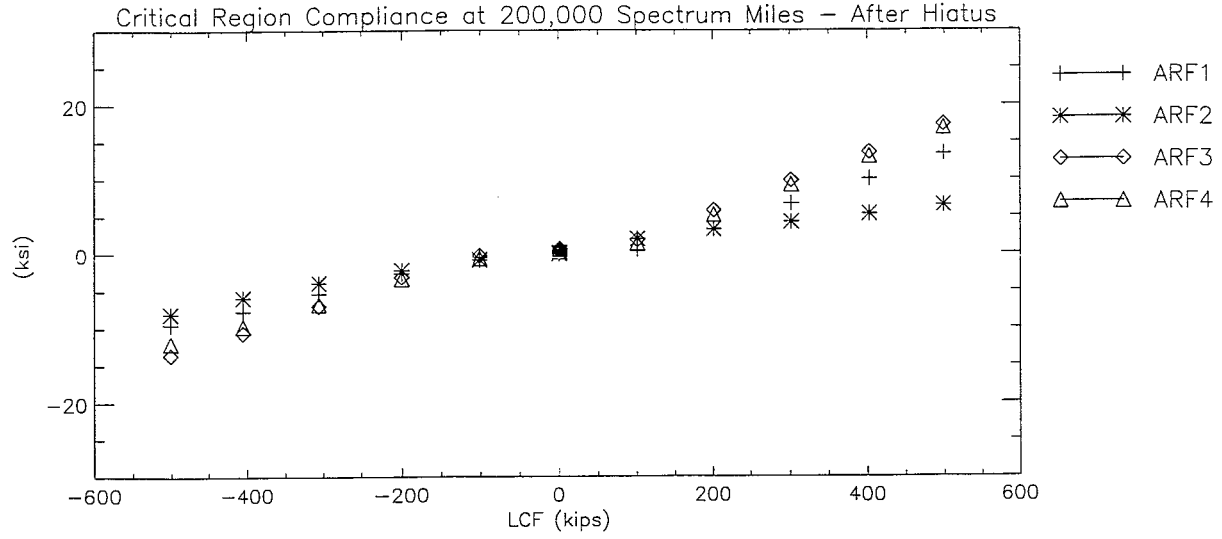


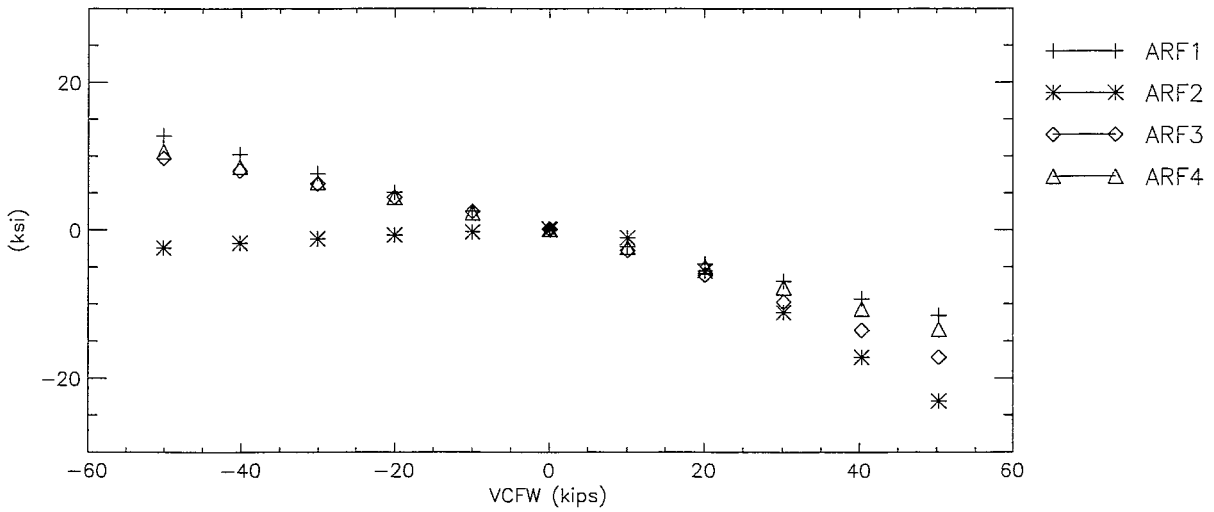
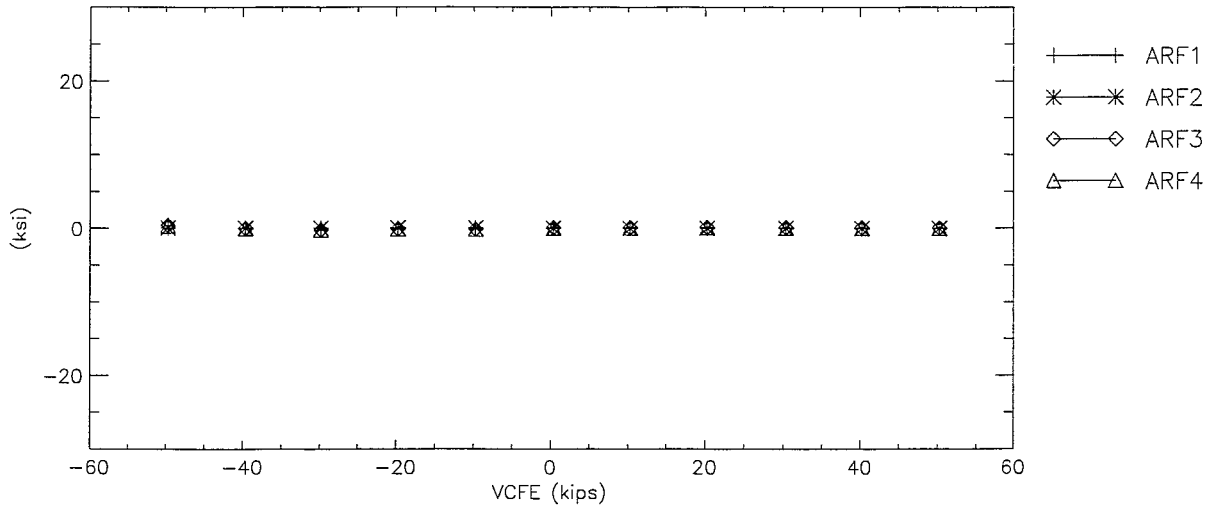
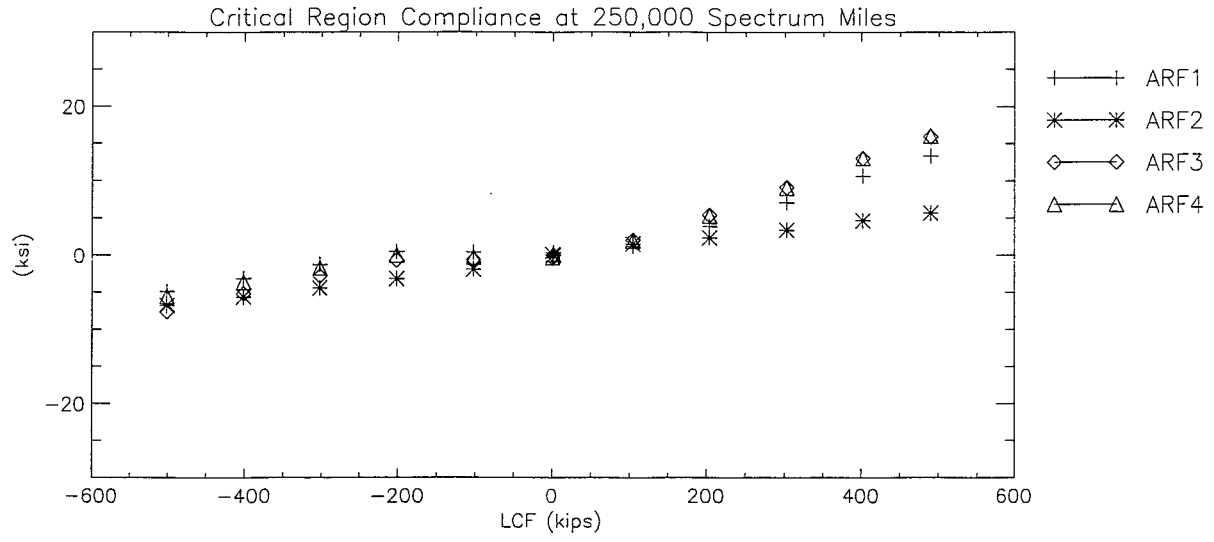


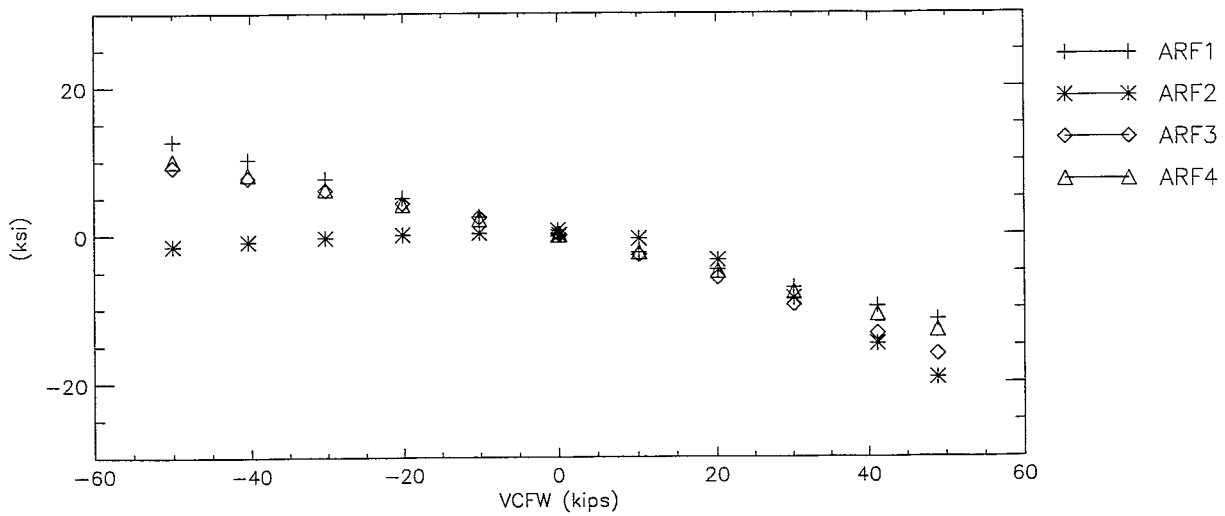
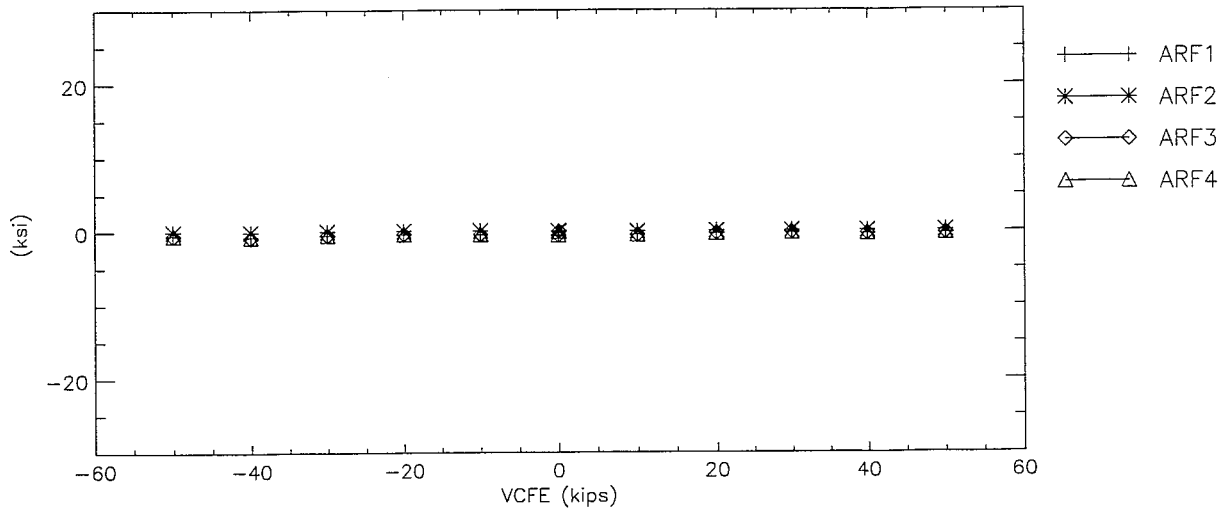
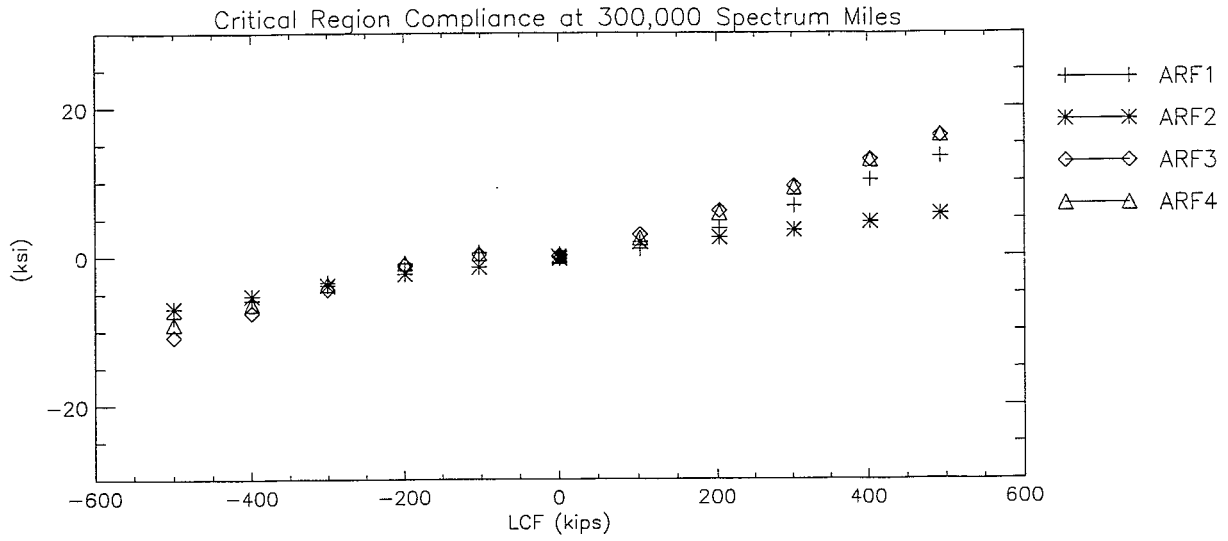












FINAL DRAFT

APPENDIX D

Car Body Compliance Sensitivities

Section D-I: LCF Buff Compliance Peaks

Section D-II: LCF Draft Compliance Peaks

Section D-III: Upward VCF Compliance Peaks

Section D-IV: Downward VCF Compliance Peaks

FINAL DRAFT

Section D-I: LCF Buff Compliance Peaks

FINAL DRAFT

Critical Region Compliance to 500 kips LCF Buff
Strain Data

	(Test 1)	(Test 2)	(Test 3)	(Test 4)	(Test 5)	(Test 6)	(Test 7)	(Test 8)	(Test 9)	spec	mi
Mileage	0	0	50,000	100,000	150,000	200,000	200,000	250,000	300,000		
LCF_D	0	0	0	0	0	0	0	0	0	kip	
LCF	-502	-503	-499	-503	-500	-502	-501	-501	-500	kip	
VCFE_D	0	0	0	1	0	0	0	0	0	kip	
VCFE	0	0	0	0	0	0	-1	0	0	kip	
VCFW_D	0	0	0	0	0	0	0	0	0	kip	
VCFW	0	0	0	0	0	0	-1	2	0	kip	
SPE	0.00	-0.17	-0.15	-0.16	-0.15	-0.13	-0.14	-0.16	-0.17	in	
VCDE	-0.18	-0.14	-0.16	-0.15	-0.14	-0.17	-0.14	-0.15	-0.16	in	
SPW	0.00	-0.14	-0.13	-0.17	-0.15	-0.10	-0.14	-0.15	-0.14	in	
VCDW	-0.17	-0.19	-0.20	-0.20	-0.20	-0.18	-0.18	-0.18	-0.20	in	
BLH1	692	636	650	587	441	334	555	609	651	ustr	
BLH2	171	153	163	119	125	158	115	156	185	ustr	
BLH3	-66	26	46	35	38	52	42	78	88	ustr	
BLHp1	21.7	21.3	22.0	20.1	14.8	11.0	19.1	21.1	22.4	ksi	
BLHp2	3.3	5.2	5.8	4.8	4.3	4.4	4.8	6.4	7.1	ksi	
BLHang	-10	-15	-16	-17	-15	-7	-18	-18	-17	deg	
BLHvM	20.3	19.2	19.7	18.2	13.2	9.6	17.2	18.8	19.8	ksi	
BLH4	459	381	388	357	359	394	341	362	392	ustr	
BLW1	314	258	178	148	210	100	153	209	196	ustr	
BLW2	406	316	226	185	261	90	177	228	207	ustr	
BLW3	192	151	101	95	89	135	81	85	101	ustr	
BLW4	253	208	160	151	143	196	128	133	148	ustr	
BRH1	-6	-38	6	-5	-14	-11	-15	9	5	ustr	
BRH2	326	237	303	271	260	300	243	293	318	ustr	
BRH3	771	639	724	682	689	728	624	714	774	ustr	
BRHp1	24.2	19.8	22.9	21.5	21.7	22.8	19.6	22.6	24.5	ksi	
BRHp2	6.4	4.2	6.3	5.6	5.3	5.8	4.8	6.3	6.7	ksi	
BRHang	4	5	5	6	6	4	5	5	5	deg	
BRHvM	21.8	18.1	20.5	19.3	19.6	20.6	17.7	20.2	21.9	ksi	
BRH4	469	396	427	402	407	446	384	416	453	ustr	
BRF1	-415	-517	-442	-459	-494	-479	-435	-441	-486	ustr	
BRF2	-427	-806	144	1837	0	0	0	0	0	ustr	
BRF3	-663	-766	-621	-636	-712	-687	-613	-641	-711	ustr	
BRF4	-617	-335	-204	-638	-703	-679	-600	-624	-698	ustr	
ALH1	-202	79	202	212	226	175	294	213	235	ustr	
ALH2	507	402	393	339	313	200	198	191	143	ustr	
ALH3	-13	-174	-180	-206	-221	-227	-214	-257	-250	ustr	
ALHp1	9.8	8.7	10.2	9.1	8.8	5.8	8.4	6.3	6.2	ksi	
ALHp2	-18.4	-12.5	-9.3	-8.9	-8.6	-7.9	-5.2	-8.1	-6.8	ksi	
ALHang	-41	37	32	29	27	24	16	21	16	deg	
ALHvM	24.8	18.5	16.8	15.6	15.1	12.0	11.9	12.5	11.2	ksi	
ALH4	332	246	219	195	185	166	134	144	149	ustr	
ALW1	-257	-453	-392	-411	-416	-347	-287	-445	-408	ustr	
ALW2	-516	-475	-419	-440	-446	-354	-313	-466	-410	ustr	
ALW3	120	50	107	87	83	193	154	51	111	ustr	
ALWp1	8.3	0.4	2.7	2.0	1.9	5.7	4.9	0.4	2.4	ksi	
ALWp2	-13.8	-16.5	-14.2	-15.0	-15.2	-11.9	-10.2	-16.2	-14.3	ksi	
ALWang	34	24	24	24	24	23	24	24	23	deg	
ALWvM	19.3	16.7	15.7	16.1	16.2	15.6	13.3	16.4	15.7	ksi	
ALW4	56	119	139	130	130	161	147	109	127	ustr	
ARF1	99	-125	-191	-165	-147	-357	-327	-168	-278	ustr	
ARF2	405	-239	-262	-246	-241	-286	-278	-233	-239	ustr	
ARF3	219	-184	-296	-260	-239	-465	-468	-262	-371	ustr	
ARF4	232	-120	-228	-191	-170	-403	-414	-192	-309	ustr	
BLBT	-354	-408	-386	-391	-414	-363	-365	-361	-361	ustr	
BLBB	273	227	216	238	299	257	242	259	265	ustr	
BRBT	-305	-383	-336	-356	-374	-346	-322	-346	-360	ustr	
BRBB	260	313	300	305	306	267	274	295	304	ustr	
ALBT	48	-374	-374	-394	-396	-377	-378	-418	-338	ustr	
ALBB	106	327	270	267	254	237	241	285	254	ustr	
ARBT	-15	-279	-293	-299	-292	-315	-330	-309	-293	ustr	
ARBB	-50	1303	193	184	176	254	237	186	205	ustr	

Critical Region Compliance to 500 kips LCF Buff
Stress Calculations

Sum	Test 1-9	Std Dev	Test 1	Test 2-6	Std Dev	Test 7-9	Std Dev	
LCF_D	0	0	0	0	0	0	0	kip
LCF	-501	1	-502	-501	2	-501	1	kip
VCFE_D	0	0	0	0	0	0	0	kip
VCFE	0	0	0	0	0	0	0	kip
VCFW_D	0	0	0	0	0	0	0	kip
VCFW	0	1	0	0	0	0	1	kip
SPE	-0.14	0.05	0.00	-0.15	0.01	-0.16	0.02	in
VCDE	-0.15	0.01	-0.18	-0.15	0.01	-0.15	0.01	in
SPW	-0.12	0.05	0.00	-0.14	0.03	-0.14	0.01	in
VCDW	-0.19	0.01	-0.17	-0.19	0.01	-0.19	0.01	in
BLH1	16.6	3.3	20.1	15.4	4.0	17.5	1.4	ksi
BLH2	4.3	0.7	5.0	4.2	0.6	4.4	1.0	ksi
BLH3	1.1	1.3	-1.9	1.1	0.3	2.0	0.7	ksi
BLHp1	19.3	3.9	21.7	17.8	4.7	20.9	1.7	ksi
BLHp2	5.1	1.2	3.3	4.9	0.6	6.1	1.2	ksi
BLHang	-15	4	-10	-14	4	-17	1	deg
BLHvM	17.3	3.6	20.3	16.0	4.4	18.6	1.3	ksi
BLH4	11.1	1.0	13.3	10.9	0.5	10.6	0.7	ksi
BLW1	5.7	1.8	9.1	5.2	1.7	5.4	0.9	ksi
BLW2	6.7	2.6	11.8	6.3	2.5	5.9	0.7	ksi
BLW3	3.3	1.1	5.6	3.3	0.8	2.6	0.3	ksi
BLW4	4.9	1.2	7.3	5.0	0.8	4.0	0.3	ksi
BRH1	-0.2	0.4	-0.2	-0.4	0.5	0.0	0.4	ksi
BRH2	8.2	0.9	9.5	8.0	0.8	8.3	1.1	ksi
BRH3	20.4	1.5	22.4	20.1	1.1	20.4	2.2	ksi
BRHp1	22.2	1.7	24.2	21.8	1.2	22.2	2.5	ksi
BRHp2	5.7	0.8	6.4	5.4	0.8	5.9	1.0	ksi
BRHang	5	1	4	5	1	5	0	deg
BRHvM	20.0	1.5	21.8	19.6	1.0	19.9	2.1	ksi
BRH4	12.2	0.8	13.6	12.1	0.6	12.1	1.0	ksi
BRF1	-13.4	1.0	-12.0	-13.9	0.9	-13.2	0.8	ksi
BRF2	2.4	20.9	-12.4	6.8	28.1	0.0	0.0	ksi
BRF3	-19.5	1.5	-19.2	-19.8	1.7	-19.0	1.5	ksi
BRF4	-16.4	5.1	-17.9	-14.8	6.6	-18.6	1.5	ksi
ALH1	4.6	4.3	-5.8	5.2	1.7	7.2	1.2	ksi
ALH2	8.7	3.6	14.7	9.5	2.4	5.1	0.9	ksi
ALH3	-5.6	2.1	-0.4	-5.8	0.7	-7.0	0.7	ksi
ALHp1	8.2	1.6	9.8	8.5	1.6	7.0	1.2	ksi
ALHp2	-9.5	3.9	-18.4	-9.4	1.8	-6.7	1.4	ksi
ALHang	18	23	-41	30	5	18	3	deg
ALHvM	15.4	4.3	24.8	15.6	2.4	11.9	0.6	ksi
ALH4	5.7	1.8	9.6	5.9	0.9	4.1	0.2	ksi
ALW1	-11.0	2.0	-7.4	-11.7	1.1	-11.0	2.4	ksi
ALW2	-12.4	1.8	-15.0	-12.4	1.3	-11.5	2.2	ksi
ALW3	3.1	1.3	3.5	3.0	1.6	3.1	1.5	ksi
ALWp1	3.2	2.6	8.3	2.5	2.0	2.6	2.2	ksi
ALWp2	-14.1	2.0	-13.8	-14.5	1.7	-13.6	3.1	ksi
ALWang	25	3	34	24	1	23	1	deg
ALWvM	16.1	1.6	19.3	16.1	0.5	15.1	1.6	ksi
ALW4	3.6	0.9	1.6	3.9	0.5	3.7	0.5	ksi
ARF1	-5.3	3.9	2.9	-5.7	2.7	-7.5	2.4	ksi
ARF2	-5.2	6.4	11.7	-7.4	0.6	-7.2	0.7	ksi
ARF3	-7.5	5.9	6.3	-8.4	3.1	-10.6	3.0	ksi
ARF4	-5.8	5.6	6.7	-6.5	3.1	-8.8	3.2	ksi
BLBT	-11.0	0.6	-10.3	-11.4	0.6	-10.5	0.1	ksi
BLBB	7.3	0.7	7.9	7.2	0.9	7.4	0.4	ksi
BRBT	-10.1	0.7	-8.8	-10.4	0.6	-9.9	0.5	ksi
BRBB	8.5	0.6	7.5	8.7	0.5	8.4	0.4	ksi
ALBT	-9.7	4.2	1.4	-11.1	0.3	-11.0	1.2	ksi
ALBB	7.2	1.7	3.1	7.9	1.0	7.5	0.7	ksi
ARBT	-7.8	2.8	-0.4	-8.6	0.4	-9.0	0.5	ksi
ARBB	8.7	11.2	-1.4	12.2	14.3	6.1	0.7	ksi

Section D-II: LCF Draft Compliance Peaks

Critical Region Compliance to 500 kips LCF Draft
Strain Data

	(Test 1)	(Test 2)	(Test 3)	(Test 4)	(Test 5)	(Test 6)	(Test 7)	(Test 8)	(Test 9)	spec mi
Mileage	0	0	50,000	100,000	150,000	200,000	200,000	250,000	300,000	
LCF_D	0	0	0	0	0	0	0	0	0	kip
LCF	501	477	493	494	493	490	498	489	493	kip
VCFE_D	0	0	0	2	0	0	0	0	0	kip
VCFE	0	0	0	0	0	0	1	0	0	kip
VCFW_D	0	0	0	0	0	0	0	0	0	kip
VCFW	0	0	0	0	0	0	-1	3	0	kip
SPE	0.00	0.05	0.09	0.06	0.07	0.12	0.11	0.06	0.05	in
VUDE	0.20	0.16	0.14	0.14	0.14	0.19	0.20	0.14	0.12	in
SPW	0.00	0.05	0.08	0.08	0.06	0.14	0.14	0.09	0.10	in
VCDW	0.17	0.16	0.17	0.18	0.17	0.20	0.19	0.19	0.16	in
BLH1	-620	-366	-318	-345	130	-440	-499	-363	-269	ustr
BLH2	-118	18	63	54	83	-88	-50	24	72	ustr
BLH3	77	92	83	76	86	14	13	44	52	ustr
BLHp1	-2.2	0.8	1.4	1.0	5.1	-2.6	-2.4	-0.2	1.2	ksi
BLHp2	-19.5	-11.8	-10.8	-11.8	3.5	-14.4	-17.0	-12.6	-9.8	ksi
BLHang	-12	-17	-21	-21	-24	-14	-19	-21	-24	deg
BLHvM	18.5	12.2	11.6	12.4	4.5	13.3	15.9	12.5	10.5	ksi
BLH4	-415	-258	-222	-234	-210	-351	-300	-234	-180	ustr
BLW1	-64	71	-6	-38	12	-51	-8	60	56	ustr
BLW2	-181	-67	-135	-171	-111	-180	-134	-53	-61	ustr
BLW3	-233	-112	-125	-137	-135	-152	-126	-99	-78	ustr
BLW4	-111	-140	-153	-172	-169	-188	-161	-131	-104	ustr
BRH1	52	80	96	98	113	25	49	92	118	ustr
BRH2	-237	-86	-41	-52	-17	-228	-156	-54	20	ustr
BRH3	-688	-431	-376	-394	-343	-686	-564	-392	-283	ustr
BRHp1	-4.1	-0.9	0.2	0.1	1.0	-4.8	-3.0	-0.1	1.8	ksi
BRHp2	-21.3	-13.2	-11.4	-11.9	-10.3	-21.6	-17.6	-11.9	-8.4	ksi
BRHang	6	10	11	11	12	8	9	11	14	deg
BRHvM	19.6	12.8	11.5	12.0	10.8	19.7	16.4	11.9	9.5	ksi
BRH4	-420	-273	-243	-256	-231	-383	-327	-253	-196	ustr
BRF1	605	538	578	583	594	580	565	559	573	ustr
BRF2	636	1425	3108	1837	0	0	0	0	0	ustr
BRF3	886	760	787	781	784	788	800	774	759	ustr
BRF4	868	342	269	795	808	815	799	779	792	ustr
ALH1	121	54	31	28	29	-79	-24	20	-1	ustr
ALH2	-646	-674	-723	-753	-742	-856	-800	-714	-685	ustr
ALH3	-140	-184	-206	-212	-206	-198	-189	-197	-166	ustr
ALHp1	14.4	11.5	11.2	11.6	11.5	10.8	11.7	10.9	10.5	ksi
ALHp2	-15.2	-16.7	-18.2	-19.0	-18.7	-21.9	-20.1	-18.0	-17.2	ksi
ALHang	-39	-39	-40	-40	-40	-43	-42	-40	-41	deg
ALHvM	25.6	24.6	25.7	26.7	26.4	28.9	27.9	25.3	24.2	ksi
ALH4	-377	-349	-363	-380	-373	-388	-384	-364	-316	ustr
ALW1	595	460	458	465	466	524	491	450	486	ustr
ALW2	465	451	462	473	465	551	509	446	471	ustr
ALW3	-70	-55	-39	-45	-49	14	-22	-44	12	ustr
ALWp1	19.4	16.2	16.4	16.7	16.6	19.4	17.9	16.0	17.4	ksi
ALWp2	1.7	0.0	0.3	0.1	0.1	2.1	0.8	0.2	2.6	ksi
ALWang	16	22	23	23	22	24	23	22	22	deg
ALWvM	18.6	16.3	16.3	16.7	16.6	18.4	17.5	15.9	16.2	ksi
ALW4	-271	-177	-174	-180	-178	-184	-183	-177	-157	ustr
ARF1	613	488	471	465	470	477	462	459	458	ustr
ARF2	851	186	203	201	203	271	223	195	194	ustr
ARF3	881	599	590	576	576	655	599	549	555	ustr
ARF4	793	586	576	565	566	625	583	553	559	ustr
BLBT	608	521	564	586	576	588	586	551	561	ustr
BLBB	436	354	346	333	393	373	381	398	404	ustr
BRBT	525	461	516	542	546	547	533	482	498	ustr
BRBB	494	509	499	502	481	494	516	540	547	ustr
ALBT	648	548	577	571	571	666	613	580	643	ustr
ALBB	481	425	412	419	404	433	424	447	441	ustr
ARBT	596	475	492	489	493	565	514	499	537	ustr
ARBB	470	604	373	368	352	407	371	374	391	ustr

Critical Region Compliance to 500 kips LCF Draft
Stress Calculations

Sum	Test 1-9	Std Dev	Test 1	Test 2-6	Std Dev	Test 7-9	Std Dev	
LCF_D	0	0	0	0	0	0	0	kip
LCF	492	7	501	490	7	494	5	kip
VCFE_D	0	1	0	0	1	0	0	kip
VCFE	0	0	0	0	0	0	1	kip
VCFW_D	0	0	0	0	0	0	0	kip
VCFW	0	1	0	0	0	1	2	kip
SPE	0.07	0.04	0.00	0.08	0.03	0.07	0.03	in
VCDE	0.16	0.03	0.20	0.15	0.02	0.15	0.04	in
SPW	0.08	0.04	0.00	0.08	0.03	0.11	0.03	in
VCDW	0.18	0.01	0.17	0.18	0.02	0.18	0.02	in
BLH1	-10.0	6.0	-18.0	-7.8	6.6	-10.9	3.4	ksi
BLH2	0.2	2.1	-3.4	0.8	2.0	0.5	1.8	ksi
BLH3	1.7	0.9	2.2	2.0	0.9	1.1	0.6	ksi
BLHp1	0.2	2.4	-2.2	1.1	2.7	-0.5	1.8	ksi
BLHp2	-11.6	6.5	-19.5	-9.1	7.2	-13.1	3.6	ksi
BLHang	-19	4	-12	-20	4	-21	3	deg
BLHvM	12.4	3.8	18.5	10.8	3.6	13.0	2.8	ksi
BLH4	-7.7	2.2	-12.0	-7.4	1.6	-6.9	1.7	ksi
BLW1	0.1	1.4	-1.9	-0.1	1.4	1.0	1.1	ksi
BLW2	-3.5	1.5	-5.2	-3.9	1.3	-2.4	1.3	ksi
BLW3	-3.9	1.3	-6.8	-3.8	0.4	-2.9	0.7	ksi
BLW4	-4.3	0.8	-3.2	-4.8	0.5	-3.8	0.8	ksi
BRH1	2.3	0.9	1.5	2.4	1.0	2.5	1.0	ksi
BRH2	-2.7	2.7	-6.9	-2.5	2.4	-1.8	2.6	ksi
BRH3	-13.4	4.3	-19.9	-12.9	4.0	-12.0	4.1	ksi
BRHp1	-1.1	2.3	-4.1	-0.9	2.3	-0.4	2.4	ksi
BRHp2	-14.2	4.8	-21.3	-13.7	4.6	-12.7	4.7	ksi
BRHang	10	2	6	10	1	11	2	deg
BRHvM	13.8	3.8	19.6	13.4	3.6	12.6	3.5	ksi
BRH4	-8.3	2.2	-12.2	-8.0	1.8	-7.5	1.9	ksi
BRF1	16.7	0.6	17.5	16.7	0.6	16.4	0.2	ksi
BRF2	22.6	32.4	18.5	36.9	38.2	0.0	0.0	ksi
BRF3	22.9	1.1	25.7	22.6	0.3	22.5	0.6	ksi
BRF4	20.2	6.5	25.2	17.6	8.0	22.9	0.3	ksi
ALH1	0.6	1.6	3.5	0.4	1.5	0.0	0.6	ksi
ALH2	-21.2	1.9	-18.7	-21.7	1.9	-21.3	1.7	ksi
ALH3	-5.5	0.7	-4.1	-5.8	0.3	-5.3	0.5	ksi
ALHp1	11.6	1.1	14.4	11.3	0.3	11.0	0.6	ksi
ALHp2	-18.3	2.0	-15.2	-18.9	1.9	-18.4	1.5	ksi
ALHang	-40	1	-39	-40	1	-41	1	deg
ALHvM	26.1	1.5	25.6	26.5	1.6	25.8	1.9	ksi
ALH4	-10.6	0.6	-10.9	-10.7	0.4	-10.3	1.0	ksi
ALW1	14.2	1.3	17.3	13.8	0.8	13.8	0.7	ksi
ALW2	13.8	1.0	13.5	13.9	1.2	13.8	0.9	ksi
ALW3	-1.0	0.8	-2.0	-1.0	0.8	-0.5	0.8	ksi
ALWp1	17.3	1.3	19.4	17.1	1.3	17.1	1.0	ksi
ALWp2	0.9	1.0	1.7	0.5	0.9	1.2	1.2	ksi
ALWang	22	2	16	23	1	22	1	deg
ALWvM	16.9	1.0	18.6	16.9	0.9	16.5	0.9	ksi
ALW4	-5.4	0.9	-7.9	-5.2	0.1	-5.0	0.4	ksi
ARF1	14.1	1.4	17.8	13.8	0.3	13.3	0.1	ksi
ARF2	8.1	6.2	24.7	6.2	1.0	5.9	0.5	ksi
ARF3	18.0	3.0	25.6	17.4	0.9	16.5	0.8	ksi
ARF4	17.4	2.2	23.0	16.9	0.7	16.4	0.5	ksi
BLBT	16.6	0.7	17.6	16.4	0.8	16.4	0.5	ksi
BLBB	11.0	0.9	12.6	10.4	0.7	11.4	0.4	ksi
BRBT	15.0	0.9	15.2	15.1	1.1	14.6	0.8	ksi
BRBB	14.8	0.6	14.3	14.4	0.3	15.5	0.5	ksi
ALBT	17.5	1.2	18.8	17.0	1.3	17.8	0.9	ksi
ALBB	12.5	0.7	13.9	12.1	0.3	12.7	0.3	ksi
ARBT	15.0	1.2	17.3	14.6	1.0	15.0	0.6	ksi
ARBB	12.0	2.3	13.6	12.2	3.0	11.0	0.3	ksi

Section D-III: Upward VCF Compliance Peaks

FINAL DRAFT

Critical Region Compliance to 50 kips Upward VCF
Strain Data

	(Test 1)	(Test 2)	(Test 3)	(Test 4)	(Test 5)	(Test 6)	(Test 7)	(Test 8)	(Test 9)	spec	mi
Mileage	0	0	50,000	100,000	150,000	200,000	200,000	250,000	300,000		
LCF_D	0	0	0	0	0	0	0	0	0	kip	
LCF	0	0	0	0	0	0	0	0	0	kip	
VCFE_D	0	0	0	0	0	0	0	0	0	kip	
VCFE	49	50	50	50	50	50	49	50	50	kip	
VCFW_D	0	0	0	0	0	0	0	0	0	kip	
VCFW	50	50	50	50	50	50	50	50	49	kip	
SPE	0.00	0.05	0.05	0.05	0.05	0.04	0.06	0.06	0.07	in	
VCDE	0.20	0.19	0.19	0.19	0.19	0.20	0.20	0.20	0.21	in	
SPW	0.00	0.06	0.04	0.05	0.03	0.05	0.05	0.06	0.06	in	
VCDW	0.25	0.24	0.23	0.23	0.23	0.24	0.23	0.24	0.24	in	
BLH1	-725	-720	-679	-671	-812	-813	-745	-671	-709	ustr	
BLH2	-595	-603	-569	-557	-559	-552	-551	-548	-564	ustr	
BLH3	-223	-227	-200	-193	-192	-173	-181	-167	-170	ustr	
BLHp1	-12.6	-12.6	-11.4	-11.1	-12.9	-12.3	-11.8	-10.3	-10.8	ksi	
BLHp2	-25.3	-25.3	-23.8	-23.4	-27.2	-27.1	-25.2	-23.2	-24.3	ksi	
BLHang	13	14	14	14	5	5	9	14	12	deg	
BLHvM	21.9	21.9	20.6	20.3	23.6	23.5	21.9	20.1	21.1	ksi	
BLH4	-380	-375	-356	-351	-351	-359	-353	-356	-376	ustr	
BLW1	9	-92	-119	-124	-133	-131	-118	-128	-134	ustr	
BLW2	-62	-174	-174	-183	-189	-168	-146	-173	-201	ustr	
BLW3	-76	-93	-112	-105	-114	-114	-98	-106	-102	ustr	
BLW4	-112	-125	-141	-129	-141	-133	-111	-127	-122	ustr	
BRH1	-334	-314	-308	-307	-304	-305	-309	-308	-310	ustr	
BRH2	-663	-626	-615	-609	-602	-615	-615	-615	-623	ustr	
BRH3	-765	-704	-686	-680	-672	-706	-699	-690	-718	ustr	
BRHp1	-16.4	-15.2	-14.8	-14.8	-14.6	-15.0	-15.1	-14.9	-15.3	ksi	
BRHp2	-27.5	-25.5	-24.9	-24.7	-24.5	-25.4	-25.3	-25.0	-25.8	ksi	
BRHang	-14	-16	-16	-16	-16	-14	-15	-16	-14	deg	
BRHvM	24.0	22.2	21.7	21.5	21.3	22.1	22.0	21.8	22.5	ksi	
BRH4	-361	-338	-327	-323	-321	-338	-336	-332	-342	ustr	
BRF1	-376	-356	-345	-348	-340	-331	-343	-348	-354	ustr	
BRF2	-2027	-1489	-5743	-4466	0	0	0	0	0	ustr	
BRF3	-629	-603	-549	-552	-539	-503	-582	-533	-509	ustr	
BRF4	-557	-245	-113	-531	-514	-489	-523	-523	-512	ustr	
ALH1	-346	-347	-340	-340	-342	-344	-337	-339	-332	ustr	
ALH2	-966	-938	-907	-888	-906	-849	-770	-878	-854	ustr	
ALH3	-843	-792	-782	-757	-775	-696	-636	-759	-728	ustr	
ALHp1	-13.6	-13.0	-13.1	-12.9	-13.1	-12.3	-12.2	-13.1	-12.6	ksi	
ALHp2	-34.0	-32.6	-31.8	-31.0	-31.7	-29.3	-26.8	-30.8	-29.8	ksi	
ALHang	-28	-29	-29	-29	-29	-31	-31	-29	-29	deg	
ALHvM	29.6	28.4	27.7	27.0	27.6	25.5	23.2	26.8	25.9	ksi	
ALH4	-422	-387	-371	-358	-367	-343	-318	-357	-340	ustr	
ALW1	-231	-259	-255	-256	-256	-245	-243	-253	-250	ustr	
ALW2	-119	-141	-145	-153	-149	-144	-154	-150	-146	ustr	
ALW3	30	16	19	19	19	20	7	19	23	ustr	
ALWp1	-1.0	-1.7	-1.5	-1.5	-1.5	-1.4	-1.8	-1.5	-1.3	ksi	
ALWp2	-7.0	-8.0	-7.9	-8.0	-7.9	-7.6	-7.7	-7.9	-7.7	ksi	
ALWang	4	4	6	7	6	7	8	7	7	deg	
ALWvM	6.6	7.3	7.2	7.3	7.3	7.0	7.0	7.2	7.2	ksi	
ALW4	-62	-63	-58	-57	-59	-55	-53	-57	-55	ustr	
ARF1	-406	-403	-408	-406	-409	-405	-405	-398	-396	ustr	
ARF2	-1029	-820	-829	-792	-811	-788	-747	-796	-667	ustr	
ARF3	-631	-602	-613	-597	-606	-613	-632	-593	-558	ustr	
ARF4	-487	-464	-475	-466	-471	-477	-502	-462	-445	ustr	
BLBT	-179	-178	-165	-181	-179	-167	-173	-179	-175	ustr	
BLBB	189	160	178	190	216	218	208	206	209	ustr	
BRBT	-179	-175	-170	-173	-169	-161	-167	-177	-175	ustr	
BRBB	182	178	175	174	172	173	169	177	184	ustr	
ALBT	-191	-186	-191	-189	-192	-181	-210	-189	-185	ustr	
ALBB	199	196	193	190	194	174	178	192	188	ustr	
ARBT	-206	-195	-200	-195	-197	-190	-214	-195	-188	ustr	
ARBB	202	0	195	190	194	187	183	193	186	ustr	

Critical Region Compliance to 50 kips Upward VCF
Stress Calculations

Sum	Test 1-9	Std Dev	Test 1	Test 2-6	Std Dev	Test 7-9	Std Dev	
LCF_D	0	0	0	0	0	0	0	kip
LCF	0	0	0	0	0	0	0	kip
VCFE_D	0	0	0	0	0	0	0	kip
VCFE	50	0	49	50	0	50	0	kip
VCFW_D	0	0	0	0	0	0	0	kip
VCFW	50	0	50	50	0	50	1	kip
SPE	0.05	0.02	0.00	0.05	0.00	0.06	0.01	in
VCDE	0.20	0.01	0.20	0.19	0.00	0.20	0.01	in
SPW	0.04	0.02	0.00	0.05	0.01	0.06	0.01	in
VCDW	0.24	0.01	0.25	0.23	0.01	0.24	0.01	in
BLH1	-21.1	1.6	-21.0	-21.4	2.0	-20.5	1.1	ksi
BLH2	-16.4	0.6	-17.2	-16.5	0.6	-16.1	0.3	ksi
BLH3	-5.6	0.6	-6.5	-5.7	0.6	-5.0	0.2	ksi
BLHp1	-11.8	0.9	-12.6	-12.1	0.8	-11.0	0.8	ksi
BLHp2	-25.0	1.5	-25.3	-25.4	1.8	-24.3	1.0	ksi
BLHang	11	4	13	10	5	12	3	deg
BLHvM	21.7	1.3	21.9	22.0	1.6	21.0	0.9	ksi
BLH4	-10.5	0.3	-11.0	-10.4	0.3	-10.5	0.4	ksi
BLW1	-3.1	1.3	0.3	-3.5	0.5	-3.7	0.2	ksi
BLW2	-4.7	1.2	-1.8	-5.2	0.2	-5.0	0.8	ksi
BLW3	-3.0	0.4	-2.2	-3.1	0.3	-3.0	0.1	ksi
BLW4	-3.7	0.3	-3.2	-3.9	0.2	-3.5	0.2	ksi
BRH1	-9.0	0.3	-9.7	-8.9	0.1	-9.0	0.0	ksi
BRH2	-18.0	0.5	-19.2	-17.8	0.3	-17.9	0.1	ksi
BRH3	-20.4	0.8	-22.2	-20.0	0.4	-20.4	0.4	ksi
BRHp1	-15.1	0.5	-16.4	-14.9	0.2	-15.1	0.2	ksi
BRHp2	-25.4	0.9	-27.5	-25.0	0.5	-25.4	0.4	ksi
BRHang	-15	1	-14	-16	1	-15	1	deg
BRHvM	22.1	0.8	24.0	21.8	0.4	22.1	0.3	ksi
BRH4	-9.7	0.3	-10.5	-9.6	0.2	-9.8	0.2	ksi
BRF1	-10.1	0.4	-10.9	-10.0	0.3	-10.1	0.1	ksi
BRF2	-44.2	63.5	-58.8	-67.8	76.4	0.0	0.0	ksi
BRF3	-16.1	1.2	-18.2	-15.9	1.0	-15.7	1.1	ksi
BRF4	-12.9	4.5	-16.2	-11.0	5.5	-15.1	0.2	ksi
ALH1	-9.9	0.1	-10.0	-9.9	0.1	-9.7	0.1	ksi
ALH2	-25.6	1.6	-28.0	-26.0	0.9	-24.2	1.6	ksi
ALH3	-21.8	1.7	-24.5	-22.1	1.1	-20.5	1.9	ksi
ALHp1	-12.9	0.5	-13.6	-12.9	0.3	-12.6	0.5	ksi
ALHp2	-30.9	2.1	-34.0	-31.3	1.2	-29.1	2.1	ksi
ALHang	-29	1	-28	-29	1	-30	1	deg
ALHvM	26.8	1.8	29.6	27.2	1.1	25.3	1.9	ksi
ALH4	-10.5	0.9	-12.2	-10.6	0.5	-9.8	0.6	ksi
ALW1	-7.2	0.3	-6.7	-7.4	0.2	-7.2	0.2	ksi
ALW2	-4.2	0.3	-3.5	-4.2	0.1	-4.3	0.1	ksi
ALW3	0.6	0.2	0.9	0.5	0.1	0.5	0.2	ksi
ALWp1	-1.5	0.2	-1.0	-1.5	0.1	-1.5	0.2	ksi
ALWp2	-7.7	0.3	-7.0	-7.9	0.2	-7.8	0.1	ksi
ALWang	6	1	4	6	1	7	1	deg
ALWvM	7.1	0.2	6.6	7.2	0.1	7.1	0.1	ksi
ALW4	-1.7	0.1	-1.8	-1.7	0.1	-1.6	0.1	ksi
ARF1	-11.7	0.1	-11.8	-11.8	0.1	-11.6	0.1	ksi
ARF2	-23.5	2.8	-29.8	-23.4	0.5	-21.4	1.9	ksi
ARF3	-17.5	0.6	-18.3	-17.6	0.2	-17.2	1.1	ksi
ARF4	-13.7	0.5	-14.1	-13.7	0.2	-13.6	0.8	ksi
BLBT	-5.1	0.2	-5.2	-5.1	0.2	-5.1	0.1	ksi
BLBB	5.7	0.6	5.5	5.6	0.7	6.0	0.1	ksi
BRBT	-5.0	0.2	-5.2	-4.9	0.2	-5.0	0.1	ksi
BRBB	5.1	0.1	5.3	5.1	0.1	5.1	0.2	ksi
ALBT	-5.5	0.2	-5.6	-5.4	0.1	-5.6	0.4	ksi
ALBB	5.5	0.2	5.8	5.5	0.3	5.4	0.2	ksi
ARBT	-5.7	0.2	-6.0	-5.7	0.1	-5.8	0.4	ksi
ARBB	4.9	1.9	5.9	4.4	2.5	5.4	0.2	ksi

Section D-IV: Downward VCF Compliance Peaks

Critical Region Compliance to 50 kips Downward VCF
Strain Data

	(Test 1)	(Test 2)	(Test 3)	(Test 4)	(Test 5)	(Test 6)	(Test 7)	(Test 8)	(Test 9)	
Mileage	0	0	50,000	100,000	150,000	200,000	200,000	250,000	300,000	spec mi
LCF_D	0	0	0	0	0	0	0	0	0	kip
LCF	1	0	0	0	0	1	0	0	0	kip
VCFE_D	0	0	0	0	0	0	0	0	0	kip
VCFE	-50	-50	-50	-50	-50	-50	-49	-50	-50	kip
VCFW_D	0	0	0	0	0	0	0	0	0	kip
VCFW	-50	-50	-50	-50	-50	-50	-52	-50	-50	kip
SPE	0.00	-0.06	-0.07	-0.06	-0.06	-0.07	-0.07	-0.06	-0.07	in
VCDE	-0.25	-0.24	-0.24	-0.23	-0.24	-0.25	-0.23	-0.25	-0.25	in
SPW	0.00	-0.05	-0.07	-0.08	-0.07	-0.08	-0.09	-0.08	-0.09	in
VCDW	-0.30	-0.25	-0.26	-0.26	-0.26	-0.26	-0.27	-0.27	-0.26	in
BLH1	755	655	621	607	980	979	797	600	560	ustr
BLH2	627	534	505	496	494	476	456	470	444	ustr
BLH3	245	162	158	163	157	147	136	131	113	ustr
BLHp1	26.5	22.6	21.5	21.0	32.2	32.2	26.2	20.5	19.1	ksi
BLHp2	13.5	10.1	9.7	9.7	13.2	12.9	11.1	8.8	7.8	ksi
BLHAng	13	13	13	13	-5	-6	-1	12	13	deg
BLHvM	22.9	19.6	18.6	18.2	28.1	28.1	22.7	17.8	16.6	ksi
BLH4	400	337	321	308	314	309	297	316	302	ustr
BLW1	-5	44	40	46	43	12	11	0	-4	ustr
BLW2	95	36	4	8	5	-49	-45	-56	-77	ustr
BLW3	73	64	73	54	62	58	52	42	46	ustr
BLW4	114	68	70	46	54	47	40	34	38	ustr
BRH1	360	321	318	320	321	325	320	328	326	ustr
BRH2	700	617	608	605	611	616	599	617	617	ustr
BRH3	799	715	708	706	716	730	711	744	740	ustr
BRHp1	28.9	25.7	25.5	25.4	25.7	26.1	25.5	26.5	26.4	ksi
BRHp2	17.5	15.7	15.6	15.7	15.8	16.1	15.8	16.4	16.2	ksi
BRHAng	-14	-13	-13	-13	-13	-12	-12	-11	-11	deg
BRHvM	25.2	22.5	22.2	22.2	22.4	22.8	22.3	23.2	23.1	ksi
BRH4	376	332	327	321	327	331	323	335	335	ustr
BRF1	372	367	355	360	359	363	357	370	363	ustr
BRF2	759	1817	0	0	0	0	0	0	0	ustr
BRF3	736	571	557	552	550	536	553	541	521	ustr
BRF4	600	237	295	530	528	532	521	523	516	ustr
ALH1	332	465	515	543	539	605	629	598	642	ustr
ALH2	910	339	346	270	288	152	132	198	157	ustr
ALH3	812	239	233	196	209	157	160	181	171	ustr
ALHp1	32.3	16.7	18.2	19.3	19.2	22.5	23.8	22.0	24.1	ksi
ALHp2	13.5	11.5	11.7	10.2	10.7	8.0	7.8	9.1	8.5	ksi
ALHAng	-27	-3	-6	-15	-14	-23	-24	-21	-23	deg
ALHvM	28.1	14.8	16.0	16.8	16.6	19.8	21.0	19.2	21.2	ksi
ALH4	399	119	112	82	91	34	34	52	26	ustr
ALW1	231	253	249	246	243	240	238	252	252	ustr
ALW2	115	167	157	149	150	152	140	153	154	ustr
ALW3	-32	-64	-74	-87	-81	-87	-98	-86	-89	ustr
ALWp1	7.0	7.7	7.5	7.3	7.3	7.1	6.9	7.5	7.5	ksi
ALWp2	1.0	-0.2	-0.5	-0.9	-0.8	-1.0	-1.3	-0.8	-0.9	ksi
ALWAng	3	12	12	11	12	12	11	11	11	deg
ALWvM	6.5	7.8	7.8	7.8	7.7	7.7	7.7	7.9	8.0	ksi
ALW4	66	25	24	18	21	17	14	17	13	ustr
ARF1	409	425	424	431	426	431	464	440	438	ustr
ARF2	1124	-97	-108	-102	-107	-108	-102	-84	-50	ustr
ARF3	660	370	348	352	343	339	374	334	318	ustr
ARF4	506	389	373	380	371	374	417	366	348	ustr
BLBT	177	174	192	163	176	186	172	167	172	ustr
BLBB	-190	-160	-178	-173	-201	-210	-187	-194	-201	ustr
BRBT	175	167	171	157	163	176	165	165	166	ustr
BRBB	-216	-208	-202	-204	-201	-208	-217	-212	-204	ustr
ALBT	179	187	182	174	168	174	172	191	159	ustr
ALBB	-186	-197	-200	-199	-199	-195	-178	-196	-204	ustr
ARBT	191	195	185	186	178	182	189	194	173	ustr
ARBB	-204	0	-193	-197	-192	-196	-217	-197	-195	ustr

Critical Region Compliance to 50 kips Downward VCF
Stress Calculations

Sum	Test 1-9	Std Dev	Test 1	Test 2-6	Std Dev	Test 7-9	Std Dev	
LCF_D	0	0	0	0	0	0	0	kip
LCF	0	0	1	0	0	0	0	kip
VCFE_D	0	0	0	0	0	0	0	kip
VCFE	-50	0	-50	-50	0	-50	0	kip
VCFW_D	0	0	0	0	0	0	0	kip
VCFW	-50	1	-50	-50	0	-51	1	kip
SPE	-0.06	0.02	0.00	-0.06	0.01	-0.07	0.01	in
VCDE	-0.24	0.01	-0.25	-0.24	0.01	-0.24	0.01	in
SPW	-0.07	0.03	0.00	-0.07	0.01	-0.09	0.01	in
VCDW	-0.27	0.01	-0.30	-0.26	0.00	-0.27	0.01	in
BLH1	21.1	4.7	21.9	22.3	5.6	18.9	3.7	ksi
BLH2	14.5	1.6	18.2	14.5	0.6	13.2	0.4	ksi
BLH3	4.6	1.1	7.1	4.6	0.2	3.7	0.3	ksi
BLHp1	24.6	4.9	26.5	25.9	5.8	21.9	3.8	ksi
BLHp2	10.8	2.0	13.5	11.1	1.8	9.3	1.7	ksi
BLHang	7	9	13	6	10	8	8	deg
BLHvM	21.4	4.3	22.9	22.5	5.1	19.0	3.3	ksi
BLH4	9.4	0.9	11.6	9.2	0.3	8.8	0.3	ksi
BLW1	0.6	0.6	-0.1	1.1	0.4	0.1	0.2	ksi
BLW2	-0.3	1.6	2.8	0.0	0.9	-1.7	0.5	ksi
BLW3	1.7	0.3	2.1	1.8	0.2	1.4	0.1	ksi
BLW4	1.6	0.7	3.3	1.7	0.3	1.1	0.1	ksi
BRH1	9.5	0.4	10.4	9.3	0.1	9.4	0.1	ksi
BRH2	18.0	0.9	20.3	17.7	0.1	17.7	0.3	ksi
BRH3	21.2	0.9	23.2	20.7	0.3	21.2	0.5	ksi
BRHp1	26.2	1.1	28.9	25.7	0.3	26.1	0.6	ksi
BRHp2	16.1	0.6	17.5	15.8	0.2	16.1	0.3	ksi
BRHang	-12	1	-14	-13	1	-11	0	deg
BRHvM	22.9	0.9	25.2	22.4	0.2	22.8	0.5	ksi
BRH4	9.7	0.5	10.9	9.5	0.1	9.6	0.2	ksi
BRF1	10.5	0.2	10.8	10.5	0.1	10.5	0.2	ksi
BRF2	8.3	18.2	22.0	10.5	23.6	0.0	0.0	ksi
BRF3	16.5	1.9	21.4	16.0	0.4	15.6	0.5	ksi
BRF4	13.8	3.5	17.4	12.3	4.2	15.1	0.1	ksi
ALH1	15.7	2.8	9.6	15.5	1.5	18.1	0.7	ksi
ALH2	9.0	6.9	26.4	8.1	2.3	4.7	1.0	ksi
ALH3	7.6	6.0	23.5	6.0	1.0	5.0	0.3	ksi
ALHp1	22.0	4.6	32.3	19.2	2.1	23.3	1.1	ksi
ALHp2	10.1	1.9	13.5	10.4	1.5	8.5	0.7	ksi
ALHang	-17	9	-27	-12	8	-23	1	deg
ALHvM	19.3	4.0	28.1	16.8	1.8	20.4	1.1	ksi
ALH4	3.1	3.4	11.6	2.5	1.0	1.1	0.4	ksi
ALW1	7.1	0.2	6.7	7.1	0.1	7.2	0.2	ksi
ALW2	4.3	0.4	3.3	4.5	0.2	4.3	0.2	ksi
ALW3	-2.2	0.6	-0.9	-2.3	0.3	-2.6	0.2	ksi
ALWp1	7.3	0.3	7.0	7.4	0.2	7.3	0.3	ksi
ALWp2	-0.6	0.7	1.0	-0.7	0.3	-1.0	0.3	ksi
ALWang	11	3	3	12	0	11	0	deg
ALWvM	7.7	0.4	6.5	7.8	0.1	7.9	0.2	ksi
ALW4	0.7	0.5	1.9	0.6	0.1	0.4	0.1	ksi
ARF1	12.5	0.4	11.9	12.4	0.1	13.0	0.4	ksi
ARF2	1.2	11.8	32.6	-3.0	0.1	-2.3	0.8	ksi
ARF3	11.1	3.1	19.1	10.2	0.3	9.9	0.8	ksi
ARF4	11.4	1.4	14.7	10.9	0.2	10.9	1.0	ksi
BLBT	5.1	0.3	5.1	5.2	0.3	4.9	0.1	ksi
BLBB	-5.5	0.5	-5.5	-5.4	0.6	-5.6	0.2	ksi
BRBT	4.8	0.2	5.1	4.8	0.2	4.8	0.0	ksi
BRBB	-6.0	0.2	-6.3	-5.9	0.1	-6.1	0.2	ksi
ALBT	5.1	0.3	5.2	5.1	0.2	5.0	0.5	ksi
ALBB	-5.7	0.2	-5.4	-5.7	0.1	-5.6	0.4	ksi
ARBT	5.4	0.2	5.5	5.4	0.2	5.4	0.3	ksi
ARBB	-5.1	1.9	-5.9	-4.5	2.5	-5.9	0.3	ksi

APPENDIX E

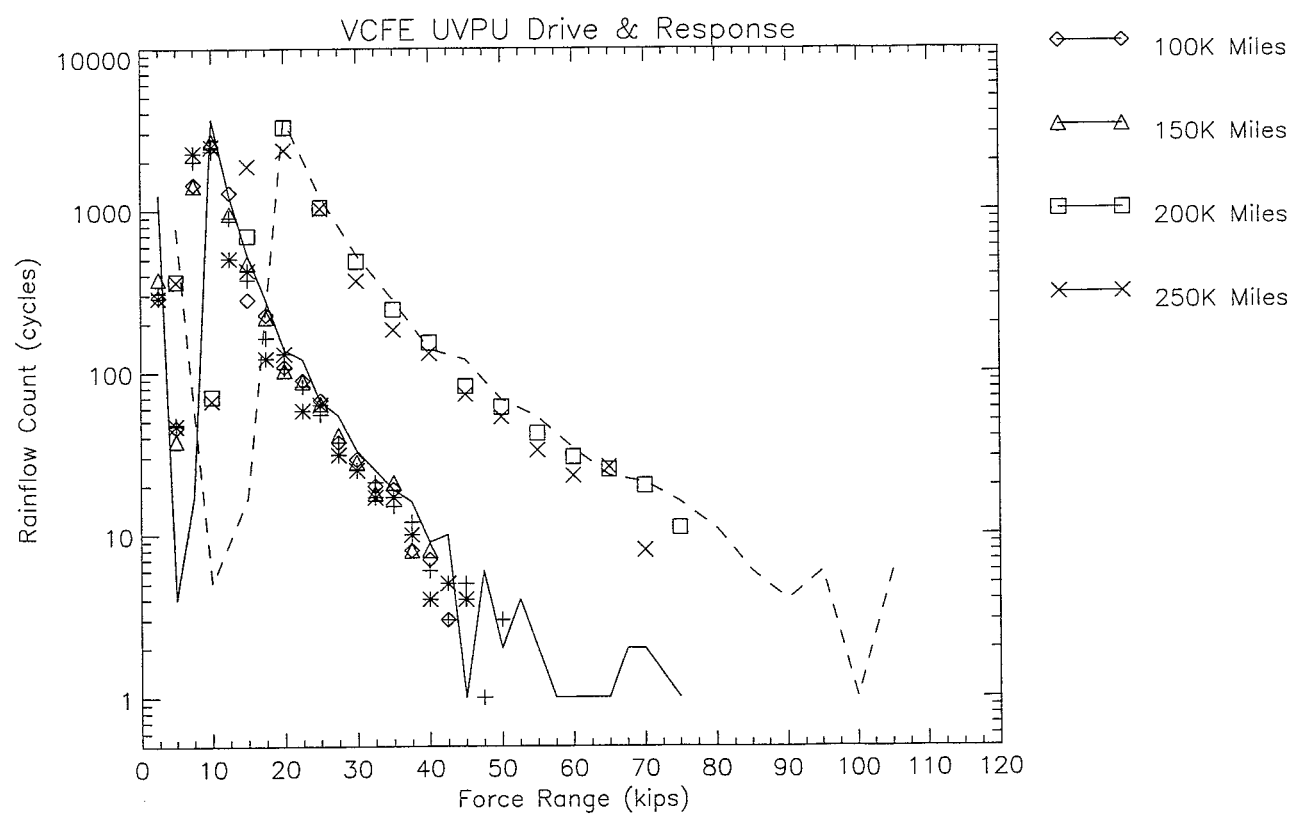
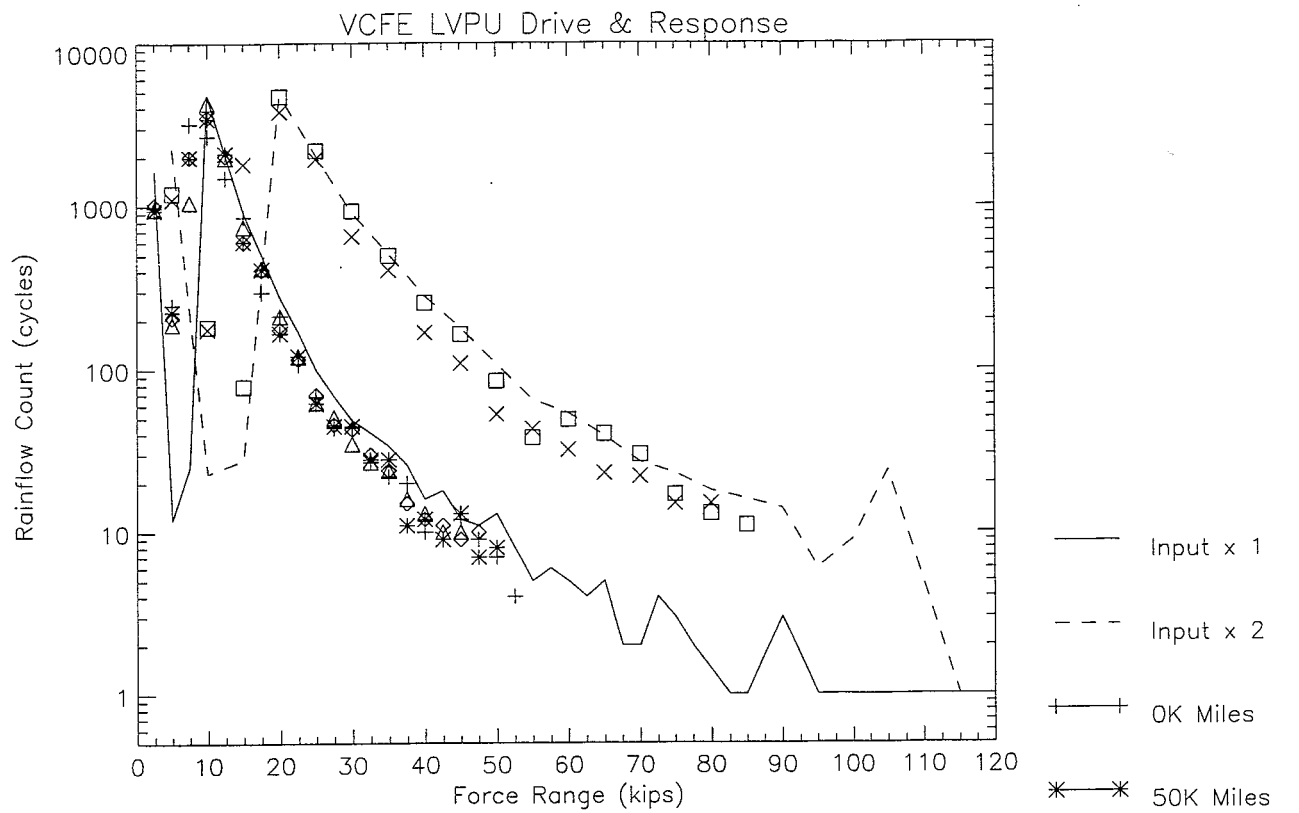
Rainflow Cycle Counted Drive and Response Data

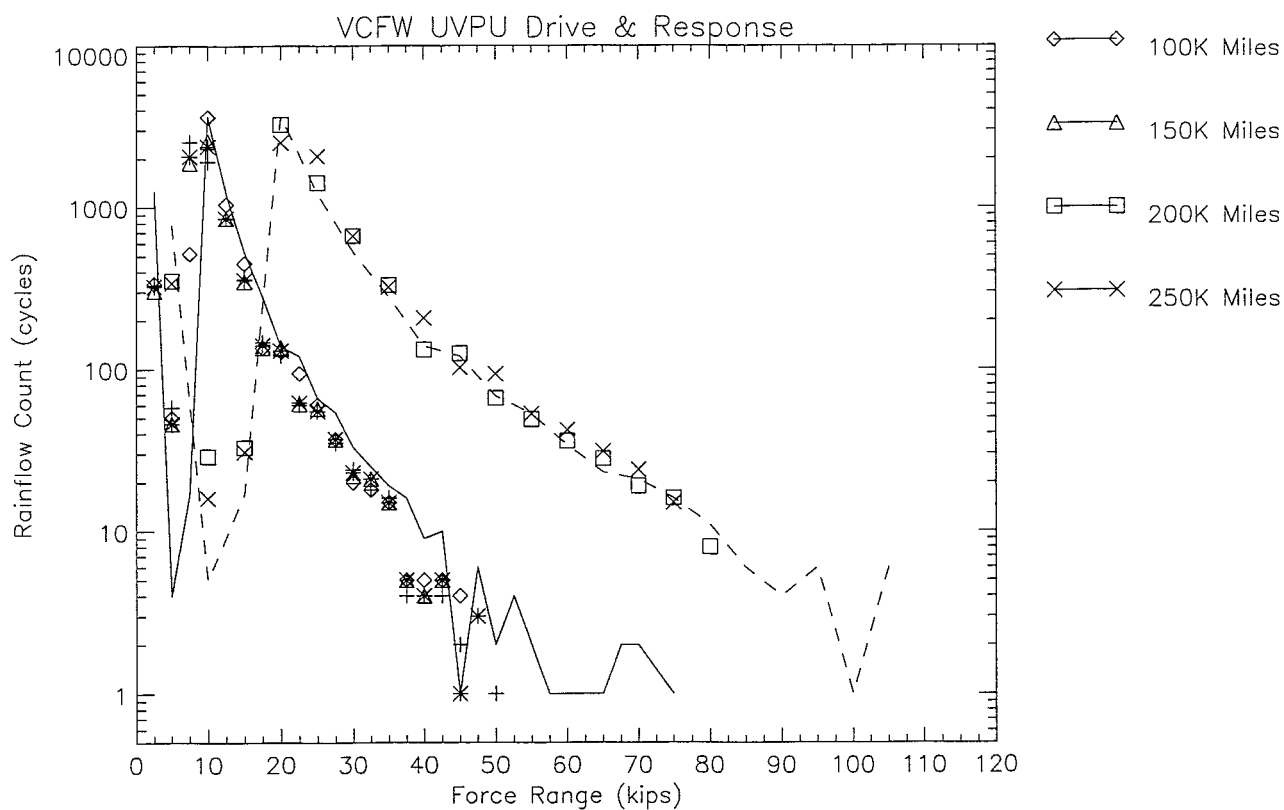
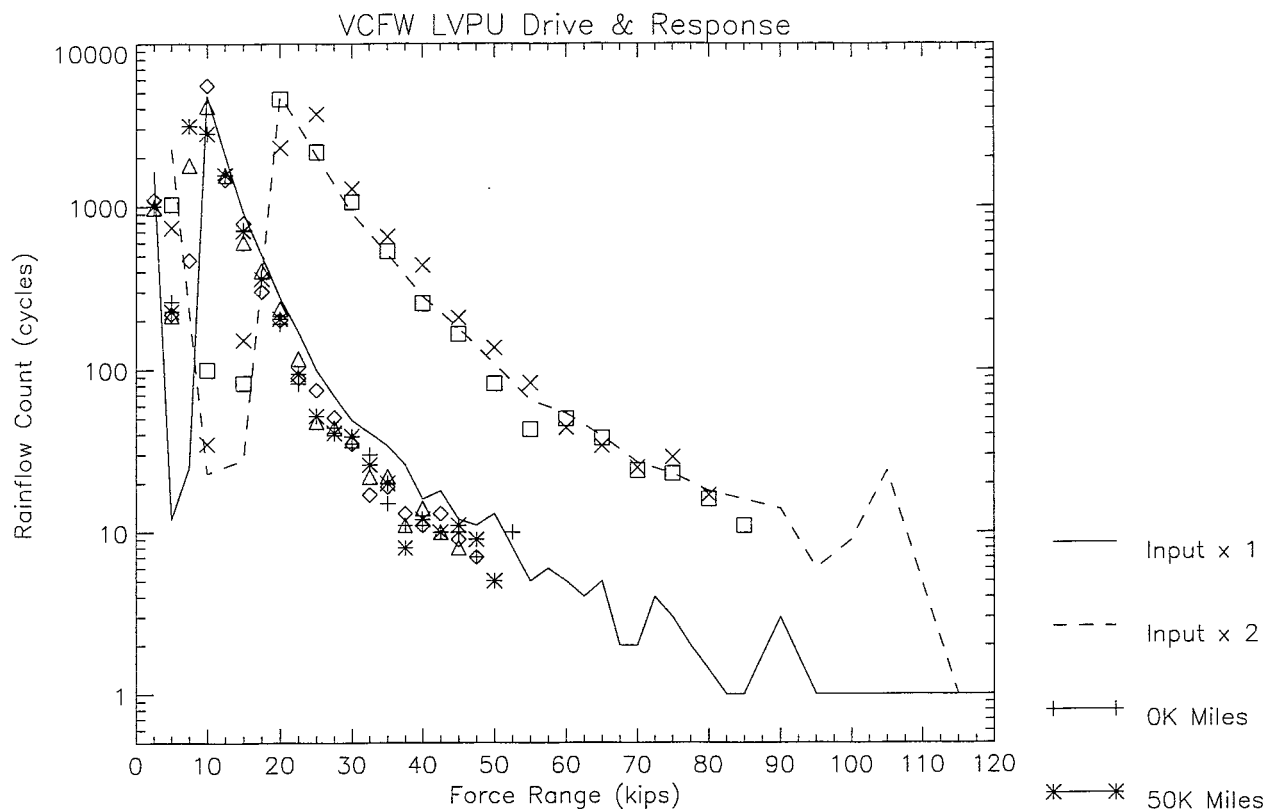
Section E-I: Vertical Coupler Force Response

Section E-II: Longitudinal Coupler Force Response

Section E-I: Vertical Coupler Force Response

FINAL DRAFT





Section E-II: Longitudinal Coupler Force Response

